



Extended-release formulations of somatostatin for ocular application and their effect on vascular endothelial growth factor as a biomarker of diabetic retinopathy

A thesis submitted in fulfilment of the requirements for the degree of Doctor of Philosophy

Uma Devi Do Jai Prakash Rai

B.Sc. (Pharmacy) (Hons) National University of Singapore 2002

School of Health and Biomedical Sciences

College of Science, Engineering and Health

RMIT University

August 2018

Declaration

I certify that except where due acknowledgement has been made, the work is that of the author alone; the work has not been submitted previously, in whole or in part, to qualify for any other academic award; the content of the project is the result of work which has been carried out since the official commencement date of the approved research program; any editorial work, paid or unpaid, carried out by a third party is acknowledged; and, ethics procedures and guidelines have been followed.

I acknowledge the support I have received for my research through the provision of an Australian Government Research Training Program Scholarship.

Uma Devi Do Jai Prakash Rai

30th August 2018

Acknowledgements

This thesis would not have been possible without the support and guidance of so many.

Foremost, I owe my deepest gratitude to my supervisors Associate Professor Simon Young, Dr Thilini Thrimawithana and Dr Celine Valery. Thank you for accepting me as your PhD student and for all your guidance, advice, patience and support in many forms. I am fortunate to have had Dr Paul Bertrand as the HDR coordinator when I started. He has always been kind, approachable and supportive. I am indebted to Professor Peter J Little who accepted me into the Discipline of Pharmacy as an Associate Lecturer, in recognition of my professional experience as a pharmacist and has given me very good advice while he was at RMIT University. I would like to specially thank Professor Ieva Stupans for always being available to listen, guide, advice and support my journey to completion of this PhD.

I must acknowledge Katherine Baverstock, one of the nicest people I have had the fortune to know. She is a role model as a mentor and a friend and has helped me through challenging times. There can be no better researcher, academic and mentor to aspire to than Dr Narin Osman. She has been incredibly generous and giving of her time, advice, materials and support with cell culture work. I have been fortunate to have been trained in cell work by Narin and thank her for her all she has done for me. Thank you to all the lecturers of the Discipline of Pharmacy who have become my second family.

In the laboratory, I have been blessed with the wonderful Fleur McAllister. Her support with keeping the laboratory running, helping with orders and maintenance of instruments has been crucial in keeping my work moving. Fleur has the best work ethic, does her job brilliantly and has inspired me with her positive words and advice. In the same way, I am eternally grateful to Paul Morrison and Mathew Pereira for sharing their technical expertise with HPLC and generous use of resources and time.

The staff at RMIT Microscopy and Microanalysis Facility (RMMF) who have been so helpful with the extensive microscopy required as part of this thesis, especially Dr Matthew Field, Dr Chaitali Dekiwadia, Dr Edwin Mayes, Mr Phil Francis and Mr Peter Rummel.

Thank you to Professor Leslie Yeo for allowing the use of his laboratory and resources as well introducing the SAW technique for the purpose of this work. Thank you to Dr Amgad Rezk and Yasmine Abbas for their help and support.

These four years have been made better and memorable with the company and friendship provided by Suzan Sam, Clare Smith, V Vien Lee, John Mishriky, Diane Gargya and Kate Polglaze.

Finally my most sincere thanks to my family and my in-laws for endless encouragement and support and my husband for being my pillar throughout my PhD journey. This thesis is dedicated to the two halves of my heart, Nikhita and Riya, who have put up with a mother who was not fully present for 4 years. Never doubt my love and devotion to you.

Manuscripts relating to this thesis

1. Rai, U. D. J., Young, S. A., Thrimawithana, T. R., Abdelkader, H., Alani, A. W., Pierscionek, B., & Alany, R. G. (2015). The suprachoroidal pathway: a new drug delivery route to the back of the eye. *Drug discovery today*, 20(4), 491-495.

A part of this work appears in Chapter 1, Section 1.2.1.5. In this paper, I authored the section on SC drug delivery: microneedles.

2. Rai, U., Thrimawithana, T. R., Valery, C., & Young, S. A. (2015). Therapeutic uses of somatostatin and its analogues: current view and potential applications. *Pharmacology & therapeutics*, 152, 98-110.

This work appears in Chapter 1, Section 1.4. I have authored this paper with advice, proof-reading and editing contributions by the other authors.

3. Rai, U., Thrimawithana, T. R., Dharmadana, D., Valery, C., & Young, S. A. (2018). Release kinetics of somatostatin from self-assembled nanostructured hydrogels. *Peptide Science*, 110(2), e23085.

This work appears in Chapter 2, starting from Section 2.1.3 to Section 2.4. I have performed all the experiments, analysis and writing with supervision, advice, proof-reading and editing contributions by the other authors. A section on Small-Angle X-Ray Scattering that appears in the published version has not been included as part of this work as the experiments were performed by D Dharmadana.

TABLE OF CONTENTS

Manuscripts relating to this thesis	iv
Table of contents	v
List of figures	ix
List of Tables	xii
List of Abbreviations	xiii
Abstract	1
CHAPTER 1 INTRODUCTION	
SECTION 1.1 ANATOMY OF THE EYE	4
1.1.1 THE FIBROUS LAYERS OF THE EYE	5
1.1.1.1 THE SCLERA	5
1.1.1.2 THE CORNEA	6
1.1.1.3 THE CONJUNCTIVA	6
1.1.2 THE VASCULAR LAYER OF THE EYE	6
1.1.3 THE NEURAL LAYER OF THE EYE	7
SECTION 1.2 OCULAR DRUG DELIVERY	7
1.2.1 ROUTES OF OCULAR DRUG DELIVERY	7
1.2.1.1 TOPICAL ADMINISTRATION	7
1.2.1.2 SYSTEMIC ROUTE	8
1.2.1.3 PERIOcular ROUTE	9
1.2.1.4 INTRAVITREAL ROUTE	10
1.2.1.5 SUPRACHOROIDAL ROUTE	11
1.2.2 BARRIERS TO ANTERIOR SEGMENT DRUG DELIVERY	12
1.2.3 BARRIERS TO POSTERIOR SEGMENT DRUG DELIVERY	12
SECTION 1.3 DIABETIC RETINOPATHY	14
1.3.1 CURRENT THERAPIES FOR THE MANAGEMENT OF DIABETIC RETINOPATHY	16
SECTION 1.4 SOMATOSTATIN	20
1.4.1 OVERVIEW OF SST BIOLOGICAL ACTIVITY	20
1.4.2 SECRETION PATHWAY AND SST ISOFORMS	21
1.4.3 SST RECEPTORS	22
1.4.3.1 SST RECEPTOR SUBTYPES	22
1.4.3.2 SST RECEPTOR DISTRIBUTION	22
1.4.3.3 SST RECEPTOR SIGNALLING MECHANISMS	24
1.4.3.4 SST ANALOGUES	27
1.4.3.5 SST RECEPTOR ANTAGONISTS	30
1.4.4 POTENTIAL USE IN DIABETIC RETINOPATHY	31
1.4.4.1 PHARMACOLOGICAL ROLE OF SST AND SST RECEPTORS IN DIABETIC RETINOPATHY	31
1.4.4.2 EFFICACY OF SST ANALOGUES IN MODELS OF DIABETIC RETINOPATHY AND CLINICAL SIGNIFICANCE	33
SECTION 1.5 THESIS OBJECTIVES	36
CHAPTER 2 PHYSICO-CHEMICAL CHARACTERISATION OF SELF-ASSEMBLED SOMATOSTATIN HYDROGELS	
SECTION 2.1 INTRODUCTION	38
2.1.1 RHEOLOGY	38
2.1.2 MODELS OF RELEASE	40
2.1.3 RELEASE KINETICS	42

2.2 MATERIALS AND METHODS.....	43
2.2.1 MATERIALS.....	43
2.2.2 METHODS.....	43
2.2.2.1 PREPARATION OF SST HYDROGELS.....	43
2.2.2.2 TRANSMISSION ELECTRON MICROSCOPY.....	44
2.2.2.3 OSCILLATORY RHEOLOGY.....	44
2.2.2.4 MONOMER RELEASE PROTOCOLS.....	45
2.2.2.5 HPLC.....	45
2.2.2.6 ASSAY BY UV SPECTROPHOTOMETRY.....	46
2.2.2.7 STATISTICAL ANALYSIS.....	46
2.3 RESULTS AND DISCUSSION.....	48
2.3.1 NANOFIBRIL STRUCTURAL CHARACTERIZATION (TEM).....	48
2.3.2 OSCILLATORY RHEOLOGY.....	50
2.3.3 MONOMER RELEASE.....	55
2.3.4 RELEASE KINETICS.....	57
2.4 CONCLUSION.....	61

CHAPTER 3 FORMULATION OF SOMATOSTATIN IN HPMC HYDROGELS

SECTION 3.1 INTRODUCTION.....	63
3.2 MATERIALS AND METHODS.....	65
3.2.1 MATERIALS.....	65
3.2.2 METHODS.....	65
3.2.2.1 PREPARATION OF HPMC GEL.....	65
3.2.2.2 RHEOLOGICAL CHARACTERIZATION OF BLANK HPMC GELS AND SST 5% W/W IN HPMC HYDROGELS.....	65
3.2.2.3 PREPARATION OF SST 5% W/W IN HPMC HYDROGELS.....	66
3.2.2.4 INVESTIGATION OF SST CONFORMATION BEFORE AND AFTER EXPOSURE TO SIMULATED LACHRYMAL FLUID.....	66
3.2.2.5 MORPHOLOGICAL CHARACTERIZATION OF HYDROGELS.....	66
3.2.2.6 RELEASE STUDY OF SOMATOSTATIN MONOMERS FROM HYDROGELS.....	67
3.2.2.7 MASS SPECTROMETRY OF RELEASED SAMPLES INVESTIGATING SST CONFORMATION UPON RELEASE.....	67
3.3 RESULTS AND DISCUSSION.....	67
3.3.1 RHEOLOGICAL CHARACTERIZATION OF AGING PROCESS OF BLANK HPMC GELS.....	67
3.3.2 RHEOLOGICAL CHARACTERIZATION OF SOMATOSTATIN-LOADED HPMC HYDROGELS.....	68
3.3.3 INVESTIGATION OF SST CONFORMATION BEFORE AND AFTER EXPOSURE TO SLF (FTIR CHARACTERIZATION OF HYDROGELS).....	73
3.3.4 MORPHOLOGICAL CHARACTERISATION OF HYDROGELS.....	77
3.3.5 RELEASE PROFILE OF SOMATOSTATIN MONOMERS FROM SST IN HPMC HYDROGELS.....	79
3.3.6 RELEASE KINETICS OF SST 5% RELEASE FROM HPMC GELS.....	80
3.3.7 MASS SPECTROMETRY OF RELEASED SAMPLES INVESTIGATING SST CONFORMATION UPON RELEASE.....	83
3.4 CONCLUSION.....	84

CHAPTER 4-PREPARATION AND CHARACTERIZATION OF SOMATOSTATIN MICROPARTICLES

4.1 INTRODUCTION.....	86
4.1.1 MICROPARTICLES.....	86
4.1.1.1 RATIONALE FOR USE OF MICROPARTICLES.....	86
4.1.1.2 CHARACTERISTICS OF MICROPARTICLES.....	86
4.1.1.3 ADMINISTRATION OF MICROPARTICLES.....	88

4.1.1.4	MICROPARTICLE USE IN OCULAR APPLICATIONS.....	88
4.1.1.5	MANUFACTURE OF MICROPARTICLES.....	89
4.1.1.6	SURFACE ACOUSTIC WAVE ATOMIZATION.....	90
4.1.2	POLYCAPROLACTONE.....	92
4.2	MATERIALS AND METHODS.....	94
4.2.1	MATERIALS.....	94
4.2.2	METHODS.....	94
4.2.2.1	OPTIMIZATION OF POLYMER CONCENTRATION AND MOLECULAR WEIGHT.....	94
4.2.2.2	PRODUCTION OF MICROPARTICLES LOADED WITH FITC-DEAE-DEXTRAN (MODEL DRUG).....	95
4.2.2.2.1	PREPARATION OF MICROPARTICLES USING SAW.....	95
4.2.2.2.2	PREPARATION OF MICROPARTICLES USING WATER-IN-OIL-IN-WATER (W/O/W) DOUBLE EMULSION METHOD.....	95
4.2.2.3	DETERMINATION OF ENCAPSULATION EFFICIENCY.....	95
4.2.2.3.1	ENCAPSULATION EFFICIENCY OF MICROPARTICLES LOADED WITH MODEL DRUG PRODUCED BY SAW TECHNIQUE.....	95
4.2.2.3.2	ENCAPSULATION EFFICIENCY OF MICROPARTICLES LOADED WITH MODEL DRUG PRODUCED BY W/O/W DOUBLE EMULSION METHOD.....	96
4.2.2.4	MORPHOLOGICAL ANALYSIS OF MICROPARTICLES.....	96
4.2.2.5	SIZING OF MICROPARTICLES.....	96
4.2.2.6	PRODUCTION OF SOMATOSTATIN-LOADED POLYMER MICROPARTICLES.....	97
4.2.2.7	RELEASE STUDIES.....	97
4.3	RESULTS AND DISCUSSION.....	97
4.3.1	ENCAPSULATION EFFICIENCY OF MODEL DRUG IN MICROPARTICLES PREPARED BY SAW TECHNIQUE.....	97
4.3.2	ENCAPSULATION EFFICIENCY OF MICROPARTICLES PRODUCED BY DOUBLE EMULSION (W/O/W) METHOD.....	98
4.3.3	MORPHOLOGICAL ANALYSIS OF MICROPARTICLES WITH FITC-DEAE-DEXTRAN (MODEL DRUG) USING SAW TECHNIQUE.....	99
4.3.4	MORPHOLOGICAL ANALYSIS OF MICROPARTICLES PRODUCED BY DOUBLE EMULSION (W/O/W) METHOD.....	100
4.3.5	ENCAPSULATION EFFICIENCY OF SST MICROPARTICLES PREPARED WITH DOUBLE EMULSION (W/O/W) METHOD.....	102
4.3.6	RELEASE STUDIES.....	104
4.3.6.1	RELEASE OF FITC-DEAE-DEXTRAN (MODEL DRUG) FROM MICROPARTICLES PREPARED WITH SAW TECHNIQUE.....	104
4.3.6.2	RELEASE OF SST FROM MICROPARTICLES PREPARED BY DOUBLE EMULSION (W/O/W) METHOD.....	107
4.4	CONCLUSION.....	110

CHAPTER 5 – INVESTIGATION OF THE EFFECTS OF SOMATOSTATIN ON THE EXPRESSION OF VEGF RECEPTOR-2 LEVELS AND VEGF SECRETION BY ARPE-19 CELLS IN HIGH GLUCOSE CONDITIONS

5.1	INTRODUCTION.....	113
5.2	MATERIALS AND METHODS.....	115
5.2.1	CULTURE OF ARPE-19 CELLS.....	115
5.2.2	MTT CYTOTOXICITY ASSAY.....	115
5.2.3	IMMUNOFLUORESCENCE STUDIES OF VEGF-R2 EXPRESSION.....	116
5.2.4	QUANTIFICATION OF VEGF SECRETION BY ELISA.....	117
5.2.5	STATISTICAL ANALYSIS.....	117
5.3	RESULTS AND DISCUSSION.....	117
5.3.1	MTT CYTOTOXICITY ASSAY.....	117
5.3.2	IMMUNOFLUORESCENCE STUDIES OF VEGF-R2 EXPRESSION.....	119
5.3.3	QUANTIFICATION OF VEGF SECRETION BY ELISA.....	125
5.4	CONCLUSION.....	129

CHAPTER 6: GENERAL DISCUSSION AND CONCLUSION

6.1 SUMMARY OF FINDINGS.....130
6.2 CONCLUSION.....139
REFERENCES.....140

LIST OF FIGURES

CHAPTER ONE

FIGURE 1.1: CROSS-SECTION OF THE HUMAN EYE.....	4
FIGURE 1.2: HEMATOXYLIN AND EOSIN (H & E) STAIN IMAGE OF POSTERIOR SEGMENT SECTIONS (15 μ M) OF A HUMAN EYE, DEPICTING THE SCLERA, CHOROID AND RETINAL ARCHITECTURE.....	5
FIGURE 1.3: OCULAR DELIVERY ROUTES.....	8
FIGURE 1.4: SCHEMATIC REPRESENTATION OF PERIOcular ROUTES OF DELIVERY	10
FIGURE 1.5: BLOOD-RETINAL BARRIER.....	13
FIGURE 1.6: PROJECTIONS FOR DIABETIC RETINOPATHY.....	15
FIGURE 1.7: INTRACELLULAR SIGNALLING CASCADES ASSOCIATED TO SOMATOSTATIN RECEPTORS IN PITUITARY CELLS.....	26
FIGURE 1.8: STRUCTURES OF SST ANALOGUES.....	27

CHAPTER TWO

FIGURE 2.1: COMPARISON OF CUMULATIVE PERCENTAGE RELEASE OF SOMATOSTATIN IN SLIDE-A-LYZER UNITS AT 48 HOURS.....	47
FIGURE 2.2 COMPARISON OF CUMULATIVE PERCENTAGE RELEASE OF SOMATOSTATIN IN EPPENDORF TUBES AT 48 HOURS.....	48
FIGURE 2.3. TRANSMISSION ELECTRON MICROGRAPHS OF (A) SOMATOSTATIN 5% W/W IN WATER (MAGNIFICATION 5000X) (B) SOMATOSTATIN 5% W/W IN 0.9% W/V NaCl (MAGNIFICATION 5000X) (C) SOMATOSTATIN 5% W/W IN SIMULATED LACHRYMAL FLUID (MAGNIFICATION 4000X)	48
FIGURE 2.4. TRANSMISSION ELECTRON MICROGRAPHS OF SST 5% WATER SAMPLES ON DAY 8.....	49
FIGURE 2.5. TRANSMISSION ELECTRON MICROGRAPHS OF SST 5% NaCl SAMPLES ON DAY 8.....	50
FIGURE 2.6. TRANSMISSION ELECTRON MICROGRAPHS SST 5% SLF SAMPLES ON DAY 8.....	50
FIGURE 2.7. COMPARISON OF THE G' (STORAGE MODULUS) OF THE SST HYDROGELS ON DAY 8 AT A FREQUENCY OF 1 HZ AT 37°C.....	52
FIGURES 2.8A AND 2.8B: FLOW SWEEP AT 25°C AND 37°C RESPECTIVELY.....	53
FIGURE 2.9 FREQUENCY SWEEP OF THE SST HYDROGELS ON DAY 8 AT 37°C.....	54
FIGURE 2.10 TEMPERATURE SWEEP OF THE SST HYDROGELS (DAY 8) FROM 20°C TO 50°C.....	54
FIGURES 2.11A AND 2.11B: COMPARISON OF CUMULATIVE PERCENTAGE SST RELEASED IN SLIDE-A-LYZER UNITS AT 48HRS AND 9HRS RESPECTIVELY.....	56
FIGURES 2.12A AND 2.12B: COMPARISON OF CUMULATIVE PERCENTAGE SST RELEASED IN EPPENDORF TUBES AT 48HRS AND 9HRS RESPECTIVELY.....	56
FIGURE 2.13: FITTING OF THE SST 5% WATER VS WATER RELEASE OVER 48 HOURS IN SLIDE-A-LYZER UNITS TO DIFFERENT MODELS OF RELEASE.....	57

CHAPTER THREE

FIGURE 3.1: CHEMICAL STRUCTURE OF METHOCCEL 65 HG® WITH 5.5-7.5% HYDROXYPROPYL SUBSTITUTION.....	65
FIGURE 3.2: CHANGES IN G' (STORAGE MODULUS) OF HPMC 3% W/W AND 6% W/W GELS DURING THE AGING PROCESS.....	68
FIGURE 3.3: COMPARISON OF THE G' (STORAGE MODULUS) OF THE DIFFERENT GELS TESTED AT DAYS 1, 7 AND DAYS 1-4 AFTER EXPOSURE TO SLF IN RELEASE CONDITIONS	70
FIGURE 3.4: COMPARISON OF THE FREQUENCY SWEEPS OF THE DIFFERENT GELS TESTED AT DAYS 1, 7 AND DAYS 1-4 AFTER EXPOSURE TO SLF IN RELEASE CONDITIONS	71
FIGURE 3.5: COMPARISON OF FLOW SWEEPS OF DIFFERENT GELS TESTED AT DAYS 1, 7 AND DAYS 1-4 AFTER EXPOSURE TO SLF IN RELEASE CONDITIONS.....	72
FIGURE 3.6: COMPARISON OF TEMPERATURE SWEEPS OF DIFFERENT GELS TESTED AT DAYS 1, 7 AND DAYS 1-4 AFTER EXPOSURE TO SLF IN RELEASE CONDITIONS.....	73
FIGURE 3.7: FTIR DATA OF THE TRANSITION IN CONFORMATION FROM RANDOM COIL TO MORE STRUCTURED B-SHEET CONFORMATIONS FOR SST 5% IN WATER, SST 5% W/W IN HPMC 3% W/W AND SST 5% IN HPMC 6% W/W UPON EXPOSURE TO RELEASE CONDITIONS IN CONTACT WITH SLF.....	75

FIGURE 3.8: SECONDARY DERIVATIVE PLOTS OF FTIR DATA COMPARING THE DIFFERENCE IN STRUCTURE BETWEEN DAY 7 AND DAY 4 OF RELEASE AFTER EXPOSURE TO SLF FOR SST 5% W/W IN WATER, SST 5% W/W IN HPMC 3% W/W AND SST 5% W/W IN HPMC 6% W/W.....	76
FIGURE 3.9: TRANSMISSION ELECTRON MICROGRAPHS OF SST 5% IN WATER AT DAY 7.....	77
FIGURE 3.10: TRANSMISSION ELECTRON MICROGRAPHS OF SST 5% IN WATER AT RELEASE DAY 4.....	77
FIGURE 3.11: TRANSMISSION ELECTRON MICROGRAPHS OF BLANK HPMC 6% W/W AT RELEASE DAY 4.....	78
FIGURE 3.12: TRANSMISSION ELECTRON MICROGRAPHS OF SST 5% W/W IN HPMC 6% W/W AT RELEASE DAY 4.....	78
FIGURE 3.13: COMPARISON OF THE RELEASE PROFILES OF SST 5% IN WATER, SST 5% W/W IN HPMC 3% W/W AND SST 5% W/W IN HPMC 6% W/W.....	79
FIGURE 3.14: RELEASE PROFILES OF SST 5% W/W IN HPMC 3% W/W AND SST 5% W/W IN HPMC 6% W/W GELS FITTED TO HYBRID MODEL OF RELEASE.....	80
FIGURE 3.15 MASS SPECTRA OF (A) SST STANDARD (B) RELEASE DAY 1 SAMPLE FROM SST 5% W/W IN HPMC 6% W/W AND (C) RELEASE DAY 10 SAMPLE FROM SST 5% W/W IN HPMC 6% W/W.....	84

CHAPTER FOUR

FIGURE 4.1 STRUCTURE OF MICROPARTICLES (MICROSPHERES AND MICROCAPSULES).....	87
FIGURE 4.2: SCHEMATIC OF THE RAYLEIGH WAVE PROPAGATION AND THE ATOMIZATION PROCESS.....	90
FIGURE 4.3: SCHEMATIC ILLUSTRATION OF THE W/O/W DOUBLE-EMULSION METHOD USED TO PREPARE PCL-PEG-PCL MICROPARTICLES.....	91
FIGURE 4.4: IMAGES UNDER FLUORESCENCE MICROSCOPE AFTER FIRST CENTRIFUGATION (A-PRE-WASH), (B- WASH #1) AND (C-WASH #2) FROM LEFT TO RIGHT RESPECTIVELY.....	100
FIGURE 4.5: SCANNING ELECTRON MICROGRAPHS OF HMW 1% POLYMER MICROPARTICLES.....	100
FIGURE 4.6: SCANNING ELECTRON MICROGRAPHS OF HMW 2% POLYMER MICROPARTICLES.....	101
FIGURE 4.7: SCANNING ELECTRON MICROGRAPHS OF HMW 5% POLYMER MICROPARTICLES.....	101
FIGURE 4.8A: CUMULATIVE PERCENTAGE RELEASE OF FITC-DEAE-DEXTRAN 0.5% W/W FROM LMW POLYMER 1% W/W MICROPARTICLES WITH SAW TECHNIQUE.....	105
FIGURE 4.8B: CUMULATIVE PERCENTAGE RELEASE OF FITC-DEAE-DEXTRAN 0.5% W/W FROM LMW POLYMER 1% W/W MICROPARTICLES WITH SAW TECHNIQUE FITTED TO EQUATION 3.1.....	105
FIGURE 4.9A: CUMULATIVE PERCENTAGE RELEASE OF SOMATOSTATIN 2.5% W/W FROM HMW POLYMER 5% W/W.....	107
FIGURE 4.9B: CUMULATIVE PERCENTAGE RELEASE OF SOMATOSTATIN 2.5% W/W FROM HMW POLYMER 5% W/W MODELLED TO EQUATION 3.1.....	108

CHAPTER FIVE

FIGURE 5.1: RESULTS OF MTT ASSAY ASSESSING CYTOTOXICITY OF APPLIED TREATMENTS ON ARPE-19 CELLS IN HIGH (25 MM) (SOLID BARS) AND NORMAL (5 MM) (SPOTTED BARS) GLUCOSE CONDITIONS.....	119
FIGURE 5.2: DOSE-RESPONSE OF VEGF-R2 EXPRESSION LEVELS IN THE PRESENCE OF SOMATOSTATIN 10^{-8} M TO 10^{-5} M IN HIGH GLUCOSE (25 MMOL/L) (SOLID BARS) AND NORMAL GLUCOSE (5 MMOL/L) (DOTTED BARS) CONDITIONS.....	121
FIGURE 5.3: EFFECT OF SOMATOSTATIN 10^{-6} M AND 10^{-7} M ON VEGF-R2 EXPRESSION LEVELS IN HIGH GLUCOSE (25 MMOL/L) (SOLID BARS) AND NORMAL GLUCOSE (5 MMOL/L) (DOTTED BARS) CONDITIONS.....	121
FIGURE 5.4: CONFOCAL IMAGES OF WELLS INCUBATED WITH (A) SST 10^{-7} M (B) SST 10^{-6} M AND (C) CONTROL IN NORMAL GLUCOSE (72 HOURS).....	122
FIGURE 5.5: CONFOCAL IMAGES OF SST 10^{-5} M SST GELLED IN (A) NORMAL GLUCOSE (B AND C) IN HIGH GLUCOSE (72 HOURS).....	122
FIGURE 5.6: CONFOCAL IMAGES OF EXPRESSION OF VEGF-R2 IN RESPONSE TO DIFFERENT SST CONCENTRATIONS IN HIGH GLUCOSE (72 HOURS) (A) SST 10^{-8} M (B) SST 10^{-7} M (C) SST 10^{-6} M (D) HIGH GLUCOSE ONLY CONTROL.....	123

FIGURE 5.7: RESULTS OF ELISA ASSAY OF EFFECT OF SOMATOSTATIN 10^{-8} M TO 10^{-5} M IN HIGH GLUCOSE (25 MMOL/L) AND NORMAL GLUCOSE (5 MMOL/L) CONDITIONS ON VEGF SECRETION AT 72 HOURS.....	123
FIGURE 5.8: RESULTS OF ELISA ASSAY OF EFFECT OF SOMATOSTATIN 10^{-8} M TO 10^{-5} M IN HIGH GLUCOSE (25 MMOL/L) (SOLID BARS) AND NORMAL GLUCOSE (5 MMOL/L) (DOTTED BARS) CONDITIONS ON VEGF SECRETION AT 72 HOURS.....	126
FIGURE 5.9: RESULTS OF ELISA ASSAY OF EFFECT OF SOMATOSTATIN 10^{-6} M AND 10^{-7} M AND RELEASE SAMPLES DAY AND DAY 10 FROM SST 5% W/W IN HPMC 6% W/W HYDROGELS IN HIGH GLUCOSE (25 MMOL/L) (SOLID BARS) AND NORMAL GLUCOSE (5 MMOL/L) (DOTTED BARS) CONDITIONS ON VEGF SECRETION AT 24 HOURS.....	126

LIST OF TABLES

CHAPTER ONE

TABLE 1.1- TABLE 1.1- SUMMARY OF THE CURRENT THERAPIES FOR DR.....	18
TABLE 1.2 –SUMMARY OF ANTI-SECRETORY FUNCTIONS OF SST.....	20
TABLE 1.3- DISTRIBUTION AND SIGNALLING MECHANISMS OF SOMATOSTATIN RECEPTORS (SSTRs)	23
TABLE 1.4- SUMMARY OF THE CURRENTLY MARKETED SST ANALOGUES.....	28
TABLE 1.5 – SUMMARY OF STUDIES OF SST ANALOGUES IN THE EYE.....	34

CHAPTER TWO

TABLE 2.1 COMPOSITION OF SIMULATED LACHRYMAL FLUID.....	43
TABLE 2.2 COMPARISON OF CUMULATIVE PERCENTAGE SOMATOSTATIN RELEASED AT 48 HOURS IN THE EPPENDORF TUBES AND SLIDE-A-LYZER UNITS.....	55
TABLE 2.3: MEAN R^2 (AND STANDARD DEVIATION) VALUES AND DESORPTION HALF TIME IN MINUTES IN SLIDE-A-LYZER UNITS.....	58
TABLE 2.4: MEAN R^2 VALUES (AND STANDARD DEVIATION) AND DESORPTION HALF-TIME IN MINUTES IN EPPENDORF TUBES.	59

CHAPTER THREE

TABLE 3.1: THE GOODNESS OF THE FIT (MEAN R^2) OF THE ABOVE MODEL TO THE SAMPLES AS WELL AS THE T_{90} (TIME TO RELEASE 90% OF SST FROM THE CORE OF THE GEL), K AND R_{MAX}	81
---	----

CHAPTER FOUR

TABLE 4.1: COMPARISON OF THE TRADITIONAL METHODS OF PEPTIDE ENCAPSULATION IN MICROPARTICLES.....	91
TABLE 4.2: COMPARISON OF PROPERTIES BETWEEN SOMATOSTATIN AND FITC-DEAE- DEXTRAN.....	97
TABLE 4.3: ENCAPSULATION EFFICIENCY OF FITC-DEAE-DEXTRAN IN MICROPARTICLES PREPARED BY SAW TECHNIQUE ANALYSING THE AMOUNT OF DRUG REMAINING IN BUFFER.....	98
TABLE 4.4: ENCAPSULATION EFFICIENCY OF FITC-DEAE-DEXTRAN IN MICROPARTICLES PREPARED BY SAW TECHNIQUE FROM DISSOLVED MICROPARTICLES.....	98
TABLE 4.5: ENCAPSULATION EFFICIENCY AND PARTICLE SIZE OF FITC-DEAE-DEXTRAN IN MICROPARTICLES PREPARED BY W/O/W METHOD.....	99
TABLE 4.6: ENCAPSULATION EFFICIENCY OF DIFFERENT CONCENTRATIONS OF SOMATOSTATIN AND HMW POLYMER USING W/O/W METHOD.....	103
TABLE 4.7: ENCAPSULATION EFFICIENCY OF SST 2.5% HMW POLYMER 2% (N=3) USING W/O/W METHOD.....	103
TABLE 4.8: MEAN R^2 , $T_{1/2}$ AND RATE CONSTANT VALUES WITH STANDARD DEVIATION FOR FITC-DEAE-DEXTRAN 0.5% W/W RELEASE FROM LMW 1% W/W POLYMER MICROPARTICLES. . . .	109
TABLE 4.9: MEAN R^2 , $T_{1/2}$ AND RATE CONSTANT VALUES WITH STANDARD DEVIATION FOR SST 2.5% W/W RELEASE FROM HMW 2% W/W POLYMER MICROPARTICLES.....	109

LIST OF ABBREVIATIONS

°C	DEGREES CELSIUS
μL	MICRO-LITERS
μM	MICROMETERS
μN.M	MICRONEWTON METER
A _D	TOTAL DIFFUSIONAL RELEASE
AGES	ADVANCED GLYCATION END-PRODUCTS
ANOVA	ANALYSIS OF VARIANCE
ARMD	AGE-RELATED MACULAR DEGENERATION
AUC	AREA UNDER THE CURVE
BAB	BLOOD AQUEOUS BARRIER
BRB	BLOOD RETINAL BARRIER
BSA	BOVINE SERUM ALBUMIN
CA.	CIRCA
C ₀	INITIAL CONCENTRATION OF ACTIVE RELEASED
C _T	THE AMOUNT OF ACTIVE AGENT RELEASED
CCK	CHOLECYSTOKININ
CM	CENTIMETER
CNS	CENTRAL NERVOUS SYSTEM
CRYO-TEM	CRYO-TRANSMISSION ELECTRON MICROSCOPY
Da	DALTON
DCM	DICHLOROMETHANE
DMEM	DULBECCO'S MODIFIED EAGLE MEDIUM
DR	DIABETIC RETINOPATHY
E	YOUNG'S MODULUS
ELISA	ENZYME-LINKED IMMUNOSORBENT ASSAY
EMA	EUROPEAN MEDICINES AGENCY
ERG	ELECTRORETINOGRAM
FBS	FETAL BOVINE SERUM
FDA	FEDERAL DRUG ADMINISTRATION
FITC	FLUORESCCEIN ISOTHIOCYANATE
FTIR	FOURIER TRANSFORM INFRARED
G	GRAM
G'	STORAGE MODULUS
G''	LOSS MODULUS
GH	GROWTH HORMONE
GIP	GASTRIC INHIBITORY POLYPEPTIDE,
GLUT-1	GLUCOSE TRANSPORTER-1
GRAS	GENERALLY REGARDED AS SAFE
H&E	HAEMATOXYLIN AND EOSIN
HPLC	HIGH PERFORMANCE LIQUID CHROMATOGRAPHY
HPMC	HYDROXYPROPYL METHYLCELLULOSE
HMW	HIGH MOLECULAR WEIGHT
HR	HOUR
Hz	HERTZ
IBRB	INNER BLOOD RETINAL BARRIER
ICH	INTERNATIONAL CONFERENCE ON HARMONISATION
IDF	INTERNATIONAL DIABETES FEDERATION
IDT	INTERDIGITAL TRANSDUCER
IGG	IMMUNOGLOBULIN G
IL-1B	INTERLEUKIN-1 BETA
ILM	INNER LIMITING MEMBRANE
INL	INNER NUCLEAR LAYER
K	FIRST-ORDER RELEASE CONSTANT

K ₀	ZERO-ORDER CONSTANT
K _B	A RELEASE CONSTANT.
kDa	KILODALTONS
LMW	LOW MOLECULAR WEIGHT
LVR	LINEAR VISCOELASTIC RANGE
M	MOLAR CONCENTRATION
MAPK	MITOGEN-ACTIVATED PROTEIN KINASE
MC	METHYLCELLULOSE
MDR	MULTI-DRUG RESISTANCE
MRP	MULTI-DRUG RESISTANCE PUMPS
MIN	MINUTE
MM	MILLIMETER
MMOL/L	MILLIMOLES PER LITER
MTT	3-(4, 5-DIMETHYLTHIAZOL-2-YL)-2, 5-DIPHENYL TETRAZOLIUM BROMIDE
MW	MOLECULAR WEIGHT
NHE1	NA ⁺ /H ⁺ EXCHANGER
NPDR	NON-PROLIFERATIVE DIABETIC RETINOPATHY
NM	NANOMETERS
NOS	NITRIC OXIDE SYNTHASE
oBRB	OUTER BLOOD RETINAL BARRIER
ON	OPTIC NERVE
ONL	OUTER NUCLEAR LAYER
Pa	PASCALS
PBS	PHOSPHATE BUFFERED SALINE
PEDF	PIGMENT EPITHELIUM DERIVED FACTOR
PEG	POLYETHYLENE GLYCOL
PCL	POLYCAPROLACTONE
PDR	PROLIFERATIVE DIABETIC RETINOPATHY
P-GP	P-GLYCOPROTEIN
PLA	POLY-LACTIC ACID
PLGA	POLY (LACTIC-CO-GLYCOLIC ACID)
PTPS	PROTEIN TYROSINE PHOSPHATASES
Q _T	THE AMOUNT OF ACTIVE AGENT RELEASED AT TIME T
Q ₀	INITIAL AMOUNT OF ACTIVE AGENT DISSOLVED
RAAS	RENIN-ANGIOTENSIN-ALDOSTERONE SYSTEM
ROS	REACTIVE OXYGEN SPECIES
RPE	RETINAL PIGMENTED EPITHELIUM
SAW	SURFACE ACOUSTIC WAVE

Abstract

The International Diabetes Federation reports 642 million adults globally will be living with diabetes by 2040. Approximately one third will go on to develop some extent of diabetic retinopathy (DR), with *ca.* 93 million current sufferers.

Current therapeutic options for DR target the late stages of the disease when vision is already significantly degraded. These treatments aim to prevent haemorrhaging using laser therapy or intraocular injections of corticosteroids and therapeutic anti-vascular endothelial growth factor (VEGF) antibodies. However, efficacy is low or variable with frequent injections required and associated with serious ocular side-effects. Moreover, all result in some degree of tissue destruction. New therapies to prevent the onset or arrest the progression of the disease before overt microvascular pathologies are therefore essential.

Somatostatin (SST) has been reported to have neuroprotective, antiangiogenic effects in addition to the regulation of water and ion transport in the retina. It is postulated that SST could attenuate key pathological changes in DR. However, studies with SST analogues such as octreotide demonstrated that systemic administration resulted in the drug reaching the retina only when there is a breakdown of the blood retinal barrier.

SST is produced by the retina and there is downregulation of SST levels in the retina of diabetic patients, correlated to retinal neurodegeneration. SST eye drops show some promise (EUROCONDOR). The purpose of this thesis was to develop a modified-release formulation of SST enhancing the treatment of diabetic retinopathy.

The physicochemical characterization of SST self-assembled hydrogels was performed to investigate the rheological and morphological properties of the self-assembled hydrogels and their influence on the mechanism and rate of SST release *in vitro*. This study demonstrated that the SST hydrogels were shear-thinning, did not exhibit thermogelation and exhibited a higher degree of structure with higher somatostatin concentration and in the presence of electrolytes. Transmission electron micrographs demonstrated the presence of nanofibrils that were narrower and denser in appearance in the presence of electrolytes. This corresponds to the higher G' (storage modulus) of the SST hydrogels in electrolytes and at a higher SST concentration. In the presence of electrolytes SST hydrogels released a lower cumulative percentage of SST monomers at 48 hours compared to those in water. The release kinetics of the SST monomers demonstrated concurrent first-order and zero-order mechanisms. However the limited release at 48 hours *in vitro* precludes these self-assembled hydrogels as depots for SST delivery.

Two formulation candidates of SST were produced and characterized. The first candidate was SST 2.5% w/w microparticles encapsulated in a triblock polymer of polycaprolactone-polyethylene glycol-polycaprolactone (PCL-PEG-PCL) prepared by the double emulsion method. Encapsulation efficiency of SST ranged from 19% to 43% of which 1.4% -4% was released over 16-24 days. Scanning electron microscopy of the microparticles showed spherical aggregates which averaged 32 μm in size. The release kinetics of somatostatin from the microparticles demonstrated first-order decay to a plateau with good mean R^2 value of 0.979.

The second formulation candidate consisted of somatostatin 5% w/w entrapped in hydroxypropyl methylcellulose (HPMC) 3% w/w or 6% w/w hydrogel. The SST in HPMC hydrogels were subjected to rheological studies and FTIR characterization, transmission electron microscopy and release studies. Rheological tests demonstrated that inclusion of SST at a concentration of 5% w/w did not alter the characteristic properties of HPMC matrices. FTIR data showed transition of SST structure from random conformations to structured organisations upon exposure to simulated lachrymal fluid (SLF). These transitions were hindered in the HPMC hydrogels compared to SST 5% w/w in water, consistent with the hypothesis that the entanglement network of HPMC acts a barrier to the interaction of the electrolytes in SLF with SST. This was supported by the TEM images. Release studies demonstrated an extended release of SST monomers from the SST/HPMC hydrogels compared to SST 5% w/w in water. The SST 5% w/w solution reached a 100% release at 6 hours. The SST 5% w/w in HPMC 3% w/w gels released a total of 45.6% incorporated SST at 96 hours whereas the SST 5% w/w in HPMC 6% w/w gels continued to release a total of 37.6% at 10 days. The release kinetics of SST 5% w/w in HPMC 3% w/w and HPMC 6% w/w hydrogels were fitted to a hybrid model of release with R^2 values of 0.998 and 0.997 respectively. Mass spectrometry confirmed the structural integrity of the SST released from hydrogels. SST 5% w/w in HPMC 6% w/w hydrogels are the most promising candidate in terms of SST delivery, with delayed SST nanofibril formation and extended duration of release in comparison to SST 5% w/w aqueous dispersions.

The safety and efficacy of SST solutions at different concentrations and that from hydrogel formulations were tested on immortalized human retinal pigment epithelium cells (ARPE-19). MTT cell viability assay was conducted to assess the effect of the release samples from SST/HPMC hydrogels and SST 10^{-7}M and 10^{-6}M on the viability of the ARPE-19 cells. The results of the MTT assay demonstrated a significant decrease in cell viability only by the Release Day 1 samples compared to control. It is postulated that the combination of the viscosity of the Release Day 1 sample with the higher concentration of SST present at 24 hours may have additive effects on the viability of the cells. The markers for assessment for efficacy were expression of vascular endothelial

growth factor receptor-2 (VEGF-R2) and secretion of VEGF by the ARPE-19 cells.

Immunofluorescence was used to assess the effect of SST concentrations (10^{-8} M to 10^{-5} M) on the expression of VEGF-R2 levels. The results of the first study showed that SST 10^{-7} M produced significant downregulation of VEGF-R2 expression in high glucose (25 mM) conditions compared to normal glucose (5 mM) conditions. The quantitative analysis of VEGF secretion in the same conditions performed by ELISA did not show any significant effect by the treatments applied in the same conditions.

In conclusion, two formulations of somatostatin for ocular delivery were developed and characterised. The microparticle formulation showed reasonable encapsulation and duration of release, however, the more promising candidate consisted of somatostatin entrapped in a HPMC network and demonstrated modified release of somatostatin over 10 days. This work has introduced HPMC as a suitable candidate for modifying the release rate of peptides. The current work also evidenced the downregulation of the VEGF receptor 2 (VEGF-R2) by somatostatin at a concentration of 10^{-7} M in high glucose (25 mM) conditions. Although further studies are warranted on other retinal cell lines and animal models with additional markers, the identification of a new polymeric carrier for the delivery of somatostatin adds to the current body of work in the search for a non-invasive treatment for diabetic retinopathy.

CHAPTER 1: INTRODUCTION

1.1 Anatomy of the Human Eye

The human eye (Figure 1.1) is a complex organ that focuses and converts light rays to electrical signals which can be converted to an image in the visual cortex of the brain. The eye can be clinically divided to anterior and posterior chambers. It can also be divided into three main layers: fibrous, vascular and neural.

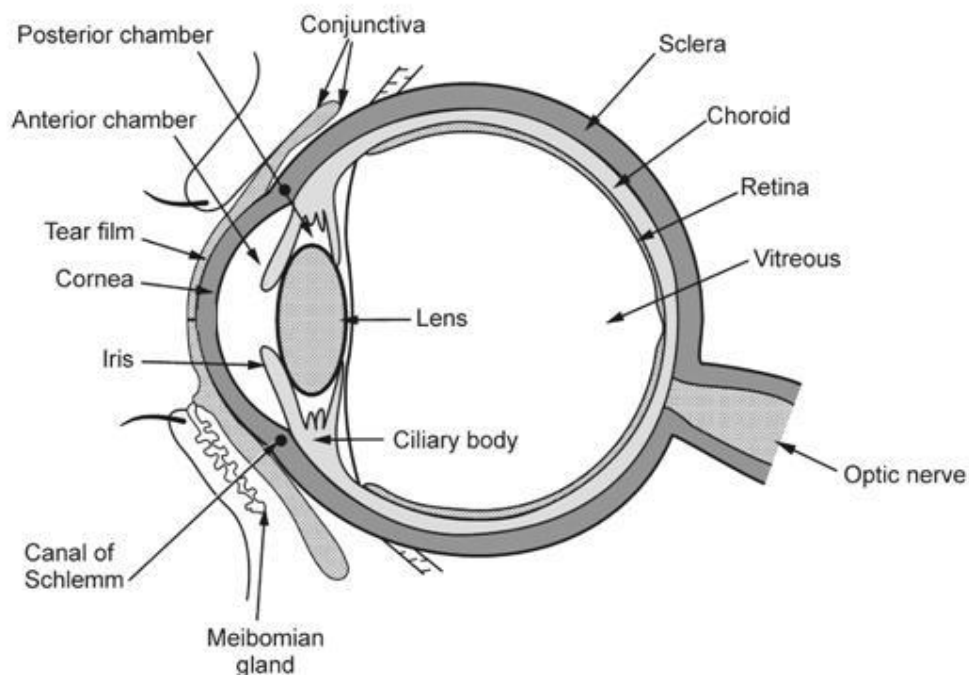


Figure 1.1: Cross-section of the human eye (Reprinted with permission from T Thrimawithana)(Thrimawithana, 2011)

The anterior chamber of the eye is located between the cornea and the iris. The posterior chamber is between the lens and the iris encompassing the vitreous humor which is almost completely surrounded by the retina. The aqueous humor fills the anterior chamber and is responsible for maintaining the shape of the eyeball, moisturizing and providing nutrients to avascular tissues like the cornea. The aqueous humor is produced by the ciliary body at a constant rate and removed at a constant amount at the base of the cornea through the Canal of Schlemm. This maintains the intraocular pressure at a constant level. The vitreous humor is a transparent, jelly-like fluid

composed of 99% water. This too maintains the shape of the eyeball, holding the lens and retina in place, maintaining the intraocular pressure and serving as a refractive medium for light entering the eye (Tate, 2009). The outer fibrous layer of the eye consists of the sclera and cornea. The middle vascular layer contains the choroid, ciliary body and iris. The inner neural layer contains the retina (Tate, 2009)(Figure 1.2).

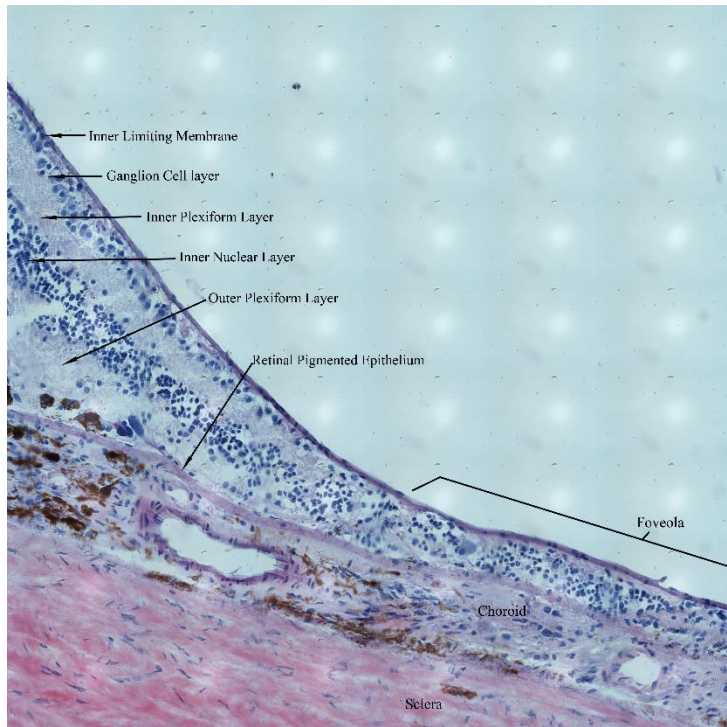


Figure 1.2: Hematoxylin and eosin (H & E) stain image of posterior segment sections (15 μ m) of a human eye, depicting the sclera, choroid and retinal architecture. (Reprinted with permission from T Thrimawithana.)

1.1.1 The Fibrous Layers of the Eye

1.1.1.1 The Sclera

The sclera, the “white of the eye”, is the posterior five-sixths of the outer eye ball. It is composed of dense collagenous connective tissue with elastic fibers, which makes it firm and opaque. It provides three main functions: it gives the eyeball its shape, protects the internal structures of the eye, and provides a surface for attachment of the ocular muscles. The sclera is a good target for drug delivery as it has an appreciable surface area of 16.3 cm² (Olsen, Aaberg, Geroski, & Edelhauser, 1998). Studies have shown that the sclera is highly permeable to hydrophilic drugs with a strong dependence on molecular radius. Lower molecular weight hydrophilic compounds can permeate through the sclera’s pores and intracellular spaces at a greater extent (Lawrence & Miller, 2004). In

vivo, proteins as large as 145 kDa were shown to penetrate through the sclera and were detected in the choroid in rabbits (Demetriades, et al., 2008; Nomoto, et al., 2009). In *ex vivo* human sclera, up to 150 kDa dextran and 149 kDa bevacizumab were able to penetrate across the sclera (Wen, Hao, & Li, 2013).

1.1.1.2 The Cornea

The cornea is the remaining one-sixth of the outer fibrous layer of the eye. The cornea is transparent and makes up the anterior section of the eyeball. There are five layers that make up the cornea, namely, the epithelial membrane, Bowman's membrane, stroma, Descemet's membrane and endothelium. The outer epithelium in the human cornea ranges in thickness between 50 to 100 μm and has 5 sub-layers. The epithelium's lipophilicity confers 90% of the eye's barrier to hydrophilic drugs and 10% of its barrier to the entry of hydrophobic drugs. The Bowman's membrane averages 8–14 μm in thickness. This layer is not regenerative and is not considered to present a barrier for the entry of drugs across the cornea. The hydrophilic stroma and constitutes ~90% of the cornea's volume. Approximately 80% of the stroma is water with the remaining weight made up of collagen, other proteins and mucopolysaccharides. The stroma is considered the main barrier to lipophilic drugs absorption across the cornea. The next layer, Descemet's membrane, is a thin regenerative 6 μm membrane, and has no appreciable impact on ocular drug absorption. Lastly, the endothelium is a single layer of cells that covers the entire posterior surface of the cornea. Gap junctions between its cells make this layer 200-fold more permeable than the epithelium. The endothelium is critical to maintaining the tonicity of the stroma through the bicarbonate dependent Na^+/K^+ -ATPase pump, which functions to control the passive movement of fluids into the stroma and the active removal out of the stroma. This pump therefore controls the transparency of the cornea and corneal thickness (Tate, 2009).

1.1.1.3 The Conjunctiva

This is a thin stratified epithelial consisting of three main regions: the bulbar epithelium, fornix epithelium and the palpebral epithelium. Although these cells are bound together by tight junctions like the cornea, the conjunctiva is more permeable to hydrophilic compounds due to more and larger paracellular epithelial pores (Lawrence & Miller, 2004).

1.1.2 The Vascular Layer of the Eye

The eye is vascularized by the short ciliary arteries that circle the optic nerve and by branches from the ophthalmic artery. The majority of the eye's blood vessels are located in the vascular layer

comprising the choroid, the ciliary body and iris. The melanin pigments contained in many of the cells in this layer contribute to the inherent black color.

The posterior section of the vascular layer (the choroid) lines the inner surface of the sclera (Tate, 2009). This layer forms the blood-ocular barrier, which tightly regulates the entry of substances into the eye from the blood. The blood-retinal barrier (BRB) is composed of the retinal vascular endothelium and the retinal pigment epithelium (RPE). The tight junctions of the BRB make up a formidable barrier to the entry of several substances from the choroidal capillaries to the retina. Efflux pumps, such as P-glycoprotein and multi-drug resistance (MDR) pumps (MRP) have been found on the RPE (Aukunuru, Sunkara, Bandi, Thoreson, & Kompella, 2001; Brian G. Kennedy & Nancy J. Mangini, 2002). These pumps limit the permeation of various xenobiotics and endogenous compounds from the choroid into the retina and vitreous (Duvvuri, Majumdar, & Mitra, 2003).

1.1.3 The Neural Layer of the Eye

The innermost layer of the posterior section of the eyeball is the retina. The retina has an outer layer of pigmented cuboidal cells and an inner light-sensitive neural layer. This neural layer has 120 million photoreceptors rod cells and 6–7 million photoreceptor cone cells and other relay neurons. Rods are responsible for vision at low light levels while the cones are active at higher light levels and are capable of colour vision (Gresh, Goletz, Crouch, & Rohrer, 2003). Light is focused on two adjoining areas of the retina, the fovea and macula. The greatest visual acuity is obtained by focusing light in the fovea since it has the greatest concentration of photoreceptors of the retina. The fovea is rod-free and has a very high density of cones. The retinal artery and vein enter and exit the retina at the optical disc, also called the “blind spot” since it does not have any photoreceptor cells (Tate, 2009). The intravitreal segment or neural layer are the most challenging area in terms of ocular drug delivery for the treatment of disorders affecting the retina, also due to the possibility of drug metabolism and excretion.

1.2 Ocular drug delivery

1.2.1 Routes of ocular drug delivery

1.2.1.1 Topical Administration

The topical route remains the most suitable and effective route of ocular drug delivery to the anterior segment of the eye (Figure 1.3). This usually involves the instillation of drops on the corneal surface but may also include ophthalmic gels or ointments instilled in the space between the lower eyelid and conjunctiva. These are generally easy to apply and have the advantage of being non-

invasive. Drug entry into the eye by the topical route follows two local pathways: corneal and conjunctival (Maurice, 2002). The corneal pathway requires the drug to traverse the cornea followed by the iris, aqueous humor, lens and ciliary body. The conjunctival pathway involves drug permeability across the conjunctiva followed by the sclera, choroid, retinal pigment epithelium and retina.

The advantage of topical administration is that hepatic first-pass metabolism is avoided and selective targeting of the drug in the anterior chamber of the eye achieved. However there is poor ocular bioavailability and typically less than 1% of the topically applied dose reaches the aqueous humor (Duvvuri, et al., 2003) and *ca.* 0.001% is anticipated to reach the posterior segment (Sigurdsson, Konráðsdóttir, Loftsson, & Stefánsson, 2007).

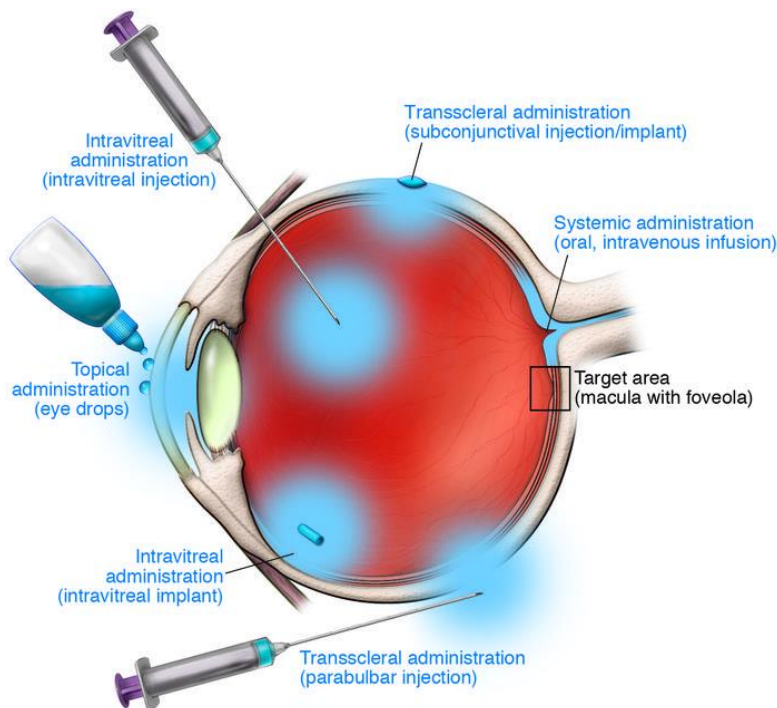


Figure 1.3: Ocular delivery routes (Reprinted with permission from Holz *et al*, 2014)(Holz, Schmitz-Valckenberg, & Fleckenstein, 2014)

1.2.1.2 Systemic Route

Systemic administration of drugs as tablets, capsules or intravenous injections to target the eye depends on the ability of the drug to traverse the blood retinal barrier (BRB). Highly lipophilic molecules such as chloramphenicol and minocycline are able to penetrate the BRB and are suitable

for systemic administration whereas hydrophilic drugs like amikacin and cefazolin do not reach the vitreous in sufficient concentrations to be effective (Boddu & Nesamony, 2013).

The disadvantages of systemic administration are that high doses and frequent administration are usually required for sufficient therapeutic concentrations to be reached at the target site. This can then result in systemic side effects (P. M. Hughes, Olejnik, Chang-Lin, & Wilson, 2005).

1.2.1.3 Periocular Route

This refers to the administration of drug using the retrobulbar, peribulbar, sub-Tenon, subconjunctival and posterior juxtасcleral pathways (Figure 1.4). This route minimizes the risk of endophthalmitis and retinal damage and is less invasive than intravitreal injection. The drug may permeate from the periocular space into the vitreous humour via three pathways, namely; the anterior chamber, systemic circulation or direct penetration. In the anterior chamber pathway, the drug can diffuse into the aqueous humour either directly across the sclera and ciliary body or indirectly via the tear fluid and cornea, followed by diffusion into the posterior chamber. In the systemic circulation route, the drug is absorbed into the general circulation via conjunctival, episcleral or choroidal vessels and later returned into the eye with blood flow. The direct penetration pathway involves several membrane barriers, which contribute to the factors affecting transscleral drug delivery to posterior ocular tissue, including diffusion across these tissues, active transport in RPE, distribution and clearance via circulation (Ranta & Urtti, 2006). While permeability across the sclera is dependent on molecular radius rather than lipophilicity or size (Jayakrishna Ambati, et al., 2000), the RPE is the rate limiting membrane for drugs via the transscleral route (J. G. Cunha-Vaz, 1976; Duvvuri, et al., 2003). Although this route affords better bioavailability to the retina and vitreous humour (about 0.01-0.1%) than the topical route (H. Kim, et al., 2004; Urtti, Pipkin, Rork, & Repta, 1990), it is still lower than that of the intravitreal route (Nakatani, et al., 2011). Up to two orders of magnitude higher volumes of drug solution can be delivered via this route compared to the intravitreal route in humans (Kalsi, Silver, & Rootman, 1991). Moreover, repeat injections under local anaesthesia can be performed without clouding of vision. Sustained drug delivery via this route is also possible to the anterior and posterior segments but risk rapid clearance through choroidal blood flow and possible systemic side effects (Ranta & Urtti, 2006).

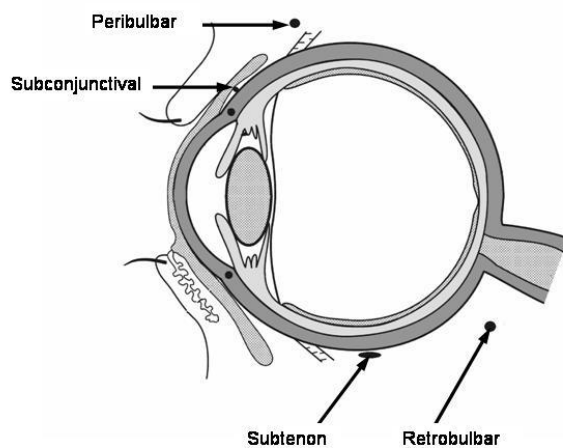


Figure 1.4: Schematic representation of periocular routes of delivery (Reprinted with permission from T Thrimawithana)(Thrimawithana, 2011)

1.2.1.4 Intravitreal route

The intravitreal injection of drugs into the eye involves direct deposition of the formulation into the vitreous humor *via* the pars plana using a 30G needle (Sarao, Veritti, Boscia, & Lanzetta, 2014). Due to the proximity of the vitreous with retina, choroid and retinal pigment epithelium (RPE) cells, intravitreal injections can achieve high drug loads and localization of the drug to the target tissue is enhanced. Drug release can also be sustained over a prolonged period of time using implant technology. However, molecules less than 500 Da tend to have a half-life of less than 3 days when applied intravitreally due to diffusion through the vitreous humour and subsequent elimination (Kaur & Kakkar, 2014). The disadvantages of intravitreal injections are the need for repeated injections which can result in retinal detachment, cataract, vitreous haemorrhage and endophthalmitis. The inner limiting membrane (ILM) comprising of a meshwork of pores ranging in size from 10 to 25 nm acts as a barrier to the movement of macromolecules from the vitreous to the retina. Kamei *et al.* (Kamei, Misono, & Lewis, 1999) have reported the failure of a 70-kDa tissue plasminogen activator to traverse the ILM on intravitreal injection. Patient acceptance is low because of the associated pain and invasiveness. Moreover, an ophthalmologist would be needed to perform such specialized injections, adding to the cost.

1.2.1.5 Suprachoroidal route

More recently, a potential drug administration site to the posterior segment of the eye – the suprachoroidal space (SCS) – has been identified and studied (Einmahl, et al., 2002; Y. C. Kim, Park, & Prausnitz, 2012). This space lies internal to the sclera and external to the choroid. It is approximately 30 μm in thickness and consists of tightly packed collagen fibres, elastic fibres, fibrocytes, melanocytes, ganglion cells and nerve plexi (Guyer, Schachat, & Green, 2006). The SCS of the eye provides a natural passageway for drugs injected across the sclera to flow quickly along the inner surface of the eye and subsequently into the posterior chamber; the flow is quick enough to warrant calling it the supra-choroidal (SC) highway. The delivery application, safety profile and pharmacokinetics of this route have been studied in rabbit and pig models for treatment of macular diseases where it has shown safety and tolerability profiles that justify further investigation in humans (Olsen, 2003).

The SCS in a pig model has been reported to expand in a dose-dependent manner to accommodate different volumes (250– 1000 μL) of an aqueous solution containing a contrast agent. The injected material rapidly diffused into the entire posterior segment in less than 8 seconds (Seiler, et al., 2011). However, a maximum volume of 200 μL is recommended for injection to avoid further expansion of this loose layer and prevent choroidal edema and potential choroidal detachment. Interestingly, the drug injected to this SCS has limited access to the vitreous body; therefore, unwanted adverse effects such as vitreous haemorrhage and opacity to the visual axis are avoided. The effects of drug lipophilicity and molecular weight on SC delivery in rabbit ex vivo eye models were studied using eight beta-blockers of different lipophilic properties and fluorescein isothio-cyanate (FITC)-dextran of a molecular weight range of 4–40 kDa. Choroidal and retinal delivery of the studied beta-blockers were enhanced; this enhancement was directly related to the increase in drug lipophilicity, with tissue levels being the highest for the lipophilic beta-blocker propranolol and the least for the hydrophilic beta-blocker atenolol. An opposite trend was seen with the delivery to the vitreous humour where drug lipophilicity showed an inverse relationship with vitreal concentration. For the effect of molecular weight (drug size), retinal and vitreal delivery were found to be significantly higher for 4 kDa FITC-dextran than for the 40 kDa counterpart, whereas sclera and choroid-retinal pigment epithelium showed higher levels with 40 kDa FITC-dextran than that estimated for 4 kDa FITC-dextran; this could be ascribed to the low diffusivity of the 40 kDa FITC-dextran (Kadam, Williams, Tyagi, Edelhauser, & Kompella, 2013). These results suggested that molecular size and lipophilicity of the drug have an impact on SC delivery and potential transit into the vitreous.

1.2.2 Barriers to anterior segment delivery

Most commercially-available eye drops dispense *ca.* 50 μL per drop; however, the eye is only able to hold 30 μL . Therefore, the rest of the applied eye drop overflows into the naso-lacrimal duct and is drained away, risking systemic absorption and resulting unintended effects (Koevary, 2003; Mishima, Gasset, Klyce, & Baum, 1966). The surface of the eye also has a rapid tear turnover of about 1 $\mu\text{L}/\text{minute}$ which results in dilution of the drug in the lacrimal fluid, affecting the concentration gradient required for diffusion of the drug across the cornea (Barar, Javadzadeh, & Omid, 2008). Moreover, enzymes and proteins present in the lacrimal fluid result in metabolism, non-productive adsorption and binding of the active ingredient.

The cornea is made up of 3 layers: a lipophilic outer epithelium, a hydrophilic stroma and a lipophilic inner endothelium (Bourlais, et al., 1998) and is thus a barrier to the diffusion of both hydrophilic and lipophilic drugs. In addition, this potential target has a smaller surface area than the conjunctiva and sclera. The conjunctiva, though made up of tight junctions, is more permeable to hydrophilic compounds than the cornea due to a greater number of and larger paracellular epithelial pores (Lawrence & Miller, 2004). It also has a surface area 17 times greater than the cornea and therefore competes with corneal drug absorption in the anterior eye (Hamalainen, Kananen, Auriola, Kontturi, & Urtti, 1997; Kaur & Kanwar, 2002).

The blood aqueous barrier (BAB), made up of the endothelium of the iris and ciliary blood vessels and non-pigmented ciliary epithelium, contains tight junctions that limit transport of solutes between the anterior and posterior segments (Raviola, 1977). Drugs that do reach the aqueous humor via fenestrated capillaries of the ciliary body tend to be readily eliminated due to the continuous outflow of aqueous humor through the Canal of Schlemm (J. Cunha-Vaz, 1979; Hornof, Toropainen, & Urtti, 2005; Janoria, Gunda, Boddu, & Mitra, 2007).

1.2.3 Barriers to posterior Segment Drug Delivery

There are a number of anatomical and physiological barriers that exist to protect the posterior eye against exogenous materials. The vitreous humour is acellular and comprises mostly water (98-99% w/w) with some collagen and glycosaminoglycans. This hydrogel forms a diffusional barrier to drug delivery to the retina, particularly to high molecular weight compounds or suspended solids (Le Goff & Bishop, 2008; Mains & Wilson, 2012).

The neural retina (separating the pigmented retinal layer from the vitreous humor) is a multilayered structure that binds to cations and limits their transport through the retina. It was demonstrated that the cationic charge was more of a limiting factor than molecular size when trying to traverse the

neural retina (Pitkänen, Ruponen, Nieminen, & Urtti, 2003). The inner limiting membrane of the neural retina has a meshwork of pores (10-25 nm) that act as a sieve keeping macromolecules from entering the retina from the vitreous (Kamei, Misono, & Lewis).

The blood retinal barrier (BRB) (Figure 1.5) is composed of tight junctions and acts as a significant barrier to drug absorption into the retina and vitreous via the systemic route (Kiernan & Lim, 2010). The retinal pigment epithelium (RPE) is the main barrier to the penetration of hydrophilic molecules and macromolecules from the sclera (Pitkänen, Ranta, Moilanen, & Urtti, 2005). The lag time increases proportionally with the molecular size (as it determines the diffusion coefficient), while small, lipophilic molecules are able to permeate the RPE as efficiently as the sclera. These can bind to melanin in the RPE, compromising their passage (Edelhauser, et al., 2010).

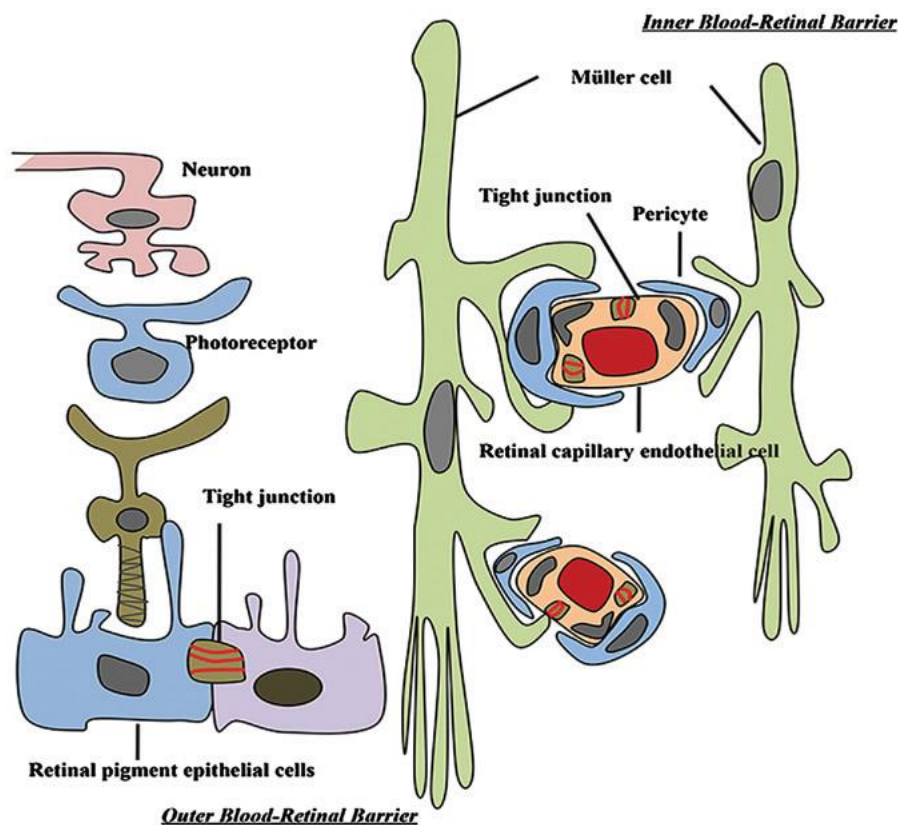


Figure 1.5: Blood-retinal barrier (Reprinted with permission from Che *et al*, 2014)(Che, Fan, & Wang, 2014)

The sclera allows drug molecules to permeate based on their hydrophilicity and molecular weight. Smaller, hydrophilic molecules are able to pass through the sclera more easily compared to their larger, more lipophilic counterparts (Berezovsky, Patel, McCarey, & Edelhauser, 2011; Prausnitz & Noonan, 1998; Thakur, Kadam, & Kompella, 2011). Lipophilic solutes and macromolecules are kept out by the pigmented nature of the choroid and especially by Bruch's membrane (Cheruvu, Amrite,

& Kompella, 2008; Moore & Clover, 2001). The choroid being highly vascularized is responsible for retinal availability of drugs administered systemically but can also sweep drugs administered by other pathways into the systemic circulation.

The human RPE contains efflux transporters such P-glycoprotein (P-gp) which act to limit the permeation of drugs from the choroid to the retina and vitreous humor (Boddu & Nesamony, 2013; P. M. Hughes, et al., 2005; B. G. Kennedy & N. J. Mangini, 2002). Conjunctival and episcleral blood and lymphatic flow can easily clear small molecules that are administered subconjunctivally. In post-mortem rabbits, blocking blood and lymphatic flow from the subconjunctival site improved drug delivery to the posterior segment significantly

1.3 Diabetic Retinopathy

The International Diabetes Federation (IDF) reports that 382 million people were diagnosed with diabetes in 2013, projected to rise to 642 million by 2040. This equates to one in ten adults developing diabetes. Diabetes provoked 5.1 million deaths and resulted in USD 548 billion dollars in global health spending in 2013. In 2017, IDF estimates the total healthcare expenditure on diabetes will reach USD 727 billion (20-79 years), which represents an 8% increase compared to the 2015 estimate. The Western Pacific, including Australia, has a diabetes prevalence greater than any other region; Australia reporting 5.14% (associated with USD 7,931 diabetes-related healthcare expenditure per person) in 2014 (Source: IDF Diabetes Atlas, 2017)

Approximately 30% of people with diabetes develop some degree of retinopathy (DR); currently the leading cause of vision loss in working age adults in the developed world. Of these, 10% have vision-threatening states such as proliferative diabetic retinopathy (PDR) (Yau, et al., 2012) The social and financial impact of visual impairment is significant to those affected and their communities more broadly (Figure 1.6).

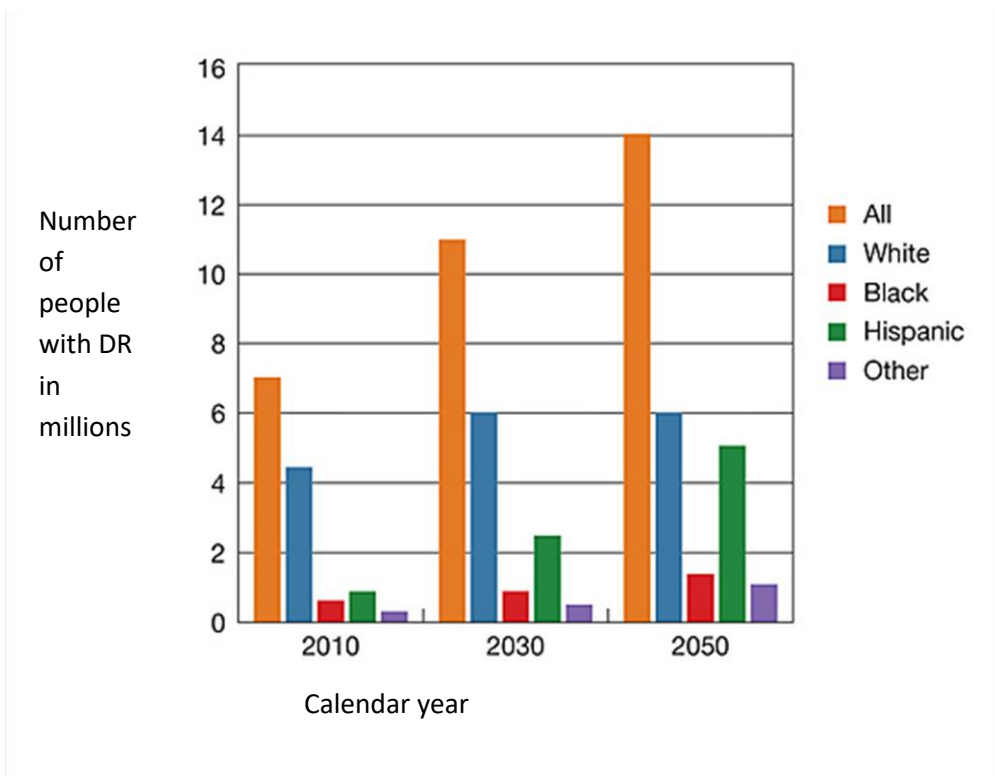


Figure 1.6: Projections for Diabetic Retinopathy in 2030 and 2050 (in millions)”, National Eye Institute, National Institutes of Health

Diabetic retinopathy can be divided in two stages. The first is non-proliferative diabetic retinopathy (NPDR) which is characterized by microaneurysms, intraretinal haemorrhaging and other microvascular aberrations.

In NPDR, loss of pericytes leads to the breakdown of the blood-retinal barrier (BRB) and in the leakage of plasma. It also results in the outpouching of the capillary walls or microaneurysms, eventually thickening of these walls causes micro-occlusion of the lumen leading to areas of ischemia and promoting the abnormal growth of new, fragile vessels in the surrounding area (Wild, Roglic, Green, Sicree, & King, 2004). There is also evidence to show that neurodegenerative changes in the retina may precede detectable changes in the microvasculature. Electroretinogram abnormalities have been detected in both humans and rats with Type 1 diabetes without any evidence of microvascular abnormalities (Di Leo, et al., 1994; Di Leo, et al., 1990; Ewing, Deary, Strachan, & Frier, 1998; Shirao & Kawasaki, 1998). High glucose levels lead to oxidative stress in the retina with the production of advanced glycation end-products (AGEs). A downregulation of neuroprotective factors such as somatostatin and pigment epithelial derived factor also play an essential role. Glutamate (a major excitatory neurotransmitter in the retina) has been found to be elevated in experimental diabetic models as well as in the vitreous fluid of patients with proliferative

diabetic retinopathy (J. Ambati, et al., 1997; Pulido, et al., 2007). Glutamate excess leads to excitotoxicity resulting in postsynaptic neuron death. The second stage is proliferative diabetic retinopathy (PDR) which is characterized by the onset of neovascularization and vitreous haemorrhage (Wilkinson, et al., 2003).

1.3.1 Current therapies for the management of diabetic retinopathy

Current therapeutic options target the late stages of diabetic retinopathy when vision is already significantly degraded. These established treatments aim to prevent haemorrhaging using laser therapy or intraocular injections of corticosteroids and therapeutic anti-vascular endothelial growth factor (VEGF) antibodies. However, efficacy is low or variable and frequent injections are required; serious ocular side-effects are possible and all result in some degree of tissue destruction. New therapies to prevent the onset or arrest the progression of the disease before overt microvascular pathologies are essential (Simo & Hernandez, 2015).

Laser photocoagulation is the main treatment for established diabetic retinopathy generally indicated in proliferative diabetic retinopathy. While the exact mechanism for how laser photocoagulation achieves its therapeutic effect is an area of active investigation, the leading hypothesis as to mechanism of laser treatment is that it reduces neovascular disease by killing retinal cells in the poorly perfused portions of the retina, reducing relative ischemia, thus decreasing the production of angiogenic factors and increasing oxygenation of the vitreous. Since photoreceptors are the most metabolically active and numerous cells in the retina, laser photocoagulation for PDR involves the purposeful destruction of a fraction of the photoreceptors. This does not restore lost vision but can ameliorate deterioration if employed in the early stages of the disease. The technique risks serious complications including loss of peripheral vision, loss of visual acuity, impaired adaptation to changes in light levels or worsening macular edema (Simo & Hernandez, 2015).

The role of intravitreal anti-vascular endothelial growth factor (VEGF) agents in proliferative diabetic retinopathy remains to be elucidated with several ongoing studies. The anti-VEGF agents are biologics that bind to the VEGF isoforms in the retina and are generally administered monthly for the first three months then every three months after. However, the optimal schedule of injections is still being investigated; currently, these are approved by the TGA but restricted to the treatment of diabetic macular edema, retinal vein occlusion and wet age-related macular degeneration. The use of these anti-VEGF agents in diabetic macular edema has been investigated in major randomized controlled clinical trials which provide robust evidence for their efficacy in preserving and improving

vision in patients with DME compared to laser therapy (Bandello, et al., 2012; N. Cheung, Wong, & Wong, 2014; Virgili, Parravano, Menchini, & Brunetti, 2012). Of the four anti-VEGF agents (ranibizumab, bevacizumab, pegaptanib and aflibercept), ranibizumab has the most evidence. Local complications from these invasive injections including endophthalmitis and retinal detachment can result. Moreover, long term use of pan-VEGF injections may be implicated in circulatory disturbances of choriocapillaris or neurodegeneration of the remaining healthy retinal tissue (D'Amore, 2007). The risk of systemic absorption of these anti-VEGF drugs remains to be addressed by long-term studies and could result in hypertension, proteinuria, impaired wound healing and increased risk of cardiovascular events (R. Simó & Hernández, 2008; Rafael Simó, Sundstrom, & Antonetti, 2014).

Intravitreal injections of corticosteroids are employed for their anti-inflammatory mechanisms and more recent studies identify neuroprotective potential (Zhang, Lai, Bao, Hambly, & Gillies, 2013). However, the incidence of complications following corticosteroid injection remains high, commonly resulting in elevated intraocular pressure and cataract formation. While there are different classes of intravitreal steroids available differing in potency and duration of action, there are two low-dose implants that can provide sustained-release delivery (the dexamethasone and flucinolone acetonide implants).

The dexamethasone implant is marketed by Allergan as Ozurdex®. This is a biodegradable polymer implant that is placed into the vitreous humour via a 22-gauge needle and releases the drug for up to six months (Yasin, Svirskis, Seyfoddin, & Rupenthal, 2014). Iluvien® is the non-biodegradable implant containing fluocinolone acetonide and once inserted into the vitreous via a 25-gauge needle, releases the drug for up to 3 years (Yasin, et al., 2014). In a randomized phase II clinical trial, Ozurdex® resulted in similar rates of improvement in visual acuity compared to bevacizumab for DME. Ozurdex® achieved superior anatomic outcomes and fewer injections with similar improvements in visual quality-of-life scores. However, more eyes treated with Ozurdex® lost vision due to cataract (Gillies, et al., 2014). Iluvien® was found to have greater risk of inducing ocular hypertension and cataract (Ciulla, Harris, McIntyre, & Jonescu-Cuypers, 2014), although the longer duration of action could potentially decrease treatment burdens on the patient and families.

Vitrectomy is the last treatment option; being both expensive and complicated this procedure is reserved for the ultimate blinding complications of diabetic retinopathy. However, the outcome after vitreo-retinal surgery remains unpredictable (Yorston, et al., 2008) and risks significant post-operative complications, including vitreous cavity haemorrhage and retinal detachment (Newman, 2010) resulting in blindness that the procedure is intended to prevent. Table 1.1 provides a summary of the discussion above.

Table 1.1- Summary of the current therapies for DR

Procedure/ Formulation	Dose/ Frequency	Side-effects	Brand & Manufacturer (if applicable)	Reference
Laser treatment Pan-retinal photo- coagulation for proliferative diabetic retinopathy	May be performed in 2 or more sessions	Moderate visual loss, some diminished visual field, reduced colour vision, and reduced contrast sensitivity	N/A	(Rafael Simó & Hernández, 2015)
Anti-VEGF agents	Monthly injections for the first five months followed by one injection every 2 months thereafter (Eylea®) Monthly injections (Lucentis®)	Conjunctival haemorrhage Endophthalmitis Retinal detachment	Aflibercept 2mg intravitreal injection- Eylea® (Regeneron Pharmaceuticals, Inc., NY, USA) Ranibizumab 0.3mg and 0.5mg intravitreal injection- Lucentis® (Genentech, Inc., Roche Group, San Francisco, CA, USA)	(R. Simó & Hernández, 2008)

Corticosteroid	Ozurdex-one implant every 6 months Iluvien and Retisert- one implant for 3 years	Infection, glaucoma, and cataract formation	Dexamethasone 700mcg intravitreal implant- Ozurdex®, (Allergan, Irvine, CA, United States Fluocinolone acetoneide 0.19mg intravitreal insert-Iluvien® (Alimera Sciences, Alpharetta, GA, United States) Fluocinolone acetoneide 0.59mg intravitreal implant- Retisert (Bausch + Lomb, NJ USA)	(Arcinue, Cerón, & Foster, 2013)
Vitrectomy	One-time procedure	Expensive, complicated treatment that requires experienced vitreoretinal specialists	N/A	(Rafael Simó & Hernánd ez, 2015)

Retinal
detachment
High
intraocular
pressure
Cataract

1.4 Somatostatin

Somatostatin (SST) is an endogeneous cyclic tetradecapeptide hormone. Primarily inhibitory in nature, this small peptide has anti-secretory and anti-proliferative effects and functions as a neurotransmitter. Originally isolated in the ovine hypothalamus and discovered as an inhibitor of growth hormone, somatostatin is now known to have widespread functions in the human body (Guillemin, 2008). The peptide is secreted throughout the central nervous system, in the gastrointestinal tract, retina, peripheral neurons and the pancreatic islets of Langerhans (Kumar & Grant, 2010).

1.4.1 Overview of SST biological activity

The anti-secretory activities of somatostatin are summarized in Table 1.2. As a neurotransmitter, somatostatin has effects on cognition, locomotor activity, sensory and autonomic functions mediated by the inhibition of release of dopamine, norepinephrine, thyroid-releasing hormone (TRH) and other lesser transmitters. In the gastrointestinal tract somatostatin inhibits exocrine secretion, gastric emptying and gall bladder contraction while inhibiting the secretion of insulin and glucagon from the pancreas.

Table 1.2 –Summary of anti-secretory functions of SST (Adapted with permission from B. Boehm)

Organ	Function
Pituitary	Reduces secretion of GH and TSH
Brain	Inhibits release of norepinephrine, TRH and corticotrophin-releasing hormone and dopamine from the midbrain.

Pancreas	Reduces secretion of insulin, glucagon and pancreatic polypeptide as well as bicarbonate and enzyme secretion.
Thyroid	Reduces secretion of T3, T4 and calcitonin.
Gastrointestinal tract	Reduces secretion of gastrin, secretin, motilin, gastric acid, enteroglucagon, CCK, VIP, GIP, intrinsic factor, pepsin, neurotensin, bile secretion and colonic fluid secretion.
Adrenals	Inhibits angiotensin II stimulated- aldosterone secretion and acetylcholine stimulated medullary catecholamine secretion.
Eye	Inhibits VEGF production

Abbreviations: CCK- Cholecystokinin, GH- growth hormone, GIP- gastric inhibitory polypeptide, TRH- thyroid-releasing hormone, TSH- thyroid- stimulating hormone, VIP- vasoactive intestinal peptide, VEGF- vascular endothelial growth factor

1.4.2 Secretion pathway and somatostatin isoforms

Initially secreted as a 116 amino acid precursor, preprosomatostatin is converted by endoproteolytic cleavage to prosomatostatin, which is then further processed into two active forms, somatostatin-28 (SST-28) and somatostatin-14 (SST-14). SST-14 is the isoform that was originally characterized (Brazeau, et al., 1973). SST-28 was later discovered as an extended SST-14 sequence to the amino-terminus (N-terminus) (van der Hoek, Hofland, & Lamberts, 2005) (Figure 1.8). The distribution of the two active isoforms is similar, although one form generally predominates over the other in different parts of the body. In the enteric neurons and peripheral nerves, SST-14 is prominent whereas SST-28 is the predominant form in the retina and intestinal mucosal cells (Hernandez, et al., 2005).

Somatostatin has an extremely short half-life of 1-3 minutes, being rapidly degraded by ubiquitously distributed peptidases in plasma and the tissues (Benuck & Marks, 1976). Consequently circulating levels of somatostatin are low at 14-32.5 pgml⁻¹ (Ensinnck, et al., 1989; Gyr, et al., 1987; Peeters, Depraetere, & Vantrappen, 1981; Penman, et al., 1981; Shoelson, Polonsky, Nakabayashi, Jaspan, & Tager, 1986; Skamene & Patel, 1984; Tsuda, et al., 1981; Vasquez, Harris, & Unger, 1982). The lack

of receptor specificity of native somatostatin, short half-life and the necessity of direct injection at the desired site of action has motivated the discovery and refinement of compounds with receptor selectivity and greater metabolic stability. Both peptide and non-peptide agonists have been synthesised (Section 2.4).

1.4.3 Somatostatin receptors

1.4.3.1 SSTR subtypes

Somatostatin binds to five subtypes of G-protein coupled transmembrane receptors (SSTR1-5) (Y. C. Patel, 1999b). The receptors are 364-418 amino acids long and share 39-57% homology in sequence. All possess seven highly conserved α -helical transmembrane domains, with most divergence occurring in the extracellular N-terminus and intracellular carboxyl terminus (C-terminus) domains. SSTR1, 3, 4 and 5 have only single subtypes, whereas two spliced variants exist for SSTR2, termed SSTR2A and SSTR2B, which differ in the length of the C-terminus domain (Kumar & Grant, 2010). SSTRs 1 to 4 bind SST-14 and SST-28 with high (nanomolar) affinity, whereas SSTR5 exhibits a 5-10-fold higher binding affinity for SST-28.

1.4.3.2 SST receptor distribution

SSTRs are widely distributed throughout the central nervous system (CNS) and periphery. Whilst all five subtypes are expressed in normal human tissues, the predominant subtypes in endocrine tissues are SSTR2 and SSTR5 (Barnett, 2003; Lamberts, van der Lely, & Hofland, 2002; Y. C. Patel, 1999b). Table 1.3 provides a summary of the distribution of the SSTRs and their signalling mechanisms.

SSTR1 triggers antiseecretory effects on growth hormone, prolactin and calcitonin. SSTR2 also inhibits secretion of growth hormone and that of adrenocorticotropin, glucagon, insulin, interferon- γ and gastric acid. SSTR5 has the same inhibitory effect on growth hormone, adrenocorticotropin, insulin and glucagon-like peptide-1 and inhibits the secretion of amylase. SSTR3 reduces cell proliferation and induces cell apoptosis, whereas the functions of SSTR4 remain largely unknown (Cejvan, Coy, & Efendic, 2003; Cervia, Petrucci, Bluet-Pajot, Epelbaum, & Bagnoli, 2002; Chisholm & Greenberg, 2002; J. Gromada, Hoy, Buschard, Salehi, & Rorsman, 2001; Hannon, et al., 2002; Strowski, et al., 2002; Strowski, et al., 2003; Weckbecker, et al., 2003; Zatelli, et al., 2002)

Table 1.3- Distribution and signalling mechanisms of Somatostatin receptors (SSTRs) (Adapted with permission from P. Dasgupta and B. Boehm)

Subtype	SSTR1	SSTR2	SSTR3	SSTR4	SSTR5
Distribution					
Brain	+	+	+	+	+
Eye		+			
Kidneys	+				
Pancreas	+	+	+		+
Pituitary					+
Heart					+
G-protein coupling via Gai1, Gai2, or Gai3	+	+	+	+	+
Inhibition of GH, insulin, and glucagon Ca ²⁺ channels		+			+
Inward-rectifying K ⁺ channel		+	+	+	+
Inhibition of Na ⁺ /H exchanger activity	+				

Activation of protein tyrosine phosphatase	+	+	+	+		
MAPK/ERK pathway	+		+		+	+
Activation of phospholipase A2					+	
Inhibition of Rho/Rac pathway	+					
STAT3 phosphorylation					+	
Inhibition of e-NOS pathway	+	+	+			
Inhibition of guanylate cyclase						+

1.4.3.3 SST receptor signalling mechanisms

All SSTRs are coupled to the pertussis toxin-sensitive G_i protein and inhibit adenylyl cyclase, thereby decreasing cyclic AMP levels (Y. C. Patel, Greenwood, Warszynska, Panetta, & Srikant, 1994). While there are similarities in signal transduction pathways, differences between the SSTRs result in

different actions effected by each receptor. Receptor endocytosis and trafficking further modulate SSTR signalling (Hofland & Lamberts, 2003).

The antisecretory effect of SST results from inhibition of exocytosis. This is mediated not only by the aforementioned suppression of cyclic AMP levels, but also by activation of various types of K⁺ channels. This includes the delayed rectifying, inward rectifying and ATP sensitive K⁺ channels. This results in membrane hyperpolarization and inhibits depolarization-induced Ca²⁺ influx through voltage-sensitive Ca²⁺ channels. Thus there is reduced intracellular Ca²⁺ and inhibition of exocytosis (Koch, Blalock, & Schonbrunn, 1988; Pace & Tarvin, 1981; Sims, Lussier, & Kraicer, 1991; Yamashita, Shibuya, & Ogata, 1986; Yatani, Codina, Sekura, Birnbaumer, & Brown, 1987). The Gi and Go protein subtypes mediate the inhibitory action of SST on Ca²⁺ (Kleuss, et al., 1991; Schlegel, Wuarin, Zbaren, Wollheim, & Zahnd, 1985). Another pathway involving a cyclic GMP –dependent protein kinase also mediates the inhibitory action of SST on neuronal calcium channels (Meriney, Gray, & Pilar, 1994).

All SSTRs with the exception of SSTR3 couple to voltage-gated K⁺ channels with SSTRs 2 and 4 being the most potent in increasing K⁺ currents (Yang, Parkington, Blake, Keating, & Chen, 2005). SSTRs 1, 2, 4 and 5 have a direct effect via coupling to N and L-type voltage sensitive Ca²⁺ channels (Fujii, et al.; Hou, Gilbert, & Barber, 1994; P. A. Smith, 2009; Tallent, et al., 1996). SST also affects exocytosis distal to secondary messengers by the downregulation of Ca²⁺-dependent phosphatase calcineurin (Jesper Gromada, Høy, Buschard, Salehi, & Rorsman, 2001; Renström, Ding, Bokvist, & Rorsman).

The antiproliferative actions of SST result from cell cycle arrest and/or apoptosis downstream from SSTR activation. SST triggers both common and unique signalling cascades upon binding to the different SSTRs. A detailed discussion of the signalling cascades for each SSTR is beyond the scope of this discussion and we refer you to Theodoropoulou *et al* 2013 for an excellent review of the subject. However, below is a summary of the signalling cascades leading to antiproliferative activity. SST inhibits growth factor receptor signalling through protein tyrosine phosphatases (PTPS) (Pan, Florio, & Stork, 1992). They are central to this process by causing the dephosphorylation of growth factor bound tyrosine kinase receptors (Pan, et al., 1992). In multiple cell systems, SST treatment increased PTP activity (Buscail, et al., 1994; T Florio & Schettini, 1996; D. B. Reardon, et al., 1996). PTPs were shown to be activated by Gai (Pan, et al., 1992) and Gai/o (Dent, et al., 1996) and SSTRs associate with the PTPs containing the cytosolic src homology 2 (SH2) domain, SHP-1 (PTP1C) and SHP-2 (PTP1D), and the membrane-anchored PTP η (DEP1) (Delesque, et al., 1995; T. Florio, et al., 2001; Frédéric Lopez, et al., 1997; F. Lopez, et al.; Massa, et al., 2004; Pagès, et al., 1999; Dean B. Reardon, Dent, Wood, Kong, & Sturgill, 1997; Srikant & Shen, 1996). Through PTPs, SST binding at SSTRs 1,2,4 and 5 lead to cell cycle arrest at G1/S boundary and at the G2/M boundary via SSTR3 (N. W. Cheung

& Boyages, 1995; Srikant, 1995). SSTRs 2 and 3 also induce apoptosis (Ferrante, et al., 2006; K. Sharma, Patel, & Srikant, 1996; Teijeiro, et al., 2002). SSTRs induce acidification which results in apoptosis via a SHP-1 dependent mechanism (Thangaraju, et al., 1999). SSTRs 1, 3 and 4 inhibit the Na⁺/H⁺ exchanger (NHE1), leading to increased intracellular acidification (C.-Y. Lin, et al., 2003; X. Lin, et al., 1996) which may be responsible for the anti-cell-migration properties of SST in certain tumor cell types (Cattaneo, Gentilini, & Vicentini, 2006; Pola, Cattaneo, & Vicentini, 2003). SSTR1 inhibits Rho GTPase, which regulates cytoskeleton organization, cell adhesion and cell motility through NHE1 (Buchan, Lin, Choi, & Barber, 2002). SSTRs 1, 2 3 and 5 block nitric oxide synthase (NOS), which is an additional pathway leading to the antiproliferative action of SST (Arena, Pattarozzi, Corsaro, Schettini, & Florio, 2005; F. Lopez, et al., 2001). Also worthy of mention is the mitogen-activated protein kinase (MAPK) pathway. The MAPK pathway mediates the mitogenic action of growth factors, cytokines and hormones (Segar & Krebs, 1995). The MAPK pathway can also halt cell growth in order to promote cell differentiation depending on the cell system and extracellular environment. SSTRs 2, 3 and 5 mediate inhibition of MAPK activity while SSTRs 1 and 4 mediate the activation of MAPK (Moller, Stidsen, Hartmann, & Holst, 2003). Figure 1.7 below summarizes the signalling pathways of SST receptors.

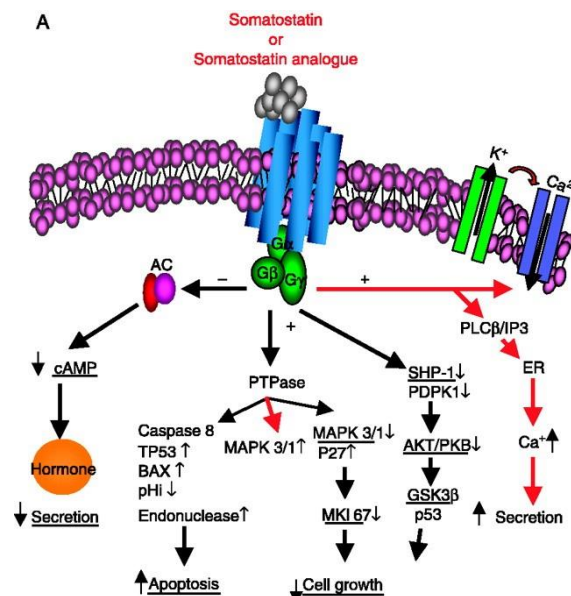


Figure 1.7: Intracellular signalling cascades associated to somatostatin receptors in pituitary cells (reprinted with permission from D Ferone *et al*, 2009)(Ferone, et al., 2009)

1.4.3.4 Somatostatin analogues

The β -turn in somatostatin structure is the pharmacophore (Modlin, Pavel, Kidd, & Gustafsson, 2010) (Figure 1.8). Amongst the variety of hexa- and octapeptide analogues that were developed, the most potent molecules are cyclic and bear a β -turn.

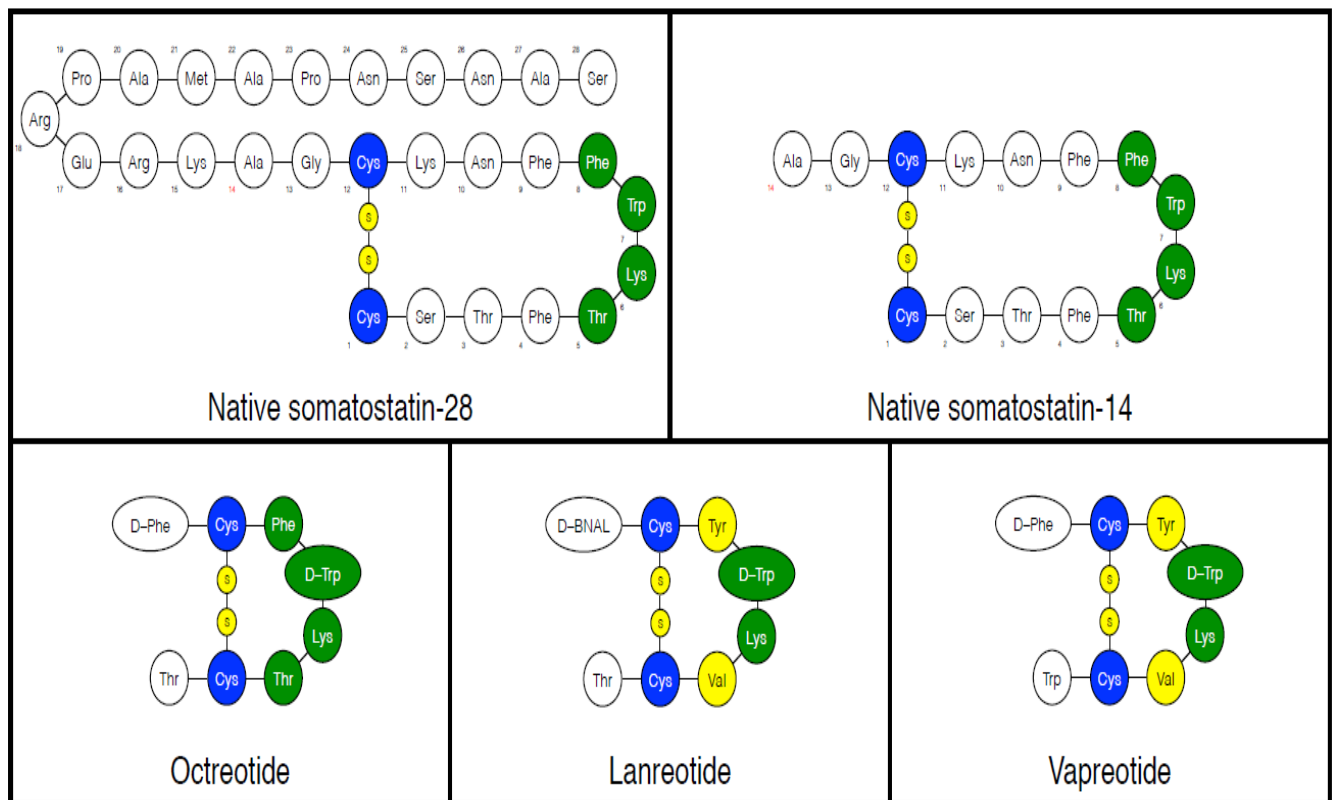


Figure 1.8 Structures of SST analogues

Within the β -turn motif of somatostatin, only phenylalanine and threonine can be substituted without compromising biological activity (Modlin, et al., 2010). The first synthetic SST agonist to be approved by the FDA was the octapeptide octreotide (SMS 201-995), marketed as Sandostatin[®]. Octreotide is available in both conventional and modified release injection (Sandostatin LAR[®]) formulations, approved in 1988 and 1998, respectively. Sandostatin LAR[®] contains octreotide distributed within polymer microspheres (Sandostatin, 2000), currently approved in the treatment of acromegaly and hormone-dependent tumors, especially those associated with the secretion of growth hormone-releasing factor and vasoactive intestinal peptide, or glucagonomas, gastrinomas, and insulinomas (Sandostatin, 2000). Thereafter was approved the octapeptide, lanreotide (BIM

23014), under the trade name Somatuline®. Initially licensed for the treatment of acromegaly, approval in Europe is extended for the treatment of symptoms associated with neuroendocrine tumors (Ipsen, 2015). Lanreotide is marketed as a slow release hydrogel formulation, under the trade name Lanreotide Autogel® or Somatuline Depot® depending on countries (Ipsen, 2015; Valéry, et al., 2003). This formulation was approved by the FDA in 2014 for the treatment of gastroenteropancreatic neuroendocrine tumors (GEP-NETs) to improve progression-free survival. Both octreotide and lanreotide bind primarily to SSTR2, with a lower affinity to SSTR3 and 5. Compared to somatostatin, both exhibit greatly-extended half-lives of 1-2 hours. In 2005, vapreotide (RC160) marketed as Sanvar®, an SST-analog with similar binding affinities to SSTR2, 3, and 5 to lanreotide and octreotide but moderate affinity to SSTR4 (Y. C. Patel, 1999a) was approved for the treatment of acute oesophageal variceal bleeding secondary to portal hypertension (Patch & Burroughs, 2002). The latest SST agonist to be approved in the EU and the USA is pasireotide (SOM-230, December 2012). This cyclohexapeptide exhibits high affinities for SSTRs 1, 2, 3 and 5 (Hasskarl, Kaufmann, & Schmid, 2011). Marketed by Novartis under the trade name Signifor®, pasireotide is licensed for the treatment of patients with Cushing’s disease. Signifor® is available as subcutaneous injection. Most recently, a novel tetradecapeptide somatostatin agonist in which the disulfide bridge has been replaced by a carbon-carbon double bond has been reported. This peptide possesses greater conformational flexibility than SST itself, and retains selectivity against SSTRs 1 and 5 (Martin-Gago, et al., 2014). Table 1.4 provides a summary of the currently available somatostatin analogues.

Table 1.4-Summary of the currently marketed SST analogues

Name	Structure	Trade name	Formulation	Indications	Receptor affinity	Half-life	References
Octreotide (SMS 201-995)	Cyclic octapeptide	Sandostatin® Sandostatin LAR®	Octreotide acetate, microsphere formulation	Acromegaly, hormone-dependent tumors	SSTR2 > SSTRs3,5	1.7-1.9h	(Sandostatin, 2000)

Lanreotide (BIM 23014)	Cyclic octapeptide	Somatuline® Somatuline Depot®/ Autogel®	Lanreotide acetate, hydrogel formulation	Acromegaly Somatuline Depot® for treatment of GEP-NETs Somatuline Autogel is also indicated treatment of symptoms of carcinoid syndrome associated with carcinoid tumours	SSTR2 > SSTRs3,5	2.5 h	(Ipsen, 2015)
Vapreotide (RC 160)	Cyclic octapeptide	Sanvar®	Immediate- release SC injections and slow- release IM formulation	Esophageal variceal bleeding secondary to portal hypertension	SSTR2 > SSTR3, SSTR5 > SSTR4	2.7 – 3.8 h	(Debiop harm, 2015) ("Vapreo tide," 2003) (Patch & Burroug hs, 2002) (Y. C. Patel, 1999b)

Pasireotide (SOM-230)	Cyclohexane	Signifor® Signifor LAR®	0.3mg, 0.6mg, 0.9mg solution for SC injection to be administere d twice daily IM injection administere d once monthly	Acromegaly, Cushing's disease	SSTRs1,2, 3,5	12 h	(Novarti sEuroph arm, 2012) (Hasskar l, et al., 2011)
--------------------------	-------------	--------------------------------	--	-------------------------------------	------------------	------	---

1.4.3.5 SST-receptor antagonists

Advances in the understanding of SST receptor antagonists have been slow. The main impetus behind the design of SST receptor antagonists is to elucidate the functions of each receptor subtype. However, due to lack of receptor specificity or mixed antagonist-agonist profile, efforts continue in the synthesis and testing of structures with antagonist activity. Below is a brief discussion of the current knowledge of SST antagonists.

A non-peptide antagonist, SRA-880, was shown to be a selective and high-affinity SSTR1 antagonist. Active in behavioural tests of anxiety, depression and bipolar disorders, SRA-880 reduced aggressive behaviour in mice without sedation or impairment of motor function. Another SST3-selective non-peptide antagonist BN-81674 competitively blocked SST-14-mediated inhibition of cAMP accumulation in a CHO-K1 cell line (Poitout, et al., 2001). It has been suggested that SSTR3 antagonists therefore have potential use as anti-apoptotic agents.

Non-peptide, highly potent and SSTR3-selective antagonists have been synthesized that show promising pharmacokinetic properties in rodents (Troxler, et al., 2010). The SST antagonist, cyclosomatostatin, has been employed in studies. One such study postulated there may be a link between somatostatin deficiency frequently detected in patients with Parkinson's disease and extrapyramidal symptoms. Cyclosomatostatin potentiated haloperidol-induced catalepsy in aged but not young rats. This action was inhibited by the SST analogue, octreotide, suggesting a link between aging, SST deficiency and extrapyramidal symptoms in the disease (Ionov & Severtsev, 2012).

Cyclosomatostatin was found to exert opioid-agonist activity in the guinea pig intestine and rat stomach fundus strip (Benko, Antwi, & Bartho, 2012). It did not exhibit the antagonist activity expected in the preparations tested. It was suggested that this opioid agonist activity of cyclosomatostatin might explain the observed antinociceptive effect when administered centrally (Bartsch, Levy, Knight, & Goadsby, 2005).

Given the role somatostatin plays in glucose homeostasis by inhibiting secretion of insulin and glucagon-like peptide 1, two novel orally bioavailable SSTR5 antagonists were studied in rodents (Sprecher, et al., 2010). These compounds are non-peptidic and exhibited receptor specificity and nanomolar binding affinity. Zucker fatty fa/fa rats and diet-induced obese mice models of diabetes were employed in these studies. The two compounds A and B performed differently in the different species. In the Zucker rats, compound A decreased glucose and insulin excursions after a single treatment in a dose-dependent manner following an oral glucose tolerance test. However, in obese mice there was a dose-dependent increase in insulin secretion by up to 72%. Compound B did not show any significant effects in the rat model. In the mouse model it showed a dose-dependent reduction of glucose excursion after 3 weeks of treatment. Hence further exploration of the role of SST antagonists in the treatment of diabetes in humans may be of value.

A highly selective SSTR2 antagonist PRL2903 was used to elucidate the anxiolytic effect of SST in the amygdala and septum of the rat brain. The complete reversal of the anxiolytic effects of SST by PRL2903 confirmed that the aforementioned effects are mediated by SSTR2 (Yeung & Treit, 2012).

1.4.4 Potential Use in Diabetic Retinopathy

1.4.4.1 Pharmacological Role of SST and SST receptors in diabetic retinopathy

SST is one of the most important neuroprotective factors synthesized by the retina, the retinal pigment epithelium (RPE) being the main source in the human eye (Hernandez, Simo, & European Consortium for the Early Treatment of Diabetic, 2013). The human retina produces significant amounts of SST with high levels reported within the vitreous fluid (Simo, et al., 2002). SSTRs are also expressed in the retina, with SSTR1 and SSTR2 being the most widely expressed (Cervia, Casini, & Bagnoli, 2008a; Klisovic, et al., 2001; Lambooi, et al., 2000). SST-28 is the main form produced in human retina (Hernandez, et al., 2005). Production of both SST and its receptors suggests a relevant autocrine action in the human retina. SST acts as a neuromodulator, regulates various ion/water transport systems and has potent anti-angiogenic properties (Hernandez, Simo-Servat, & Simo, 2014).

Retinal neurodegeneration is an early event in the pathogenesis of diabetic retinopathy (Simo, Hernandez, & European Consortium for the Early Treatment of Diabetic, 2012). Amongst other neuroprotective factors, SST which functions as an endogenous neuroprotective peptide is downregulated in the diabetic eye (Carrasco, et al., 2007). The main hallmarks of retinal neurodegeneration are apoptosis and glial activation, which are already present in the retinas of diabetic donors without any microcirculatory abnormalities (J. Ambati, et al., 1997; Pulido, et al., 2007). Glutamate is the main excitatory neurotransmitter in the retina and elevated levels are linked to “excitotoxicity” which leads to neurodegeneration (Kowluru, Engerman, Case, & Kern, 2001; Lieth, LaNoue, Antonetti, & Ratz, 2000). This excitotoxicity of glutamate is mediated by the over-activation of ionotropic glutamate receptors, over-expressed in streptozotocin-induced diabetic rats (Ng, Zeng, & Ling, 2004; Santiago, et al., 2009). Oxidative stress, advanced glycation end-product receptor upregulation and renin-angiotensin-aldosterone system (RAAS) activation also play a role in the retinal neurodegeneration induced by diabetes mellitus.

SST has been shown to inhibit glutamate release via the SSTR2 receptor (Bigiani, et al., 2004; Cervia, Martini, et al., 2008; Kokona, et al., 2012; N. Mastrodimou, Lambrou, & Thermos, 2005). Consequently SST may ameliorate glutamate neurotoxicity by regulating the amount of glutamate available to glutamate receptors. There is also evidence that shows that SST, via SSTR2, protects against ischemic damage to the retina by limiting vascular endothelial growth factor (VEGF) release under ischemic conditions (D. Cervia, E. Catalani, M. Dal Monte, & G. Casini, 2012). SST and analogues may also exert an antiangiogenic effect by reducing endothelial cell proliferation and neovascularization. Amongst multiple mechanisms, this effect may have contributed to the inhibition of postreceptor signalling events of peptide growth factors observed, including IGF-1, VEGF, epidermal growth factor, bFGF and PDGF (Baldysiak-Figiel, Lang, Kampmeier, & Lang, 2004; Davis, Wilson, & Grant, 2001; L. E. Smith, et al., 1997; Wilson, Davis, Caballero, & Grant, 2001). Studies in transgenic mice have shown that SSTR2 activation may protect against angiogenesis (Dal Monte, Cammalleri, Martini, Casini, & Bagnoli, 2007). However, this has not been demonstrated in murine diabetic models. It is worth noting that non-diabetic models are usually used to mimic retinal neovascularization instead (Ramos, et al., 2013).

Additionally, SST has a potential anti-permeability effect in the retina that has not been widely explored. On the apical side of the RPE there are various ion/water transport systems and SSTR2 is highly expressed there (Lambooj, et al., 2000). Thus there is a role for SST in the prevention of diabetic macular edema may be postulated.

1.4.4.2 Efficacy of SST analogues in models of diabetic retinopathy and clinical significance

Several studies have been conducted in animal models of diabetes to investigate the efficacy of SST analogues in diabetic retinopathy. Although a twice daily administration of octreotide injection in rats failed to inhibit hypoxia-induced retinal neovascularization (Averbukh, et al., 2000), beneficial effects were reported for SST analogues in other animal models. In a mouse model of oxygen induced retinopathy, Woc4D and octreotide decreased blood vessel tufts and extra-retinal neovascularization in an equally effective manner (Higgins, Yan, & Schrier, 2002). Normal mice treated with a SSTR2 agonist, seglitide (MK 678), showed a 44% decrease in ischemia induced retinal neovascularization (L. E. Smith, et al., 1997). A nonpeptide SST agonist (L-779976) selective for SSTRs 2 and 3 was studied in neonatal mice. Oxygen-induced retinal neovascularization was found to decrease by about 50% (Grant & Caballero, 2002). Wu *et al* demonstrated a reduction in bFGF-induced corneal angiogenesis by SST in a rat corneal pocket model (P. C. Wu, et al., 2003). SST eye drops have been administered to streptozocin-induced diabetic rats and it was demonstrated that SST reaches the vitreous and retina after topical administration and prevents retinal neurodegeneration (Hernandez, Garcia-Ramirez, et al., 2013). The effect of SST on changes in the electroretinograms of early streptozocin-induced diabetic rats was investigated by Sun et al. The latent periods of the a-wave and the b-wave in the SST treatment group were shorter than those in the control group at the 8th week of treatment, although still longer than in non-diabetic rats (Y. D. Sun, et al., 2014).

In a case report, Lanreotide Autogel[®] (Somatuline[®] Autogel[®]) was administered to two diabetic patients with bilateral persistent cystoid macular edema. Authors reported improved vision in 3 out of 4 eyes. Foveal thickness was reported to be reduced and Health Related Quality of Life (HRQOL) scores increased, although, visual acuity was not shown to be significantly improved (Hernaiz-Ortega, Soto-Pedre, & Pinies, 2008). However, in 2001, a larger study showed that 3 years of octreotide treatment in type 1 diabetes patients with advanced proliferative retinopathy significantly reduced vitreous haemorrhage and improved visual acuity (Boehm, Lang, Jehle, Feldman, & Lang, 2001). Grant et al demonstrated that octreotide treatment retarded the progression of advanced retinopathy and delayed the time to laser photocoagulation (Grant, et al., 2000) Earlier clinical studies on diabetic patients are summarized in Table 1.5. Together, these studies present a strong case for the therapeutic use of SST or a suitable analogue in diabetic eye conditions such as retinopathy or macular edema. A multicentric phase II-III randomized controlled clinical trial has recently been completed in Europe to compare the efficacy of brimonidine and SST eye drops in retinal neurodegeneration and microvascular impairment (EUROCONDOR -278040).

Eligible patients with type 2 diabetes (n = 449) were randomly allocated to one of 3 investigation groups: placebo, somatostatin 0.1% and brimonidine tartrate 0.2%. They all had one drop administered to each eye twice daily. The primary outcome was the change in implicit time assessed by multifocal electroretinography (mfERG) between baseline and at the end of follow-up (96 weeks). The results of this clinical trial revealed that SST and brimonidine were only useful in patients with pre-existing retinal neurodysfunction, in which the worsening of implicit time was prevented (Simó-Servat, Hernández, & Simó, 2018).

Table 1.5 – Summary of studies of SST analogues in the eye

DR stage	Study duration	No. of patients	Treatment	Results	Reference
Type 1 diabetes	Group A: 20 weeks Group B: 3 days – 16 weeks	15 patients	Group A: octreotide sc injection 3 x 50 µg/day Group B: Octreotide continuous sc infusion 500µg/day	Group A: Visual acuity minus 2 lines in 3 out of 4 patients Group B: no change in visual acuity in 5 patients, improvement in 1 patient. Retinal haemorrhages and further laser treatment not prevented.	(Hyer, Sharp, Brooks, Burrin, & Kohner, 1989)

Early diabetic Retinopathy	12 months	11 IDDM 9 controls 7 pts and 7 controls completed the study	Octreotide Continuous sc infusion (up to 400 µg/day)	No effects, no observable difference between groups	(Kirkegaard, et al., 1990)
Proliferative retinopathy	3 months	8 patients	Continuous infusion of SSTR2-specific agonist BIM23014	Significant abrogation of vascular leakage in 2 patients	(McCombe, Lightman, Eckland, Hamilton, & Lightman, 1991)
PDR progressing despite photocoagulation	6-20 months	4 IDDM no controls	Octreotide Continuous infusion 44µg/ day	Neovascularization stopped in 2 patients	(Mallet, et al., 1992)
Severe non-proliferative DR, non- high risk PDR	15 months	16 pts (8 pts: treated 8 pts: controls	Octreotide 600–3000 µg/day. Continuous infusion or sc injection	Failure to eliminate the need for photocoagulation therapy though levels of GH or IGF-1 reduced in all patients	(Grant, Mames, Cooper, Caballero, & Fitzgerald, 1996)

Case report, type 1 diabetic	3 months		Octreotide sc injection 3 x 50µg/ day	Hemorrhages completely resorbed, numbers of microaneurysms reduced	(H. K. Lee, et al., 1988)
Idiopathic cystoid macular edema	12 weeks	Case report 1 patient	Octreotide Sc injection 3 x 100µg/ day	Macular edema dried, visual acuity improved	(Kuijpers, Baarsma, & van Hagen, 1998)
IDDM	6 months	27 patients	Octreotide 200 µg/day	Reduced endothelial dysfunction and attenuation of vitreous haemorrhages after full scatter laser coagulation	(Clemens, et al., 1999)

1.5 Thesis Objectives

The hypothesis that somatostatin may prevent or slow down the progression of diabetic retinopathy if an effective formulation for delivery to the retina can be developed is advanced. The ultimate aims of the current work are development of an extended-release formulation of somatostatin with the potential for delivery of somatostatin to the retinal pigment epithelium cells and to investigate the modulation of a key receptor subtype implicated in diabetic retinopathy. To this end the following aims and objectives are advanced:

Aim 1: Determine the impact of SST self-assembly on release and formulation characteristics of the self-assembled hydrogels.

Objective: To perform rheological characterization, morphological studies, and investigate the reversibility of SST hydrogel formation for formulation optimisation.

Aim 2: Design and optimise an ocular formulation of SST.

Objective 1: To assess the suitability of SAW devices and traditional methods to manufacture microparticles encapsulating SST and perform stability and release studies upon these.

Objective 2: To produce a hydrogel formulation of SST in a polymeric carrier that extends the duration of release and perform characterisation and release studies on the formulation candidate.

Aim 3: Assessment of *in vitro* toxicity and effect on vascular endothelial growth factor receptor-2 (VEGF-R2) expression and VEGF secretion.

Objective: To perform *in vitro* studies on ARPE-19 cells to assess the cytotoxicity of an extended-release formulation and to investigate the effect of SST released from an extended-release formulation on VEGF-R2 expression and VEGF secretion.

CHAPTER 2: PHYSICOCHEMICAL CHARACTERIZATION OF SELF-ASSEMBLED SOMATOSTATIN HYDROGELS

2.1 Introduction

In this chapter, the rheological properties of self-assembled somatostatin hydrogels are studied and related to structure with transmission electron microscopy. The reversibility of somatostatin nanofibril formation as well as the kinetics of release of somatostatin monomers from hydrogels formed in different media are investigated. The purpose of physicochemical characterization is to provide an insight into the mechanical and flow properties of the self-assembled hydrogels and their influence on the mechanism and rate of somatostatin release *in vitro*.

2.1.1 Rheology

Peptide-based hydrogels are an important class of biomaterials with potential use in drug delivery. A primary experimental method to explore the physical properties of these hydrogels is rheology. Rheology provides gain a fundamental understanding of peptide hydrogel mechanical properties and underlying molecular mechanisms. This is important for determining whether these biomaterials are potentially suitable for biotechnological applications. Rheology is the primary experimental method with which researchers explore the viscoelastic properties of hydrogels.

The field of rheology theory, measurements and equipment is well introduced in books on the subject, e.g. Mezger(Mezger, 2006). Small deformation rheology experiments are performed on hydrogels to assess mechanical properties quantitatively (Ross-Murphy, 1994). By small deformation, the measurement is meant to be carried out within linear viscoelastic region of a material, a window of applied strain values within which the measured hydrogel properties are independent of the magnitude of imposed strain (Mezger, 2006). Typical small deformation tests are small amplitude oscillatory shear (SAOS) measurement as well as creep and creep recovery tests.

For controlled-strain rheometers, shear strain is applied to the sample in a sinusoidal oscillation,

$$\gamma(t) = \gamma_0(\sin \omega t) \quad \text{Equation 2.1}$$

and the measured shear stress is a phase-shifted sine wave with

$$\tau(t) = \tau_0(\sin \omega t + \delta) \quad \text{Equation 2.2}$$

in which ω is the applied angular frequency and δ is the phase difference between the two waves whereas for stress-controlled rheometers, the shear stress is applied as

$$\tau(t) = \tau_0(\sin \omega t) \quad \text{Equation 2.3}$$

and the resulting shear strain is measured as

$$\gamma(t) = \gamma_0(\sin \omega t + \delta). \quad \text{Equation 2.4}$$

For a purely elastic material, the strain and stress waves are in phase ($\delta = 0^\circ$) while a purely viscous response has the two waves out of phase by 90° ($\delta = 90^\circ$). Viscoelastic materials give rise to a phase-angle between 0° and 90° (Kavanagh & Ross-Murphy, 1998; Mezger, 2006).

In small amplitude oscillatory shear measurements, the shear storage modulus, G' , loss modulus, G'' , and loss factor, $\tan \delta$, are critical hydrogel properties monitored against time, frequency and strain. G' , the storage modulus, measures the deformation energy stored during shear process of a test material (i.e. the elasticity of the material) and G'' , the loss modulus, is representative of the energy dissipated during shear (i.e. the flow response of the material). If $G'' > G'$ ($\tan \delta > 1$), the sample behaves more like a viscous liquid while, conversely, when $G' > G''$, and, thus, $\tan \delta < 1$, the sample behaves more like an elastic solid (Mezger, 2006).

For gel samples, these parameters are often measured as a function of time, strain and frequency. Gelation can be actively observed by monitoring the temporal evolution of G' and G'' . Monitoring the moduli vs. strain helps one determine the linear viscoelastic region within which G' and G'' are independent of shear strain. Frequency sweeps (measurement of the moduli vs. frequency) elucidate the behaviour of the hydrogel at short vs. long time scales. The frequency dependence of the moduli is a critical hydrogel characteristic to observe since a single material behaves like an elastic solid ($G' > G''$) at a high frequency/fast timescale but behave more like a liquid ($G'' > G'$) at low frequency/longer time scales. It is thus imperative to observe rheological behaviour in a time-frame of relevance to the application.

In addition to the measurements described above, it is essential to assess the properties of hydrogels during flow as well as their abilities to retain or recover their solid form morphology and rigidity after experiencing shear flow or large strain. Shear-thinning thixotropic hydrogels can be excellent candidates for injectable therapeutic delivery vehicles. Monitoring rheological behavior and structural evolution of these gels during and after flow can help delivery during syringe injection and the ability of the material to stay localized after injection against possible biological forces *in vivo*.

2.1.2 Models of release

Drug release models can be empirical or mechanistic models. Empirical models are based on the experimental behaviour of the system studied without considering any physical mechanisms. However such a model does not provide any information on the mechanisms that control the process and therefore cannot be used to predict the effect of a change in conditions on the release rate.

Mechanistic or mathematical models are based on the physical mechanisms that influence the release process and therefore can be used to make predictive stimulations. To be employed, the validity of the model against experimental data must be established.

While many models are predicated upon diffusion equations, models also need to account for the morphology of the structure through which diffusion takes place (Langer & Peppas, 1983b; Narasimhan & Peppas, 1997). Drug release mechanisms can be classified as diffusion-controlled, chemically controlled, osmotically controlled and swelling-and/or dissolution-controlled. The commonly used models of release are discussed briefly below.

Zero-order kinetics

$$C_t = C_0 + K_0 t \quad \text{Equation 2.5}$$

where C_t represents the amount of active agent released during the time t , C_0 is the initial concentration of active released (generally, $C_0 = 0$), and K_0 is the zero-order constant.

For zero-order kinetics, the release of an active agent is only a function of time and the process takes place at a constant rate independent of the concentration of the active agent.

First-order kinetics

$$\ln \left(\frac{Q_t}{Q_0} \right) = kt \quad \text{Equation 2.6}$$

where Q_t is the amount of active agent released at time t , Q_0 is the initial amount of active agent dissolved and k is the first-order release constant.

This states that the change in concentration of the active agent with respect to time is dependent only on the concentration.

Higuchi model

$$Q_t = K_H t^{1/2} \quad \text{Equation 2.7}$$

where Q_t is the amount of active agent released at time t and K_H is the release constant of Higuchi.

The Higuchi model (Higuchi, 1961) relates the concentration of the active agent to the square root of time, representing a linear function. However this model makes a number of assumptions which make it only valid in the case of polymers that do not swell significantly on contact with water.

Hixson-Crowell model

$$(1 - f_1)^{1/3} = 1 - K_\beta t \quad \text{Equation 2.8}$$

where $f_1 = 1 - (W_i/W_0)$ Equation 2.9

and represents the fraction of drug dissolved on time t , W_0 is the initial amount of the drug in the system; W_i is the amount remaining in the system on time t and K_β is a release constant.

This model (Hixson & Crowell, 1931) applies to dosage forms in which dissolution happens in planes parallel to the surface of the dosage form e.g. tablets. The surface decreases proportionally over time and the geometrical form remains constant. A linear function is represented when the cube root of the non-released fraction is related with time. When this model is used, it is assumed that drug release is limited by dissolution velocity and not by diffusion, which can occur through the polymeric matrix.

Korsmeyer-Peppas model

$$M_t/M_\infty = kt^n \quad \text{Equation 3.0}$$

Where M_t and M_∞ are cumulative amounts of drug released at time t and infinite time, respectively. This is a comprehensive semi-empirical equation (Ritger & Peppas, 1987) to describe drug release from polymeric forms. It was developed specifically for the release of drug molecules from polymeric matrices like a hydrogel. It is useful when the release mechanisms are unknown or more than one type of phenomenon of drug release is involved. This model involves the superposition of drug transport, relaxation and diffusion mechanisms. The exponent n relates the release is by drug diffusion ($n=0.5$) or zero-order ($n=1$) and due to swelling/relaxation of polymer chains. When $0.5 < n < 1$, the release is defined by both diffusion and swelling.

2.1.3. Release kinetics

Somatostatin-14 reversible self-assembly into nanofibrils was previously reported (Anoop, et al., 2014; Maji, et al., 2009; W. van Grondelle, et al., 2007; van Grondelle, et al., 2013). This intrinsic propensity of the peptide is currently thought to be biologically relevant to its conditions of storage within normal hypothalamic secretory granules, as a wide range of other human neuropeptide hormones (Anoop, et al., 2014; Maji, et al., 2009). The spontaneous assembly of somatostatin-14 into flexible liquid crystalline nanofibrils was shown in water (above 3% w/w) and in 150mM sodium chloride (NaCl) (0.5% w/v and above) (W. van Grondelle, et al., 2007). Nanofibril self-assembly was therein mentioned to result in the formation of hydrogels in water with or without NaCl or other salts (calcium and phosphate). The width of the nanofibrils was found to decrease in the presence of these salts, coupled with an enhanced propensity to form nanofibrils - decrease in critical concentration of assembly - and an enhanced nanofibril lateral association. Both phenomena were attributed to the screening of electrostatic repulsions between the cationic self-assembling peptides by the additional ions in the media (W. van Grondelle, et al., 2007; van Grondelle, et al., 2013).

It is of interest to investigate if the propensity of somatostatin to self-assemble would lend to a depot formulation of the peptide, which can release monomers at a controlled rate. However, the fibrils would have to release the peptide monomers at a rate sufficient for therapeutic activity to occur. Of the somatostatin analogues, lanreotide has been shown to self-assemble into large nanotubes and form self-assembled hydrogels (Valery, et al., 2004; Valéry, et al., 2003), from which lanreotide monomers are released in a sustained manner. This property led to the formulation marketed as Lanreotide Autogel® (Wolin, et al., 2016). Although the release of somatostatin-14 from nanofibrils formed in the presence of heparin and mannitol has been previously shown for low peptide concentrations (0.2% w/w) (Anoop, et al., 2014), there is currently no published data on the rheology and release kinetics of somatostatin hydrogels.

Hydrogels for the delivery of non-peptide actives in the treatment of ocular disorders have been investigated, both self-assembling supramolecular nanofibers as well as nano-composite hydrogels (Li, et al., 2014; Li, Zhang, & Chen, 2013).

This study aims to investigate the release kinetics of somatostatin-14 from the hydrogels it spontaneously forms in aqueous media and in the presence of electrolytes. As discussed above, SST was shown to prevent retinal neurodegeneration following topical administration to diabetic rats at concentrations of 0.2% and 1% (Hernandez, Garcia-Ramirez, et al., 2013). It has been reported that daily administration is required for up to 16 days to achieve this response (Hernandez, Garcia-

Ramirez, et al., 2013). In this study, we investigate the release kinetics of SST from SST gels formed at higher peptide concentrations (1%, 2.5% and 5%), in order to determine its potential to provide a platform for sustained release of SST. The gels were formed in either water or simulated lachrymal fluid (SLF) to determine the effects of electrolytes present in ocular tissue on release of the peptide.

While investigating the feasibility of ocular formulations for the treatment of diabetic retinopathy from somatostatin self-assembled hydrogels, we report on the correlation between the monomer release kinetics and the rheological properties of the hydrogels.

2.2 Materials and Methods

2.2.1. Materials

Somatostatin-14 of sequence Ala-Gly-Cys-Lys-Asn-Phe-Phe-Trp-Lys-Thr-Phe-Thr-Ser-Cys (cyclic, MW=1638 Da) was purchased as an acetate salt from Polypeptide Laboratories (Sweden). According to the Manufacturer's certificate of analysis, the peptide purity is 99.6%.

Sodium azide and the chemicals used to prepare the simulated lachrymal fluid were purchased from Sigma Aldrich (St Louis, MO). MilliQ water was used in the preparation of all media. The composition of simulated lachrymal fluid can be found in Table 2.1 (Ceulemans & Ludwig, 2002).

Table 2.1 Composition of simulated lachrymal fluid (Ceulemans & Ludwig, 2002).

Composition (in water)	Amount (g/L)
NaCl	6.3118
KCL	1.7893
NaHCO ₃	2.1842
CaCl ₂	0.0444
MgCl ₂	0.0477
Adjusted to pH 7.4 (+/- 0.1) with 0.1N HCL	

2.2.2 Methods

2.2.2.1. Preparation of somatostatin hydrogels

Somatostatin 2.5% w/w and 5% w/w were investigated in 0.9% w/v NaCl and in simulated lachrymal fluid. Somatostatin 5% w/w was also prepared in distilled water as this is above the minimum concentration required for nanofibril formation in the absence of electrolytes (SST 3% w/w) (W. van Grondelle, et al., 2007). The concentrations are expressed in weight per weight as the volume changes during the gelation process.

Somatostatin acetate powder was weighed and dissolved in the relevant medium to reach the required concentration in Eppendorf tubes. The tubes were then vortexed for 30 seconds to ensure complete dissolution of the somatostatin powder and then incubated at 37 °C.

The gels (SST 2.5% w/w and 5% w/w) formed in 0.9% w/v NaCl and in simulated lachrymal fluid took 48 hours to form and were analysed by rheometry on days 1, 2 and 8. Higher concentration gels (SST 5% w/w) formed in water took a longer time to form (16 days) and were analysed on days 1, 2, 8 and 16.

2.2.2.2 Transmission electron microscopy (TEM)

Transmission electron microscopy (TEM) was used to characterise the morphology of the nanofibrils. Negative staining by uranyl acetate was performed to contrast the nanostructures, using the same protocol as reported in van Grondelle *et al.* 2007. Stained samples deposited on formvar and carbon-coated 200 mesh copper grids (Proscitech, Australia) were examined with a JEOL 1010 transmission electron microscope operating at 100 kV.

2.2.2.3. Oscillatory rheology

The rheological properties of the somatostatin gels were determined using an ARG2 Rheometer (TA Instruments, UK). A stainless steel 40mm parallel plate geometry with gap of 500 µm was employed. The removal of the gels was performed as gently as possible from the containers to minimize disruption of the structure. The gels were given an hour to equilibrate at the investigated temperature to relax to the resting condition prior to analysis. According to the review by Pochan *et al* (Sathaye, et al., 2015), parallel plate rheometers are a good choice for hydrogels containing large domain sizes like hierarchically assembled fibers. Zero gap calibration and same gap was set for all measurements as recommended by the authors. A solvent trap was used to eliminate the evaporation of water from the gel periphery. Oscillation amplitude sweeps were used to confirm the linear viscoelastic region. Frequency sweeps (0.1-10 Hz) at 25°C and 37 °C and temperature sweeps (1 Hz, 20-50 °C) were then conducted. Measurements were performed in triplicate.

2.2.2.4. Monomer release protocols

The release characteristics of self-assembled somatostatin hydrogels were investigated in both water and simulated lachrymal fluid (Table 2.1) with 0.01% sodium azide to prevent microbial growth in the media. As the rheological properties of the somatostatin hydrogels in 0.9% w/v NaCl and SLF were similar and our interest is in simulating release in a media relevant to the physiological environment of the eye, only SLF was used to investigate release.

SST monomer release was investigated using two previously reported methods for peptide self-assembled hydrogels; either with the hydrogel in direct contact with the relevant medium in a 1.5 mL Eppendorf tube (Branco, Pochan, Wagner, & Schneider, 2009) or in a Slide-A-Lyzer mini dialysis unit system comprising a dialysis regenerated cellulose and polypropylene membrane with a 3.5kDa cut-off (Thermo Fisher Scientific, USA) (Anoop, et al., 2014).

Prior to both release protocols, somatostatin-14 samples were incubated at 37° C, for 48 hours for the gels prepared in SLF or 16-20 days for the gels prepared in water, to allow gelation to occur. The study was commenced when the gels formed completely on visual observation. As this is a variable process depending on nucleation (Harper & Lansbury, 1997), the time taken for the gels to completely form ranged from 16-20 days in water.

Release medium (water or SLF; 500 µL) with 0.01% w/v sodium azide was placed directly on top of the gels in Eppendorf tubes. The Eppendorf tubes were then closed and sealed with Parafilm. The gels formed in the Slide-A-Lyzer units were dialysed against the same volume of release medium in capped centrifuge tubes. The assembled units were then placed in a shaking water bath at 37° C. At various time intervals (1, 2, 4, 6, 9, 24 and 48 h), an appropriate aliquot 400 µL of 500 µL) was removed for analysis by UV spectrophotometry. Given the high solubility of somatostatin in aqueous media (> 70mg/mL) and the turnover of 80% of buffer volume at each sampling point, this approaches sink conditions *in vivo* in the ocular environment with tears or blood flow. The units were reassembled and replaced in the shaking water bath. We have followed the protocol reported by Anoop *et al* who investigated the reversibility of somatostatin fibril formation (Anoop, et al., 2014). The experiments were performed in triplicate.

2.2.2.5. HPLC

The stability of somatostatin in the media at 37 °C over 48 hours was determined by HPLC (Flexar, Perkin Elmer, USA). The method described by Valery et al (W. van Grondelle, et al., 2007) was adapted and modified to suit the instrument used. This method was validated according to ICH guidelines. Chromatography was performed on a Phenomenex C18 column (5 µm particle size, 150 x

4.6 mm). Trifluoroacetic acid (TFA) 0.1% v/v in water was used as mobile phase and acetonitrile with 0.1% v/v TFA was used as organic eluent. Separation was carried out at ambient temperature, at a flow rate of 1 mL/min, with a gradient from 5% to 68% of organic eluent in the mobile phase in 55 min. Detection was performed at 280 nm. The HPLC method was used to validate UV analysis.

2.2.2.6. Assay by UV spectrophotometry

Calibration curves obtained by dilutions of somatostatin (0.0005% w/w - 0.05% w/w) in both water and SLF (with 0.01% w/v sodium azide) were used. The aliquots taken from the release medium were diluted to 2000 μ L with the corresponding medium to reach concentrations in the same range as the calibration curves. The diluted aliquots were placed in quartz cuvettes and subjected to analysis by UV in a T60U Spectrophotometer (PG Instruments, UK).

Absorbance at 280nm was measured and the cumulative percentage released over 48 hours was calculated based on calibration curves. The experiments were performed in triplicate.

2.2.2.7. Statistical analysis

A two-way ANOVA with Tukey's multiple comparisons test was performed to assess if the differences in the cumulative percentage released at 48 hours were significant amongst the different concentrations of SST and medium within each group.

The analysis shows that the differences between all except the ones marked 'ns' were significant.

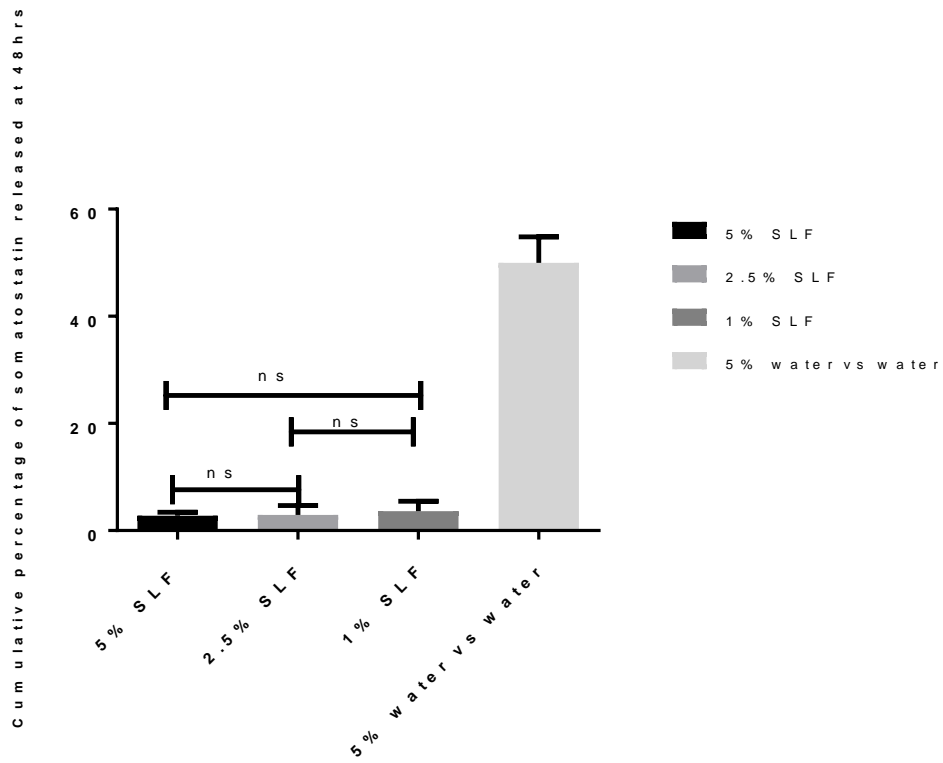


Figure 2.1: Comparison of cumulative percentage release of somatostatin in Slide-A-Lyzer units at 48 hours (ns-not significantly different) (n=3, error bars= SD)

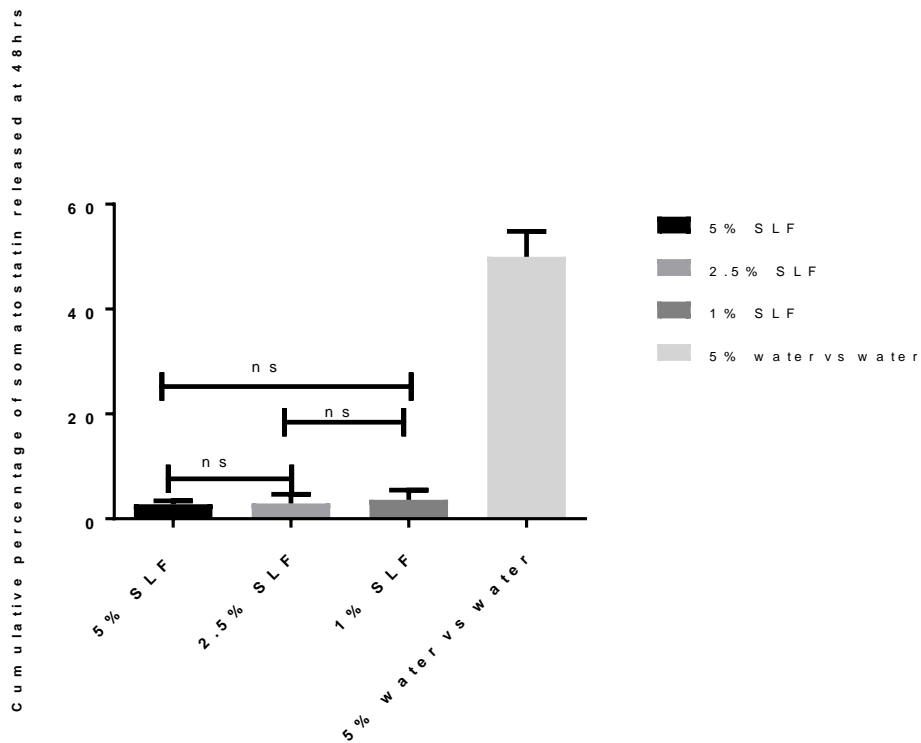


Figure 2.2: Comparison of cumulative percentage release of somatostatin in Eppendorf tubes at 48 hours (ns-not significantly different) (n=3, error bars= SD, 5% water gel vs simulated lachrymal fluid not represented because the experiment ended at 9hrs)

2.3. Results and Discussion

2.3.1. Nanofibril structural characterisation (TEM)

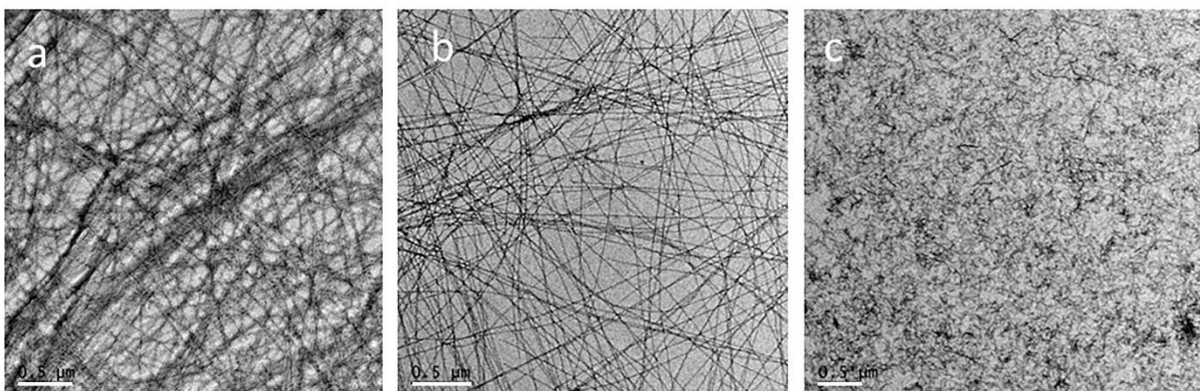


Figure 2.3. Transmission electron micrographs of (a) Somatostatin 5% w/w in water (magnification 5000x) (b) Somatostatin 5% w/w in 0.9% w/v NaCl (magnification 5000x) (c) Somatostatin 5% w/w in simulated lachrymal fluid (magnification 4000x). Scale bars (a, b and c) 0.5 μ m. Samples were equilibrated for 8 days.

The morphology of somatostatin nanofibrils in water, NaCl and SLF was investigated by transmission electron microscopy on gelled samples. Figure 2.3 shows that the nanofibrils in the presence of electrolytes are narrower and more dense in appearance compared to the nanofibrils formed in the absence of electrolytes. The average width of the nanofibrils in water was 15.8nm, 12.6nm in NaCl and 10.8nm in SLF (Image J)(Abràmoff, Magalhães, & Ram, 2004). These are larger than the mean widths reported by W. van Grondelle *et al* (W. van Grondelle, et al., 2007) of somatostatin nanofibrils in water and 150 mM NaCl. This could be due to the density of the nanofibrils in our samples which made it harder to distinguish between single nanofibrils and laterally associated ones. W. van Grondelle, *et al* also observed a reduced nanofibril width in the presence of electrolytes. As discussed by van Grondelle *et al* (W. van Grondelle, et al., 2007), this is likely to be due to the electrostatic shielding of the positive charges on the peptide by the electrolytes, enhancing lateral association. As published in our paper “Release kinetics of somatostatin from self-assembled nanostructured hydrogels” (Rai, Thrimawithana, Dharmadana, Valery, & Young, 2017) in Section 3.1, the small angle X-ray scattering (SAXS) patterns obtained for the different somatostatin hydro-gels (Figure 5 in the paper) show an increase in intensity as a function of the ionic strength of the buffers, especially at low q range. The corresponding scattering patterns do not correspond to the Guinier regime (q_0) for molecular species but rather to scattering by large semi-flexible structures q_1 – q_2). This trend confirms the higher density of assembled structures/nanofibrils as a function of the ionic strength. The pH of somatostatin solutions in aqueous media is $\text{pH } 4.7 \pm 0.3$ (W. van Grondelle, et al., 2007). At this pH, the peptide exhibits a net charge of 2. Chloride ions in both NaCl and SLF solutions and carbonate ions in SLF are likely to shield this positive charge and enhance lateral association. Figures 2.4,2.5 and 2.6 are TEM images of SST hydrogels at different magnifications.

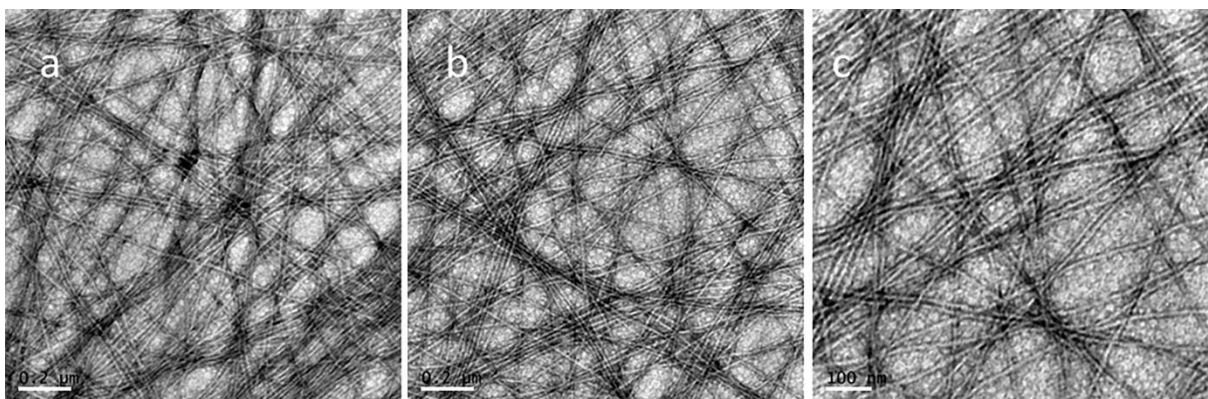


Figure 2.4. Transmission electron micrographs of SST 5% w/w water samples on day 8. Scale bars for (a and b) -0.2 μm (12,000x magnification) and (c) -100 nm (20,000x magnification)

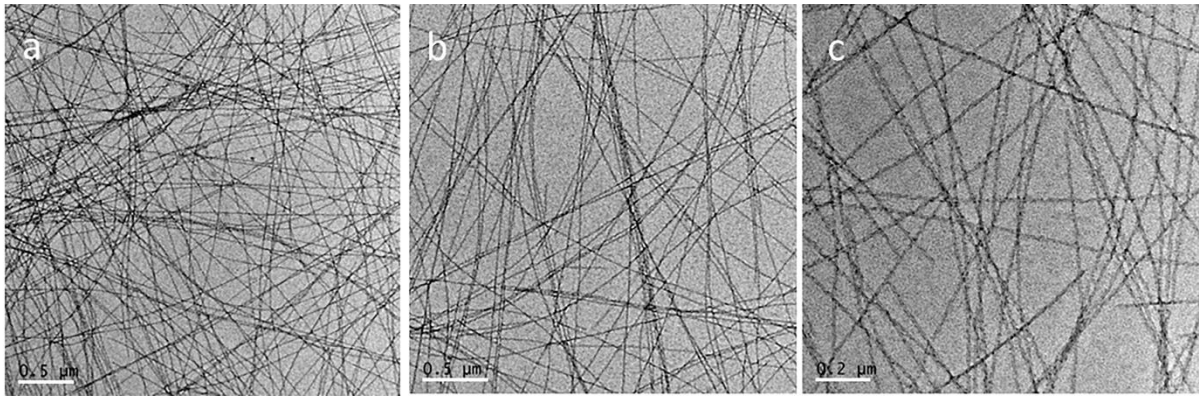


Figure 2.5. Transmission electron micrographs of SST 5% NaCl samples on day 8. Scale bars for (a and b) -0.5 μm (5,000x magnification) and (c) -0.2 μm (12,000x magnification).

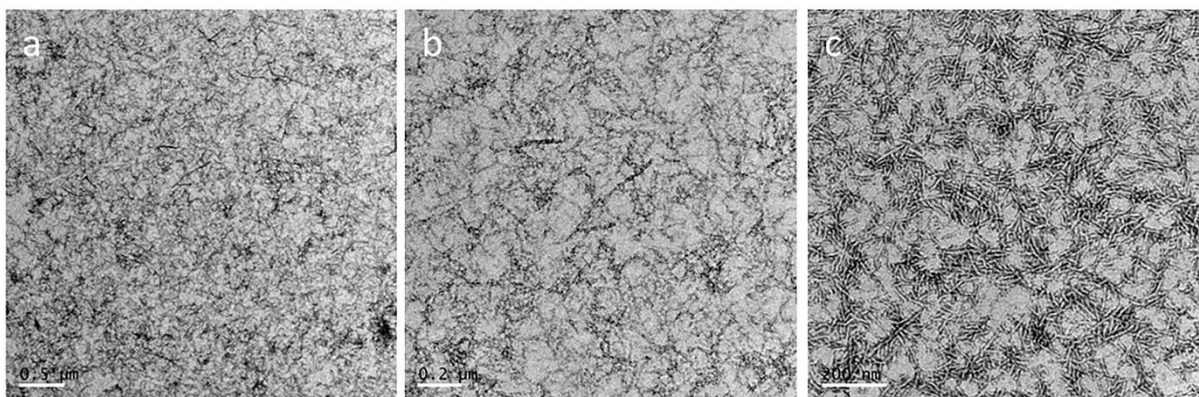


Figure 2.6. Transmission electron micrographs SST 5% SLF samples on day 8. Scale bars for (a) - 0.5 μm (4000x magnification), (b) - 0.2 μm (10,000 magnification) and (c) - 200nm (15,000 magnification).

2.3.2. Oscillatory rheology

The rheological studies showed that somatostatin formed a gel with higher storage modulus (G') at higher SST concentrations and in the presence of electrolytes as shown in Figure 2.7. All the concentrations tested exhibited shear-thinning properties, with declining viscosity as shear rate increased (Figures 2.8a and 2.8b). The frequency sweeps showed a trend to increase in moduli with increasing frequency (Figure 2.9). As high frequencies represent shorter timescales and low frequencies are representative of longer timescales, this indicates a lowering of the stiffness of the gel over longer time period. For example, the G' of SST 5% in NaCl hydrogel at 1 Hz was 80888 compared to 89816 at 10 Hz. Similarly, for SST 2.5% hydrogel in SLF the G' was 42882 at 1 Hz and 52145 at 10 Hz. However the G' remained higher than G'' at all frequencies indicating the SST hydrogel structure was not destroyed. At a frequency of 1 Hz, the G' of SST 2.5% in NaCl was 5809 compared to the G'' of 2277. The G' remained higher than the G'' at a frequency of 10 Hz (10381 vs

4591 respectively). Temperature sweeps showed a progressive decrease in G' and G'' with increasing temperature from 20 °C to 50 °C characteristic of materials in the absence of thermogelation (Figure 10). The G' of SST 5% hydrogel in NaCl decreased from 159406 at 20 °C to 43531 at 50 °C and from 16190 at 20 °C to 2735 at 50 °C for SST 2.5% hydrogel in NaCl. Thixotropic behavior was observed in plots of shear rate against stress. Several examples of hydrogel moduli are available for comparison (Aggeli, et al., 1997; Caplan, Schwartzfarb, Zhang, Kamm, & Lauffenburger, 2002; Collier, et al., 2001). The moduli of the SST hydrogels are equal to, or greater than, that of moduli reported for comparable hydrogel systems.

Pochan, Schneider and co-workers have developed 2 self-assembling peptides, MAX1 and MAX8, with β -hairpin turns as possessed by SST (Yan, et al., 2010). These hydrogels exhibited shear-thinning behaviour and flowed easily when injected through a syringe with recovery of the structure after flow. Thixotropic behaviour was also observed and a theory was advanced as to the mechanisms of shear-thinning in the hydrogels. It was proposed that the hydrogel network fractures into domains as shear is applied to allow for flow and upon removal of shear, the fractured domains percolate and self-heal into gels of original stiffness (Yan, et al., 2010). Loveday and co-workers investigated the rheological characteristics of β -lactoglobulin, which forms amyloid-like fibrils upon heating. Fibrillar samples also demonstrated shear-thinning properties (Loveday, Wang, Rao, Anema, & Singh, 2012).

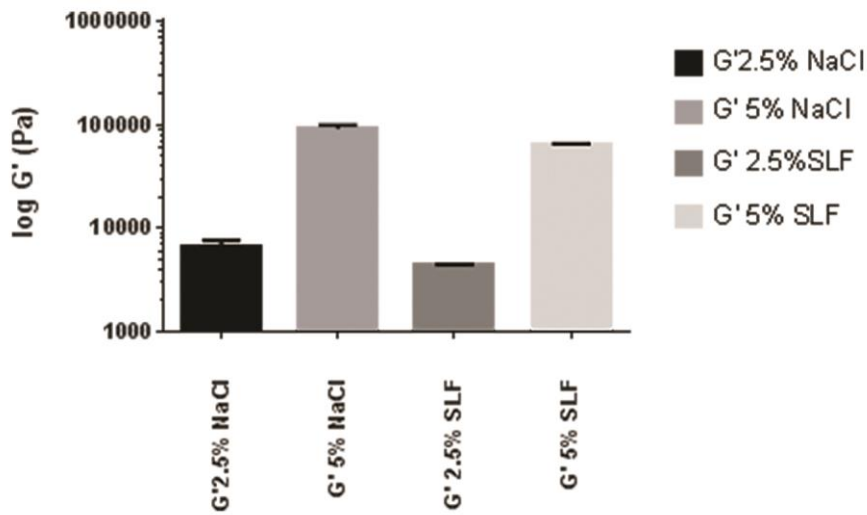
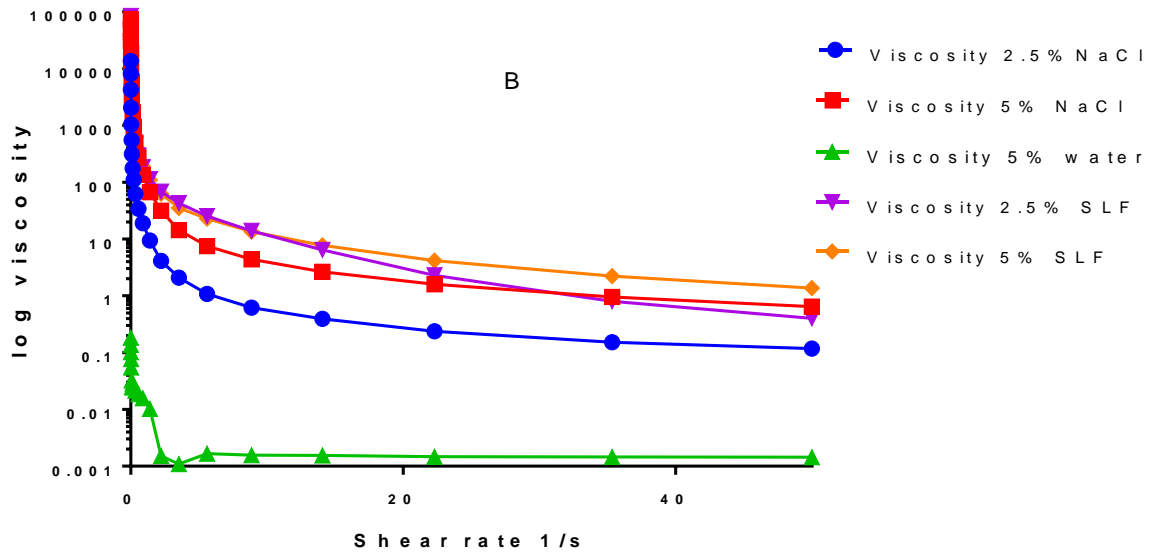
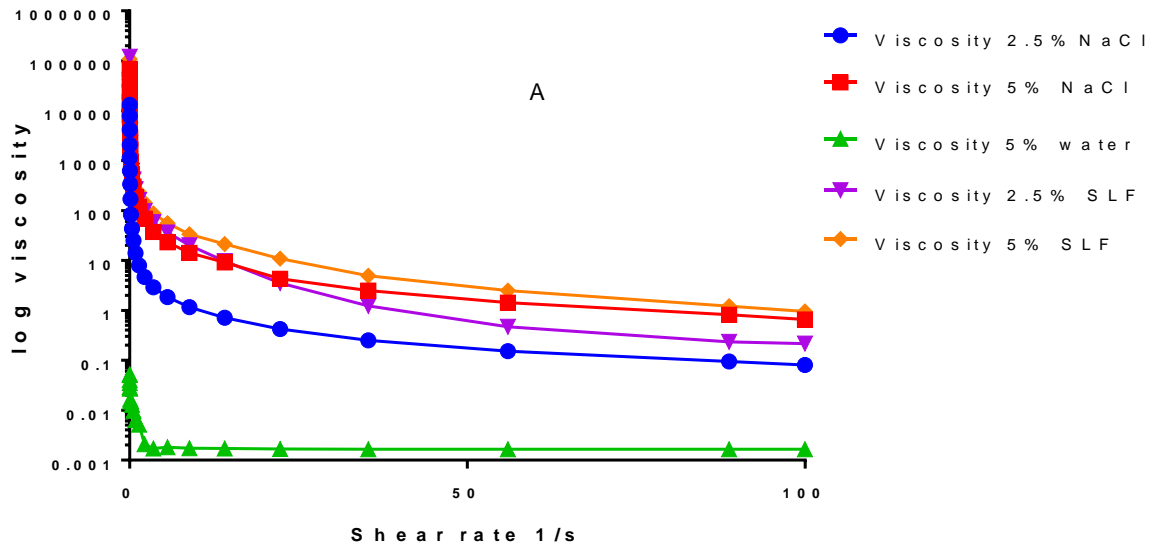


Figure 2.7. Comparison of the G' (storage modulus) of the SST hydrogels on day 8 at a frequency of 1 Hz at 37°C (n=3, error bars represent standard deviation). SST 5% w/w in water formed viscous solutions with negligible G' (elasticity) below reliable instrument detection and are therefore, not included for comparison.



Figures 2.8a and 2.8b: Flow sweep at 25°C and 37°C respectively (n=3)

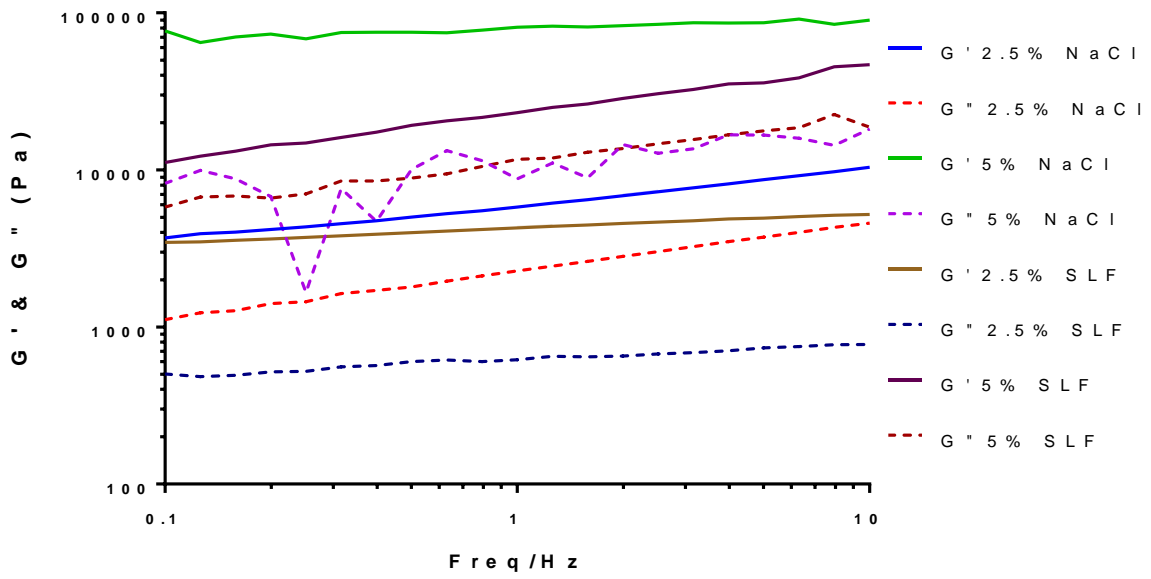


Figure 2.9 Frequency sweep of the SST hydrogels on day 8 at 37°C (n=3)

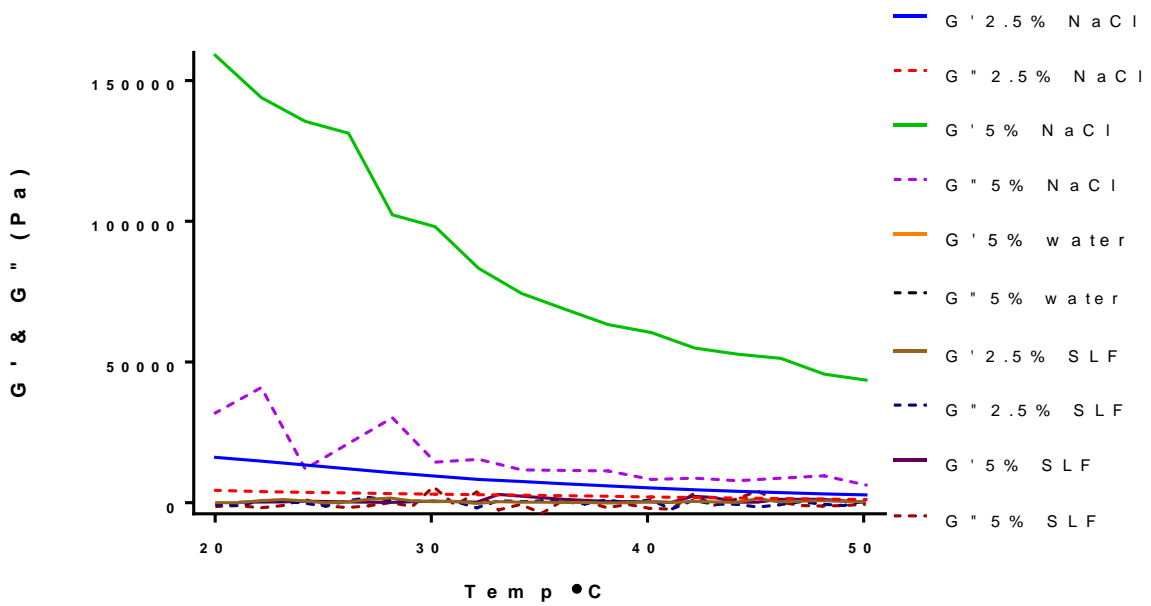


Figure 2.10 Temperature sweep of the SST hydrogels (day 8) from 20°C to 50°C (n=3).

2.3.3. Monomer release

Table 2.2 Comparison of cumulative percentage somatostatin released at 48 hours in the Eppendorf tubes and Slide-a-Lyzer units

Gels tested	Average of cumulative percentage somatostatin released at 48 hours in Eppendorf tubes	Average of cumulative percentage somatostatin released at 48 hours in Slide-a-Lyzer units
SST 5% SLF	3.37%	0.99%
SST 2.5% SLF	2.95%	0.74%
SST 1% SLF	3.60%	0.53%
SST 5% water vs water	49.99%	25.8%
SST 5% water vs SLF	38.03% (at 9 hours)	3.01%

From Table 2.2, it can be seen that the SST gels in water released significantly higher percentage of SST monomers compared to the SST gels formed in SLF both in the Eppendorf tubes and the Slide-a-Lyzer units ($p < 0.0001$) (Figures 2.1 and 2.2). There were no significant differences amongst the cumulative percentage released by the SST gels formed in SLF in the Eppendorf tubes or the Slide-a-Lyzer units. Rheological studies demonstrate that that SST forms stiffer gels in the presence of electrolytes (Figure 2.7). This could be due to the favouring of self-assembly as reported by van Grondelle *et al* (W. van Grondelle, et al., 2007) supported by our observation that these gels formed more quickly at 48 hours compared to 16 days required for the gels formed in water. The experiment with the water gels against SLF in the Eppendorf tubes was concluded at 9 hours as solid layer of opaque gel had formed at the release interface.

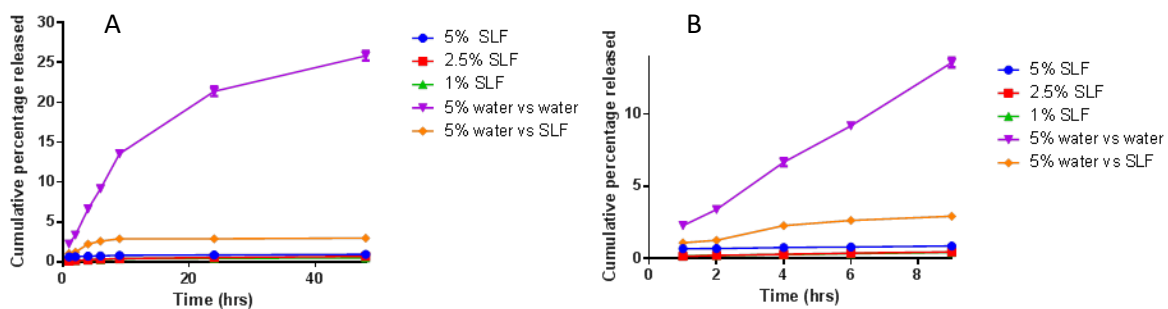
A similar observation was made with the water gels in the Slide-A-Lyzer units dialysed against SLF. The initially transparent gel turned opaque as the electrolytes from the SLF outside diffused through the dialysis membrane into the somatostatin sample rendering it identical to the gels formed in the presence of electrolytes. This may account for the lower cumulative percentage released from the SST 5% water gel dialysed against SLF at 48 hours compared to the SST 5% water gel dialysed against water.

There was a higher percentage of release from the gels in the Eppendorf tubes compared to the Slide-a-Lyzer units (Table 2.2). While it is likely that somatostatin was released from the samples in both the Eppendorf tubes and Slide-a-Lyzer units via erosion and diffusion release mechanisms

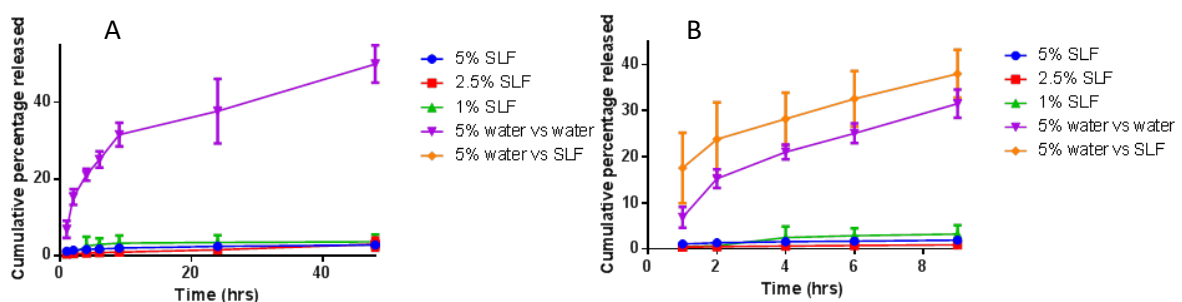
(Bamba, Puisieux, Marty, & Carstensen, 1979; Gohel, Panchal, & Jogani, 2000; Roy & Rohera, 2002), possible obstruction of cellulose membrane in the Slide-A-Lyzer units may have contributed to the observed low release and be a limitation of this method of investigating release from hydrogels.

Cumulative percentages of SST release versus time in and against different media are shown in Figures 2.11 and 2.12. From the variation in release of SST between the SST gels in direct contact with the medium versus the ones in the Slide-a-Lyzer units, certain mechanistic inferences can be made. Primarily, that erosion plays a significant role in release of SST monomers from the water gels.

Erosion also plays a role in the release of SST from the gels in SLF, though the difference is only three-fold between the Eppendorf tubes and Slide-a-Lyzer units. This can be attributed to the viscoelasticity of gels formed in the presence of electrolytes. Also, the nanofibrils in the presence of electrolytes are possibly more stable due to the enhancement of lateral association.



Figures 2.11a and 2.11b: Comparison of cumulative percentage SST released in Slide-a-Lyzer units at 48hrs and 9hrs respectively (n=3, error bars represent standard deviation)



Figures 2.12a and 2.12b: Comparison of cumulative percentage SST released in Eppendorf tubes at 48hrs and 9hrs respectively (n=3, error bars represent standard deviation)

2.3.4 Release kinetics

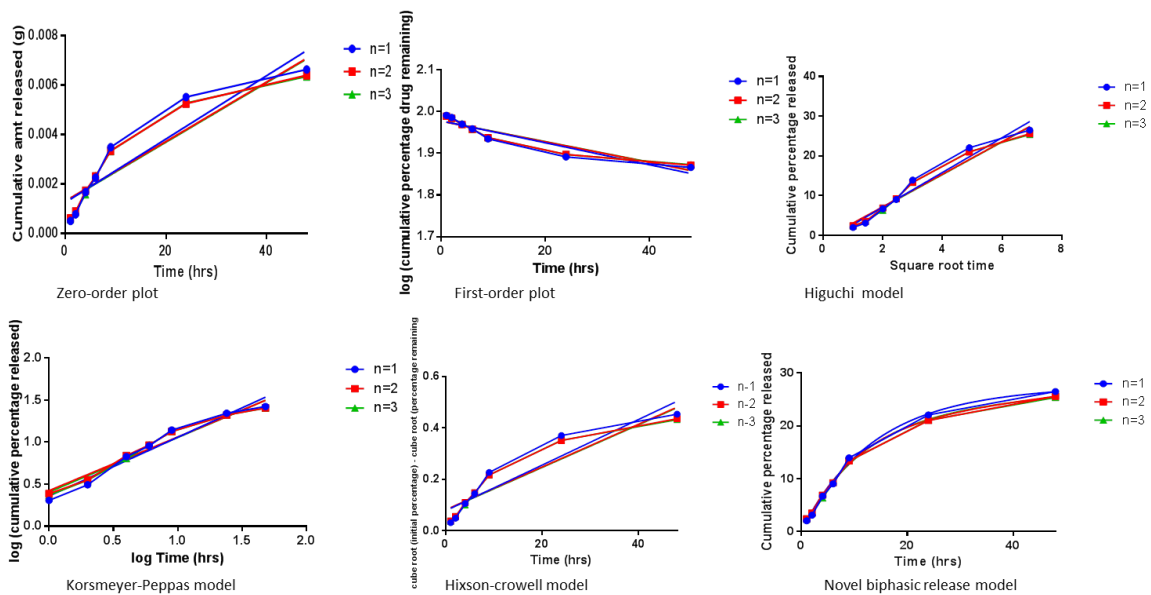


Figure 2.13: Fitting of the SST 5% w/w water vs water release over 48 hours in Slide-a-Lyzer units to different models of release ($n=3$)

In order to elucidate the mechanism of release of the SST monomers, the data was fitted to zero and first-order models as well as Higuchi (Higuchi, 1961), Korsmeyer-Peppas (Korsmeyer, Gurny, Doelker, Buri, & Peppas, 1983) and Hixson-Crowell (Hixson & Crowell, 1931) cube root models. The SST 5% water gel dialysed against water in the Slide-a-Lyzer unit is shown as a representative in Figure 2.13 fitted to the different release models.

The mean R^2 values are provided in Tables 2.3 and 2.4 for the release in both the Slide-a-Lyzer units and Eppendorf tubes respectively. For the majority, the best R^2 values were obtained for the Higuchi model, which is typical for systems where drug release is governed purely by diffusion (Higuchi, 1961).

Table 2.3: Mean R² (and standard deviation) values and desorption half time in minutes in Slide-a-Lyzer units.

	Mean R ² ± SD				
	SST 5% SLF	SST 2.5% SLF	SST 1% SLF	SST 5% Water vs Water	SST 5% Water vs SLF
Zero-order	0.780±0.0487	0.858±0.031	0.751±0.023	0.868±0.005	0.408±0.037
First-order	0.780±0.039	0.859±0.031	0.752±0.024	0.889±0.004	0.408±0.035
Higuchi	0.893±0.033	0.959±0.019	0.894±0.016	0.968±0.003	0.588±0.039
Korsmeyer-Peppas	0.919 ±0.056	0.976±0.011	0.946±0.018	0.967±0.005	0.764±0.032
Hixson-crowell	0.779±0.05	0.859±0.031	0.752±0.024	0.882±0.005	0.409±0.038
Hybrid release model	0.880±0.076	0.989 ±0.005	0.966 ±0.039	0.998 ±0.001	0.791 ±0.296
Half-time of diffusional release process (hours ⁻¹)	0.284	2.27	1.734	8	2.086
Total diffusional release %	0.749± 0.213	0.405± 0.071	0.398± 0.179	22.8± 2.72	2.69± 0.739

Table 2.4: Mean R² values (and standard deviation) and desorption half-time in minutes in Eppendorf tubes.

	Mean R ² ± SD				
	SST 5% SLF	SST 2.5% SLF	SST 1% SLF	SST 5% Water vs water	SST 5% Water vs SLF
Zero-order	0.821±0.144	0.967±0.022	0.467±0.118	0.793±0.069	0.949±0.024
First-order	0.822±0.144	0.967±0.023	0.468±0.118	0.850±0.068	0.964±0.022
Higuchi	0.928±0.095	0.958±0.067	0.634±0.125	0.899±0.048	0.982±0.021
Korsmeyer-Peppas	0.969±0.043	0.966±0.038	0.771±0.088	0.887±0.054	0.983±0.019
Hixson-crowell	0.821±0.144	0.967±0.022	0.468±0.118	0.833±0.069	0.959±0.023
Hybrid release model	0.896±0.033	0.9±0.158	0.909±0.068	0.896±0.088	0.974±0.045
Half-time of diffusional release process (hours ⁻¹)	0.706	0.95	3.227	3.128	0.662
Total diffusional release %	1.62± 0.22	0.711±0.177	3.79± 0.638	25.4± 12.1	20.5± 5.53

The pattern of release appears to be bimodal consistent with the hypothesis that different release mechanisms predominate at different times rather than the same mechanism determining the rate of release. As release from most gel samples demonstrated bimodal properties, a hybrid model conceived as being the sum of adsorbed material release (first-order) and erosional release (zero-order) was developed. We advance that the observed rapid but incomplete initial release may proceed as a result of the more rapid release of material adsorbed onto the surface of the gel with

the expectation that such adsorption follows a Langmuir Adsorption Isotherm(Foo & Hameed, 2010). As the release of adsorbed material is depleted, release then slows to a zero-order rate, perhaps related to the erosion of the gel matrix. The hybrid model conceived is represented by:

$$R = k_0 t A_D + (1 - \exp^{-k_1 t}) \quad \text{Equation 2.10}$$

Where:

R = cumulative release (%)

k_0 = zero-order release constant (erosion)

A_d = total diffusional release

k_1 = first-order release rate constant (diffusion)

t = time

and

$$t_{1/2r} = \ln(2) / k_1$$

where $t_{1/2r}$ = half-time of diffusional release process

k_1 = first-order release rate constant (diffusion)

Such a model has no linear solution or approximation. Rather, to fit experimental data to such a model requires iterative curve fitting to be employed. In this work, GraphPad Prism was employed to optimize model parameters to experimental data.

Testing the fit of experimental data to accepted release models and the novel hybrid release model demonstrated mean R^2 values obtained by fitting the data to the novel hybrid release model to be superior except in the case of 5% SST gels (the most rigid tested) where erosional release would be anticipated to be minimal. Moreover, this observation is consistent with the Langmuir Adsorption Isotherm where higher concentrations of SST would be anticipated to result in higher adsorbed surface concentrations of release. Alternatively, such first-order release ordinarily may be explained by diffusional release where an increase in concentration of releasing substrate would result in a corresponding increase in release rate. However, in this case, the diffusing substrate and the structural component of the gel are the same such that increasing the concentration of the diffusing substrate above the gel threshold would reduce diffusional release. These observations establish the

first-order release (or first-order region of release in the case of biphasic release patterns) to be more likely to be due to the release of adsorbed material from the cortex rather than the diffusional release of material from the core.

From the fit achieved to the novel hybrid model, the half-time of diffusional release process ($t_{1/2r}$) may be estimated from the first-order release rate constant (k_1). This demonstrates that the times were shorter for the release in the Eppendorfs compared to the Slide-A-lyzer units. This is likely to be due to direct contact of the gel with the medium which would facilitate both desorption and erosional release. Moreover, the 5% SLF gels released more quickly than the 2.5% SLF gels. Whilst from rheological tests it may be inferred that 5% SLF gels would erode more slowly (having a higher G'), there may be more SST monomers adsorbed on the surface of the gel and closer to the surface compared to the 2.5% SLF gels. In contrast, for 1% and 2.5% SLF gel release times are similar in the Slide-a-Lyzer units but are significantly more rapid in the Eppendorf tubes with the lower concentration gels releasing more quickly. These lower concentration gels demonstrate greatly reduced G' thus, having a lesser structure, erode readily in direct contact with the medium.

It is difficult to compare the data of the SST 5% water gels directly between the Eppendorf tubes and Slide-a-Lyzer units due to the variation in time scale of the experiments. The observation of reduced release rate with time in contact with the electrolytes in solution is consistent with the increase in nanofibril structure observed in an environment of higher electrolyte presence (Figure 2.3). This suggests some diffusion of ions into the SST gel of lower structure (Figure 2.7).

2.4. Conclusions

The rheological tests indicate that the SST hydrogels are shear-thinning. The storage modulus (G') of the SST hydrogels increases with increasing SST concentration and in the presence of electrolytes. Here, for the first time, we have investigated the rheological properties and release kinetics from self-assembled SST hydrogels. We propose that the release kinetics of SST monomers from the hydrogels follow a hybrid model where both zero-order and first-order release occur, predominating at different times.

This study indicates that SST self-assembled hydrogels have the potential to act as a depot for SST delivery as the release of monomers has been demonstrated. However, it remains questionable that the amount released is adequate to achieve therapeutic benefit in the retina. The cumulative percentage of release ranging from 2.95% to 3.60% from the self-assembled SST hydrogels in SLF at 48 hours seems low; although release over an extended period of time may be sufficient. The amount of SST in the vitreous of non-diabetic human subjects has been found to be 113.5 pg/mL

(Hernandez, et al., 2005), which is lower than the amount of SST released from the hydrogels. It has been observed that the presence of electrolytes results in a slower release, which has to be considered as electrolytes will be present in the physiological milieu.

While there are no clinical formulations of somatostatin for ocular use currently on the market, there are a number of studies of somatostatin on retinal cultures and animal models. The concentrations studied ranged from 10^{-11} to 10^{-5} M on retinal cell cultures (Davide Cervia, Elisabetta Catalani, Massimo Dal Monte, & Giovanni Casini, 2012; Cervia, Martini, et al., 2008; Niki Mastrodimou, Kiagiadaki, Hodjarova, Karagianni, & Thermos, 2006). Therefore the amount released from SST hydrogels investigated in this study may be of clinical relevance, however this warrants further investigation using cell culture studies and/or in-vivo experiments.

Given the above considerations, formulation strategies were explored in the following chapters to extend the duration of release as well as to increase the cumulative amount released in comparison to the self-assembled SST hydrogels studied in this chapter. The next chapter (Chapter 3) investigates a hydrogel formulation of SST in a polymeric carrier while Chapter 4 explores two different methods to manufacture microparticles encapsulating SST with the same intent of extending duration and amount of SST released.

CHAPTER 3: FORMULATION OF SOMATOSTATIN AND HPMC HYDROGELS

3.1. Introduction

Hydrogels are described as cross-linked networks of hydrophilic polymers capable of retaining large amounts of water yet remaining insoluble and maintaining their three-dimensional structure. Hydrogels have been studied for a wide range of biomedical and pharmaceutical applications, including contact lenses, tissue engineering, diagnostics, drug delivery, vascular prostheses, and coating for stents and catheters. There are a number of comprehensive reviews on hydrogels available in the literature (Censi, Di Martino, Vermonden, & Hennink, 2012). The hydrophilic polymers used to create hydrogels need to be physically and/or chemically cross-linked to prevent dispersion. Hydrogels can be prepared from natural and synthetic polymers and can consist of homopolymers, copolymers, and interpenetrating or double polymeric networks (Censi, et al., 2012).

The high water content and soft nature of hydrogels render them as biocompatible materials. They are similar to natural extracellular matrices and minimize tissue irritation and cell adherence (Park & Park, 1996). Their porous structure and high water content allow them to accommodate high loads of water-soluble compounds, including therapeutically active proteins and peptides. Unlike other delivery systems (microparticles, emulsions, etc.), where preparation conditions are sometimes detrimental to proteins due to the use of organic solvents and protein denaturing processes, like homogenization, exposure to interfaces, and shear forces, hydrogel preparation procedures are beneficial in preserving protein stability. Finally, proteins have a limited mobility or are immobilized in the hydrogel network, which is favorable for preservation of their mostly fragile 3D structure. All these unique properties of hydrogels have raised increasing interest in their use as reservoir systems for proteins that are intended to be released from the hydrogel matrix in a controlled fashion to maintain a therapeutic effective concentration of the protein drug in the surrounding tissues or in the circulation over an extended period of time. Proteins can be physically incorporated in the hydrogel matrix, and their release is governed by several mechanisms, such as diffusion, swelling, erosion/degradation, or a combination of these mechanisms (Censi, et al., 2012).

Changes in the concentration, molecular weight or polymer architecture of the hydrogel allow fine-tuning of protein release. Other strategies to tailor drug release from hydrogels exist; these rely on reversible protein–polymer interaction or encapsulation of the protein in a secondary delivery system such as micro- or nanoparticles dispersed in the hydrogel network (Holland, Tabata, & Mikos, 2005; Singh, Suri, & Roy, 2009).

In addition, injectable hydrogels that can be administered in a minimally invasive manner are of interest due to patient acceptance. Syringeability, defined as the ability to pass easily through a hypodermic needle or transfer from a vial prior to injection, and ease of delivery for pre-formed hydrogels are desirable.

Cellulose derivatives such as methylcellulose (MC), carboxymethylcellulose sodium (CMC) and hydroxypropyl methylcellulose (HPMC) are naturally occurring polymers with thermoresponsive properties. The structure of Methocel 65 HG[®] used in this study is provided in Figure 3.1. These are commercially available in various products for the treatment of dry eyes, including Celluvisc[®] (CMC sodium 1%), Genteal[®] gel (HPMC 0.3%) and PAA HPMC gel[®] (HPMC 0.3%). Aqueous solutions of MC and HPMC form gels at lower concentrations (1–10% w/w) (Sarkar, 1979) and temperatures of 40–50 °C and 75–90 °C, respectively (Pal, Paulson, & Rousseau, 2013). The presence of salts or a higher degree of cellulose ether substitution decreases the phase transition temperature of cellulose derivatives (Ambrosio, Demitri, & Sannino, 2011; Bain, et al., 2012). The inclusion of salts and alterations in concentration influence sol-gel transition temperature of MC (Arvidson, et al., 2013; Xu, Li, Zheng, Lam, & Hu, 2004), with the transition occurring at a lower temperature in the presence of certain salts (salt-assisted) and at higher temperatures in the presence of others (salt-suppressed).

Preclinical studies have been done with anti-VEGF agents bevacizumab and ranibizumab incorporate in *in situ* gelling formulations using polymers like hyaluronic acid-dextran (Yu, Lau, Lo, & Chau, 2015), alginate-chitosan hydrogel (Osswald & Kang-Mieler, 2016), silk-based hydrogels (Lovett, et al., 2015) and diels-alder hydrogels (Kirchhof, et al., 2015). There is strong interest in peptide delivery through hydrogels for the reasons outlined above, with special focus on stimuli sensitive delivery (Mandal, et al., 2018).

In this study, a hydrogel of somatostatin in HPMC was formulated in an attempt to modulate the release of somatostatin monomers compared to the self-assembled hydrogels that were studied in Chapter 2. The release kinetics were studied using the protocol described in Chapter 2 and the gels were further characterised by rheological studies, transmission electron microscopy (TEM) and FTIR.

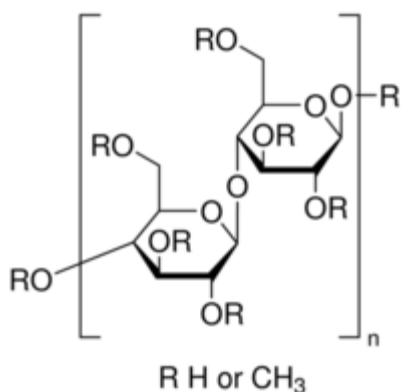


Figure 3.1: Chemical structure of Methocel 65 HG[®] with 5.5-7.5% hydroxypropyl substitution (Reference: Sigma-Aldrich product information)

3.2 Materials and methods

3.2.1 Materials

Somatostatin-14 of sequence Ala-Gly-Cys-Lys-Asn-Phe-Phe-Trp-Lys-Thr-Phe-Thr-Ser-Cys (cyclic, MW=1638 Da) was purchased as an acetate salt from Polypeptide Laboratories (Sweden). According to the Manufacturer's certificate of analysis, the peptide purity is 99.6%.

Methocel 65 HG[®], sodium azide and all the chemicals used to prepare the simulated lachrymal fluid were purchased from Sigma Aldrich (St Louis, MO, USA). Milli-Q water was used in the preparation of all media. The composition of simulated lachrymal fluid can be found in Chapter 2, Table 2.1. (Ceulemans & Ludwig, 2002).

3.2.2 Methods

3.2.2.1 Preparation of HPMC gel

HPMC 3% w/w gel was prepared by dispersing the appropriate quantity of Methocel 65 HG powder into hot (freshly boiled) water. Powder was added to the water gradually to avoid clumping. Sodium azide was added to a concentration of 0.01% w/v to prevent any bacterial growth. The suspension was then refrigerated at 4°C for 7 days to allow the entanglement network to relax and for aging to occur.

3.2.2.2 Rheological characterization of blank HPMC gels and SST 5% w/w in HPMC hydrogels

The aging process of the HPMC 3% w/w and 6% w/w gels was characterised over the course of 15 days for the 3% w/w gel and 19 days for the 6% w/w gel. The rheological properties of all the gels investigated were determined using an ARG2 Rheometer (TA Instruments, UK). A stainless steel

40mm parallel plate geometry with gap of 500 μm was employed. The removal of the gels was done as gently as possible from the containers to minimize disruption of the structure. The gels were then given an hour to equilibrate prior to analysis. A solvent trap was used to eliminate the evaporation of water from the gel periphery. Oscillation amplitude sweeps were used to confirm the linear viscoelastic region. Frequency sweeps (0.1-100 Hz) at 20°C were then conducted. In addition for the SST 5% in HPMC hydrogels, temperature sweeps (1 Hz, 20°C to 80°C) were conducted. Measurements were performed in triplicate.

3.2.2.3 Preparation of SST 5% w/w in HPMC hydrogels

After the aging of the blank HPMC 6% gels at 4°C for 7 days, 0.5g of SST 5% w/w and HPMC 3% w/w gels were prepared. This was done by adding a 0.25 g solution of SST in Milli-Q water to 0.25g of HPMC 6% w/w gel in an Eppendorf tube. The SST 5% w/w in HPMC 6% w/w gels were prepared by diluting HPMC 8% w/w gel to yield the final concentration. The mixture was then vortexed until thoroughly mixed and then allowed to equilibrate at 4°C for an additional 7 days.

3.2.2.4 Investigation of SST conformation before and after exposure to simulated lachrymal fluid

Based on the release profile of SST from the hydrogels, FTIR characterization was performed on Days 1 and 7 after preparation of the SST 5% HPMC hydrogels and during the release studies every 24 hours for up to 4 days.

ATR-FTIR spectra were measured using a Tensor II Bruker Spectrometer equipped with an ATR attachment. The spectra are shown to result from the average of 32 scans. Each spectrum was scanned over the range of 4000-1000 cm^{-1} , using a 4 cm^{-1} resolution. All spectra were baseline corrected and the water signal was removed by subtraction of respective solvent (blank) spectrum recorded the day of the experiment. Spectragryph 1.2 was used to obtain the second derivative of the spectrum.

3.2.2.5 Morphological characterization of hydrogels

Transmission electron microscopy (TEM) was used to characterise the morphology of the hydrogels. Negative staining by uranyl acetate was performed to contrast the nanostructures, using the same protocol as reported in van Grondelle et al. 2007. Stained samples deposited on formvar and carbon-coated 200 mesh copper grids (Proscitech, Australia) were examined with a JEOL 1010 transmission electron microscope operating at 100 kV.

3.2.2.6 Release study of somatostatin monomers from HPMC hydrogels

Release medium (SLF; 500 μ L) with 0.01% w/v sodium azide was placed directly on top of the gels which were prepared in 1.5mL Eppendorf tubes. The Eppendorf tubes were then closed and sealed with Parafilm. The assembled units were then placed in a water bath at 37 °C, agitated at 30 RPM. At various time intervals (1, 2, 4, 6, 24, 48, 72, 96h and every 24 hours up to day 10), the receptor compartment/medium (500 μ L) was removed for analysis by HPLC. The receptor medium was replenished with fresh medium immediately. Given the high solubility of somatostatin in aqueous media (> 70mg/mL) and the replacement of the whole buffer volume at each sampling point, this approaches sink conditions *in vivo* in the ocular environment with tears or blood flow. The units were reassembled and replaced in the shaking water bath. The experiments were performed in triplicate.

3.2.2.7 Mass spectrometry of released samples investigating SST conformation upon release

Mass spectrometry was performed on the release samples from SST 5% w/w in HPMC 6% w/w at Release Day 1 and Release Day 10 to confirm that the native structure of somatostatin released from the hydrogels was preserved. The samples were compared to a freshly-made solution of SST 5% w/w in water. Bruker AutoFlex Matrix Assisted Laser Desorption/Ionisation (MALDI) Time of Flight (TOF) - Mass Spectrometer (MALDI-TOF-MS) was used to perform the experiment. Sample size of 1 μ L was spotted onto the target.

3.3 Results and discussion

3.3.1 Rheological characterization of aging process of blank HPMC gels

The amplitude sweeps of the HPMC 3% w/w and 6% w/w gels show that a torque of 50 μ N.m is within the linear viscoelastic region of the gels at all time points tested. The frequency sweeps of both the HPMC 3% w/w and 6% w/w gels show a progressive decline of the G' (storage modulus) at higher frequencies indicating that the gels tend to stiffen over longer time periods (Figure 3.3). There is an increase in the G' of the HPMC 3% gel until day 7 after which it remains stable until day 15 (Figure 3.2). This data shows that the entanglement network is not sufficiently relaxed and requires 7 days for aging to occur. Hence, the gels are aged for 7 days before and after mixing with somatostatin. The G' of the HPMC 6% w/w gel on the other hand was unstable although displaying an upward trend until day 14 (Figure 3.2). The HPMC 6% w/w gels were aged in the same way as the HPMC 3% w/w gels as the total aging time before and after mixing in somatostatin adds up to 14 days. The aging of HPMC gels has been documented (Hakert, Eckert, & Müller, 1989) and it has been

shown that the rheological behaviour of HPMC gels in water does not change after aging for up to 140 days (Daneluzzi). The purpose of allowing the HPMC gels to be fully aged is to eliminate the impact of the aging process on the release of somatostatin monomers.

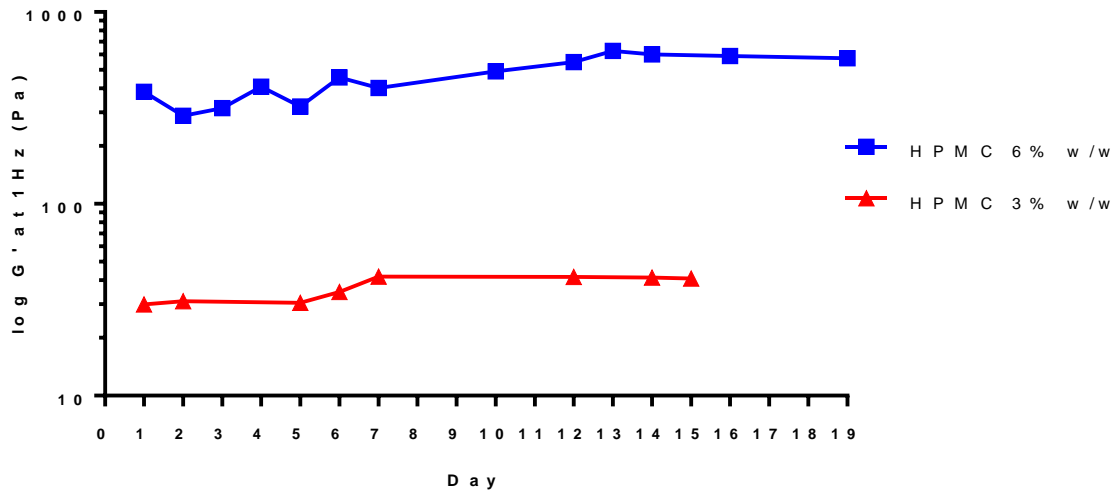


Figure 3.2: Changes in G' (storage modulus) of HPMC 3% w/w and 6% w/w gels during the aging process

3.3.2 Rheological characterization of somatostatin-loaded HPMC hydrogels

Rheological studies as described in section 3.2.2.2 were conducted on SST 5% w/w water solutions, HPMC 3% w/w and 6% w/w gel and SST 5% w/w in HPMC 3% w/w and 6% w/w gels on Days 1 and 7 after being prepared and every day for the first 4 days of release. The amplitude sweeps show that a torque of 50 $\mu\text{N}\cdot\text{m}$ falls within the linear viscoelastic region for all the samples tested. Therefore, subsequent studies were performed at 50 $\mu\text{N}\cdot\text{m}$. The frequency sweeps show a progressive decline in the G' (storage modulus) of the blank HPMC 3% w/w and 6% w/w gels and SST 5% w/w in HPMC 3% w/w and 6% w/w gels. This indicates that the gels are stiffer at longer time frames (low frequencies) and less at shorter time frames (higher frequencies). This means that the inclusion of SST in the HPMC gel does not alter this property of the HPMC gels. The frequency sweeps of the SST 5% w/w aqueous solution on the other hand shows an increase in G' as the frequency increases. This finding supports data presented in Chapter 2 of the frequency sweeps done on SST aqueous solutions and those in the presence of electrolytes. The flow sweeps indicate that all samples tested are shear-thinning and will flow more easily with the application of shear as the viscosity falls. This is

a desirable property should the formulation be administered as an injection. The temperature sweeps show that the gels with HPMC undergo thermogelation *ca.* 65°C. There is an increase in G' from 65°C onwards. This is a characteristic property of HPMC matrices (Joshi, 2011). This is not observed with the SST 5% w/w aqueous samples where there is a decline in G' with increasing temperatures. This is consistent with materials that do not undergo thermogelation. A comparison of the G' of the SST 5% w/w in HPMC 3% w/w gels at 1Hz at the different time points tested show that the G' initially decreases as the gel is diluted with the addition of the SLF on top then significantly increases on Day 4 of release. This correlates with the end of the release of somatostatin monomers as detected by HPLC based on our release data. This may be attributed to formation of nanofibrils, resulting in an increase in the stiffness of the gel. The same applies to the SST 5% w/w aqueous samples where the G' is highest on Day 4 of release. Data from Rai et al (Rai, et al., 2017) shows that SST in the presence of electrolytes forms stiffer hydrogels which explains the highest G' of the sample exposed the longest to electrolytes. For all blank HPMC samples, the trend is opposite with the lowest G' after 4 days of release. This can be attributed to the dilution of the HPMC hydrogels with the presence of SLF on top removed and replaced every 24 hours. The SST 5% w/w in HPMC 6% w/w gels show the same trend in the change in G' as the SST 5% w/w in HPMC 3% w/w gels. Although there is an initial decrease in G' upon exposure to SLF when the release study is commenced and an increase on Day 4 of the release, these changes are smaller in magnitude. This can be attributed to the higher stiffness of the SST 5% w/w in HPMC 6% w/w gels (G' of 510.4 Pa) at the starting point of release studies (Day 7) compared to a G' of 96.8 Pa of the SST 5% w/w in HPMC 3% w/w gels at the same time point. The difference in magnitude of G' of the SST 5% w/w in HPMC 3% w/w gels between release day 3 and 4 was 927 Pa whereas for the SST 5% w/w in HPMC 6% w/w gels the difference was 178 Pa. When HPMC matrix comes in contact with water, the polymer begins to swell and forms a protective gel around the drug content, leading to a sustained release of drugs (J. L. Ford, 1999). The stiffer 6% w/w HPMC matrix would be more resistant to the diluting effects of the SLF and provide a stronger barrier to the interaction of the electrolytes in the SLF with the entrapped somatostatin. This may be a possible reason for the longer duration of release (over 10 days) compared to 4 days for the SST 5% w/w in HPMC 3% w/w gels.

In similar work, Liang and co-workers (Liang, et al., 2010) investigated the potential ocular application of self-assembled peptide containing a RGD (arginine-glycine-aspartic acid) sequence as well as a hydrophobic FMOC tail in the rabbit eye. The G' of the hydrogel studied was between 200-250 Pa. The G' of the self-assembled hydrogel studied falls between the G' of the SST 5% w/w in HPMC 6% w/w hydrogel and SST 5% w/w in HPMC 3% w/w in our work. Subconjunctival and intracamerular injection of the peptide hydrogel into the rabbit eye showed that the biocompatibility was

similar to that of commercial sodium hyaluronate injection. A more extensive discussion of similar hydrogels in the literature is found in Chapter 2.

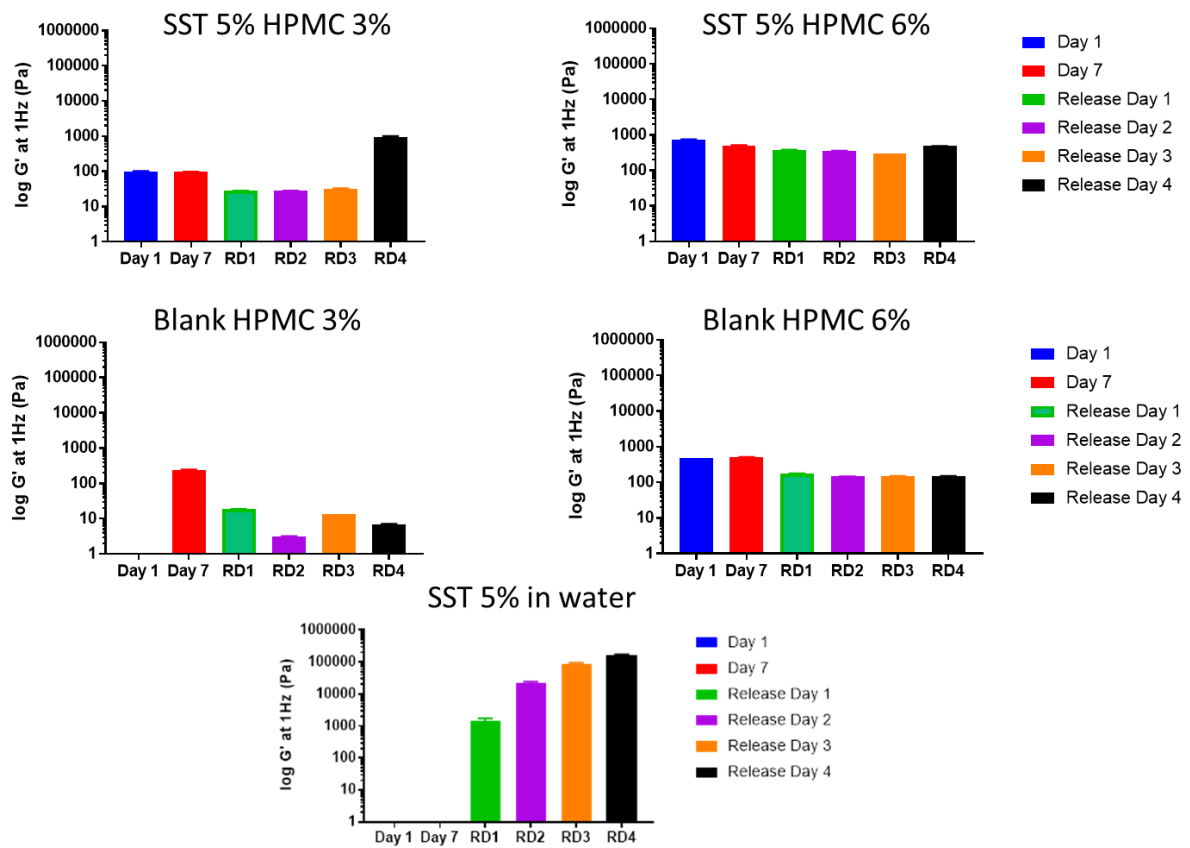


Figure 3.3: Comparison of the G' (storage modulus) of the different gels tested at Days 1, 7 and days 1-4 after exposure to SLF in release conditions ($n=3$; error bars = SD)

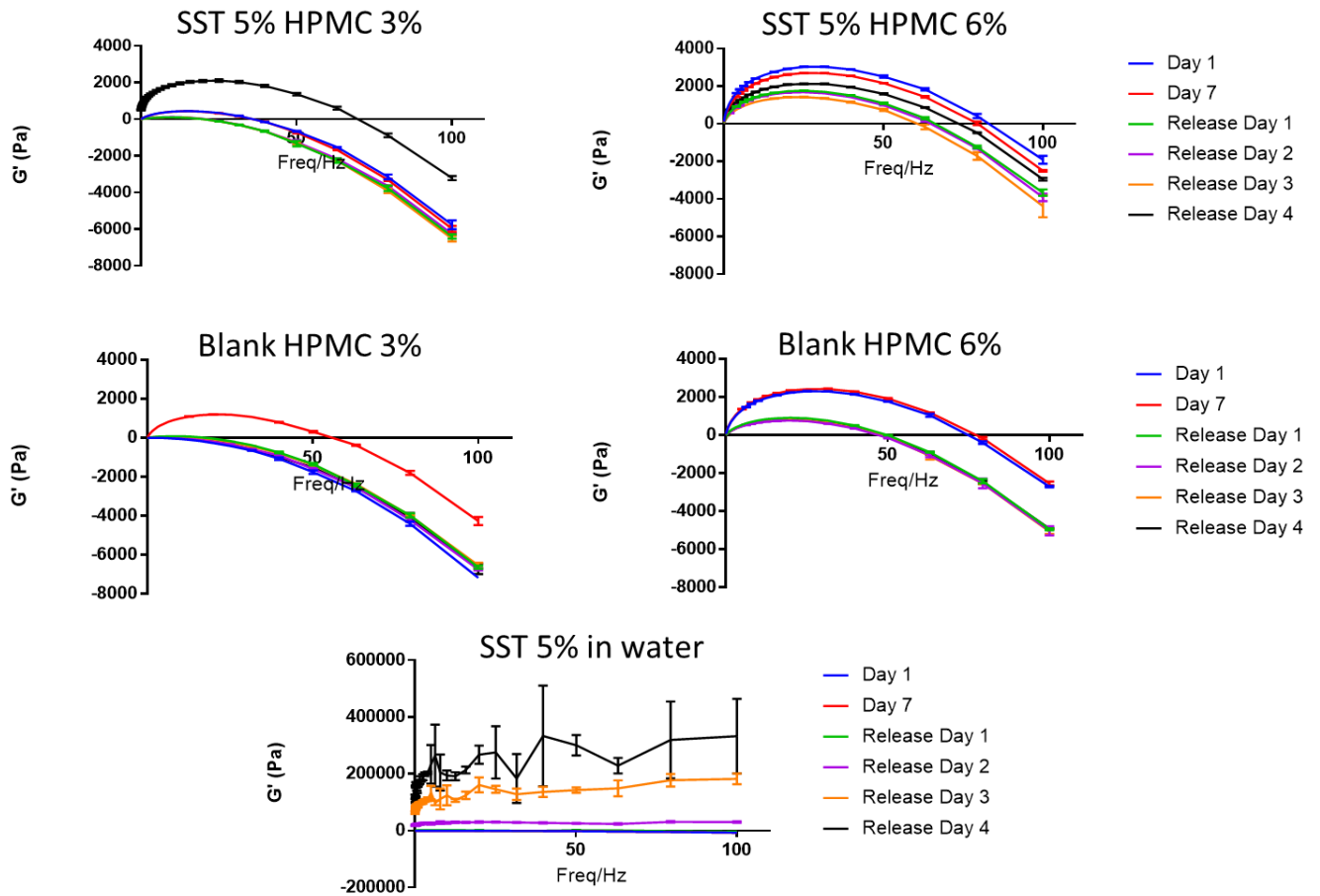


Figure 3.4: Comparison of the frequency sweeps of the different gels tested at Days 1, 7 and days 1-4 after exposure to SLF in release conditions (n=3; error bars =SD)

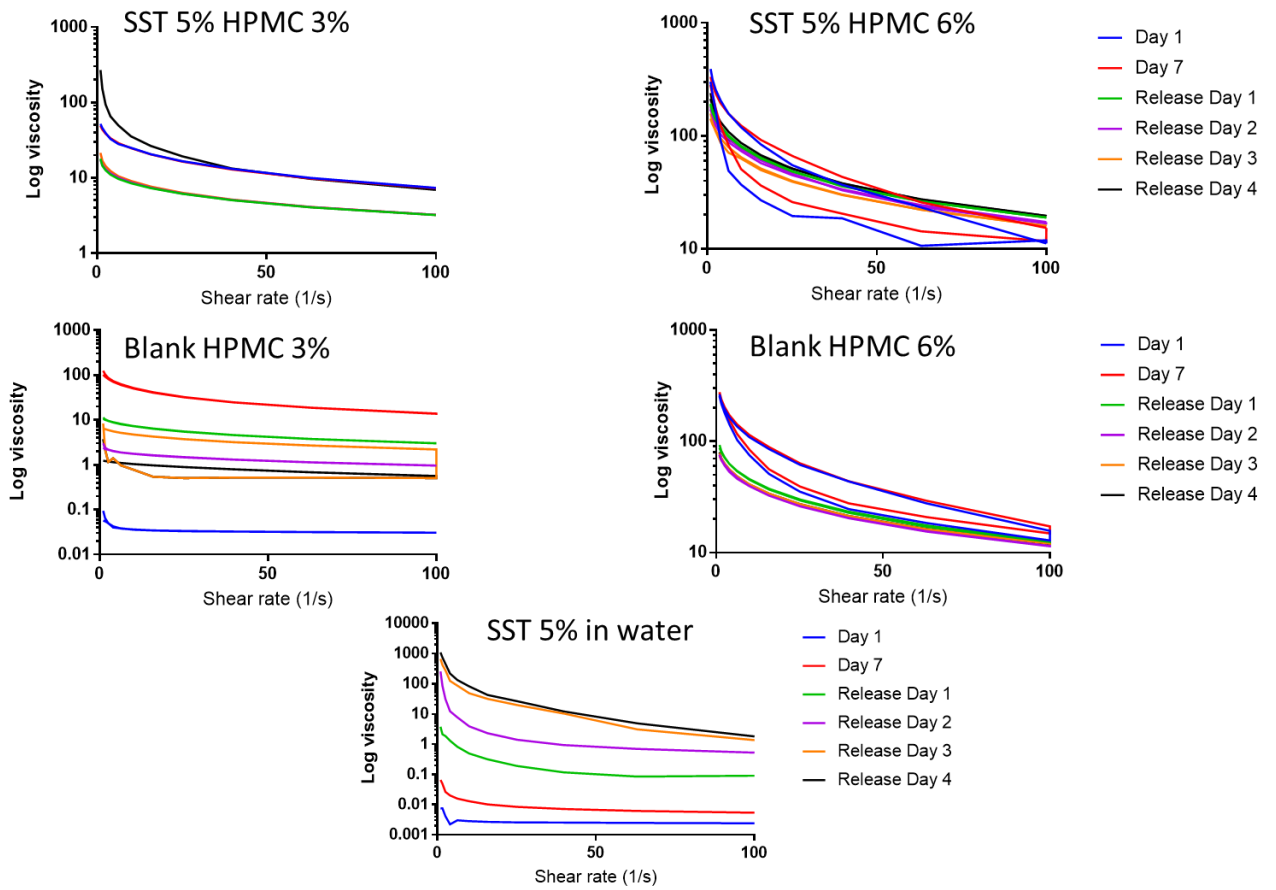


Figure 3.5: Comparison of flow sweeps of different gels tested at Days 1, 7 and days 1-4 after exposure to SLF in release conditions (n=3)

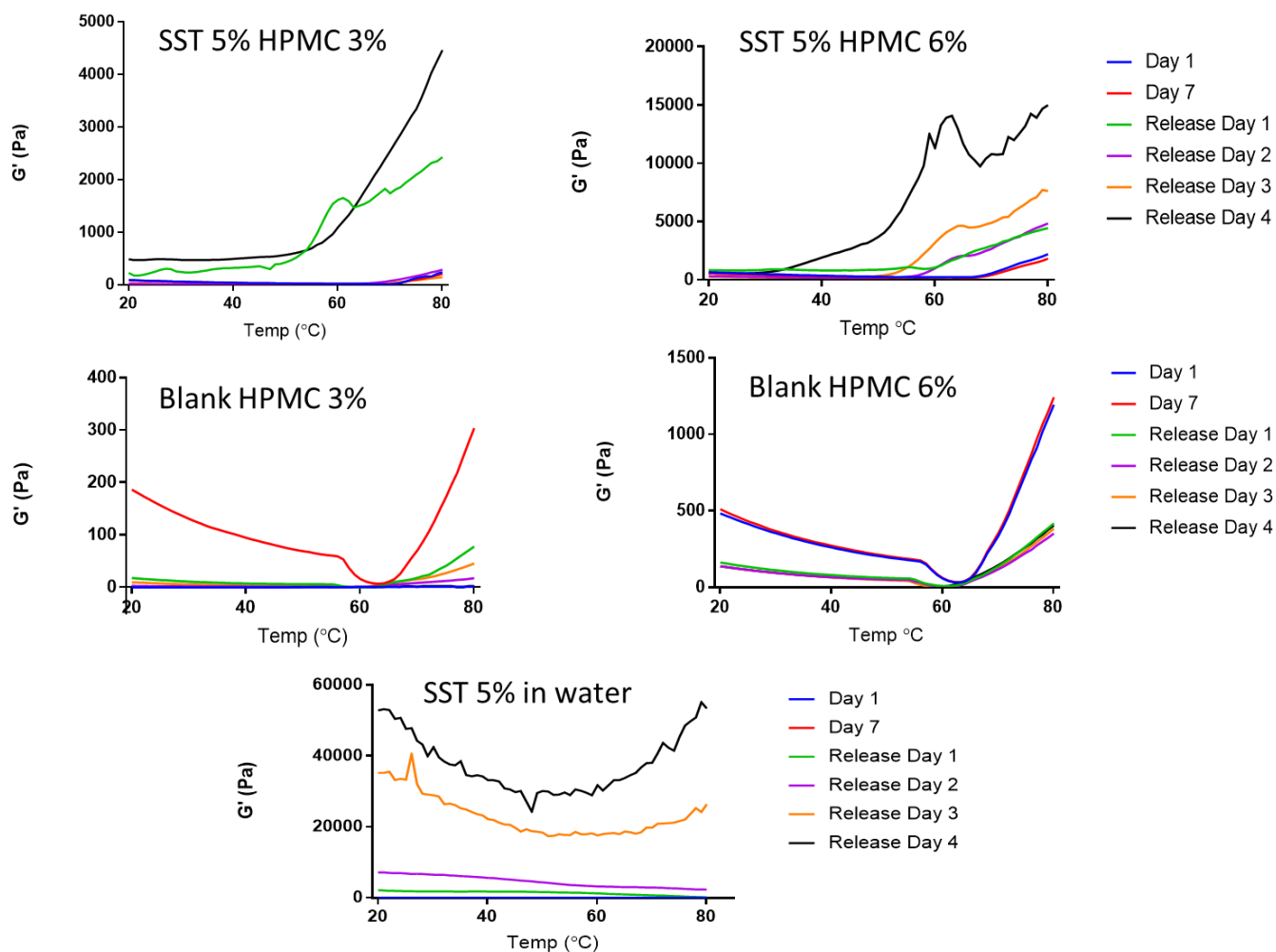


Figure 3.6: Comparison of temperature sweeps of different gels tested at Days 1, 7 and days 1-4 after exposure to SLF in release conditions (n=3)

3.3.3 Investigation of SST conformation before and after exposure to simulated lachrymal fluid (FTIR characterization of hydrogels)

The SST 5% in HPMC 3% and 6% were characterized on Days 1 and 7 after being prepared and every day for the first four days of release studies. This was performed to investigate the transition of SST from a random coil conformation to structured β -sheets.

The analysis was focused on amide I vibrations ($1600\text{--}1700\text{ cm}^{-1}$), which are attributed to vibrational stretching modes of the backbone carbonyl groups. The corresponding wavenumbers can be assigned to different strengths/types of hydrogen bonds and can indicate secondary structure types (Hiramatsu & Kitagawa, 2005; Krimm & Bandekar, 1986). The vibration at 1643 cm^{-1} is assigned to random conformations while the combination of vibrations around 1615 and 1675 cm^{-1} is attributed to antiparallel β -sheet secondary structure and the vibration around 1663 cm^{-1} to a turn secondary

structure. This combination is typical of a β -hairpin backbone conformation, which corresponds to the bioactive Somatostatin-14 conformation (Barth, 2007; Holladay & Puett, 1976; Holladay, Rivier, & Puett, 1977; W. van Grondelle, et al., 2007).

The FTIR data below (Figure 3.7) shows the SST becomes more structured once the gel is exposed to SLF. There are less of the random conformations and a transition to more structured organisations of the parallel and anti-parallel β -sheets. This has been discussed at length by Valery and co-workers (W. van Grondelle, et al., 2007). They have found that the self-assembly process of somatostatin is sensitive to the presence of electrolytes (such as those found in SLF). The self-association into higher structures and nanofibril lateral association is enhanced in the presence of electrolytes compared to in pure water. Our data supports the observations by Valery *et al.* Figure 3.8 is a secondary derivative plot which shows that the transition from a random coil conformation to structured β -sheets is hindered when somatostatin is entrapped within the HPMC matrix, thus delaying the formation of nanofibrils.

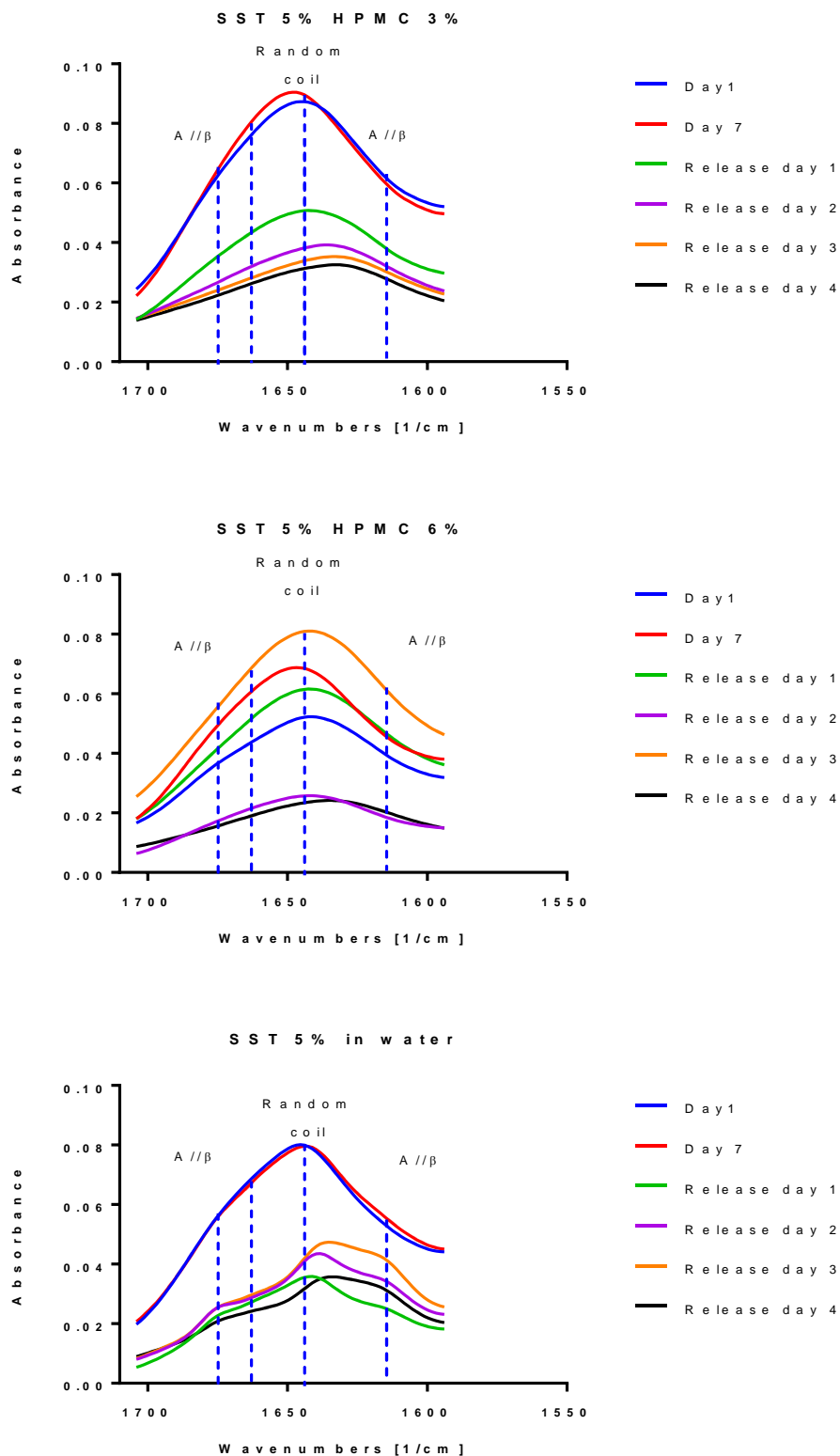


Figure 3.7: FTIR data of the transition in conformation from random coil to more structured β -sheet conformations for SST 5% in water, SST 5% w/w in HPMC 3% w/w and SST 5% in HPMC 6% w/w upon exposure to release conditions in contact with SLF. Water/SLF spectrum was subtracted.

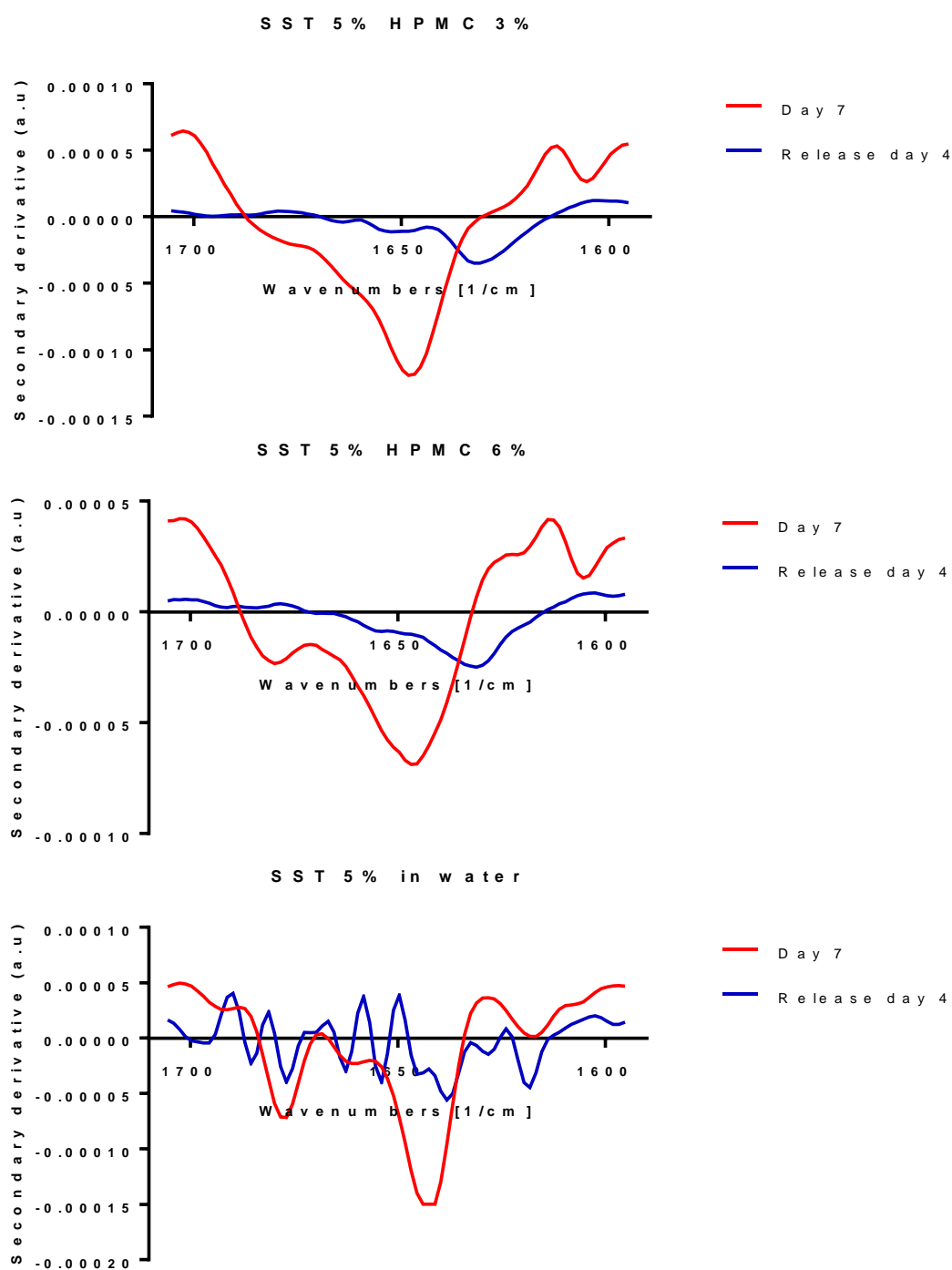


Figure 3.8: Secondary derivative plots of FTIR data comparing the difference in structure between Day 7 and Day 4 of release after exposure to SLF for SST 5% w/w in water, SST 5% w/w in HPMC 3% w/w and SST 5% w/w in HPMC 6% w/w. Water/SLF spectra has been subtracted.

3.3.4 Morphological characterisation of hydrogels

SST 5% w/w in water, SST 5% w/w in HPMC 6% w/w and blank HPMC 6% w/w gels were observed by transmission electron microscopy at Days 1 and 7 and Day 4 of the release study after exposure to SLF. The method of preparation of the stained gels is as described above and is the same as used for morphological characterization of the self-assembled SST hydrogels in Chapter 2.

There were no structures observed in SST 5% in water at Day 1. This is consistent with our observations from Chapter 2 that in pure water, self-assembly of somatostatin takes about a week.

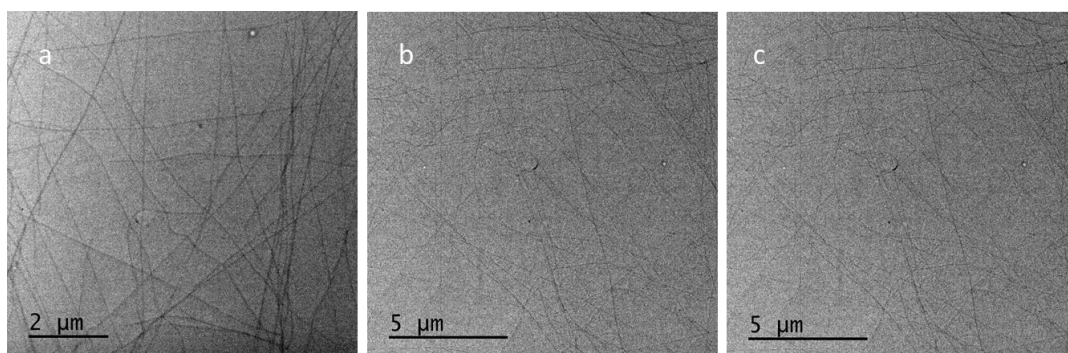


Figure 3.9: Transmission electron micrographs of SST 5% in water at Day 7 (a) magnification 2000x (b and c) magnification 1200x.

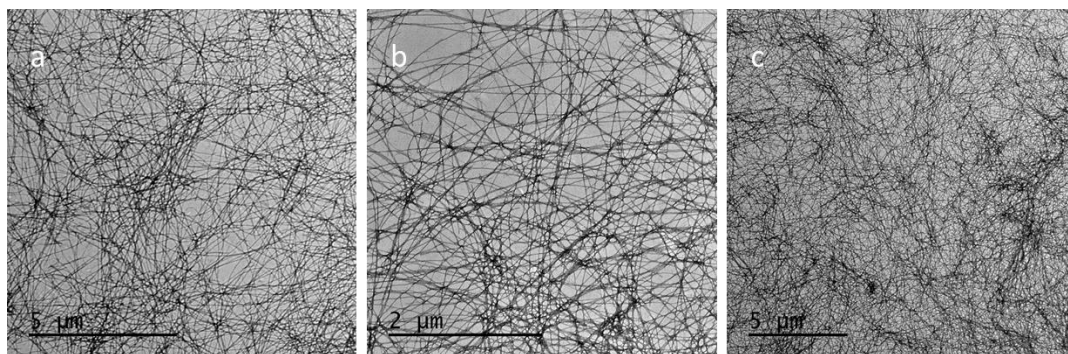


Figure 3.10: Transmission electron micrographs of SST 5% in water at Release Day 4 (a) magnification 1500x (b) magnification 4000x and (c) magnification 1000x.

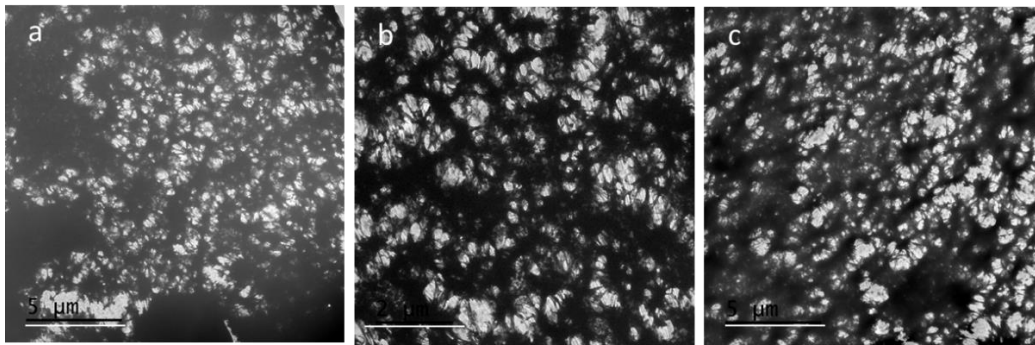


Figure 3.11: Transmission electron micrographs of blank HPMC 6% w/w at Release day 4 (a) magnification 1000× (b and c) magnification 2000×. Scale bars (a and c) 5 μm and (b) 2 μm.

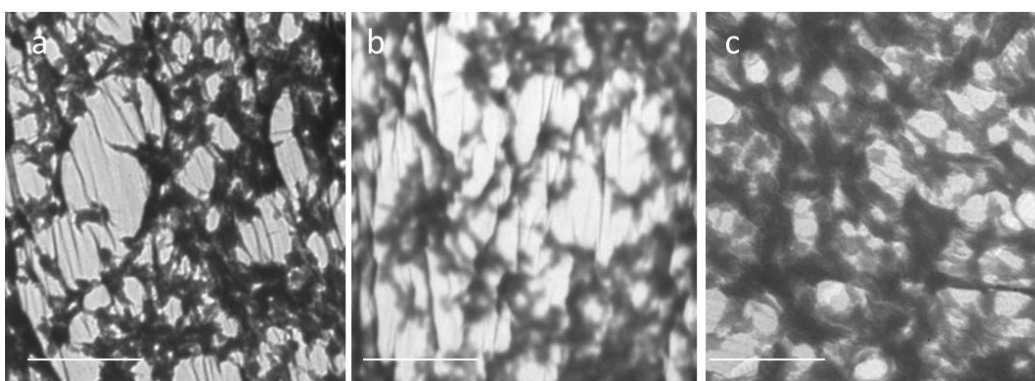


Figure 3.12: Transmission electron micrographs of SST 5% w/w in HPMC 6% w/w at Release day 4 (a and c) magnification 600× and (b) magnification 750×. Scale bars (a and c) 10 μm and (b) 5 μm.

Figure 3.9 demonstrates that at Day 7 prior to release studies, self-assembly of somatostatin into nanofibrils in SST 5% w/w in water samples has begun. After exposure to SLF on release Day 4, the extensive network of nanofibrils is apparent as per Figure 3.10. The TEM micrographs of blank HPMC 6% w/w consist of a thick entanglement network that is dense and heavily stained with uranyl acetate. It was a challenge to perform TEM on the HPMC-containing samples as the gels were highly viscous. The SST 5% w/w in HPMC 6% w/w and blank HPMC 6% w/w gels on day 7 could not be viewed as the gels were too heavy for the grids and the mesh was torn or they were stained too strongly for any structures to be differentiated. However, some images of the SST 5% w/w in HPMC 6% w/w on release day 4 were obtained although in most of the grids the mesh was torn. Figure 3.12 demonstrates the presence of a network similar to the blank HPMC 6% w/w gels although less dense. There are no apparent fibrillar structures such as found in Figure 3.10.

Bodvik et al (Bodvik, et al., 2010) have studied the aggregation and network formation of HPMC using cryo-TEM, amongst other techniques. In comparison to methylcellulose which forms fibrillar structures, the bulkiness of the hydroxypropyl groups leads to the formation of globular aggregates in HPMC. The TEM images appear to support the hypothesis from the FTIR results that the presence of HPMC delays the nanofibril formation of somatostatin when exposed to electrolytes. However, it is impossible to make a definitive conclusion given the difficulties of characterising a thick hydrogel with TEM. Cryo-TEM, performed properly, may provide more information about the structural characteristics of the SST and HPMC hydrogels.

3.3.5 Release profile of somatostatin monomers from SST in HPMC hydrogels

The release study was conducted as described above on SST 5% w/w solution, SST 5% w/w in HPMC 3% w/w and HPMC 6% w/w gels. Conditions were kept the same for all samples. The SST 5% w/w solution reached a 100% release at 6 hours. The SST 5% w/w in HPMC 3% w/w gels released a total of 45.6% at 96 hours and there was no further release (no detectable peaks by HPLC) whereas the SST 5% w/w in HPMC 6% w/w gels continued to release a total of 37.6% at 10 days when the experiment was stopped, however, the release was ongoing.

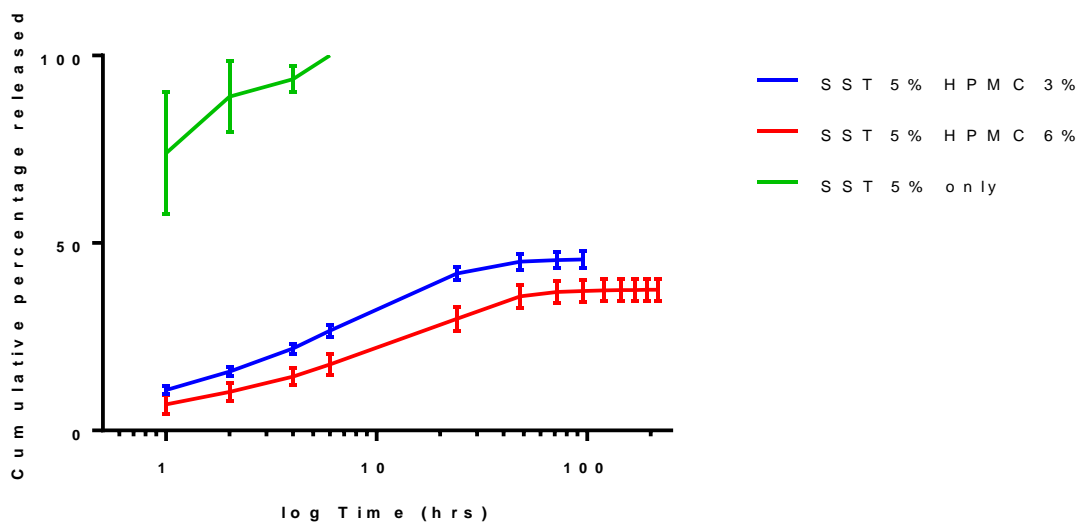


Figure 3.13: Comparison of the release profiles of SST 5% in water, SST 5% w/w in HPMC 3% w/w and SST 5% w/w in HPMC 6% w/w. (n=3, Error bars = SD)

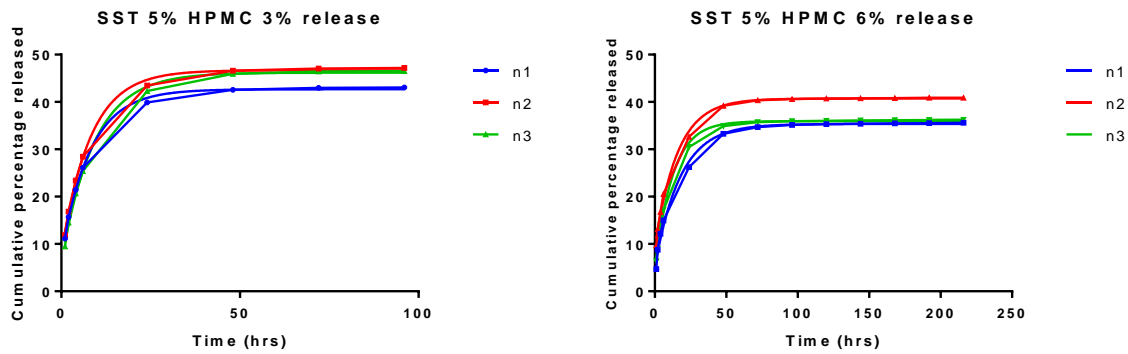


Figure 3.14: Release profiles of SST 5% w/w in HPMC 3% w/w and SST 5% w/w in HPMC 6% w/w gels fitted to hybrid model of release (equation 4.1) (n=3)

3.3.6 Release kinetics of SST 5% release from HPMC gels

Based on prior published work relating to a hybrid model of release (Rai, et al., 2017), the graphs were fitted to the equation below using GraphPad (version 7.02).

$$\text{Cumulative percentage released} = r + (R_{max} - r) \times (1 - e^{-kt}) \quad \text{equation 3.1}$$

Where

r = the cumulative percentage released when time is zero.

R_{max} = cumulative percentage released at infinite times.

k = the first-order release rate constant (diffusion)

t = time

and

$$t_{90} = \ln(100/90)/k \quad \text{equation 3.2}$$

where t_{90} is the time to release 90% of SST from the core of the gel and k is the first-order release rate constant (diffusion).

Table 3.1: The goodness of the fit (mean R^2) of the above model to the samples as well as the t_{90} (time to release 90% of SST from the core of the gel), k and R_{max} .

Gel tested	Mean $R^2 \pm SD$	Mean $k \pm SD$	Mean $R_{max.} \pm SD$	Mean $t_{90} \pm SD$
SST 5% HPMC 3%	0.998 ± 0.0002	0.118 ± 0.008	45.2 ± 2.19	19.6 ± 1.46
n= 3				
SST 5% HPMC 6%	0.997 ± 0.002	0.067 ± 0.013	37.3 ± 2.94	35.3 ± 6.29
n= 3				

As can be seen from Table 3.1, the release kinetics of the somatostatin monomers from the SST in HPMC gels fit well (R^2 values between 0.997-0.998) to the proposed hybrid model of release. The time taken for 90% of SST to be released from the core (t_{90}) of the SST 5% w/w HPMC 3% w/w gels averages 19.6 hours while the t_{90} for the SST 5% w/w HPMC 6% w/w gels averages 35.3 hours. This is consistent with the observation that a higher concentration of HPMC produced gels that could release somatostatin for 10 days compared to 4 days for the lower HPMC concentration hydrogels. It is hypothesized that the swelling of the HPMC matrix when in contact with the SLF acts as a barrier to the ease of interaction of the electrolytes in the SLF with SST. This is more effective when the G' of the HPMC matrix is higher, as in the case of the SST 5% w/w in HPMC 6% w/w gels which have a G' of *ca.* 500 Pa at day 7 compared to G' *ca.* 100 Pa of the SST 5% HPMC 3% w/w gels (Figure 3.4).

The initial higher percentage of release for both sets of gels tested can be attributed to the diffusional release of SST monomers adsorbed on the surface of the hydrogels. However, with continued release conditions, erosional release would come into play with the expectation that the more rigid HPMC 6% w/w matrix would erode more slowly than the HPMC 3% w/w matrix. Results in Chapter 2 have shown that release of SST monomers becomes undetectable once nanofibrils are formed which are stable in the presence of electrolytes (W. van Grondelle, et al., 2007). This is likely to be the explanation for no further detected release from the SST 5% HPMC 3% w/w gels after 4

days. The SST 5% w/w HPMC 6% w/w gels offer a formulation candidate that delays SST nanofibril formation in the presence of electrolytes and extends the duration of release.

In comparison to the self-assembled somatostatin hydrogels studied in Chapter 2, these hydrogels have demonstrated a longer duration of release of somatostatin monomers. Although the SST 5% w/w in water gel released *ca.* 38% SST monomers in SLF at 9 hours (Chapter 2, Table 2.2), the entrapment of SST in HPMC has extended the duration of release to 4 and 10 days (experiment stopped) with a similar cumulative amount released. The concentrations released are in the order of 10^{-5} M, which fall in the upper range of concentrations reported to be effective in cell and animal studies. Chapter 5 discusses the results of such studies in more detail.

Such extended release has been previously reported with polymers of erosional degradation. For example, Misra and co-workers (Misra, et al., 2009) synthesized a series of water-based small dimensional hydrogel systems composed of NIPAAm monomer and Dex-lactateHEMA macromer using UV photopolymerization at room temperature. These thermoresponsive hydrogels were hydrolytically degradable and were able to load insulin with up to 98% loading efficiency during synthesis. The hydrogels achieved one week of insulin release which involved both diffusion and degradation mechanisms of the hydrogels.

Comparing our data to an extended release self-assembled hydrogel, the somatostatin analogue, lanreotide, is formulated as a supersaturated aqueous solution in a ready-to-use prefilled syringe for deep subcutaneous injection under the trade name Somatuline Autogel®. It is administered once every 28 days (Castinetti, Saveanu, Morange, & Brue, 2009; Roelfsema, Biermasz, Pereira, & Romijn, 2008). The injection exhibited linear pharmacokinetic profiles in healthy subjects with a half-life of about 21-22 days (Hu & Tomlinson, 2010). Although the longest duration of release exhibited in this study was 10 days *in vitro*, further work *in vivo* remains to be investigated.

On the other hand, Pochan and Schneider (Branco, et al., 2009) studied the release of probes of different sizes from a class of self-assembling peptides that undergo triggered hydrogelation in response to physiological pH and salt conditions (pH 7.4, 150 mM NaCl) to form mechanically rigid, viscoelastic gels. It was found that the mechanism of release was by solely by diffusion and dependent on the size of the probe. The full release from these hydrogels ranged from days to months, increasing with an increase in the size of the probe. This is in contrast to our SST in HPMC hydrogels where erosion plays a role in the release of SST monomers, particularly in the later stages of release.

A commercial example of an *in situ* gelling thermosensitive hydrogel for delivery of a glycoprotein is ReGel® (made up of PLA-PEG-PLGA triblock copolymer). It was used to deliver commercially available interleukin-2, proleukin (Chiron®) in a depot formulation. The fully bioactive protein was released in a 3–4-day period and weekly administration in animal models improved tumor stasis and survival and was purported to have negligible side effects as compared to conventional interleukin-2 administration (Rathi, Zentner, & Jeong, 2000).

In this work, we have shown that extended release of somatostatin, which is otherwise challenging to deliver due to its short half-life and self-assembly in the presence of electrolytes, is possible via entrapment in HPMC. This formulation retains the advantages of hydrogels as previously discussed in Section 3.1 and having the potential to be delivered via topical or intra-ocular administration, pending animal studies.

3.3.7 Mass spectrometry of released samples investigating SST conformation upon release

Mass spectrometry was performed on the release samples from SST 5% w/w in HPMC 6% w/w at Release Day 1 and Release Day 10 as described above. This was done to confirm that the native structure of somatostatin released from the hydrogels was preserved. The samples were compared to a freshly-made solution of SST in water. The mass spectra revealed that the native structure of somatostatin was preserved upon release from the HPMC gel matrix.

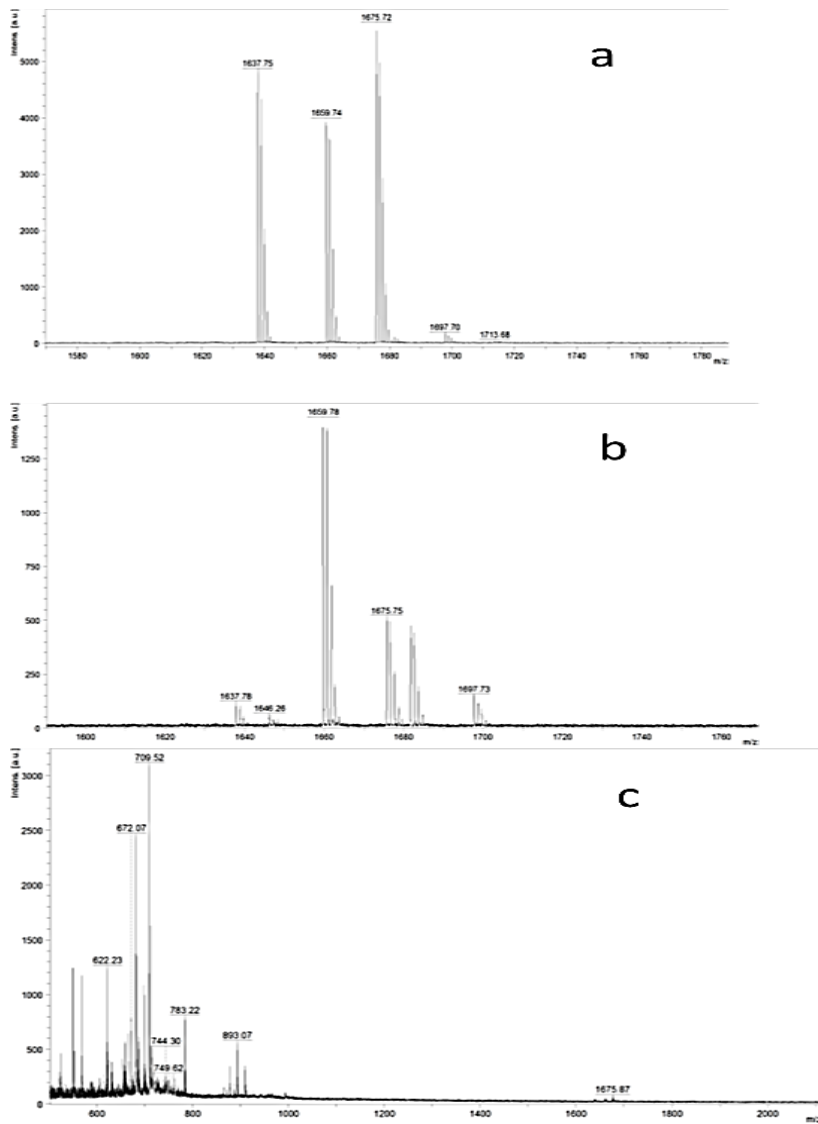


Figure 3.15 Mass spectra of (a) SST standard (b) Release Day 1 sample from SST 5% w/w in HPMC 6% w/w and (c) Release Day 10 sample from SST 5% w/w in HPMC 6% w/w. Note: the SST peak in spectra (c) is very small reflecting the amount released at Day 10.

3.4 Conclusion

A hydrogel formulation of somatostatin in a higher concentration of HPMC (6% w/w) that could release somatostatin for 10 days compared to 4 days for the lower HPMC (3% w/w) concentration was developed and characterized. The total cumulative percentage released from these hydrogels was similar to that from a SST 5% w/w in water hydrogel but over a period of days rather than hours. A release model was developed that fits well to the release profile of somatostatin from the hydrogels. Here, we have a formulation candidate that delays somatostatin nanofibril formulation in

the presence of electrolytes and extends the duration of release. Hence, the SST 5% w/w in HPMC 6% w/w hydrogels were chosen to proceed with safety and efficacy tests on an in vitro cell line.

CHAPTER 4: PREPARATION AND CHARACTERIZATION OF SOMATOSTATIN

MICROPARTICLES

4.1 Introduction

4.1.1 Microparticles

4.1.1.1 Rationale for use of microparticles

Delivery of a protein drug may require multiple daily administrations to achieve therapeutic efficacy. In order to improve patient compliance and convenience, sustained release dosage forms have been developed (Cohen, Yoshioka, Lucarelli, Hwang, & Langer, 1991; Leach, et al., 2005). In the last three decades, many therapeutic proteins and peptides have been microencapsulated in biodegradable polymers, mainly poly(lactic acid) (PLA), poly(glycolic acid) (PGA), and poly(lactic-co-glycolic acid) (PLGA) (Lam, Duenas, Daugherty, Levin, & Cleland, 2000; Morlock, Kissel, Li, Koll, & Winter, 1998; Pean, et al., 1999; Takada, Yamagata, Misaki, Taira, & Kurokawa, 2003). The use of biodegradable polymers as a carrier for peptide drugs assumes that the release of a loaded peptide drug depends mainly on the degradation kinetics of the polymer. The degradation kinetics of PLGA can be adjusted by changing the lactide/glycolide ratio and molecular weight (MW) (Frangione-Beebe, Rose, Kaumaya, & Schwendeman, 2001). This is not always the case because other factors of the formulation can also affect the drug release kinetics, and can be more dominant than the degradation kinetics of a polymer. These factors include interactions between the polymer and the drug, size of the microspheres and excipients present (Varde & Pack, 2004).

4.1.1.2 Characteristics of microparticles

An ideal microparticle formulation should have reasonably high encapsulation efficiency, loading capacity, and sustained release of the loaded protein with retained bioactivity (Jain, 2000). The high protein loading and high encapsulation efficiencies are most critical simply due to the high price of therapeutic proteins (Jain, 2000).

For an injectable formulation, the size of microparticles should be small enough for going through a fine needle. While intravitreal injection of solutions or liquid formulations like Verisome[®] can be delivered via 30G needles (Section 1.2.1.4), polymeric steroid implants have been delivered using 22G and 25G needles (Section 1.3.1). Similarly, polymeric microparticles would have to be delivered through needles of 22–25G (inner diameters of 394–241 μ m) to facilitate syringeability and injectability. Microparticles with diameters much smaller than that of a needle are essential, in order to minimize potential blockage of the needle as well as vascular blockages. The particle size and size

distribution are also important for protein release rate as the total surface area for protein delivery depends on the particle size (Berkland, Kim, & Pack, 2001). As particle size decreases, the surface area-to-volume ratio increases. Thus, for a given rate of drug diffusion through the microsphere, the movement of drug out of the microsphere increases with decreasing particle size. In addition, water may penetrate more quickly due to the shorter distance from the surface to the centre of the particle. For poorly water-permeable polymers like polyanhydrides, a decrease in particle size increases surface area-to-volume ratio resulting in faster release rates (per mass of polymer) from smaller polyanhydride microspheres (Varde & Pack, 2004).

Microparticles fall in the size range of 1-1000 μm and can be termed microcapsules for reservoir structures or microspheres for matrix systems (Figure 4.1) (Yasukawa, et al., 2004). Microcapsules are formed by a core that contains the drug and is surrounded by a layer of a polymer or a mixture of several polymers. In the microspheres, the active substance is dispersed in the polymeric network. Matrix structure is preferred for biodegradable systems as the drug is dispersed in the polymer.

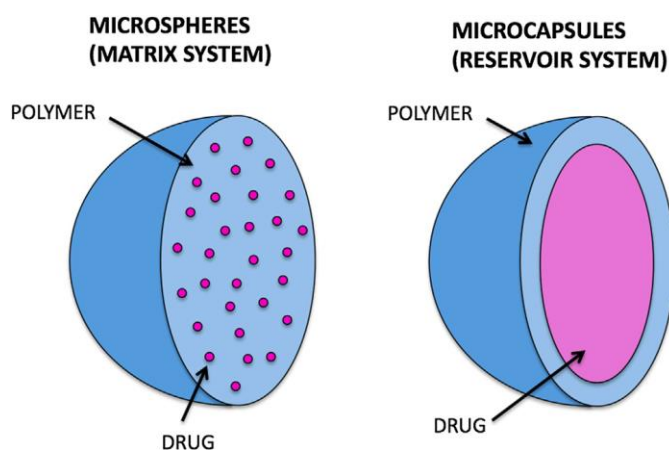


Figure 4.1: Structure of microparticles (microspheres and microcapsules). In the microspheres, the active substance is dispersed within the polymeric matrix, while microcapsules have drug in the core, which is surrounded by a polymeric layer. Reprinted with permission from Herrero-Vanrell *et al.* (R. Herrero-Vanrell, Bravo-Osuna, Andres-Guerrero, Vicario-de-la-Torre, & Molina-Martinez, 2014)

Once administered, microparticles can disappear or remain at the site of administration after releasing the drug depending on the characteristics of the polymer.

Microspheres are good candidates to be used in personalized medicine as different amounts of particles can be administered depending on patient needs. For intraocular purposes, they must be biocompatible, safe and stable, demonstrating predictable degradation kinetics. All these requirements can be achieved by the adjustment of the manufacturing parameters (R. Herrero-Vanrell, et al., 2014).

4.1.1.3 Administration of microparticles

Microspheres are usually injected as a conventional suspension with Balanced Salt Solution or phosphate buffer but sometimes viscous vehicles, such as hydroxypropyl methylcellulose or hyaluronic acid are used to prevent clogging of needles during microsphere injections and improve syringeability and injectability (dos Santos, et al., 2006; Rocio Herrero-Vanrell & Refojo, 2001). A force of 12N over 10s is considered acceptable (Xie, et al., 2014).

4.1.1.4 Microparticle use in ocular applications

In the management of chronic posterior eye diseases biodegradable microspheres are preferred since they are degraded *in vivo*, either enzymatically or chemically to produce biocompatible, toxicologically safe by-products which are further eliminated by the normal metabolic pathways (X. S. Wu, 1995). For this reason, biodegradable polymers such as gelatin, albumin, polyorthoesters, polyanhydrides and polyesters are preferred for the synthesis of intraocular microspheres, as they do not require removal from the injection site after delivering the drug (R. Herrero-Vanrell, et al., 2013). The derivatives of poly (lactic) acid (PLA), poly (glycolic) acid (PGA) and their copolymers poly (lactic-co-glycolic) acid (PLGA) are the most employed and have been approved for clinical use by the U.S. Food and Drug Administration (FDA) and the European Medicines Agency (EMA). Different devices such as implants, scleral plugs, pellets, discs, films, and rods have been prepared from these erodible polymers for delivery of therapeutics to the posterior segment of the eye (Yasukawa, et al., 2004). Their use as injectable devices has become more popular over the last few decades.

For intraocular administration, a large variety of bioactive compounds has been included in microspheres (e.g. antiproliferatives, antiinflammatories, immunosuppressants, antibiotics and even biological therapeutic agents). Some examples are dexamethasone, budesonide, cyclosporine, anti-VEGF aptamers and ganciclovir (R. Herrero-Vanrell, et al., 2014). For the treatment of posterior segment diseases, microspheres can be administered by intravitreal, periocular or suprachoroidal injection (Rocío Herrero-Vanrell, 2011; Rocio Herrero-Vanrell & Refojo, 2001; Paganelli, et al., 2010; Yasukawa, et al., 2004).

Intraocular microspheres allow the release of the encapsulated drug, bypassing the blood ocular barrier. The main advantage of these formulations is that they can release the drug over weeks or months with a single administration, achieving the same therapeutic effect as multiple injections. For example, Veloso *et al* (Veloso, Zhu, Herrero-Vanrell, & Refojo, 1997) tested the antiviral effect of ganciclovir released from PLGA microspheres to avoid frequent intravitreal ganciclovir injections. The study showed that the microspheres controlled the progression of the disease in treated rabbit

eyes over 14 days with no adverse tissue reaction observed after 8 weeks. Control eyes were injected with blank microspheres. Sustained release of active substances from microspheres reduces the need for frequent administrations and enhances patient compliance. This strategy has gained attention, especially in chronic diseases that require low concentrations of the active substances for a long period of time (Patricia Checa-Casalengua, et al., 2011). Injection volumes of 50-100 μL can be delivered, although larger volumes can be accommodated in periocular spaces. Microparticles with sizes 1 μm and 10 μm in a volume of 50 μL were administered into the suprachoroidal space of New Zealand white rabbits with no inflammation or abnormalities observed and persisted for 2 months (S. R. Patel, et al., 2012).

4.1.1.5 Manufacture of microparticles

Microparticles can be manufactured by a variety of techniques including solvent extraction/evaporation from emulsion, aggregation by pH adjustment/heat, coacervation (phase separation), interfacial polymerization, ionic gelation and spray-drying. For encapsulation of proteins, double emulsion (water-in-oil-in-water) method (described further in Figure 4.2), inclusion of stabilizers (Freitas, Merkle, & Gander, 2005) or the formation of a solid-in-oil-in-water emulsion are preferred as these techniques have shown effective protection of the biologically active (secondary, tertiary or quaternary) structure of the protein (Patricia Checa-Casalengua, et al., 2011). Table 4.1 below provides a summary of the advantages and disadvantages of the aforementioned methods. This provides a rationale for the SAW technique being explored in this chapter. The advantage of this technique is the avoidance of the use of high temperatures or residual organic solvents that may denature thermolabile peptides or proteins. It is also time efficient due to the reduction in the number of steps and processing time required in comparison to traditional techniques like double solvent emulsion evaporation (Benoit, Baras, & Gillard, 1999), phase separation (Coccoli, et al., 2008; Morita, Sakamura, Horikiri, Suzuki, & Yoshino, 2000) or spray drying (Gander, Johansen, Nam-Trân, & Merkle, 1996).

A final sterilization step is preferred for microparticles with autoclaving, gamma irradiation and ethylene oxide being most commonly employed. Thermally-sensitive microparticles are preferentially sterilised by gamma irradiation (25 kGy), however, this can induce structural changes in both the polymer and drug through dose-dependent chain scission as well as reduction of the polymer molecular weight. This can affect the behaviour of the final product. Strategies like the use of dry ice during sterilization of microspheres with low molecular weight drugs and use of antioxidants combined with protein drugs can help minimise the aforementioned changes (Amrite, Ayalasonmayajula, Cheruvu, & Kompella, 2006; P. Checa-Casalengua, et al., 2012; Rocio Herrero-

Vanrell & Ramirez, 2000; Martínez-Sancho, Herrero-Vanrell, & Negro, 2004; Mohanan, Gander, Kündig, & Johansen, 2012).

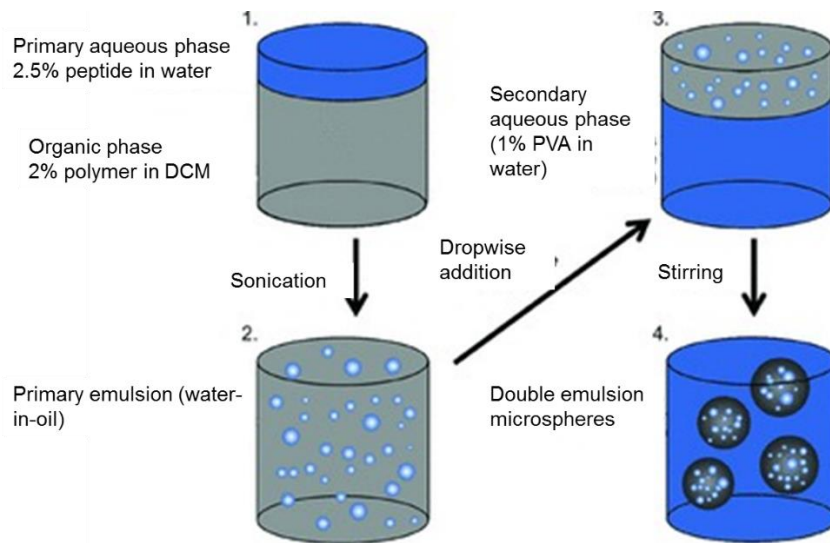


Figure 4.2: Schematic illustration of the w/o/w double-emulsion method used to prepare PCL-PEG-PCL microparticles. Adapted from Thatcher *et al*, (Thatcher, Welch, Eberhart, Schelly, & DiMaio, 2012)

4.1.1.6 Surface acoustic wave atomization

Surface acoustic wave (SAW) atomizers can be utilised for the straightforward, rapid, and energy efficient production of protein-loaded polymer microparticles. The apparatus consists of a drop of liquid on a device. A SAW is a sound wave transmitted through a piezoelectric substrate (solid) which results in longitudinal waves being diffracted into the liquid at an angle (Rayleigh) due to the mismatch between the velocities of sound in solid and liquid. As power is increased, the surface of the liquid drop vibrates and the entire drop may move or simply atomize (Figure 4.3). An increase in power and vibration amplitude of the SAW causes atomization of the drop, producing a fine continuous mist of droplets ejected from the surface of the drop. The device used is an interdigital transducer (IDT) with aluminium/titanium electrodes sputter-deposited on a piezoelectric substrate. A sinusoidal electrical signal matching the operating frequency is applied to the IDT using a RF signal generator and RF power amplifier. The strong acoustic streaming drives effective mixing within the pre-atomized drop. Therefore, the protein polymer solution is well mixed prior to atomization and it is conceivable that the protein is atomized together with the polymer solution and encapsulated within the polymer shell. It was found that there was a decrease in the particle size produced with an increase in SAW frequency. A higher polymer concentration also showed smaller and more

homogeneous particles. In one study by Alvarez *et al* (Alvarez, Friend, & Yeo, 2008), approximately 55% of bovine serum albumin (BSA) survived atomization and emerged intact from the particles.

SAW devices are already widely employed in a host of telecommunications applications, for example, as inexpensive multiplexing signal filters in mobile phones, demonstrating how they may be mass produced through standard microfabrication technology and the potential of these devices in the development of a miniaturized integrated device for *in situ* protein encapsulation for portable drug delivery.

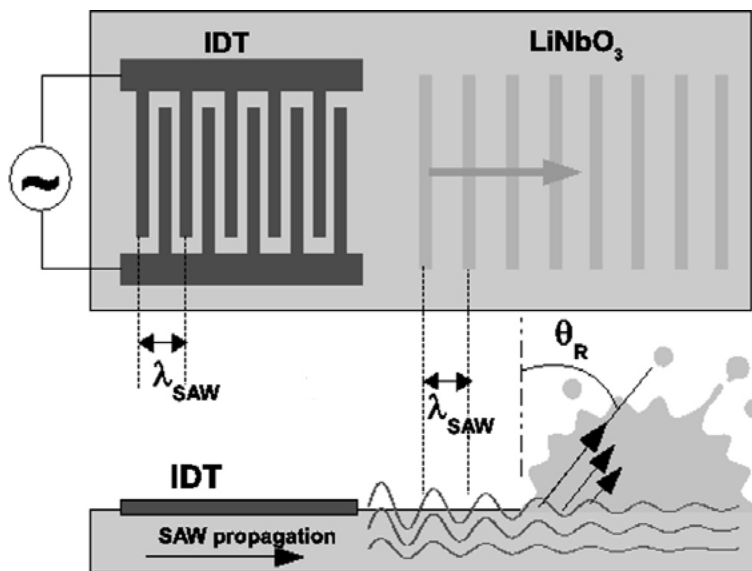


Figure 4.3: Schematic of the Rayleigh wave propagation and the atomization process. Reprinted with permission from L Yeo (Alvarez, et al., 2008)

Table 4.1: Comparison of the traditional methods of peptide encapsulation in microparticles

Method	Advantage	Disadvantage	Commercial application
Phase separation	Suitable for water-soluble & water-insoluble drugs Selection of solvents easier	Agglomeration of particles Complex process depending on several kinetic parameters Requires removal of large quantities of organic phase	Sandostatin® LAR Trelstar™ depot Decapeptyl® SR Somatuline® LA

		from the microspheres	
Spray Drying	Rapid Convenient Easy to scale up Mild conditions	Significant loss of product-adhesion of microparticles to the inner walls of the spray-dryer	Parlodel LAR™
Double-emulsion method	Successful encapsulation of peptides	Traces of organic solvents Various formulation & process variables significantly affect encapsulation & release	RISPERDAL® CONSTA® Vivitrol® Lupron Depot® Enantone Depot® Trenantone® Enantone Gyn

4.1.2 Polycaprolactone

Polycaprolactone (PCL) is a biocompatible polymer with a slow biodegradation caused by its molecular weight dependent surface hydrophobicity and crystallinity (Dash & Konkimalla, 2012). Polycaprolactone has a glass transition temperature of 60°C and melting point ranging between 59°C and 64°C, depending on its crystalline nature (Barbato, La Rotonda, Maglio, Palumbo, & Quaglia, 2001; Sinha, Bansal, Kaushik, Kumria, & Trehan, 2004). PCL is a bioerodible polymer that undergoes type III erosion, which means that it leads to the formation of small, soluble molecules, by cleavage of the polymeric chains. There are 2 distinct phases, namely non-enzymatic cleavage and enzymatic fragmentation (Chen, Bei, & Wang, 2000; Jenkins & Harrison, 2006; Sinha, et al., 2004). In PCL formulations, the random nonenzymatic cleavage starts in the amorphous region that is auto-catalyzed by carbonyl end groups of fragmented polymeric chain and needs water to occur (Chen, et al., 2000; Sinha, et al., 2004). The internal fragmentation produces fragments of length depending on the initial molecular weight of polymer. The weight loss from the formulation starts when the length of PCL fragments produced becomes small enough (below 5000) to be diffused through the polymeric matrix to the media at a much later stage (4–6 months) of PCL degradation. This bulk process is generally accompanied by enzymatic surface erosion characterized by grooves and cracks on the surface. Hydrolysis of ester bonds in the PCL matrix leads to break down to their constituent monomer, the ϵ -hydroxycaproic acid that then undergoes phagocytosis (Merkli, Tabatabay, Gurny, & Heller, 1998).

The compatibility of PCL with a wide range of drugs enables uniform drug distribution in the polymer matrix and the slow degradation facilitates drug release up to several months (Hakkarainen & Albertsson, 2002; Sinha, et al., 2004). The physical, chemical and mechanical properties of PCL can be modified by co-polymerization which can help tailor a desired crystallinity, solubility and degradation pattern (Dash & Konkimalla, 2012). Poly (ethylene glycol) (PEG), which is hydrophilic, non-toxic and absent of antigenicity and immunogenicity is a candidate to be attached to PCL, forming PCL-PEG copolymers. The PCL-PEG copolymers have better hydrophilicity and shorter degradation times than PCL alone (Chen, et al., 2000; Huang, et al., 2004; Koenig & Huang, 1995; Moon, Lee, Han, & Byun, 2002). Many researchers have investigated thermosensitive triblock (TB) copolymers (A-B-A or B-A-B) composed of PLA/polycaprolactone (PCL)/PLGA blocks (A) and PEG block (B) for their applicability in the development of sustained delivery formulation (Ghalanbor et al., 2012; Kapoor et al., 2015; Lucke et al., 2002). In general, one may expect that increasing the content of the more rapidly degrading monomer would increase the release rate and this is often the case (S. Y. Lin, Chen, Teng, & Li, 2000; Shen, Kipper, Dziadul, Lim, & Narasimhan, 2002; Spenlehauer, Vert, Benoit, & Boddaert, 1989). In this study, we have investigated PCL-PEG-PCL triblocks of two different molecular weights, namely PCL_{1k}-PEG_{2k}-PCL_{1k} and PCL_{5k}-PEG_{2k}-PCL_{5k}.

PCL is widely used in the pharmaceutical and biomedical fields as a biomaterial (e.g., suture, osteosynthetic material, artificial skin, or support of cellular regeneration) or in extended-release drug delivery systems targeting specific tissues within the body because of its lack of toxicity (Hiljanen-Vainio, Karjalainen, & Seppälä, 1996; Sinha, et al., 2004). The utilization of PCL in ophthalmology, especially for delivery through the intraocular route has been poorly explored. Beeley and co-workers (Beeley, et al., 2005) developed a subretinal drug delivery system made of PCL encapsulating triamcinolone acetonide as the drug. The developed device was implanted into the subretinal space of six rabbits. No complications were observed during the 4-week follow-up period showing that PCL is well tolerated by the retinal tissue and that the implant can provide sustained drug release for a period of at least 4 weeks. Silva-Cunha et al (Silva-Cunha, Fialho, Naud, & Behar-Cohen, 2009) investigated the *in vivo* release profile obtained from dexamethasone loaded PCL implants into the vitreous of pigmented rabbits. The study showed that the drug was released slowly for 25 weeks, possibly controlled by diffusion through the channels and pores. The release profile obtained showed long-term, well-controlled, stable release of dexamethasone in the vitreous humour with no significant peaks or valleys of drug release that could result in toxicity or no therapeutic effect. At 55 weeks, approximately 79% of dexamethasone was still present in the implants confirming the slow release of the drug and also the possibility of drug release for a period of 2 years. The use of PCL-PEG copolymers as drug delivery systems has been reviewed in detail by

Wei and co-workers (Wei, et al., 2009), including the delivery of biomacromolecules. In one study (Zhou, Deng, & Yang, 2003a), PCL-PEG microparticles containing human serum albumin were prepared by the double emulsion (water-in-oil-in water) method and it was found that the loading efficiency for PCL-PEG microparticles was higher compared with the PCL homopolymer. In another study (Erdemli, Usanmaz, Keskin, & Tezcaner, 2014), PEG-PCL-PEG microparticles were prepared by double emulsion-solvent evaporation method and their properties were compared with those of PCL microparticles. Immunoglobulin G (IgG) was loaded into the microparticles. PEG-PCL-PEG microparticles had higher encapsulation efficiency of *ca.* 74% compared to *ca.* 54% for PCL microparticles. *In vitro* cytotoxicity tests revealed that both PEG-PCL-PEG and PCL microparticles had no toxic effects on 3T3 fibroblastic cell line and fibroblast-like synoviocytes.

4.2 Materials and methods

4.2.1 Materials

Somatostatin-14 of sequence Ala-Gly-Cys-Lys-Asn-Phe-Phe-Trp-Lys-Thr-Phe-Thr-Ser-Cys (cyclic, MW=1638 Da) was purchased as an acetate salt from Polypeptide Laboratories (Sweden), with a peptide purity of 99.6%.

FITC-DEAE-Dextran (MW= 3-5kDa) and Polyvinyl alcohol (87-90% hydrolyzed, mw 30-70 kDa) (PVA) were from Sigma-Aldrich (USA). Poly (ϵ -Caprolactone)-Polyethylene Glycol-Poly (ϵ -Caprolactone) of two different weights (PCL_{5k}-PEG_{2k}-PCL_{5k} and PCL_{1k}-PEG_{2k}-PCL_{1k}) were from Polysciences (USA). Dichloromethane was from RCI Labscan (Thailand). Water purified with Milli-Q system (Merck, Millipore Australia) with a resistivity of 18.2 M Ω .cm (at 25°C) was used in the preparation of all reagents and experiments. Ethanol absolute was from Merck (Germany) and glacial acetic acid was from Fagron Pharmaceuticals (USA).

4.2.2. Methods

4.2.2.1 Optimization of polymer concentration and molecular weight

The PCL_{1k}-PEG_{2k}-PCL_{1k} triblock polymer was chosen as the candidate for production of microparticles via the SAW technique as this is readily soluble in ethanol. Ideally, the polymer and the drug would be soluble in the same solvent for optimum results. Since somatostatin is soluble in ethanol but not in dichloromethane, we proceeded with the lower molecular weight triblock copolymer. The concentration of the polymer that could be used with the SAW technique was limited by the resulting viscosity of the polymer solution in ethanol. A series of polymer solutions (0.5% w/v, 1 %

w/v, 2% w/v) were prepared and nebulised on the hydra device. It was found that 1% w/v of the PCL_{1k}-PEG_{2k}-PCL_{1k} dissolved in ethanol could be nebulised easily and was selected as the concentration to proceed with.

4.2.2.2 Production of microparticles loaded with FITC-DEAE-Dextran (model drug)

4.2.2.2.1 Preparation of microparticles using SAW

Polymer 1%w/v (PCL_{1k}-PEG_{2k}-PCL_{1k}) and 0.5% w/v of FITC-DEAE-Dextran, (mw: 3-5kDa) were dissolved in 50% ethanol and 50% of Milli-Q water (0.6mL in total). The solution was vortexed. A volume of 0.1 mL of the solution was nebulised into a glass bottle using a hydra device at a frequency of 14.4 Mhz and an amplitude of 110 mV on an Agilent N9310A RF Signal Generator. Each bottle was immediately wrapped in aluminium foil.

4.2.2.2.2 Preparation of microparticles using water-in-oil-in-water (w/o/w) double emulsion method

Briefly, an aqueous solution of FITC-DEAE-Dextran and sodium chloride was prepared. The required amount of high molecular weight (PCL_{5k}-PEG_{2k}-PCL_{5k}) polymer or low molecular weight (PCL_{1k}-PEG_{2k}-PCL_{1k}) polymer was weighed and then dissolved in dichloromethane (DCM) forming the oil phase. The primary emulsion was formed through probe sonication (QSONICA LLC, United States) at three different time intervals (2, 4 and 8 seconds), with an amplitude of 35%. The external aqueous phase consisted of a 1% w/w PVA and 5% w/w NaCl in Milli-Q water which was added to the primary emulsion in separate quantities up to 7.1 mL. The mixture was then magnetically stirred at high speed for 3 hours in a fume hood to allow the evaporation of the organic solvent. The remaining microparticles were then wrapped in aluminium foil to protect them from light and stored at 4°C for further analysis.

4.2.2.3 Determination of encapsulation efficiency

4.2.2.3.1 Encapsulation efficiency of microparticles loaded with FITC-DEAE-Dextran produced by SAW technique

Glass bottles were rinsed out with 2 mL of Milli-Q water in small increments and the contents transferred to centrifuge tubes. The tubes were centrifuged at 4000 RPM for 10 minutes. The supernatant was removed and analysed in plate reader for fluorescence. 2 mL of Milli-Q water was added to each tube and vortexed to resuspend and wash the particles. The centrifugation was repeated twice more with the supernatant being removed for analysis after each wash. A drop

containing the particles from each tube was placed on a glass slide to look under the fluorescence microscope and SEM. The particles were then dissolved in 0.5 mL ethanol and 0.5 mL SLF was added for the FITC-DEAE-dextran to preferentially partition into. The solution was vortexed. The aliquots of the solution were analysed using fluorescence spectrophotometer at excitation 485nm and emission at 538nm (Flexstation 3 Molecular Devices LLC, USA).

4.2.2.3.2. Encapsulation efficiency of microparticles loaded with FITC-DEAE-Dextran produced by w/o/w double emulsion method

The slurry obtained after 3 hours of high speed stirring was centrifuged at a speed of 4000 RPM for 10 minutes. The resulting supernatant was then analysed using a fluorescence spectrophotometer (Flexstation 3 Molecular Devices LLC, USA) plate reader at excitation 485nm and emission 538nm to determine the amount of FITC-DEAE-Dextran that was not encapsulated. The microparticles were then resuspended in 2mL of the external aqueous phase and centrifuged again at 4000rpm for 10 minutes. The supernatant was removed for analysis as Wash 1. This step was repeated once more to obtain Wash 2. Two washes were performed to remove any model drug adsorbed on the surface of the microparticles.

Appropriate aliquots of the supernatant after each washing step were analysed in the abovementioned plate reader for fluorescence at excitation wavelength of 485nm and emission at 538nm. Concentrations were determined with reference to calibration curves ($R^2 = 0.9952$).

4.2.2.4 Morphological analysis of microparticles

Scanning electron microscopy was performed to analyse particle morphology. Briefly, dried microparticles were applied to carbon film positioned on an aluminium stub. Surface of particles on carbon film was sputter-coated for 60s with Au-Pd alloy followed by imaging with a scanning electron microscope (SEM, Tescan Vega).

Fluorescence microscopy (Olympus BX60) was also used to visually confirm encapsulation of the model drug as well as the shape of the microparticles generated using the SAW technique.

4.2.2.5 Sizing of microparticles

The size distribution of the microparticles was determined using a wet dispersion technique in a Mastersizer 3000 (Malvern Instruments, United Kingdom). The sizing was performed at room temperature (22°C) at a 1.46 refractive index of PCL-PEG- PCL and an absorbance index of 0.01 nm.

4.2.2.6 Production of somatostatin-loaded polymer microparticles

The double emulsion (w/o/w) method as previously described (Section 4.2.2.2.2) was followed to encapsulate somatostatin in the microparticles as this method provided high encapsulation of model drug in comparison to the SAW technique. Somatostatin 2.5 % w/v and 5% w/v were investigated. The high molecular weight polymer, PCL_{5K}-PEG_{2K}-PCL_{5K} was investigated at 2 % w/v and 5 % w/v concentrations.

4.2.2.7 Release studies

In vitro release profiles of somatostatin were conducted by adding 3 mL of SLF to the microparticles and placed in a shaking water bath (Paton industries, Australia) at 37 °C. Two mL of the SLF was removed for analysis at each time point with replacement of an equal volume of fresh SLF to maintain sink conditions. Analysis of the amount of somatostatin released was performed using the validated HPLC method described in Chapter 2. Calculations were performed with respect to the area under the curve of a known standard concentration (0.25 mg/ml of somatostatin dissolved in 0.1% v/v glacial acetic acid in Milli-Q water) assayed on the same day.

4.3 Results and Discussion

4.3.1. Encapsulation efficiency of FITC-DEAE-Dextran in microparticles prepared by SAW technique

Fluorescein isothiocyanate–dextran-DEAE (FITC-dextran-DEAE) was used as a model drug due to a similar molecular weight and cationic charge to somatostatin. It was used in place of somatostatin in preliminary work to identify the most appropriate sonication time, polymer molecular weight and polymer concentration required to produce microparticles with the highest drug encapsulation efficiency. Table 4.2 below provides a comparison between somatostatin and FITC-DEAE-Dextran.

Table 4.2: Comparison of properties between somatostatin and FITC-DEAE-Dextran

Properties	FITC-DEAE-Dextran	Somatostatin
Molecular weight (Da)	3000-5000	1638
Aqueous solubility	>25mg/mL	>70mg/mL
Charge at pH 7.4	+2	+2

Table 4.3: Encapsulation efficiency of FITC-DEAE-Dextran in microparticles prepared by SAW technique analysing the amount of drug remaining in buffer (sample replicates are defined as S1, S2 and S3 respectively)

Wash #	S=1 % of drug not encapsulated (w/v)	S=2 % of drug not encapsulated (w/v)	S=3 % of drug not encapsulated (w/v)
Pre-wash	8.85%	7.95%	5.70%
1	0.11%	0.048%	0.132%
2	0.005%	0.004%	0.008%

Table 4.4: Encapsulation efficiency of FITC-DEAE-Dextran in microparticles prepared by SAW technique from dissolved microparticles

Wash #	Average % of drug encapsulated (w/v) (n=3)
1	0.322%
2	0.035%
3	0.028%

Based on the data above (Table 4.3), approximately 6% - 9% of the FITC-Dextran-DEAE was detected in the washing steps. That would mean that there should be approximately 94% of the model drug should be encapsulated. However, upon dissolution of the microparticles, it was revealed that only 0.03% of the drug is actually encapsulated after 3 washes (Table 4.4). In this instance, the polymer-drug solution was manually deposited in volumes of 10 μ L at a time on the SAW device until the entire 100 μ L was nebulised. The set-up was not enclosed which resulted in loss of the nebulised drug and polymer to the environment and may explain the poor encapsulation efficiencies in our results.

4.3.2 Encapsulation efficiency of microparticles produced by double emulsion (w/o/w) method

The optimisation and characterisation of microparticle preparation was conducted in two phases. As shown in Table 4.5, the highest encapsulation efficiency (*ca.* 65%) was achieved with 5% of the HMW polymer when the sample was sonicated for 2 seconds. The HMW 5% sample sonicated for 2

seconds and the HMW 2% samples also produced relatively high encapsulation efficiencies. The LMW samples generally produced no encapsulation. A possible reason for this could be the similar molecular weights of FITC-DEAE-Dextran (3000-5000 Da) and the LMW polymer (4000 Da). Due to the lack of favourable encapsulation efficiencies with the LMW samples, their size was not characterized. The size of the microparticles produced by the HMW polymer at different sonication times has been provided below in Table 4.5.

Table 4.5: Encapsulation efficiency and particle size of FITC-DEAE-Dextran in microparticles prepared by w/o/w method

Polymer Concentration (% w/v)	Sonication Time (seconds)	Encapsulation Efficiency (%)		Average Particle Size (μm)	
		LMW	HMW	LMW	HMW
1%	2	0	57.0	-	-
	4	0	55.8	-	22.6
	8	0	53.7	-	63.7
2%	2	NA	56.6	-	27.9
	4	NA	61.5	-	26.5
	8	NA	64.8	-	62.9
5%	2	NA	64.9	-	50.1
	4	NA	56.7	-	51.4
	8	NA	50.0	-	47.0

4.3.3 Morphological analysis of microparticles with FITC-DEAE-Dextran using SAW technique

Figure 4.4 demonstrates the formation of polydisperse polymer-drug conjugates from the SAW technique that do not resemble microparticles. This may be due to the nebulized droplets impacting on the surface of the collection vessel i.e. the glass bottle before getting a chance to dry and form completely. In the work done by Alvarez et al (Alvarez, Yeo, Friend, & Jamriska, 2009), the set-up included a drying tube with a trajectory length of 50cm. In our case, the SAW device had to be inserted into the glass collection bottle as far in as possible to prevent loss to the atmosphere.

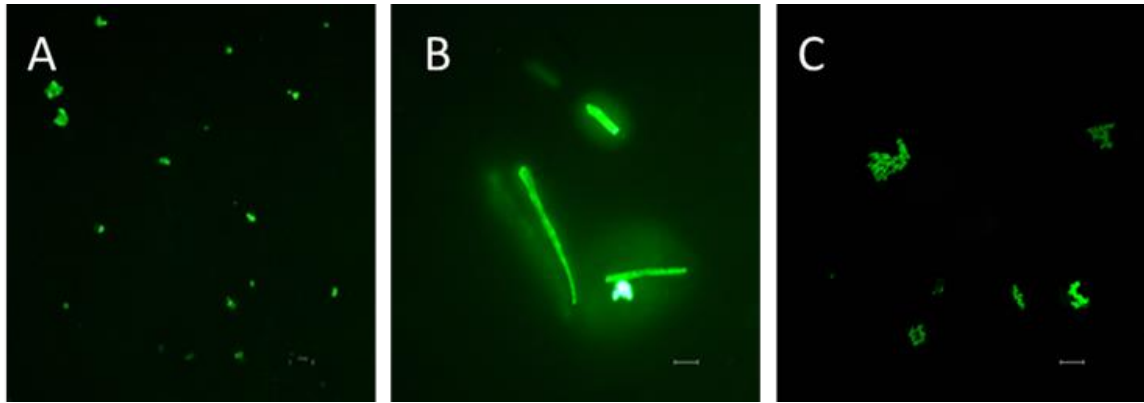


Figure 4.4: Images under fluorescence microscope after first centrifugation (A-pre-wash), (B- wash #1) and (C-wash #2) from left to right respectively. Scale bars for A, B and C- 18 μm .

4.3.4 Morphological analysis of microparticles produced by double emulsion (w/o/w) method

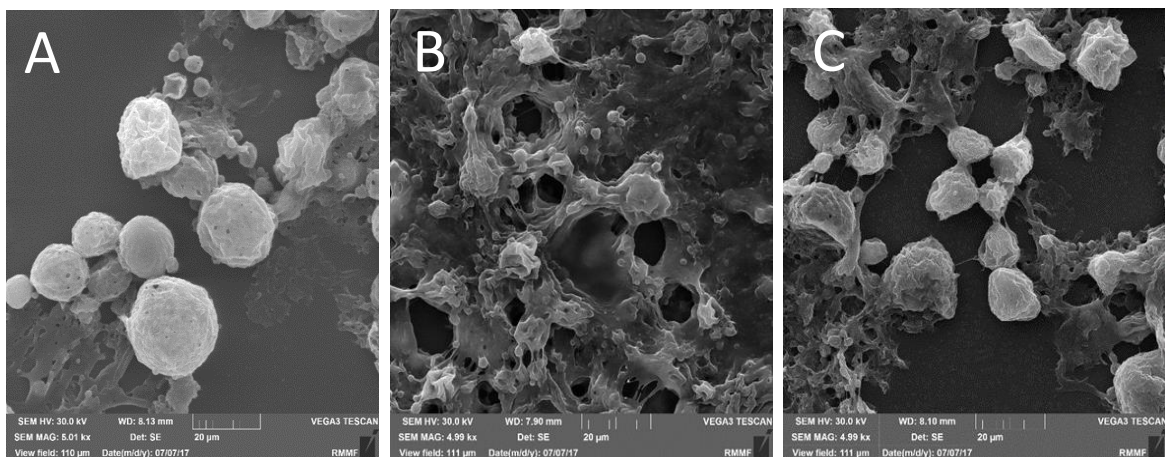


Figure 4.5: Scanning electron micrographs of HMW 1% polymer microparticles. Sonication times - A- 4 seconds, B- 8 seconds and C- 10 seconds. Scale bars for A, B and C- 20 μm .

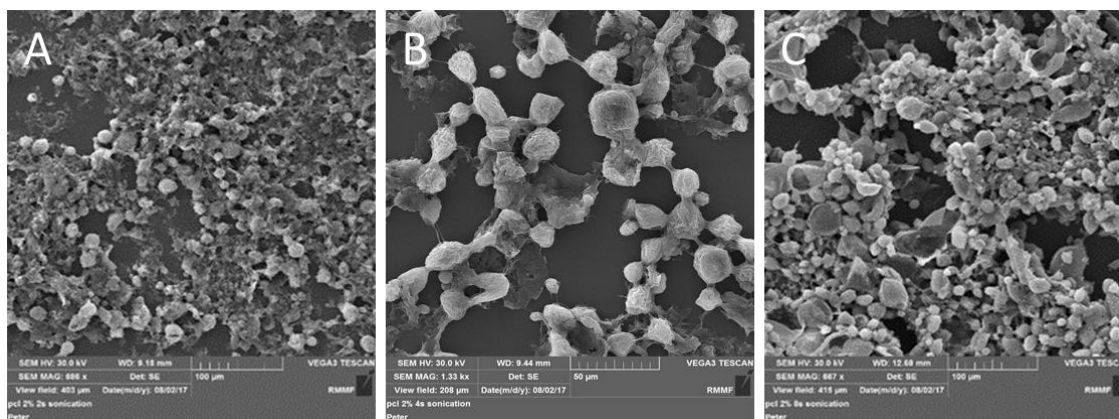


Figure 4.6: Scanning electron micrographs of HMW 2% polymer microparticles. Sonication times – A- 2 seconds, B- 4 seconds and C- 8 seconds. Scale bars for A and C- 100 µm, B – 50 µm.

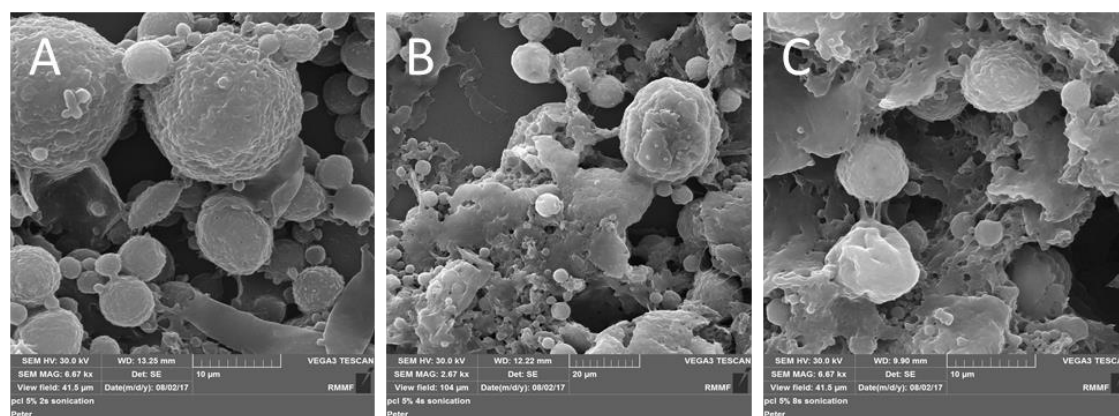


Figure 4.7: Scanning electron micrographs of HMW 5% polymer microparticles. Sonication times – A- 2 seconds, B- 4 seconds and C- 8 seconds. Scale bars for A and C- 10 µm, B – 20 µm.

The microparticles prepared using the double-emulsion method (Figures 4.5-4.7) are better formed morphologically and more spherical in appearance. However, a longer sonication time of 8 seconds reveals more of the polymer being present in a “mesh” compared to the samples subjected to shorter sonication times. Although the encapsulation efficiencies were not significantly different, the SEM images reveal more discrete microparticles formed in the 4 second sonication duration compared to samples from 8 seconds of sonication, particularly in Figures 4.5A and 4.6B. Figure 4.5C illustrates that 10 seconds of sonication results in a tangled network of polymer rather than discrete microparticles. This is likely to be due to more heat generated with a longer duration of sonication, leading to change in the morphology of the microparticles. In the case of Figure 4.7 (high molecular weight polymer 5%), the microparticles are better formed at 2 seconds sonication (Figure 4.7A) compared to 4 seconds (Figure 4.7B) and 8 seconds (Figure 4.7C). However, the average size of the HMW 5% microparticles was 50.1µm which was larger than HMW 2% microparticles with an average

size of 26.5µm. Comparing to other microparticles administered periodically (R. Herrero-Vanrell, et al., 2014) with particle sizes of about 30 µm, the latter particle size is preferable. For this reason, HMW 2% with a sonication time of 4 seconds was selected as the candidate for somatostatin encapsulation, with Figure 4.6B demonstrating the formation of discrete microparticles with a mean size of 26.5µm (sized by laser diffraction analysis).

4.3.5 Encapsulation efficiency of SST microparticles prepared with double emulsion (w/o/w) method

HMW polymer at 2% w/w and 5% w/w with a sonication time of 4 seconds was investigated with SST 2.5% and 5% w/w. There were a number of strategies employed in an attempt to improve the encapsulation efficiency. Both the drug and the polymer were tested at 2 different concentrations to see if increasing the concentration of either drug or polymer would improve the percentage encapsulated. It was found that SST 5% w/w produced a very low encapsulation of 4.3%. The SST solution transitioned from a solution to gel rapidly after dissolution in water and the gel was not adequately dispersed by the probe sonication or high speed mixing. Based on the work done by Hermann *et al* (Herrmann & Bodmeier, 1998), SST was dissolved in acetate buffer instead of Milli-Q water in the dissolution step. This did not result in a significant improvement in the encapsulation efficiency. Based on preliminary work done with SST in combination with HPMC, it was hypothesized that the positive charges on SST may be shielded by HPMC in solution and therefore may improve encapsulation of the hydrophilic SST into the hydrophobic triblock co-polymer. This also yielded a negative result with no encapsulation produced. This information is summarised in the table below (Table 4.4). Based on the encapsulation efficiency, SST 2.5% w/w in HMW polymer 2% w/w microparticles were manufactured for release studies and further characterization.

Table 4.6: Encapsulation efficiency of different concentrations of somatostatin and HMW polymer using w/o/w method

Concentration of SST (% w/w)	Concentration of HMW polymer (% w/w)	Encapsulation efficiency
2.5%	2%	43.4%
2.5%	5%	19.7%
2.5% (dissolved in acetate buffer)	2%	21.1%
2.5% (dissolved in HPMC 0.5% solution)	2%	0%
5%	2%	4.31%

Table 4.7: Encapsulation efficiency of SST 2.5% HMW polymer 2% (n=3) using w/o/w method

Sample	Encapsulation efficiency	Mean \pm SD
1	43.4%	29.8 \pm 12.2
2	26.6%	
3	19.6%	

The data in Table 4.5 shows that the method of production of the microparticles produces encapsulation efficiencies with a large standard deviation. This could be due to the very small volumes that are being investigated where a small variation in a particular condition (e.g. the position of the probe during sonication) can lead to a large effect on the final amount encapsulated. The probe sonicator was not fixed in place and had to be set up manually for each sonication. For each sample sonicated, the tilt of the probe and the depth of the probe into the sample would vary despite best attempts at consistency. The high encapsulation achieved in Sample 1 indicates that a good encapsulation with this method is achievable providing that conditions are kept favourable and scale-up for industrial manufacture is also possible.

Vaishya *et al* (Vaishya, Mandal, Patel, & Mitra, 2015) investigated the encapsulation of octreotide in PCL-PEG-PCL triblocks (PCL_{10k}-PEG_{2k}-PCL_{10k}) amongst other polymers. The purpose was to determine the effect of polymer type on the release kinetics and acylation of octreotide. The method of microparticle production was the double-emulsion method. The encapsulation efficiency achieved was 45% with a complete release of octreotide over 3 months. In the work done by Vaishya and co-

workers, triethyl amine (TEA) was used to make the octreotide hydrophobic by adjusting the pH and it was dissolved in methanol to keep it in solution.

The encapsulation of FITC-DEAE-Dextran was improved by using sodium chloride in the aqueous solution. The chloride ions shielded the positive charges on the model drug and allowed more of it to be entrapped within the hydrophobic polymer matrix. However, this approach did not work with somatostatin due to its propensity to self-associate and transition into a gel in the presence of electrolytes. As discussed earlier, the somatostatin solution with sodium chloride gelled quickly and could not be dispersed by probe sonication process or high-speed mixing. Acetate buffer, which is weaker electrolyte solution, was then investigated. The results in Table 4.4 show there was no significant improvement in the encapsulation efficiency. Another option was to adjust the pH of the solution to the isoelectric point (pI) of somatostatin. The calculated pI of somatostatin is 8.3 (W. van Grondelle, et al., 2007). However, increasing the pH to 8.3 accelerates the degradation of somatostatin (Herrmann & Bodmeier, 2003) and the effect on the native structure is unknown.

Herrmann et al (Herrmann & Bodmeier, 1998) formulated microparticles of somatostatin in PLGA and PLA using various modifications of the oil-in-water solvent evaporation method. They achieved high encapsulation efficiencies of 63.7% to 84.4%. The theoretical drug loading was 2% w/w. The hydrophilic nature of PLGA and PLA may have contributed to the better entrapment of somatostatin within the polymer. Somatostatin analogues currently on the market, for example Sandostatin LAR[®], Signifor LAR[®] and Somatuline LA[®], are all microspheres prepared with PLGA as the polymer matrix. However, PCL-PEG-PCL was picked as the polymer candidate for this study due to a possible longer degradation time than PLGA and the fact that it does not acidify the microenvironment as it degrades. PLGA degrades into lactic and glycolic acids resulting in the acylation of the drug (Ghassemi, et al., 2012) as well as acidification of the area of administration which may cause inflammation. This is an undesirable effect in diabetic retinopathy, where inflammatory mediators contribute to deterioration (X. Zhang, Wang, Barile, Bao, & Gillies, 2013).

4.3.6 Release studies

4.3.6.1 Release of FITC-DEAE-Dextran (model drug) from microparticles prepared with SAW technique

Release studies were conducted on the microparticles with LMW polymer 1% w/w and FITC-DEAE-Dextran 0.5% w/w. Although the encapsulation efficiency was very low as discussed above, the release studies were conducted to investigate the release profile. The release studies were

conducted as described above with the additional protection of the microparticles from light by wrapping the centrifuge tubes in aluminium foil.

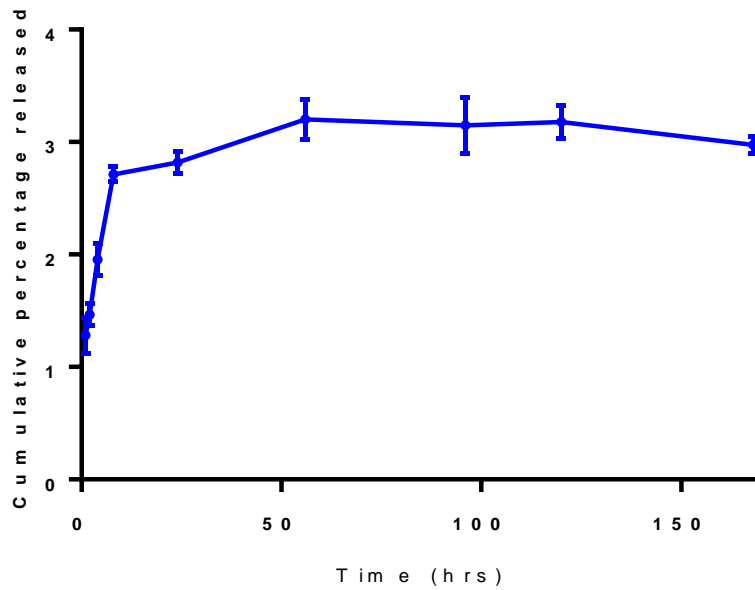


Figure 4.8a: Cumulative percentage release of FITC-DEAE-Dextran 0.5% w/w from LMW polymer 1% w/w microparticles with SAW technique (n=3; error bars = SD)

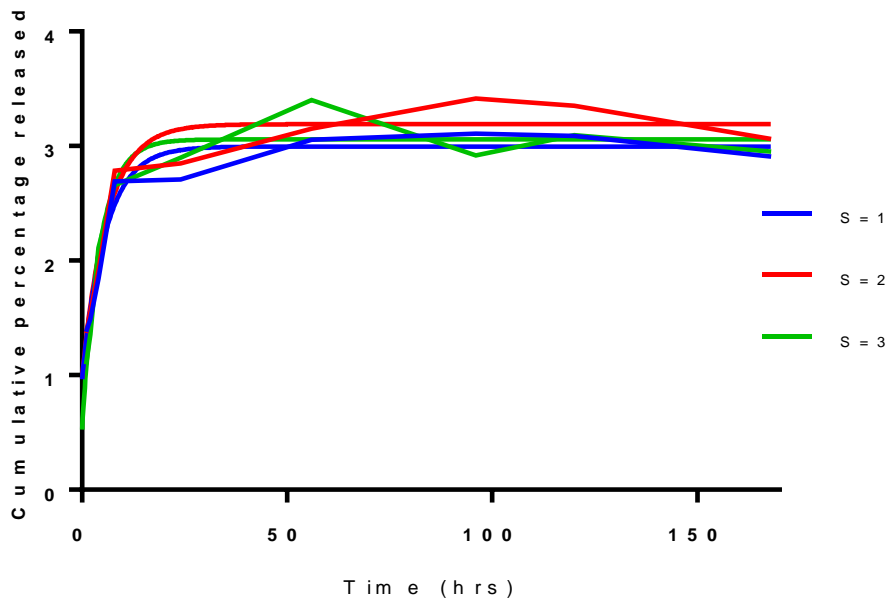


Figure 4.8b: Cumulative percentage release of FITC-DEAE-Dextran 0.5% w/w from LMW polymer 1% w/w microparticles with SAW technique fitted to equation 4.1.

The study revealed a very low percentage release- *ca.* 3% cumulative release at day 7. The experiment was concluded at day 7 as fluorescence was undetectable after that.

Due to the poor results of the encapsulation and release study, this technique was not further investigated as a possible candidate for formulation of SST microparticles.

In comparison to our results, Alvarez *et al* (Alvarez, et al., 2008) demonstrated the encapsulation of BSA (molecular weight of 66 kDa) in PCL (molecular weight 65 kDa). The microparticles produced were in the order of 10 μ m in size and the encapsulated protein survived the process with a yield of 55%. Confocal microscopy was used to visually confirm the uniform distribution of the fluorescent-conjugated protein within the polymer shell. Although they did not investigate the release kinetics of the encapsulated BSA from the microparticles, ELISA was used to assess if the native conformation of BSA was preserved by dissolving the microparticles. The encapsulation efficiency was not reported.

There are a number of possible reasons that the SAW technique did not work well in our endeavours to encapsulate somatostatin and FITC-DEAE-Dextran. The set-up used by Alvarez and co-workers was sophisticated and involved 2 separate syringes containing the polymer dissolved in an organic solvent and protein in aqueous solution respectively. The mixture was dispensed onto the SAW devices at a fixed flow rate and the nebulized mist was passed through a drying tube before being collected at the end.

In this instance, the polymer-drug solution was manually deposited in volumes of 10 μ L at a time on the SAW device until the entire 100 μ L was nebulised. The set-up was not enclosed which resulted in loss of the nebulised drug and polymer to the environment and may explain the poor encapsulation efficiencies in our results. The bottle for collection of the microparticles generated was held at close proximity. This does not allow sufficient drying time for the microparticles but was necessary to minimise loss to the environment. We were limited to using the same solvent for drug and polymer which excluded investigation of the high molecular weight polymer. In the case of somatostatin, there was a visible thick deposit of the peptide on the SAW device during the nebulisation of the polymer-peptide solution which resulted in a failure of efficient encapsulation. The images from fluorescence microscopy show polydisperse polymer-drug conjugates (Figure 4.4).

It is possible that results may be improved with the use of an enclosed experimental set-up that minimises loss to the environment and an automatic dispensing device that would make the process more efficient. Given that the molecular weight of somatostatin is a fraction of that of BSA and both exhibit a net positive molecular charge, these factors should not adversely affect encapsulation. The

set-up would also have permitted experiments with the higher molecular weight polymer to enable comparison with the current results. The combination of poor results and the interests of time and economy with regards to the amount of somatostatin expended led to this technique not being further explored.

4.3.6.2 Release of SST from microparticles prepared by double emulsion (w/o/w) method

SST 2.5% w/w HMW polymer 2% w/w microparticles were tested for release. The method used was as previously described (Section 4.2.2.7). HPLC was used to quantify the amount of somatostatin released as per the method described in Chapter 2.

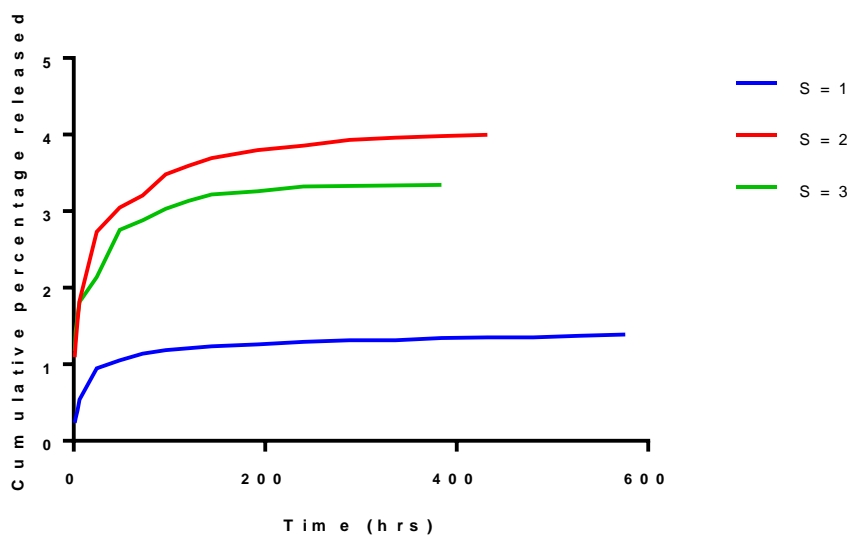


Figure 4.9a: Cumulative percentage release of somatostatin 2.5% w/w from HMW polymer 5% w/w (n=3)

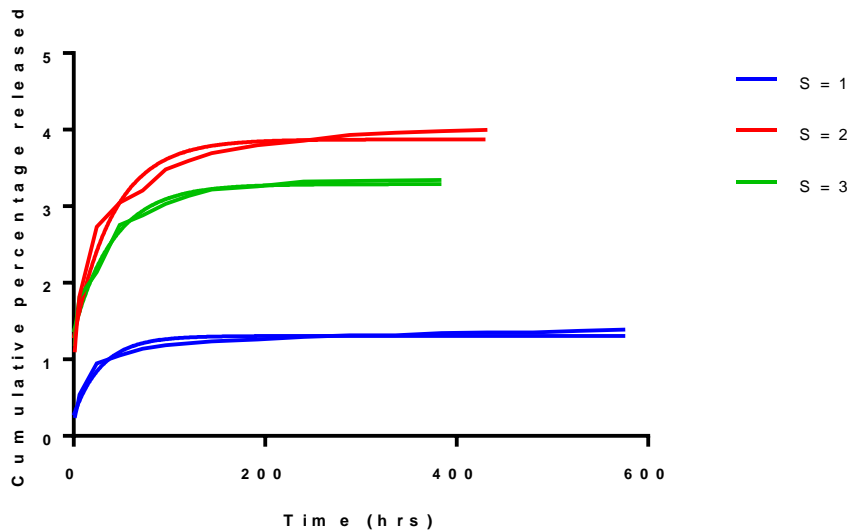


Figure 4.9b: Cumulative percentage release of somatostatin 2.5% w/w from HMW polymer 5% w/w (n=3) modelled to equation 4.1.

The results above show us that the sample (S=1) with the highest percentage of somatostatin encapsulated produced the longest duration of release for 24 days but the lowest cumulative release at about 1.4%. The highest cumulative percentage of somatostatin released was from sample S=2 at about 4% for 18 days. Sample S=3 had a cumulative release of about 3.3% for 16 days. The sampling was stopped when no further released somatostatin was detected by the HPLC for 3 consecutive days.

Fitting of the data from Figures 4.8 and 4.9 was done to the equation below (a first-exponential decay to plateau model) using GraphPad Prism (Version 7.02) curve-fitting software.

$$\text{Cumulative percentage released} = A (1 - e^{-kt}) \quad \text{equation 4.1}$$

where A = cumulative percentage released at infinite times

k = first-order release rate constant

t = time

and $t_{1/2} = \ln 2/k$

The tables below report the goodness of the fit (R^2) of the above model to the individual samples as well as the $t_{1/2}$ (time to release 50% of SST from the microparticles) and k (the rate constant).

Table 4.8: Mean R^2 , $t_{1/2}$ and rate constant values with standard deviation for FITC-DEAE-Dextran 0.5% w/w release from LMW 1% w/w polymer microparticles.

Sample	R^2	Mean $R^2 \pm$ SD	$t_{1/2}$ (hours)	Mean $t_{1/2} \pm$ SD	k	Mean k \pm SD
S=1	0.957	0.957 \pm	3.98	3.74 \pm	0.174	0.189 \pm
S=2	0.951	0.006	4.23	0.641	0.164	0.035
S=3	0.963		3.01		0.229	

Table 4.9: Mean R^2 , $t_{1/2}$ and rate constant values with standard deviation for SST 2.5% w/w release from HMW 2% w/w polymer microparticles.

Sample	R^2	Mean $R^2 \pm$ SD	$t_{1/2}$ (hours)	Mean $t_{1/2} \pm$ SD	k	Mean k \pm SD
S=1	0.975	0.979 \pm 0.004	20.8	26.4 \pm 4.81	0.033	0.027 \pm 0.006
S=2	0.978		29.1		0.024	
S=3	0.983		29.2		0.024	

In general, the drug release from a modified release system such as microparticles can be controlled by various mechanisms, such as dissolution, diffusion, partitioning, osmosis, swelling, and erosion. Diffusion of the drug is dependent on the structure through which the diffusion takes place, and polymer morphology has to be considered (Langer & Peppas, 1983a). A hydrophilic drug incorporated in a matrix can be released easily by diffusion compared to a hydrophobic or less water-soluble drug. Hydrophobic drug release is dependent on polymer swelling and/or matrix erosion. The same active agent, when incorporated in a polymeric matrix, can present different behaviours due to differences in solubility and participation of the different processes outlined above (Agnes, 2003).

The mechanism of PCL biodegradation has been discussed above. Hydrophilic drugs like somatostatin tend to accumulate at the interface of the microparticles during the formulation processes and are released by desorption at the initial period of release (Dash & Konkimalla, 2012).

This results in a biphasic pattern of release where the initial burst release is much higher than for lipophilic drugs. This can be seen from the release profile of the drugs in Figures 4.8 and 4.9 where there is a higher percentage released initially which then slows to lower rate of release.

In comparison, Sandostatin LAR[®] exhibited a concentration-time profile with a limited initial burst release of octreotide, an erosion phase from weeks 3-5, and a slowly declining concentration to day 52 (Petersen, Bizec, Schuetz, & Delporte, 2011). This is a once-monthly formulation that is administered intramuscularly. Somatuline LA[®] which contains PLGA microparticles of biodegradable polymer containing lanreotide exhibits drug release in a biphasic pattern, that is, an early release of the peptide localized at the surface of the copolymer during the first 2 days after administration, followed by sustained release of lanreotide for about 1 week, starting at day 4, as a result of enzymatic breakdown of the microspheres, and then followed by an exponential decrease in drug release over the course of 14 days (Roelfsema, et al., 2008).

4.4 Conclusion

Based on the results from our work, the following conclusions can be drawn. Firstly, only the low molecular weight polymer (PCL_{1K}-PEG_{2K}-PCL_{1K}) was suitable for use with the SAW technique. This is due to the requirement that both the peptide and polymer had to be soluble in the same solvent (ethanol). The high molecular weight polymer (PCL_{5K}-PEG_{2K}-PCL_{5K}) could not be used because it would not dissolve in ethanol and somatostatin is not soluble in dichloromethane. Hence the suitability of use for that particular triblock copolymer (PCL_{5K}-PEG_{2K}-PCL_{5K}) for the SAW technique could not be evaluated. It must be mentioned that Alvarez et al (Alvarez, et al., 2009) have demonstrated encapsulation of BSA in PCL (molecular weight 65 kDa) with 54% of the BSA surviving the atomization process. The low molecular weight polymer (PCL_{1K}-PEG_{2K}-PCL_{1K}) encapsulated a negligible amount of FITC-DEAE-Dextran using the SAW technique. Although we did not succeed with the triblock copolymers using the SAW technique, it does not mean it will not work with a more sophisticated set-up with an enclosed apparatus, long drying tube and an automatic dispensing system for the polymer-peptide solution/dispersion as demonstrated by Alvarez et al (Alvarez, et al., 2009). The double-emulsion method worked better with the high molecular weight polymer compared to the low molecular weight polymer. As previously discussed in Section 4.3.1, the low molecular weight samples produced no encapsulation, possibly due to the similar molecular weights of FITC-DEAE-Dextran (3000-5000 Da) and the LMW polymer (4000 Da). The high molecular weight polymer produced good encapsulation efficiencies with the FITC-DEAE-Dextran ranging from 50% to ca. 65% at different polymer concentrations and sonication times (Table 4.5). However, with somatostatin, the encapsulation efficiency was lower and variable, ranging from 19%-43%. Vaishya

et al (Vaishya, et al., 2015) attempted the encapsulation of a synthetic somatostatin analogue-octreotide in a PCL_{10k}-PEG_{2k}-PCL_{10k} triblock copolymer using the same double-emulsion method. An encapsulation efficiency of 45% was achieved with this triblock polymer and the release studies demonstrated complete release of octreotide over 3 months. In their case, they were able to increase the hydrophobicity of octreotide using TEA, thus achieving a higher encapsulation efficiency. It cannot be assumed that the molecular weight of their chosen triblock copolymer affected the encapsulation efficiency since they did not compare to another triblock with a different molecular weight although the degradation times are indeed affected by polymer molecular weight (Makadia & Siegel, 2011). While we attempted the use of counter-ions to shield the positive charges on somatostatin, the propensity of self-assembly proved to be a drawback. The calculated pI of somatostatin is 8.3 (Wilmar Van Grondelle, et al., 2007) and adjusting the pH to 8.3 may affect the stability of the peptide. Based on the results of Herrmann and Bodmeier (Herrmann & Bodmeier, 1998), triblock polymers of PLGA may yield better encapsulation efficiencies using the double-emulsion method. We cannot predict if all triblock polymers will behave the same way without experimentation but it is reasonable to postulate that a hydrophilic peptide may be more easily entrapped in PLGA-PEG triblock polymers due to the higher hydrophilicity of that polymer combination. The triblock polymer chosen in our study was selected based on work by Vaishya's group encapsulating octreotide, a somatostatin analogue (Vaishya, et al., 2015). Wei, Qian and co-workers (Wei, et al., 2009) have published a thorough review on the use of PCL-PEG copolymers as drug delivery vehicles. In terms of production by the double-emulsion method, different kinds of PCL-PEG microspheres containing human serum albumin (HSA) were successfully prepared (Zhou, Deng, & Yang, 2003b) and the experimental parameters of the methods were investigated (Zarnbaux, et al., 1998). Similarly, microspheres based on PCL-PEG copolymer containing bovine serum albumin were prepared by adopting double emulsion method (J.-H. Kim & Bae, 2004). Such PCL-PEG copolymers have also been studied for protein delivery, for example, human serum albumin (HSA) was encapsulated in PCL-PEG microparticles using the double emulsion method with higher encapsulation efficiencies than PCL. Anionic PCL-PEG nanoparticles were prepared by modified emulsion solvent evaporation method with human basic fibroblast growth factor (bFGF) adsorbed onto the surface of nanoparticles by electrostatic interaction. In vitro release studies indicated a controlled release of bFGF from PCL-PEG-bFGF complex.

This study attempted the encapsulation of somatostatin in a PCL-PEG-PCL triblock polymer which has not been done before. A non-traditional technique using surface acoustic waves and a traditional double emulsion method were used. The results show that encapsulation and release of somatostatin is possible with the use of this triblock polymer, although low. The encapsulation

efficiency as well as the duration of release can be improved. Further work can be done to improve the amount of somatostatin entrapped by the polymer and that may also help to extend the duration of release. This was demonstrated by the sample 1 with SST 2.5% w/w and HMW polymer 2% w/w. In addition Wei and group (Wei, et al., 2009) suggest that addition of lipases to release buffers for studies with PCL microparticles more closely simulate the *in vivo* milieu. *In vitro* degradation profiles of biodegradable polymers frequently do not sympathize with the data of *in vivo* degradation experiments due to the presence of enzymes (M. P. Wu, Tamada, Brem, & Langer, 1994) and it has been reported that the *in vivo* degradation of PCL is significantly accelerated when in the presence of PCL-degrading enzymes, namely lipases, in the body (H. Sun, Mei, Song, Cui, & Wang, 2006). A study by Wu and co-workers (C. Wu, Jim, Gan, Zhao, & Wang, 2000) found that the presence of the microbial *Pseudomonas* lipase enhanced the degradation rate of PCL nanoparticles 1000-fold compared with purely hydrolytic degradation. An investigation on the effect of PEG incorporation on the biodegradation characteristics of PCL demonstrated that (Li et al., 2002) in the presence of *Pseudomonas* lipase, enzymatic degradation of PCL was not altered by the incorporation of PEG for both diblock and triblock copolymers compared to a PCL homopolymer. Bei's group, however, found that the degradation rate of PCL-PEG increased with increase in PEG content and in the presence of lipase (Bei, Li, Wang, Le, & Wang, 1998). The studies discussed provide considerations for future work, such as the addition of lipases to the release medium and difference in degradation times with higher PEG content.

CHAPTER 5 – INVESTIGATION OF THE EFFECTS OF SOMATOSTATIN ON THE EXPRESSION OF VEGF RECEPTOR-2 LEVELS AND VEGF SECRETION BY ARPE-19 CELLS IN HIGH GLUCOSE CONDITIONS

5.1 Introduction

The retinal pigment epithelium (RPE) plays a crucial role in retinal physiology and is responsible for the diffusion of nutrients to the retina from choroidal blood vessels by forming the blood–retinal barrier (BRB)(Luna, et al., 1997). The RPE secretes various growth factors to maintain the extracellular environment of the photoreceptors (Sheedlo, Li, & Turner, 1992) and it is where the phagocytosis of outer segments of photoreceptors occurs (Bok, 1993). RPE cells also produce various cytokines (Adamis, et al., 1993; Rafael Simó, Villarroya, Corraliza, Hernández, & Garcia-Ramírez, 2010) implicated in ocular diseases such as diabetic retinopathy,(Aiello, et al., 1994; Funatsu, Yamashita, Nakanishi, & Hori, 2002; Vogt, et al., 2006), choroidal neovascularization and diabetic macular edema (Funatsu, Yamashita, Ikeda, et al., 2002). Amongst the various growth factors and cytokines secreted by the RPE are vascular endothelial growth factor (VEGF), pigment epithelium-derived growth factor (PEDF), fibroblast growth factor (FGF) and platelet derived growth factor (PDGF). Vascular endothelial growth factors (VEGF) comprise a family of mitogenic proteins consisting of multiple homologs (Rafael Simó, et al., 2014). The RPE is the main source of VEGF in the posterior eye and expresses diffusible isoforms of VEGF, namely VEGF₁₆₅ and VEGF₁₂₁ but not VEGF₁₈₉ which is the cell-associated form. VEGF₁₆₅ is the predominant form and is found both circulating as well as bound to the cell and extracellular matrix. VEGF₁₂₁ is freely soluble while VEGF₁₈₉ and VEGF₂₀₆ are completely sequestered in the extracellular matrix (Rafael Simó, et al., 2014).

RPE cells express both receptors VEGF-R1 and VEGF-R2 for VEGF (Kociok, et al., 1998). VEGF-R2 is expressed on the apical side of the RPE but the secretion of VEGF in response to high glucose or hypoxia is basal (Blaauwgeers, et al., 1999). This is thought to be directed towards the VEGF-R2 receptors expressed by the endothelium of the choriocapillaris facing the RPE layer (Blaauwgeers, et al., 1999). VEGF-R2 is mainly responsible for the mitogenic, angiogenic, and permeability-enhancing effects of VEGF(Ferrara, 2004). While there is some discussion about the VEGF-R2 possibly being autocrine in function (Klettner, Westhues, Lassen, Bartsch, & Roider, 2013), upregulation of VEGF-R2 in early pre-clinical diabetic retinopathy was observed in streptozotocin-induced diabetic rats in ganglion cell layers, inner and outer nuclear layers as well as the RPE(Hammes, Lin, Bretzel, Brownlee, & Breier, 1998). There is increased expression of VEGF-R2 in human diabetic retinopathy correlated to the presence of leaky retinal vessels (Witmer, et al., 2002) which was linked to the effects of VEGF on vascular permeability (Schlingemann, Hofman, Vrensen, & Blaauwgeers, 1999).

VEGF produced by RPE cells has been implicated in the induction of choroidal neovascularization and macular degeneration (Grossniklaus, et al., 2002; Ohno-Matsui, et al., 2001; Schwesinger, et al., 2001). Increased VEGF expression has been noted to precede retinal proliferative changes in diabetic rats (Sone, et al., 1999). However, it should be noted that VEGF does have important constitutive functions in the healthy adult retina. VEGF is a survival factor for endothelial cells and important for the maintenance of the choroid (Gerber, et al., 1998; Saint-Geniez, Kurihara, Sekiyama, Maldonado, & D'Amore, 2009). Additionally, VEGF protects the RPE, Müller cells, photoreceptors, and retinal neurons from hypoxia-induced apoptosis via a direct trophic effect as well as through angiogenesis (Byeon, et al., 2010; K. M. Ford, Saint-Geniez, Walshe, Zahr, & D'Amore, 2011; Nishijima, et al., 2007; Saint-Geniez, et al., 2008), and may save axotomized ganglion cells from delayed cell death (Kilic, et al., 2006).

ARPE-19 is a rapidly growing, spontaneously evolved human cell line which was purified by selective trypsinization of a primary RPE culture. ARPE-19, established by Dunn et al. (Dunn, Aotaki-Keen, Putkey, & Hjelmeland, 1996) retains many properties characteristic of RPE cells (Trevino, Schuschereba, Bowman, & Tsin, 2005) including defined cell borders, an overall 'cobblestone' appearance and noticeable pigmentation. The cell line is widely used in cell biology and biochemical studies (Geiger, Waters, Kamp, & Glucksberg, 2005; R. K. Sharma, Orr, Schmitt, & Johnson, 2005). Lynn and co-workers (Lynn, et al., 2017) investigated if the secretion of VEGF-A was comparable to those from primary RPE cells isolated from human donors. Their study showed that ARPE-19 monolayers secreted VEGF at levels comparable to VEGF levels secreted by the primary RPE cells (Blaauwgeers, et al., 1999). ARPE-19 cells have been used as *in vitro* models to study the effects of high glucose in diabetes in a number of studies which have been thoroughly discussed by Szabadfi and co-workers (Szabadfi, Pinter, Reglodi, & Gabriel, 2014).

The physiological role of somatostatin in the retina and possible beneficial effects in diabetic retinopathy have been discussed at length in Chapter 1. Expression of SSTR1 and SSTR2 in RPE cells, both *in vitro* and *in vivo*, have been demonstrated (Katz, Klisovic, O'Dorisio, Lynch, & Lubow, 2002; Klisovic, et al., 2001). Somatostatin is produced in the human retina (van Hagen, et al., 2000) along with expression of its receptors, with SSTR1 and SSTR2 being the most widely expressed (Cervia, Casini, & Bagnoli, 2008b; Klisovic, et al., 2001; Lamboojij, et al., 2000). It has been postulated that somatostatin acts through its receptors to downregulate VEGF secretion in human RPE cells, amongst other effects (Sall, Klisovic, O'Dorisio, & Katz, 2004), hence, ARPE-19 cells were chosen for this study. In this chapter, we investigate the possible effects on cell viability of somatostatin in solution, released somatostatin from the SST 5% w/w in HPMC 6% w/w hydrogels as well as blank

HPMC using a 3-(4, 5-dimethylthiazol-2-yl)-2, 5-diphenyl tetrazolium bromide (MTT)-based cell viability assay. The effect of somatostatin on VEGF-R2 expression by ARPE-19 cells in both high and normal glucose conditions is investigated. The amount of VEGF secreted by the ARPE-19 cells in the same conditions is quantified with an Enzyme-Linked Immunosorbent Assay in the presence of somatostatin in solution as well as somatostatin released at 24 hours (Release Day 1) and 10 days (Release Day 10) from the SST 5% w/w in HPMC 6% w/w hydrogels.

5.2 Materials and Methods

5.2.1 Culture of ARPE-19 cells

ARPE-19 was obtained from American Type Culture Collection (Manassas, VA) and cultured under conditions as described by a number of studies (M. Villarroel, Garcia-Ramírez, Corraliza, Hernández, & Simó, 2011; Marta Villarroel, García-Ramírez, Corraliza, Hernández, & Simó, 2009). The cells were cultured under normoglycemic (5.5 mmol/L D-glucose) or hyperglycemic (25 mmol/L D-glucose) conditions at 37°C under 5% (v/v) CO₂ in Dulbecco's Modified Eagle Medium (DMEM)(Thermo Fisher Scientific, Life Technologies Australia) supplemented with 10% (v/v) fetal bovine serum (FBS)(Gibco, Life Technologies Australia) and penicillin/streptomycin/glutamine (Gibco, Life Technologies Australia). ARPE-19 cells between passages 10- 20 were used and the media was changed every third day.

5.2.2 MTT cell viability assay

The effects on cell viability of 10⁻⁷ M and 10⁻⁶ M somatostatin, Release Day 1 and Release Day 10 samples from SST 5% w/w in HPMC 6% w/w hydrogels and blank HPMC 6% w/w hydrogels was assessed in ARPE-19 cells using the In Vitro Toxicology Assay Kit; MTT based (Sigma-Aldrich, St Louis, MO) as per the manufacturer's instructions. ARPE-19 cells seeded onto 96-well plates (Corning, USA) at a density of 10⁴ cells per well were allowed to grow for 3 days. After serum starvation for 24h, cells were exposed to samples as above and incubated for 24 hours. Background control wells without cells contained 50 µL 3-(4, 5-dimethylthiazol-2-yl)-2, 5-diphenyl tetrazolium bromide (MTT) reagent and 50 µL of cell culture media. After treatment with 50 µL of MTT reagent and 50 µL of cell culture media for 3 hours at 37 °C, 150 µL MTT solubilization solution was added to each well. Levels of formazan reaction product were determined by measuring the absorbance at 570 nm in a plate reader (Clariostar, BMG Labtech, Germany).

5.2.3 Immunofluorescence studies of VEGF-R2 expression

The ARPE-19 cells were seeded in 12-well plates (Corning, USA) at a density of 10^4 cells per well. They were serum-deprived for 24 hours before stimulation with glucose for experiments. The confluent cells exposed to different concentrations of glucose (normal glucose [NG, 5 mM] or high glucose [HG, 25mM] in the presence or absence of somatostatin at 10^{-5} M to 10^{-8} M for 24 hours and 72 hours. The experiment was performed in triplicate for 10^{-7} M and 10^{-6} M somatostatin concentrations at 72 hours. The cells were fixed with methanol (which had been stored at -20°C prior to use) for 15 minutes at room temperature. The methanol was decanted and the wells were washed twice with ice-cold PBS. The cells were then incubated with 1% bovine serum albumin (BSA) (Sigma Aldrich, St Louis, MO) in PBS for 30 minutes at room temperature. This was done to block non-specific binding of the primary antibody. The 1% BSA solution was decanted and the wells rinsed with PBS. A rabbit polyclonal antibody to VEGF receptor 2 (ab2349) (Abcam, UK) was applied at a 1/100 dilution to all wells except the negative controls. The cells were incubated with the primary antibody overnight at 4°C . The next morning, cells were washed thrice with ice-cold PBS. The secondary antibody, a goat polyclonal secondary antibody to rabbit IgG - H&L (Alexa Fluor[®] 488) (ab150077) (Abcam, UK) was applied to all the wells at a 1/500 dilution. The plates were incubated in the dark for one hour at room temperature. Both primary and secondary antibodies were diluted in 1% BSA in PBS. The cells were washed thrice again in ice-cold PBS for 15 minutes in the dark. The last step was the application of DAPI (4', 6-Diamidino-2-phenylindole dihydrochloride) (Sigma-Aldrich, St Louis, MO) at a concentration of $1\ \mu\text{g}/\text{mL}$ into each well for the visualization of cell nuclei. The wells were then visualized using Nikon Eclipse Ti-E (inverted) confocal microscope (Nikon Instruments, Japan). The emission (bandwidth) for FITC ranged from 496 to 535 nm. The images were then analysed using the NIS-Elements Analysis Software (Nikon Instruments, Japan). Analysis of each image was done the same way by doing a count for the number of fluorescent objects. The background fluorescence was subtracted using the software and the "clean, smooth and separate" features were used for picking up distinct fluorescent spots. Restrictions for area and circularity were applied as well as using the same range for fluorescence intensity for all images analysed. The object count thus obtained for each image was then recorded and the mean calculated from the triplicate of wells.

5.2.4 Quantification of VEGF secretion by ELISA

ARPE-19 cells were seeded on a 12-well plate (Corning, USA) and allowed to reach near confluence. The cells were grown in conditions as described above in HG and NG, as well as in the presence of somatostatin at 10^{-5} M to 10^{-8} M for 72 hours, with triplicate wells for each condition. The study was repeated with Release Day 1 and Day 10 samples from SST 5% w/w in HPMC 6% w/w hydrogels and 10^{-7} M and 10^{-6} M somatostatin with 24 hour incubation. The cell culture medium was collected and centrifuged at 1400 RPM for 1 minute to remove any debris. The resulting supernatant was used for the estimation of VEGF by solid-phase sandwich Enzyme-Linked Immunosorbent Assay (ELISA) (Invitrogen, Life Technologies, USA) according to the manufacturer's protocol. This kit recognizes human VEGF₁₆₅ and VEGF₁₂₁ isoforms. At the end of the protocol, a plate reader (Clariostar, BMG Labtech, Germany) was used to read the absorbance of the wells at of 450 nm.

5.2.5 Statistical analysis

Results were subjected to statistical analysis with ANOVA (GraphPad Prism version 7.02, GraphPad Software, San Diego California USA), followed by post hoc analysis according to Dunnett or Neuman-Keuls and $p < 0.05$ was considered statistically significant.

5.3 Results and Discussion

5.3.1 MTT cytotoxicity assay

The results of the MTT assay (Figure 5.1) were analysed using one-way ANOVA with multiple comparisons test. In both high and normal glucose conditions, only release Day 1 samples caused significantly more cytotoxicity (65% and 62% respectively) compared to control ($p < 0.005$). Release day 1 samples also caused more VEGF to be released in the ELISA assay as discussed in section 5.3.3. It was observed during the course of the release studies that when sampling the release buffer above the somatostatin 5% w/w in HPMC hydrogels at 24 hours, the sample withdrawn was of thicker consistency and more difficult to withdraw than that of simulated lachrymal fluid alone. The release Day 1 samples were very viscous when sampled from above the SST 5% w/w in HPMC 6% w/w hydrogels. This is likely to be due to the presence of diluted HPMC in the release buffer at the interface of the hydrogel by the SLF placed on the gel. The viability of the cells is likely to be adversely affected with a viscous layer applied on them. This would result in the high percentage of cytotoxicity observed. The concentration of SST that is present in the release Day 1 samples (in the order of 10^{-5} M) is higher compared to the other treatments, contributing to the effect caused by the

viscosity of the HPMC. In contrast, by release Day 10, lower levels of cytotoxicity were observed (11% vs 65% in high glucose and 62% vs 35% in normal glucose). The effect of macromolecules such as methylcellulose contributing to a higher viscosity in cell culture media is discussed by Khorshid *et al* (Khorshid, 2005). It is inferred that viscosity most likely affects the diffusional motions of molecules in and out of the space between cell and substratum. Tuvia *et al* (Tuvia, et al., 1997) have found that extracellular fluid macroviscosity can affect cell membrane activities and have proposed that the effect of solvent viscosity on a solute (proteins or cells) is determined by the size ratio of the viscous cosolvent to the solute; while for proteins the macromolecules are too big to affect their microenvironment, for cells they can be viewed as a microenvironment. Yedgar's group (Yedgar & Reisfeld, 1990) have proposed that extracellular fluid viscosity can affect cellular and biochemical processes as well. Hughes *et al* (P. Hughes, Delahaye, Boix, Chang, & Lyons, 2005) found that HPMC up to a concentration of 1.2% diminishes ARPE-19 cell viability by about 20-40% especially at 24 hours incubation (as per the MTT assay). They hypothesize an effect on mitochondrial dehydrogenase by HPMC treatment. In this study, only the samples from Release Day 1 demonstrated significant cytotoxicity. These samples had the highest concentration of somatostatin released as well as being highly viscous due to the dilution of the HPMC hydrogel at the interface with the release buffer.

An additional explanation for the observed results is provided by a study done by Papadaki's group (Papadaki, Tsilimbaris, Pallikaris, & Thermos, 2010). Their group investigated the effect of somatostatin in concentrations ranging from 10^{-10} M to 10^{-4} M on the viability of human RPE cells (D407 cell line) using a MTT assay. They reported a decrease in cell viability in a concentration-dependent manner for SST concentrations 10^{-8} – 10^{-4} M. The SST concentrations in the Release Day 1 samples in our study fall within that range. While there was an observed decrease in cell number due to SSTR1 and SSTR5-mediated apoptosis, Papadaki *et al* found that activation of SSTRs 2, 3 and 4 led to inhibition of cell growth via antiproliferative actions. The anti-proliferative actions of SST have been discussed in Chapter 1. A possible combination of the actions discussed by Papadaki and group coupled with the viscosity of the samples may have led to the results in this study. The SST concentrations found in the Release Day 10 samples are much lower, in the order of 10^{-8} M, below the range reported by Papadaki's group. It must also be taken into account that other studies conducted on cells with somatostatin (as previously discussed in Section 5.3.2) have not reported any cytotoxicity with their tested concentrations. HPMC is generally regarded as safe (GRAS) and is widely applied in drug and food formulations. In fact, cellulose derivatives, specifically hydroxyethylcellulose and sodium carboxymethylcellulose, were investigated as candidates for ophthalmic viscosurgical devices (Andrews, Gorman, & Jones, 2005). According to the authors, these

polymers were chosen due to their known biocompatibility and ocular acceptability. The MTT assay presents the results from the application of a static layer of viscous HPMC on the cells. This is not representative of the dynamic ocular environment *in vivo*. However, the MTT assay was conducted as part of the safety assessment of the SST 5% w/w in HPMC 6% w/w hydrogels, which have not been studied elsewhere in combination.

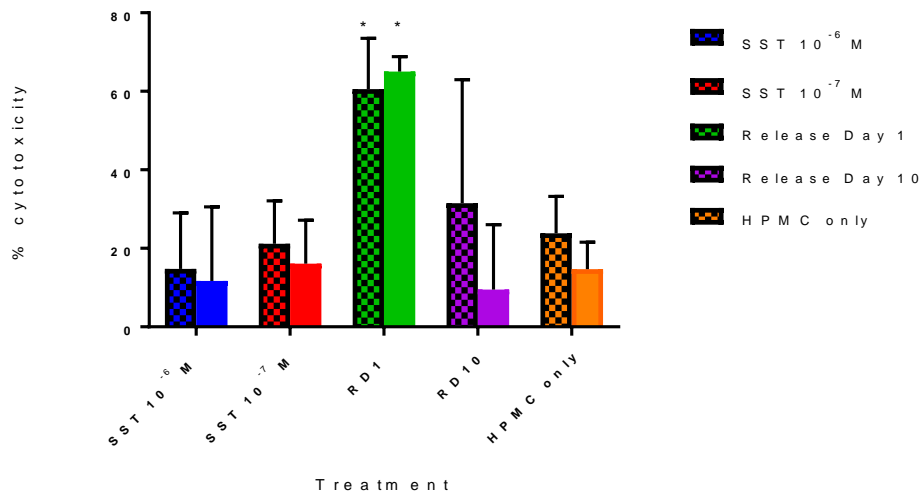


Figure 5.1: Results of MTT assay assessing cytotoxicity of applied treatments on ARPE-19 cells in high (25 Mm) (solid bars) and normal (5 mM) (spotted bars) glucose conditions. Data shown are mean \pm SD (n = 3). The symbol * denotes a significant increase in cytotoxicity compared to control wells grown in same conditions with no treatments applied.

5.3.2 Immunofluorescence studies of VEGF-R2 expression

A pilot study was performed as previously described (Section 5.2.3) to determine the concentration of somatostatin that significantly affects the expression of the VEGF-R2 levels in the ARPE-19 cells. The cells were incubated with somatostatin 10⁻⁸M TO 10⁻⁵ M in both high and normal glucose conditions. Although the supplier recommends culture of the cells at 18 mM glucose, in this study, 5.5 mM glucose was picked as representative of physiological glucose levels and 25 mM glucose as high glucose conditions. A study by Heimsath Jr. *et al* (Heimsath Jr, et al., 2006) recommends that 5.5 mM glucose be included as a euglycemic concentration when studying VEGF release from ARPE-19 cells. Heimsath and co-workers found that a high level of glucose (18 mM) led to a significant

increase in VEGF secretion from the ARPE-19 cells compared to 5.5 mM glucose at all tested time points.

The results of our pilot immunofluorescence study are shown in Figure 5.2. Statistical analysis as described above (Section 5.2.5) showed that treatment with SST 10^{-6} M and 10^{-7} M produced a significant ($p < 0.05$) downregulation of the expression of VEGF-R2 compared to control wells in high glucose at 72 hours. In normal glucose media, there were no significant differences in VEGF-R2 expression between the treatment and control wells. The experiment was then repeated further on two separate occasions at 72 hours with only the 2 concentrations of SST that had showed significant results in the pilot study. The VEGF-R2 expression assays were conducted on three different occasions on three different batches of ARPE-19 cells in order to give a true triplicate, with triplicate wells for each treatment. The data as presented is obtained from three separate assays \pm S.D. It is acknowledged that the error bars are large, however, it is not uncommon for in vitro biological assays. The triplicate assays were performed with 2 different batches of antibodies and some variances may occur inevitably although all other conditions were kept the same. Similarly large error bars have been found in the following (Kannan, et al., 2006; Saenz-de-Viteri, et al., 2016; Senthilkumari, Sharmila, Chidambaranathan, & Vanniarajan, 2017).

The results of the triplicate studies (Figure 5.3) reveal that only SST 10^{-7} M produced a significant downregulation of VEGF-R2 expression levels in high glucose conditions. There were no significant differences in VEGF-R2 expression between the control wells and the treatment wells in normal glucose conditions. The same experiment performed with 24 hours incubation with SST 10^{-6} M and 10^{-7} M did not show any significant effects on the expression of VEGF-R2 in the ARPE-19 cells in both high and normal glucose conditions. This may mean that a change in the expression levels of the VEGF-R2 in response to high glucose conditions may possibly take longer than 24 hours to occur or may not be detected by the immunofluorescence study at 24 hours.

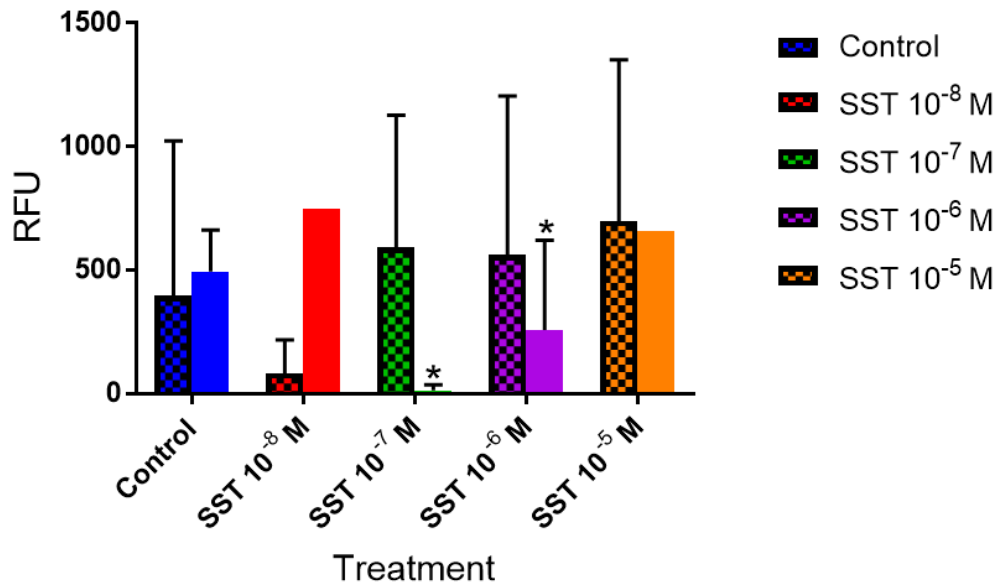


Figure 5.2: Dose-response of VEGF-R2 expression levels in the presence of somatostatin 10^{-8} M to 10^{-5} M in high glucose (25 mmol/L) (solid bars) and normal glucose (5 mmol/L) (dotted bars) conditions. Results are presented as mean + SD. (* indicates the concentrations that were significantly different to control wells)

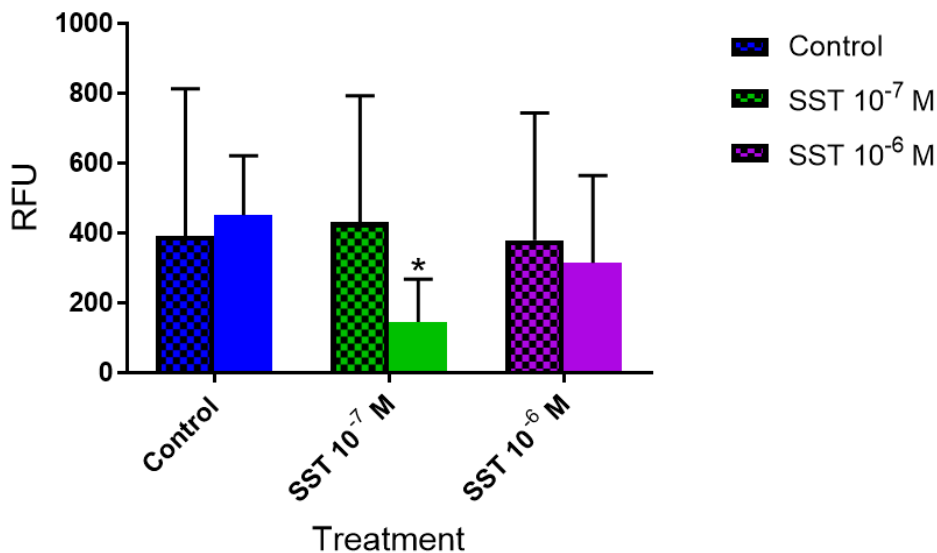


Figure 5.3: Effect of somatostatin 10^{-6} M and 10^{-7} M on VEGF-R2 expression levels in high glucose (25 mmol/L) (solid bars) and normal glucose (5 mmol/L) (dotted bars) conditions (n=3). Results are presented as mean + SD. (* indicates the concentrations that were significantly different to control wells)

The images below (Figures 5.4 to 5.7) are a representative of the confocal images taken of the cells in the treatment and control wells. SST 10^{-5} M formed a gel (Figure 5.6) in the presence of the electrolytes in the cell culture media which acted as a barrier to the binding of the primary antibody to the VEGF-R2. This is consistent with the reported self-assembly of SST at lower concentrations in the presence of electrolytes (Wilmar Van Grondelle, et al., 2007) such as those found in the culture medium than in the absence of electrolytes. Therefore, those wells were unable to be analysed as the gel layer on the cells prevented an accurate determination of the VEGF-R2 expression through the binding of the primary and secondary antibodies.

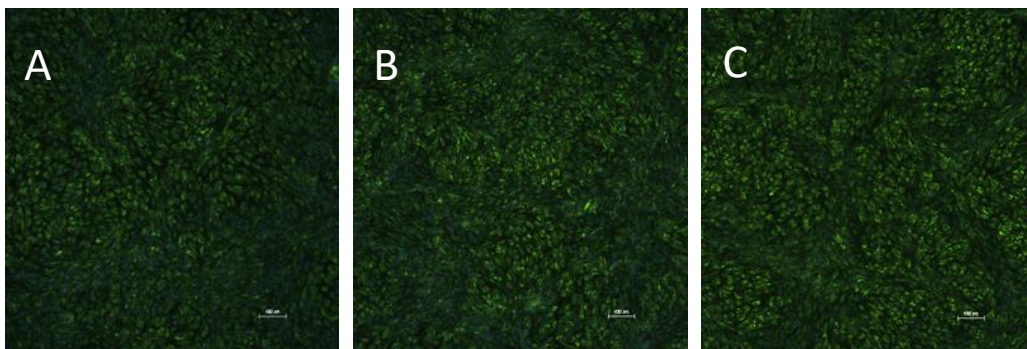


Figure 5.4: Confocal images of wells incubated with (A) SST 10^{-7} M (B) SST 10^{-6} M and (C) control in high glucose at 72 hours.

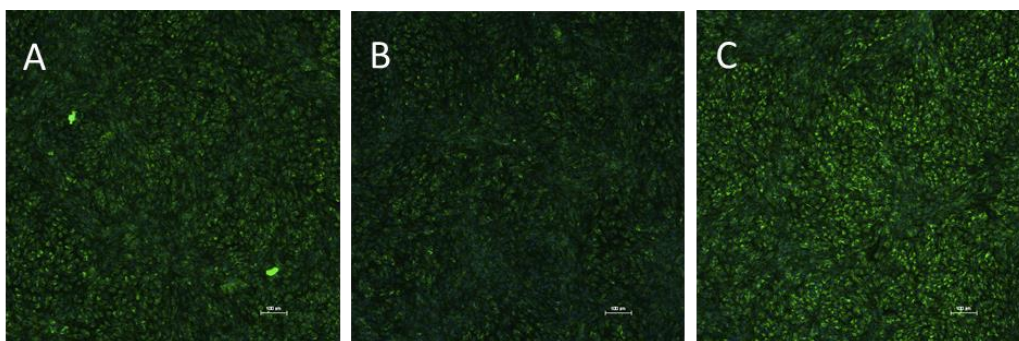


Figure 5.5: Confocal images of wells incubated with (A) SST 10^{-7} M (B) SST 10^{-6} M and (C) control in normal glucose at 72 hours.

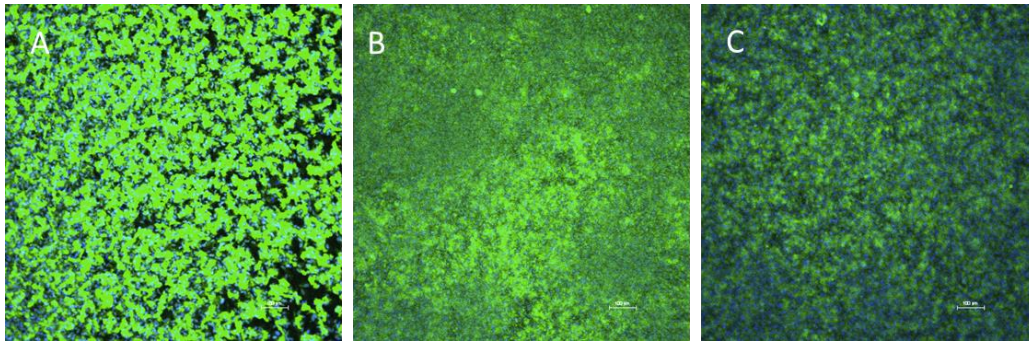


Figure 5.6: Confocal images of SST 10^{-5} M SST gelled in (A) normal glucose (B and C) in high glucose at 72 hours.

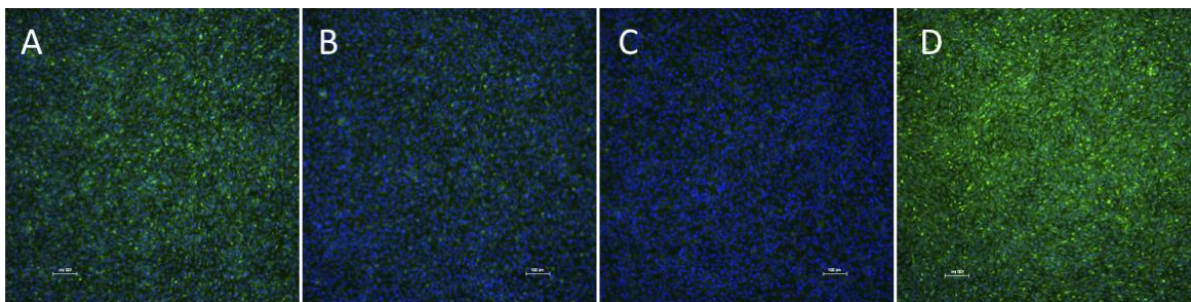


Figure 5.7: Confocal images of expression of VEGF-R2 in response to different SST concentrations in high glucose at 72 hours. (A) SST 10^{-8} M (B) SST 10^{-7} M (C) SST 10^{-6} M (D) high glucose only control

To the best of our knowledge from a review of current literature, this is the first study investigating the effect of SST on the expression of VEGF-R2 in ARPE-19 cells in high glucose conditions alone.

Figures 5.7 of representative wells illustrate the response of the ARPE-19 cells to the presence of SST with regard to VEGF-R2 expression in high glucose. The confocal images in Figure 5.7 show less fluorescence in the wells with SST 10^{-7} M and 10^{-6} M compared to the control well in high glucose.

The results of the study overall suggest a downregulation of VEGF-R2 expression in ARPE-19 cells by SST 10^{-7} M in high glucose.

Hyperglycemia results in a variety of metabolic imbalances and vascular changes in the retina prior to clinical diagnosis of DR and is established as a major risk factor for the development and progression of DR (Klein, Klein, Moss, & Cruickshanks, 1998). Since transport of glucose into the retina does not rely on insulin but occurs instead through the glucose transporter-1 (Glut-1) (Sone, Deo, & Kumagai, 2000), hyperglycaemia leads to high intracellular glucose levels, leading to the formation of free radicals (oxidative stress) and a state of intracellular 'pseudohypoxia' (Williamson, et al., 1993).

The formation of advanced glycation end products (AGEs) as a result of hyperglycemia are found to be increased in diabetic retina (Stitt, et al., 1997). These AGEs cause increased oxidative stress and subsequent cell death, leading to a gradual loss of retinal cells. For these reasons, high glucose conditions alone were applied to the cells in this study.

VEGFRs are also upregulated in non-proliferative diabetic retinopathy (G. Smith, McLeod, Foreman, & Boulton, 1999). As previously discussed in Section 5.1, upregulation of VEGFR-2 in early preclinical DR was observed in streptozotocin-induced DM in rats (Hammes, et al., 1998) and the presence of VEGFR-2 correlated with the presence of leaky retinal vessels (Witmer, et al., 2002) in humans. This may suggest that the vascular expression of VEGFR-2 enables the effects of VEGF-A such as increased vascular permeability in areas with established DR (Schlingemann, et al., 1999). Induction by VEGF-A itself can upregulate VEGF-R2 expression, as was shown in the monkey retina in a monkey model of VEGF-induced retinopathy (Witmer, et al., 2002). Summarily, upregulation of VEGF-R2 is seen in the pathological changes caused by VEGF and can be induced by VEGF itself. This explains the rationale behind our immunofluorescence study as we sought to determine if SST had any effects on VEGF-R2 expression. In this regard, the results of our study are promising in the investigation of the relationship between SST and VEGF, through the expression of VEGF-R2 on the apical surface of the ARPE-19 cells. It is conceivable to hypothesize that a downregulation of VEGF-R2 expression by SST may result from a decrease in VEGF secretion. This hypothesis was investigated in Section 5.3.3.

In studies done with SST analogues, octreotide was applied to mouse retinal explants in hypoxic conditions with analyses of VEGF secretion and VEGF-R2 expression (Mei, et al., 2011). Mei *et al* found that octreotide decreased VEGF secretion as well as inhibited the phosphorylation of VEGF-R2 in the conditions studied, thus inhibiting the downstream effects of VEGF-R2 activation. The effects of octreotide were postulated to be due to actions on SSTR2, which is consistent with work done by Dal Monte *et al* (Dal Monte, et al., 2007) in a transgenic mouse model of hypoxia-induced neovascularization. Hypoxia increased the expression of VEGF and its receptors, VEGF-R1 and VEGF-R2 and somatostatinergic function at SSTR2 reduced this increase. In the context of the results of the current study, this provides a hypothesis of the mechanism of VEGF-R2 downregulation by SST. This is further supported by the work of Klisovic *et al* (Sall, et al., 2004) demonstrating that action on SSTR2 by somatostatin and its analogue, octreotide, reduced downstream VEGF synthesis by inhibition of phosphorylation of IGF-1R in ARPE-19 cells. VEGF-R2 expression was not assessed.

Klisovic and co-workers found SST 10^{-11} M to 10^{-9} M to be most effective for reduction of VEGF synthesis. This is in contrast to our study which found SST 10^{-7} M to be most effective in the downregulation of VEGF-R2, in the range of SST 10^{-8} M to 10^{-5} M investigated, keeping in mind that

the markers are different. While there are multiple studies done on the effect of SST on VEGF secretion, these studies are usually performed under different conditions to the current study, such as under hypoxic conditions and with no assessment or report of VEGF-R2 expression. As such, it can perhaps be hypothesized that this study has investigated the expression of VEGF-R2 as a “proxy” for the effects of SST on VEGF secretion. These results then led to the study discussed in the following section (5.3.3) to assess VEGF secretion directly.

5.3.3 Quantification of VEGF secretion by ELISA

Based on the results from the immunofluorescence studies, an ELISA assay was conducted as described above with SST 10^{-8} M to 10^{-5} M applied to the cells and incubated for 72 hours. The results of the ELISA assay (Figure 5.8) show that SST did not have a statistically significant effect on the amount of VEGF secreted in high glucose and normal glucose conditions. It was hypothesized that the effect of SST on VEGF secretion may occur prior to the change in the expression of VEGF-R2 (at 72 hours), as reported in our results from Section 5.3.2. There were a number of studies that investigated the changes in VEGF secretion by retinal cells at shorter time points ranging from 4 hours to 48 hours (Heimsath Jr, et al., 2006; Mugisho, et al., 2018; Sall, et al., 2004; S. X. Zhang, Wang, Gao, Parke, & Ma, 2006). The study was thus repeated at the 24hr time-point in high and normal glucose conditions (Figure 5.9). The treatments applied were SST 10^{-6} M and 10^{-7} M and release samples from SST 5% w/w in HPMC 6% w/w hydrogels at day 1 and day 10. Levels of VEGF secretion are higher in high glucose compared to normal glucose conditions at both 24 hours (Figure 5.8) and 72 hours (Figure 5.9), although not significantly so. At both time points studied, there was no significant down-regulation of VEGF secretion by the treatments applied compared to controls in high and normal glucose conditions (Figures 5.8 and 5.9). Paradoxically, there was a significant increase in the amount of VEGF secreted in the wells treated with SST 10^{-7} M and release Day 1 samples in high glucose conditions only (Figure 5.9). This may be attributed to the highly viscous nature of the release day 1 samples which may have an irritant effect on the cells when applied. This correlates to the results of the MTT assay in Section 5.3.1. No explanation can be offered for the significant increase in VEGF levels in the wells treated with SST 10^{-7} M at 24 hours, as this effect was not observed in the 72 hour study (Figure 5.8) and requires further investigation.

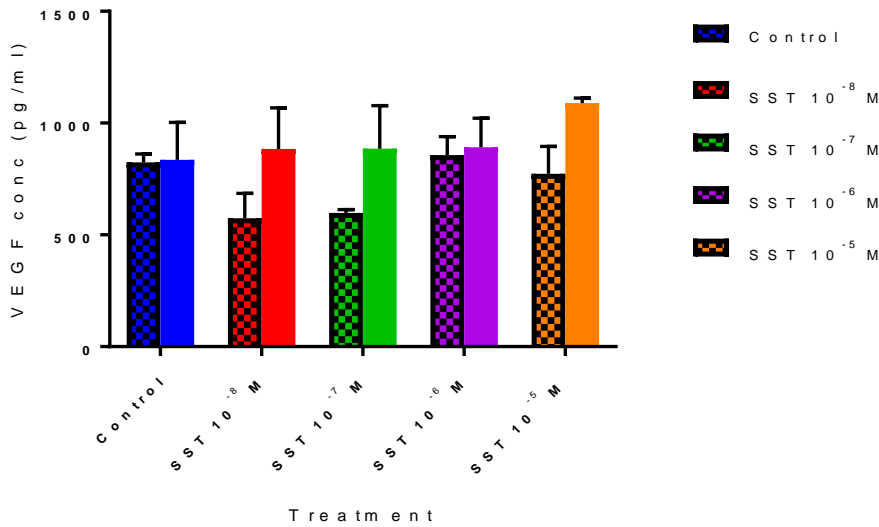


Figure 5.8: Results of ELISA assay of effect of somatostatin 10⁻⁸ M to 10⁻⁵ M in high glucose (25 mmmol/L) (solid bars) and normal glucose (5 mmol/L) (dotted bars) conditions on VEGF secretion at 72 hours. (n=3). Results are presented as mean + SD. (* indicates the concentrations that were significantly different to control wells). There were no significant differences between control and treatments in normal and high glucose conditions.

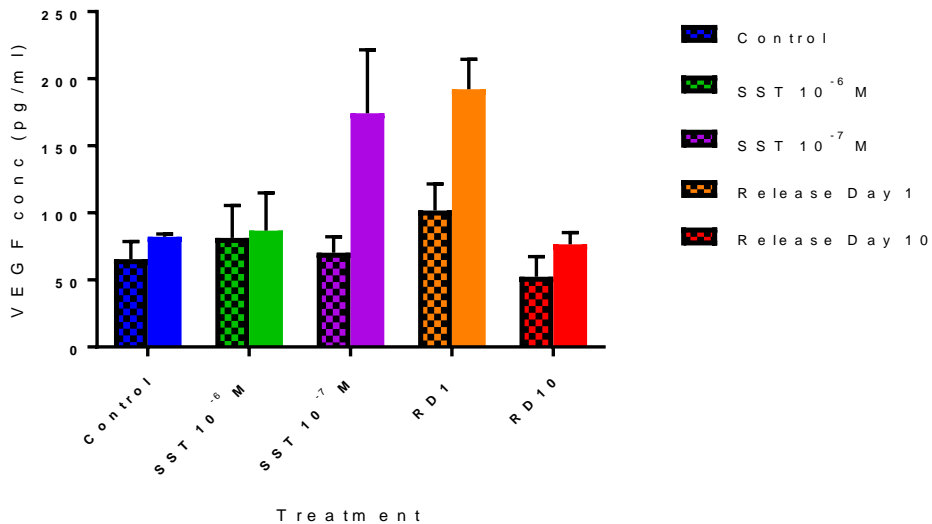


Figure 5.9: Results of ELISA assay of effect of somatostatin 10⁻⁶ M and 10⁻⁷ M and Release samples Day and Day 10 from SST 5% w/w in HPMC 6% w/w hydrogels in high glucose (25 mmmol/L) (solid bars) and normal glucose (5 mmol/L) (dotted bars) conditions on VEGF secretion at 24 hours. (n=3). Results are presented as mean + SD. (* indicates the concentrations that were significantly different

to control wells). A paradoxical significant increase in VEGF levels were seen in wells treated with SST 10^{-7} M and Release Day 1 samples from SST 5% w/w in HPMC 6% w/w hydrogels.

There are a number of studies in the literature that have been conducted under different conditions to this study and may provide some hypotheses for the results above. Rupenthal and Green (Mugisho, et al., 2018) subjected ARPE-19 cells to culture in HG conditions alone (15 mM glucose), a combination of pro-inflammatory cytokines 10 ng/mL TNF- α and 10 ng/mL IL-1 β or a combination of high glucose, 10 ng/mL TNF- α and 10 ng/mL IL-1 β . Levels of VEGF secretion, amongst other markers were assessed 24 hours post-treatment. The authors found that HG alone did not produce a significant increase in VEGF secretion compared to the group challenged with the combination of inflammatory cytokines and HG. This is consistent with the findings in our study, as the levels of VEGF between the control wells in high glucose and normal glucose conditions were not significantly different. The combination of inflammatory cytokines and HG significantly increased VEGF release ($p < 0.0001$) with VEGF concentrations being more than double its baseline level in the study by Rupenthal *et al.* This implies that high glucose alone, in the absence of other factors involved in the pathology of DR, may be insufficient to affect levels of VEGF release by the ARPE-19 cells.

With regards to the VEGF levels determined by the ELISA assay, we are not the first to report no effect on VEGF secretion by somatostatin-14. Studies by Lawnicka and co-workers (Ławnicka, et al., 2000) have been unable to demonstrate the inhibitory effects of somatostatin-14 or octreotide in concentrations of 10^{-14} to 10^{-6} M on VEGF secretion in vitro, in HeCa10 mouse endothelial cells. Although somatostatin and octreotide displayed antiproliferative activity in HeCa10 cells, they did not suppress VEGF levels in the culture supernatant. The authors concluded that the abrogation in VEGF secretion by somatostatin agonists may be primarily an in vivo effect, which may not be observed in certain cell types as in vitro experimental systems. Of the few studies that have assessed the impact of high glucose alone on VEGF secretion, Sone's group (Sone, et al., 1996) reported that VEGF production in bovine cultured RPE cells was significantly elevated at 10 days, but not by 1 or 3 day exposure to 16.5 mM glucose compared to a 5.5 mM glucose group. In the context of the current study, this may mean that in the absence of other cytokines, a longer duration of study is required to detect an increased level of VEGF secretion in high glucose conditions.

According to another school of thought, it has been suggested that hyperglycemia might not be responsible for all clinical aspects of diabetic retinopathy, since there are numerous cases of this pathology without evident hyperglycemia (Chan, Cole, & Hanna, 1985; Harrower & Clarke, 1976), raising the question if hyperglycemia per se is necessary or sufficient for the establishment of the disease (Antonetti, et al., 2006; Barber, et al., 2001). Diabetic retinopathy also presents

characteristics of a low grade chronic inflammatory disease, characterized by increased production of cytokines (Carmo, Cunha-Vaz, Carvalho, & Lopes, 1999; Kowluru & Odenbach, 2004).

In a study similar to this study, Senthilkumari (Senthilkumari, Sharmila, Chidambaranathan, & Vanniarajan, 2016) investigated VEGF-mRNA expression as well VEGF secretion by ARPE-19 cells in normal glucose (5 mM) as well as two different concentrations of high glucose (25 mM and 50 mM) at 72 hours. In that work, although there was a significant upregulation of VEGF mRNA at 72 hours at both high glucose concentrations tested versus normal glucose, only the VEGF secretion (measured by ELISA) in 50 mM glucose was significantly different to normal glucose conditions. These results are consistent with the current findings of the VEGF secretion at 72 hours in 25 mM glucose.

The assessment of VEGF mRNA was also performed by Wang and co-workers (Wang, et al., 2012), who reported the increased expression of VEGF mRNA and protein (assessed by Western Blot) at 48 hours in ARPE-19 cells cultured in 30, 40 and 50 mM glucose compared to normal (5.5mM) glucose. The implications of the results of Wang's study for this work suggest the use of a different technique in addition to ELISA for the quantification of VEGF secretion as well as a higher level of glucose for HG conditions.

A study that used the same cell line and glucose concentrations as this study was performed by Miranda and Simó (Miranda, et al., 2011). However, the markers assessed did not include VEGF. The treatment investigated (fenofibrate) was applied for 72 hours (days 16, 17 and 18 of culture). It was found that high glucose alone and in combination with hypoxia triggered increased levels of stress markers and the induction of pro-apoptotic factors. Reactive oxygen species (ROS) were elevated and the integrity of tight junctions was disrupted in this study. This suggests that in further work, markers such as pro-apoptotic factors in addition to VEGF may be investigated.

Summarising the studies discussed above in the context of this study, significant effects of somatostatin on VEGF secretion may have been detected at a longer duration of incubation in HG, higher glucose levels (30-50 mM), the addition of inflammatory cytokines and/or with use of additional techniques like Western Blot. There are several studies that have been conducted on various retinal cell types, retinal explants and animal models that have demonstrated a variety of beneficial effects in the retina resulting from somatostatin at different concentrations (Akopian, Johnson, Gabriel, Brecha, & Witkovsky, 2000; Arroba, et al., 2016; Baldysiak-Figiel, et al., 2004; Bigiani, et al., 2004; D. Cervia, et al., 2012; Cervia, Martini, et al., 2008; Cervia, et al., 2002; Dal Monte, et al., 2007; Kokona, et al., 2012; Kouvidi, Papadopoulou-Daifoti, & Thermos, 2006; Niki Mastrodimou, et al., 2006; N. Mastrodimou, et al., 2005; Wilson, et al., 2001). In these studies, a

variety of markers have been evaluated in response to somatostatin in different conditions, however, VEGF was chosen for this study as its role in the pathology of diabetic retinopathy is established. This hypothesis is supported by the anti-VEGF agents that are currently on the market. Future work with different retinal cell types, a series of higher glucose concentrations, inclusion of inflammatory cytokines and/or hypoxic conditions can be undertaken with analysis at more time-points. A positive control using one of the commercial anti-VEGF agents would make for a good comparison with SST.

5.4 Conclusion

The most promising formulation candidate, SST 5% w/w in HPMC 6% w/w hydrogel was tested for safety and efficacy on ARPE-19 cells as well as somatostatin solutions at different concentrations. Release samples from day 1 and day 10 were picked as they represent the highest and lowest concentrations of SST released from the formulation. The immunofluorescence studies demonstrate that SST 10^{-7} M produced a significant downregulation of VEGF receptor 2 (VEGF-R2) levels in high glucose at 72 hours. The ELISA assay, however, did not show any significant effects on the amount of VEGF secreted from any of the treatments applied. This may be due to the conditions of the study in comparison to other work discussed in Section 5.3.3, including the glucose concentration for high glucose conditions, time-points assessed and the absence of other factors like inflammatory cytokines and hypoxia. Future work may focus on varying the conditions as mentioned above based on existing literature for further investigation. The addition of another technique (e.g. Western Blot) and inclusion of other markers (e.g. proapoptotic factors or stress kinases) should be explored. The inclusion of a commercial anti-VEGF agent for comparison would be ideal. Results of the MTT assay demonstrate that the concentrations of SST 10^{-7} M and 10^{-6} M, blank HPMC and release Day 10 samples did not cause significant cytotoxicity. Supra-physiological concentrations of SST compounded by the viscosity due to HPMC in the Release Day 1 samples resulted in significant cytotoxicity in a static *in vitro* cell study. Therefore, further evaluation in an animal model would provide clarification to these results as it is more representative of an *in vivo* environment.

CHAPTER 6: GENERAL DISCUSSION AND CONCLUSION

6.1 Summary of findings

Diabetes poses one of the greatest challenges to current healthcare systems worldwide. According to the International Diabetes Federation, an estimated 415 million adults globally were living with diabetes in 2015, with this figure set to rise to 642 million by 2040, constituting some 10% of the global adult population aged between 20 and 79. Diabetic retinopathy (DR) is a common complication of diabetes and can result in severe visual impairment. It is currently the leading cause of irreversible vision loss of people with diabetes (Dall, et al., 2014; Mohamed, Gillies, & Wong, 2007). DR affects the small blood vessels of the retina of the eye in people with diabetes. The vessels swell and leak liquid into the retina, blurring the vision and sometimes leading to blindness (Wild, et al., 2004). Persistent hyperglycaemia can damage small blood vessels (microvasculature) in organs such as the eye, leading to DR (Cade, 2008). It is estimated that approximately 93 million people worldwide have DR, and that a third of the global diabetic population are expected to develop some form of retinopathy in their lifetime (R. Lee, Wong, & Sabanayagam, 2015).

There are a number of treatments available for sight-threatening DR such as laser treatment (photocoagulation), intra-vitreous anti-VEGF drugs, intra-vitreous steroid injections, and vitrectomy. However, these treatments are associated with serious complications and are only used at the late stages of the disease to reduce the rate of disease progression.

The postulated therapeutic effects of somatostatin (SST) in the retina have been described in Chapter 1, Section 1.4.4. A tremendous amount of work done by Simó and co-workers in the ocular formulation of SST has seen the investigation of SST eye drops in clinical trials (EUROCONDOR) (Simó-Servat, et al., 2018). This clinical trial revealed that SST was only useful in patients with pre-existing retinal neurodysfunction and suggests screening to identify patients in whom neuroprotective treatment might be of benefit. Thus, the purpose of this thesis was to develop a modified-release formulation of SST for the treatment of diabetic retinopathy.

The eye has a number of properties that make it well suited to targeted drug delivery strategies, including its relative accessibility for delivery, limited size which can reduce the amount of drug required, and inner barriers, which limit drug clearance (Hosoya, Tomi, & Tachikawa, 2011). However, unlike the anterior segment, topical delivery to the posterior segment is limited by pre-corneal drainage, the lipoidal nature of the corneal epithelium, and systemic circulation absorption, which leads to low drug bioavailability – typically less than 5% (Gaudana, Ananthula, Parenky, & Mitra, 2010; Mishra, Bagui, Tamboli, & Mitra, 2011; Urtti, 2006). Therefore, subconjunctival

(between the conjunctiva and the sclera) or intravitreal injections are the most common routes of administration for drug delivery to the posterior segment of the eye (S. H. Kim, Lutz, Wang, & Robinson, 2007).

In this work, two modified-release formulations of somatostatin were developed. Somatostatin microparticles were intended for intra-ocular administration, particularly the suprachoroidal or scleral route. Whereas, somatostatin in HPMC hydrogel formulation, the more promising candidate, may be administered topically as an ophthalmic gel. In the early stages of diabetic retinopathy with no discernible changes to vision, it would be difficult to persuade patients to an injectable formulation. However, the patient acceptance of a topical formulation that does not require frequent administration is likely to be higher.

The first experimental chapter of this thesis (Chapter 2) investigates and characterises the properties of self-assembled somatostatin hydrogels. Somatostatin self-assembly in water and in the presence of electrolytes has been reported (W. van Grondelle, et al., 2007). Lanreotide, a somatostatin analog, exhibits similar self-assembly properties (Valery, et al., 2004) and has been marketed as a sustained-release monthly subcutaneous injection (Somatuline Autogel®). The purpose of Chapter 2 was to determine if self-assembled somatostatin hydrogels had the potential to act as a depot for the sustained release of somatostatin monomers. The hydrogels were extensively characterised with regard to their rheological properties, morphology using transmission electron microscopy and release kinetics of the somatostatin monomers from the hydrogels. The rheological studies showed that somatostatin formed a gel with higher storage modulus (G') at higher SST concentrations and in the presence of electrolytes (Figure 2.7). All the concentrations tested exhibited shear-thinning properties, with declining viscosity as shear rate increased. This is a favorable property for administration via intra-ocular injection. The frequency sweeps showed a trend to increase in moduli with increasing frequency. As high frequencies represent shorter timescales and low frequencies are representative of longer timescales, this indicates a lowering of the stiffness of the gel over longer timescales. This is beneficial as the administration of the gel will not become more difficult over a period of use or storage. However the G' remained higher than G'' at all frequencies indicating the SST hydrogel structure was not destroyed. This indicates that the SST hydrogels retain the properties of a gel over longer periods of time. Temperature sweeps showed a progressive decrease in G' and G'' with increasing temperature from 20 °C to 50 °C characteristic of materials in the absence of thermogelation. Thixotropic behavior was observed in plots of shear rate against stress. The thixotropic feature is favourable, relevant in view of transforming an initially viscous hydrogel into a thin product, easy to deliver to the desired site. The moduli of the SST hydrogels are equal to, or

greater than, that of moduli reported for comparable hydrogel systems (Aggeli, et al., 1997; Caplan, et al., 2002; Collier, et al., 2001).

In summary, the rheological studies showed that the somatostatin hydrogels were shear-thinning, did not exhibit thermogelation and exhibited a higher degree of structure with higher concentration and in the presence of electrolytes. This was correlated to morphological analysis. Transmission electron micrographs demonstrated the presence of nanofibrils that were narrower and denser in appearance in the presence of electrolytes. This corresponds to the higher G' (storage modulus) of the SST hydrogels in electrolytes and at a higher concentration as discussed in Chapter 2.

The release studies revealed that the hydrogels in the presence of electrolytes released a lower cumulative percentage of somatostatin monomers at 48 hours compared to those in water. The release kinetics of the somatostatin monomers were fitted to a hybrid model of release, indicating concurrent first-order (diffusion of adsorbed SST monomers) and zero-order (erosional release) mechanisms of release. The pattern of release appears to be a bimodal consistent with the hypothesis that different release mechanisms predominate at different times rather than the same mechanism remaining predominant. The observed rapid but incomplete initial release may proceed as a result of the more rapid release of material adsorbed onto the surface of the gel. As the release of adsorbed material is depleted, release then slows to a zero-order rate, perhaps related to the erosion of the gel matrix. The low percentage of monomer release (2.95% to 3.6%) at 48 hours *in vitro* revealed the low potential of these self-assembled hydrogels to follow the path of lanreotide. Although the initial release from SST 5% w/w in water hydrogels in SLF was high (cumulative release of 38%), the release stopped at 9 hours as a solid gel layer formed on top of the hydrogel. Electrolytes are ubiquitous in the physiological environment and therefore, would provide the ideal environment for self-assembly of somatostatin to occur. It is important to note, however, that *in vitro* release characteristics are likely to be very different to those observed *in vivo* and merely provide a means of comparison between the different samples tested. The limitations of this study were the short duration of the study (48 hours) and the method of peptide quantification. The duration of the study could have been extended further to determine further release of monomers had a more sensitive method of detection been used. For these reasons, HPLC was used for the quantification of somatostatin release in the following chapters.

Maji *et al* (Maji, et al., 2008) have studied the potential of amyloids as a long-acting depot for peptides. Maji *et al* reported that certain peptides formed very stable fibrils, which released peptides so slowly that an effective concentration of the drug for action was not attained. While the amyloid fibrils formed are stable, there must be a thermodynamic equilibrium condition between

the fibrils and monomers. If the monomer release is insufficient for effective drug concentrations, then there is failure of the depot formulation. Although the same group (Anoop, et al., 2014) has demonstrated the reversibility of somatostatin fibril formation, that study was conducted at much lower concentrations of somatostatin (0.2% w/v) than in the current study and in the presence of heparin an aggregation inducer. The results from Chapter 2 show that self-assembled somatostatin hydrogels form very stable fibrils in the presence of electrolytes and once formed, release only a low percentage of somatostatin present in the hydrogel. This discovery then led to efforts to modulate the formation of the nanofibrils in an attempt to increase the cumulative percentage released which culminated in the work in Chapter 3.

In Chapter 3, a hypothesis was explored regarding strategies to hinder somatostatin nanofibril formation. Somatostatin 5% w/w was entrapped in hydroxypropyl methylcellulose (HPMC) 3% w/w and 6% w/w hydrogels and aged for 7 days. The time required for relaxation of the HPMC entanglement networks was determined by rheological analysis. The SST in HPMC hydrogels were subjected to extensive rheological studies consisting of amplitude sweeps, frequency and flow sweeps as well as temperature sweeps. The frequency sweeps showed a progressive decline in the G' (storage modulus) of the blank HPMC 3% w/w and 6% w/w gels and SST 5% w/w in HPMC 3% w/w and 6% w/w gels. This indicates that the gels are stiffer at longer timescales (low frequencies) and less at shorter timescales (higher frequencies). This means that the inclusion of SST in the HPMC gel does not alter this property of the HPMC gels. In contrast, the frequency sweeps of the SST 5% w/w aqueous solution showed an increase in G' as the frequency increased, consistent with our data in Chapter 2. The flow sweeps indicated all samples tested were shear-thinning and will flow more easily with the application of shear. This is a desirable property should the formulation be administered as an injection or as a topical formulation. The temperature sweeps showed that the HPMC gels undergo thermogelation at 65°C, a characteristic property of HPMC matrices (Joshi, 2011). This is not observed with the SST 5% w/w aqueous samples where there is a decline in G' with increasing temperatures. This is consistent with materials that do not undergo thermogelation. There was a decrease in the G' of the SST 5% in HPMC 3% w/w hydrogel initially as the gel is diluted with the addition of the SLF on top then significantly increases on Day 4 of release. This correlated with the end of the release of somatostatin monomers as detected by HPLC based on our release data. This may be attributed to formation of nanofibrils, resulting in an increase in the stiffness of the gel. The same applies to the SST 5% w/w aqueous samples where the G' is highest on Day 4 of release. For all blank HPMC samples, the G' was lowest after 4 days of release. This can be attributed to the dilution of the HPMC hydrogels with the presence of SLF on top removed and replaced every 24 hours. The SST 5% w/w in HPMC 6% w/w gels exhibited the same trend in the change in G' as the

SST 5% w/w in HPMC 3% w/w gels but smaller in magnitude. The stiffer 6% w/w HPMC matrix would be more resistant to the diluting effects of the SLF and provide a stronger barrier to the interaction of the electrolytes in the SLF with the entrapped somatostatin. This may explain the longer duration of release (10 days and continuing) compared to 4 days for the SST 5% w/w in HPMC 3% w/w gels.

FTIR characterization of SST 5% w/w in HPMC 3% w/w and 6% w/w was performed on Days 1 and 7 of aging and for four days of release after exposure to SLF. These data showed that there is transition of SST structure from random conformations (1643 cm^{-1}) to parallel and anti-parallel β -sheets (1615 cm^{-1} and 1675 cm^{-1}) upon exposure to SLF. These transitions are hindered in the HPMC hydrogels compared to SST 5% in water, which is consistent with the hypothesis that the entanglement network of HPMC acts a barrier to the interaction of the electrolytes in SLF with SST. The secondary derivative plot (Figure 3.8) demonstrates a higher degree of structure in the SST aqueous solutions in SLF compared to SST 5% w/w in HPMC 3% w/w and 6% w/w hydrogels. Transmission electron micrographs of SST 5% aqueous solutions at Day 7 of aging and Release day 4 demonstrate increased density of nanofibrils after exposure to SLF (Figures 3.9 and 3.10). In the TEM micrographs of SST 5% w/w in HPMC 6% w/w hydrogels (Figure 4.12), however, there are no visible SST nanofibrils at Release Day 4. The micrographs demonstrate a network similar to those of blank HPMC 6% w/w hydrogels (Figure 3.11). The challenge of performing microscopy on these samples was the viscosity of the HPMC hydrogels. The formvar-coated copper grids had a fragile mesh which was easily broken by the weight of the hydrogels, resulting in many grids that were unable to be imaged. With the limitations, however, the TEM images appear to support the hypothesis that SST nanofibril formation is delayed by the presence of HPMC when exposed to electrolytes.

Release studies conducted on the SST 5% w/w in HPMC 3% w/w and HPMC 6% w/w hydrogels demonstrated an extended release of SST monomers from the SST/HPMC hydrogels compared to SST 5% w/w in water. The SST 5% w/w solution reached a 100% release at 6 hours. The SST 5% w/w in HPMC 3% w/w gels released a total of 45.6% incorporated SST at 96 hours and there was no further release (no detectable peaks by HPLC) whereas the SST 5% w/w in HPMC 6% w/w gels continued to release a total of 37.6% at 10 days when the experiment was stopped, however, the release had not concluded. The release kinetics of SST 5% w/w in HPMC 3% w/w and HPMC 6% w/w hydrogels were fitted to a hybrid model of release (Equation 3.1) with R^2 values of 0.998 and 0.997 respectively. The time taken for 90% of SST to be released from the core of the hydrogels for the SST 5% w/w in HPMC 6% w/w hydrogels (35.3 hours) is almost double that of SST 5% w/w in HPMC 3% w/w hydrogels (19.6 hours). The initial higher percentage of release from both samples is attributed

to diffusional release that is later superseded by erosional release. The higher stiffness of the HPMC 6% w/w hydrogel leads to a longer duration of release of 10 days compared to 4 days for the HPMC 3% w/w hydrogel. Mass spectrometry was performed to confirm the structural integrity of the somatostatin released from the SST 5% w/w in HPMC 6% w/w hydrogels. Therefore, SST 5% w/w in HPMC 6% w/w hydrogels are the most promising candidate in terms of SST delivery, with delayed SST nanofibril formation and extended duration of release in comparison to SST 5% w/w aqueous dispersions.

Chapter 4 describes a second formulation approach to extend duration of SST release. Microparticles of somatostatin were synthesized by two different techniques. The use of surface acoustic waves (SAW) was attempted to encapsulate the model drug (FITC-DEAE-Dextran) in a triblock co-polymer of polycaprolactone-polyethylene glycol-polycaprolactone (PCL-PEG-PCL). The model drug was used in place of somatostatin to optimize parameters of the process prior to using somatostatin itself. Alvarez et al (Alvarez, et al., 2008) had demonstrated the encapsulation of bovine serum albumin (BSA) in polycaprolactone microparticles using the SAW technique. However, experiments with FITC-DEAE-Dextran revealed low encapsulation efficiencies (0.03%) and a very low percentage of cumulative release (3%), which stopped after 7 days. Attempts were made with somatostatin but the experiment was unsuccessful due to the visible deposition of the peptide on the SAW device. This technique was limited to the use of the lower molecular weight triblock (PCL_{1k}-PEG_{2k}-PCL_{1k}) as the set-up did not permit the use of two immiscible solvent systems.

The production of somatostatin microparticles was then attempted using the traditional double emulsion method. PCL-PEG-PCL was selected as the polymer candidate in this work. It was hypothesized that the duration of release may be extended in comparison to PLGA due to the crystalline nature of PCL resulting in slower degradation. In this study, the method published by Vaishya et al (Vaishya, et al., 2015) to synthesize PCL-PEG-PCL microparticles encapsulating octreotide, a somatostatin analogue, was adapted. FITC-DEAE-Dextran was used as the model drug to optimize the parameters (drug and polymer concentration, polymer molecular weight and sonication time). The encapsulation efficiency of the model drug was relatively high (61.5%) with a polymer concentration of 2% w/w and drug concentration of 2.5% w/w. The same parameters were applied to the synthesis of somatostatin microparticles with this technique. The results from our study showed that the encapsulation efficiency of somatostatin was highly variable (ranging from 19% to 43%). The release profiles of somatostatin from the microparticles were similarly variable in the cumulative percentage released (1.4% -4%) and duration of release (16-24 days). The microparticles were characterised morphologically using scanning electron microscopy. The images

showed spherical aggregates, resembling microspheres to a larger degree than the polydisperse irregularly-shaped products of the SAW technique. The microparticles were analysed for size and determined to average 32 μm , ranging from 10.9 μm to 50.4 μm . The release kinetics of somatostatin from the microparticles were fitted to a first-order decay to plateau model with good mean R^2 value of 0.979.

In comparison to the current results, Herrmann and Bodmeier (Herrmann & Bodmeier, 1998) had produced somatostatin microparticles using different molecular weights of poly-lactic acid (PLA) and poly-(lactic/glycolic) acid (PLGA). Different methods like oil-in-water dispersion, oil-in-water co-solvent and water-in oil-in water double emulsion were investigated. The authors reported good encapsulation efficiencies ranging from 64% to 85%. They performed a release study for 7 days, showing about 10%-25% somatostatin released in that duration. This indicates better results with PLA and PLGA in comparison to PCL-PEG-PCL. However, this remains too variable for clinical application.

Vaishya *et al* used the PCL_{10k}-PEG_{2k}-PCL_{10k} to encapsulate octreotide, an analogue of somatostatin. An encapsulation efficiency of 45% was achieved with this triblock polymer. The release studies demonstrated complete release of octreotide over 3 months. It is important to note that the microparticles were suspended in a polymeric thermosensitive gel of the same composition as the microparticles, which had the effect of further extending duration of release.

As discussed in Chapter 4, the encapsulation of somatostatin in the polymer used was not successful due to the inability to shield the charges. This was due to the reported self-assembly properties in the presence of electrolytes. Another limitation in the technique used was the ultrasonication step. Variation in the position of the ultrasound probe despite best attempts at consistency and the small volumes tested led to considerable effects on the variable encapsulation efficiency.

This work shows promise of somatostatin encapsulation in PCL-PEG-PCL triblock polymer with further optimization of parameters. Current results show a reasonable encapsulation efficiency of *ca.* 30% and a duration of release ranging from 16 to 24 days. Further work should focus on strategies to improve the amount of somatostatin encapsulated, for example, pH adjustment, co-solvents, solid dispersion method and consistency of technique.

In Chapter 5, the safety and efficacy of somatostatin solutions at different concentrations and released somatostatin from the SST 5% w/w in HPMC 6% w/w hydrogels were tested on immortalized human retinal pigment epithelium cells (ARPE-19). MTT cell viability assay was used to assess the safety of the Release day and Release Day 10 samples as well as SST 10^{-7} M and 10^{-6} M.

The results of the MTT assay demonstrated a significant negative effect on cell viability (*ca.* 65%) by the Release Day 1 samples compared to control in both high and normal glucose conditions. However, Release day 10 samples (*ca.* 11%), SST 10^{-6} M (*ca.* 14%), SST 10^{-7} M (*ca.* 17%) and blank HPMC (*ca.* 15%) did not result in a significant effect on cell viability. It is thus postulated that the combination of the viscosity of the Release Day 1 sample with the higher concentration of SST present at 24 hours may have additive effects on the viability of the cells. The MTT assay measures the viability of cells by the ability to reduce MTT, a yellow water-soluble tetrazolium dye, primarily by the mitochondrial dehydrogenases, to purple coloured formazan crystals. Somatostatin has anti-proliferative properties via actions at SSTs 2,3 and 4 and may decrease viability in a concentration-dependent manner (Papadaki, et al., 2010). The concentrations of SST released in the first 24 hours from the SST 5% w/w in HPMC 6% w/w gels are in the order of 10^{-5} M, which resulted in the formation of a gel in the wells in our immunofluorescence studies. This is due to the propensity of SST to self-assemble in the presence of electrolytes, such as those found in the cell culture medium. A viscous, gel layer formed on the cells in a well could conceivably reduce their viability, explaining the results of our MTT assay. This is consistent with the finding that the Release Day 10 samples, which are both less viscous and have lower concentrations of SST (in the order of 10^{-8} M) that did not impact cell viability.

The markers for assessment for efficacy were expression of vascular endothelial growth factor receptor-2 (VEGF-R2) and secretion of VEGF by the ARPE-19 cells. Immunofluorescence was used to assess the effect of SST on the expression of VEGF-R2 levels at SST concentrations from 10^{-8} M to 10^{-5} M. The results of the first study showed that SST 10^{-7} M and 10^{-6} M produced significant downregulation of VEGF-R2 expression in high glucose (25 mM) conditions compared to normal glucose (5 mM) conditions. Based on this study, the experiment was repeated twice more with SST 10^{-7} M and 10^{-6} M. The statistical analysis of the results in triplicate revealed that only SST 10^{-7} M resulted in a significant downregulation of VEGF-R2 expression in high glucose conditions.

The quantitative analysis of VEGF secretion in the same conditions was performed by ELISA at two time points of 24 hours and 72 hours. These studies showed no significant difference in the amount of VEGF secreted between the SST concentrations tested (10^{-8} M to 10^{-5} M) and control wells in high glucose versus normal glucose conditions. Somatostatin released from SST 5% w/w in HPMC 6% w/w hydrogels on Release Day 1 and Release Day 10 was also applied to the cells and incubated for 24 hours before the ELISA assay. The Release Day 1 samples paradoxically resulted in a significant increase in VEGF secretion in high glucose conditions. This is hypothesized to be due to the highly viscous nature of the Release Day 1 samples, which have a high amount of HPMC.

The results from Chapter 5 are equivocal and require clarification in future work. The current study shows that SST 10^{-7} M results in a significant downregulation of VEGF-R2 expression by the ARPE-19 cells at 72 hours. The results from the ELISA assay, however, do not support that finding in terms of the effect on quantity of VEGF secreted. Both studies were performed at 24 hours and 72 hours. As highlighted in the literature, the experiments to quantify VEGF release may need to be repeated with analysis at shorter time points (e.g. 4 hours) more frequently but extending beyond 72 hours. In addition, comparison of results in the presence of inflammatory cytokines in the media versus in high glucose alone could be performed. The presence of inflammatory mediators would be more representative of the milieu in diabetic retinopathy. It is difficult to draw meaningful conclusions from one assay in one retinal cell line. However, this still adds to the existing body of work contributing to the search for treatments for diabetic retinopathy. As the stated end point could not be reached, the hypothesis in this instance is incorrect.

In addition, it is postulated that somatostatin inhibits the post-receptor signalling events of peptide growth factors such as VEGF, which may account for the preliminary data of the downregulation of VEGF-R2 expression without significant effects on VEGF secretion. It is worth noting that although the VEGF secretion levels in high glucose conditions were higher, they were not significantly so. This supports the discussion that in vitro studies on a single cell line in only high glucose cannot replicate the complexity of biological systems. The decision was made not to proceed further with additional cell-based studies primarily because this is not the focus of the thesis and preliminary data on safety and effect on VEGF/VEGF-R2 had been obtained on ARPE-19 cells, which is the only cell line we had access to at the time of this research work.

Future work will focus on the above as well as investigating the effect of SST on other retinal cell lines, such as the Müller cells. The Müller cells are macroglial cells that react to neuronal apoptosis by aberrant expression of glial fibrillary acidic protein (GFAP) in diabetes. Müller cells are involved in the modulation of blood flow, vascular permeability and cell survival in the retina. In addition, their processes surround all the blood vessels in the retina. It could be reasonably conceived that these cells are key players in the pathogenic events in the diabetic eye (Simo, et al., 2012). Studies on healthy animals to assess the biocompatibility of SST 5% in combination with HPMC 6% w/w can be conducted prior to efficacy tests on diseased animal models. This will be a more accurate assessment of potential irritant effects of the SST 5% w/w in HPMC 6% w/w hydrogels compared to the static conditions of cell studies.

6.2 Conclusion

In conclusion, this work resulted in the development and characterization of two formulations of somatostatin for ocular delivery. The microparticle formulation has shown reasonable encapsulation and duration of release, however, further optimisation can be done to improve both parameters. The more promising candidate consists of somatostatin entrapped in a HPMC network and has demonstrated modified release of somatostatin over 10 days. This work has introduced HPMC as a suitable candidate for modifying the release rate of peptides. The FTIR data demonstrating a hindering of nanofibril self-assembly may provide a platform for the investigation of HPMC in the delivery of other self-assembling moieties. The combination of SST with HPMC provides aqueous loading of the peptide with no denaturing conditions and 100% loading. The SST 5% w/w in HPMC 6% w/w hydrogels are shear-thinning, which facilitates their application topically or as an injectable.

The current work has also evidenced the downregulation of the VEGF receptor 2 (VEGF-R2) by somatostatin at a concentration of 10^{-7} M in high glucose (25 mM) conditions. At this concentration, there was no reduction in cell viability. Although further studies are warranted to investigate effects on other retinal cell lines and animal models with additional markers, the identification of a new polymeric carrier for the delivery of somatostatin adds to the current body of work in the search for a non-invasive treatment for diabetic retinopathy.

REFERENCES

- Abràmoff, M. D., Magalhães, P. J., & Ram, S. J. (2004). Image processing with ImageJ. *Biophotonics international*, 11, 36-42.
- Adamis, A. P., Shima, D. T., Yeo, K.-T., Yeo, T. K., Brown, L. F., Berse, B., Damore, P. A., & Folkman, J. (1993). Synthesis and secretion of vascular permeability factor/vascular endothelial growth factor by human retinal pigment epithelial cells. *Biochemical and biophysical research communications*, 193, 631-638.
- Aggeli, A., Bell, M., Boden, N., Keen, J., Knowles, P., McLeish, T., Pitkeathly, M., & Radford, S. (1997). Responsive gels formed by the spontaneous self-assembly of peptides into polymeric β -sheet tapes.
- Agnes, E. J., & Gonzales Ortega, G. (2003). *Mathematical models and physicochemical of diffusion*. (Vol. 19).
- Aiello, L. P., Avery, R. L., Arrigg, P. G., Keyt, B. A., Jampel, H. D., Shah, S. T., Pasquale, L. R., Thieme, H., Iwamoto, M. A., & Park, J. E. (1994). Vascular endothelial growth factor in ocular fluid of patients with diabetic retinopathy and other retinal disorders. *New England Journal of Medicine*, 331, 1480-1487.
- Akopian, A., Johnson, J., Gabriel, R., Brecha, N., & Witkovsky, P. (2000). Somatostatin modulates voltage-gated K⁺ and Ca²⁺ currents in rod and cone photoreceptors of the salamander retina. *Journal of Neuroscience*, 20, 929-936.
- Alvarez, M., Friend, J., & Yeo, L. Y. (2008). Rapid generation of protein aerosols and nanoparticles via surface acoustic wave atomization. *Nanotechnology*, 19, 455103.
- Alvarez, M., Yeo, L. Y., Friend, J. R., & Jamriska, M. (2009). Rapid production of protein-loaded biodegradable microparticles using surface acoustic waves. *Biomicrofluidics*, 3, 014102.
- Ambati, J., Canakis, C. S., Miller, J. W., Gragoudas, E. S., Edwards, A., Weissgold, D. J., Kim, I., Delori, F. C., & Adamis, A. P. (2000). Diffusion of high molecular weight compounds through sclera. *Investigative ophthalmology & visual science*, 41, 1181-1185.
- Ambati, J., Chalam, K. V., Chawla, D. K., D'Angio, C. T., Guillet, E. G., Rose, S. J., Vanderlinde, R. E., & Ambati, B. K. (1997). Elevated gamma-aminobutyric acid, glutamate, and vascular endothelial growth factor levels in the vitreous of patients with proliferative diabetic retinopathy. *Archives of ophthalmology*, 115, 1161-1166.
- Ambrosio, L., Demitri, C., & Sannino, A. (2011). Superabsorbent cellulose-based hydrogels for biomedical applications. In *Biomedical Hydrogels* (pp. 25-50): Elsevier.
- Amrite, A. C., Ayalasomayajula, S. P., Cheruvu, N. P. S., & Kompella, U. B. (2006). Single Periocular Injection of Celecoxib-PLGA Microparticles Inhibits Diabetes-Induced Elevations in Retinal PGE₂, VEGF, and Vascular Leakage. *Investigative ophthalmology & visual science*, 47, 1149-1160.
- Andrews, G. P., Gorman, S. P., & Jones, D. S. (2005). Rheological characterisation of primary and binary interactive bioadhesive gels composed of cellulose derivatives designed as ophthalmic viscosurgical devices. *Biomaterials*, 26, 571-580.
- Anoop, A., Ranganathan, S., Das Dhaked, B., Jha, N. N., Pratihari, S., Ghosh, S., Sahay, S., Kumar, S., Das, S., Kombrabail, M., Agarwal, K., Jacob, R. S., Singru, P., Bhaumik, P., Padinhateeri, R., Kumar, A., & Maji, S. K. (2014). Elucidating the role of disulfide bond on amyloid formation and fibril reversibility of somatostatin-14: relevance to its storage and secretion. *J Biol Chem*, 289, 16884-16903.
- Antonetti, D. A., Barber, A. J., Bronson, S. K., Freeman, W. M., Gardner, T. W., Jefferson, L. S., Kester, M., Kimball, S. R., Krady, J. K., & LaNoue, K. F. (2006). Diabetic retinopathy: seeing beyond glucose-induced microvascular disease. *Diabetes*, 55, 2401-2411.
- Arcinue, C. A., Cerón, O. M., & Foster, C. S. (2013). A comparison between the fluocinolone acetonide (Retisert) and dexamethasone (Ozurdex) intravitreal implants in uveitis. *Journal of Ocular Pharmacology and Therapeutics*, 29, 501-507.

- Arena, S., Pattarozzi, A., Corsaro, A., Schettini, G., & Florio, T. (2005). Somatostatin Receptor Subtype-Dependent Regulation of Nitric Oxide Release: Involvement of Different Intracellular Pathways. *Molecular Endocrinology*, *19*, 255-267.
- Arroba, A. I., Mazzeo, A., Cazzoni, D., Beltramo, E., Hernández, C., Porta, M., Simó, R., & Valverde, Á. M. (2016). Somatostatin protects photoreceptor cells against high glucose-induced apoptosis. *Molecular Vision*, *22*, 1522-1531.
- Arvidson, S. A., Lott, J. R., McAllister, J. W., Zhang, J., Bates, F. S., Lodge, T. P., Sammler, R. L., Li, Y., & Brackhagen, M. (2013). Interplay of Phase Separation and Thermoreversible Gelation in Aqueous Methylcellulose Solutions. *Macromolecules*, *46*, 300-309.
- Akunuru, J. V., Sunkara, G., Bandi, N., Thoreson, W. B., & Kompella, U. B. (2001). Expression of multidrug resistance-associated protein (MRP) in human retinal pigment epithelial cells and its interaction with BAPSG, a novel aldose reductase inhibitor. *Pharmaceutical Research*, *18*, 565-572.
- Averbukh, E., Halpert, M., Yanko, R., Yanko, L., Peer, J., Levinger, S., Flyvbjerg, A., & Raz, I. (2000). Octreotide, a somatostatin analogue, fails to inhibit hypoxia-induced retinal neovascularization in the neonatal rat. *International journal of experimental diabetes research*, *1*, 39-47.
- Bain, M. K., Bhowmick, B., Maity, D., Mondal, D., Mollick, M. M. R., Rana, D., & Chattopadhyay, D. (2012). Synergistic effect of salt mixture on the gelation temperature and morphology of methylcellulose hydrogel. *International Journal of Biological Macromolecules*, *51*, 831-836.
- Baldysiak-Figiel, A., Lang, G. K., Kampmeier, J., & Lang, G. E. (2004). Octreotide prevents growth factor-induced proliferation of bovine retinal endothelial cells under hypoxia. *The Journal of endocrinology*, *180*, 417-424.
- Bamba, M., Puisieux, F., Marty, J. P., & Carstensen, J. T. (1979). Release mechanisms in gelforming sustained release preparations. *International Journal of Pharmaceutics*, *2*, 307-315.
- Bandello, F., Cunha-Vaz, J., Chong, N. V., Lang, G. E., Massin, P., Mitchell, P., Porta, M., Prunte, C., Schlingemann, R., & Schmidt-Erfurth, U. (2012). New approaches for the treatment of diabetic macular oedema: recommendations by an expert panel. *Eye (Lond)*, *26*, 485-493.
- Barar, J., Javadzadeh, A. R., & Omid, Y. (2008). Ocular novel drug delivery: impacts of membranes and barriers. *Expert Opin Drug Deliv*, *5*, 567-581.
- Barbato, F., La Rotonda, M. I., Maglio, G., Palumbo, R., & Quaglia, F. (2001). Biodegradable microspheres of novel segmented poly (ether-ester-amide) s based on poly (ϵ -caprolactone) for the delivery of bioactive compounds. *Biomaterials*, *22*, 1371-1378.
- Barber, A. J., Nakamura, M., Wolpert, E. B., Reiter, C. E. N., Seigel, G. M., Antonetti, D. A., & Gardner, T. W. (2001). Insulin rescues retinal neurons from apoptosis by a phosphatidylinositol 3-kinase/Akt-mediated mechanism that reduces the activation of caspase-3. *Journal of Biological Chemistry*, *276*, 32814-32821.
- Barnett, P. (2003). Somatostatin and somatostatin receptor physiology. *Endocrine*, *20*, 255-264.
- Barth, A. (2007). Infrared spectroscopy of proteins. *Biochimica et Biophysica Acta (BBA) - Bioenergetics*, *1767*, 1073-1101.
- Bartsch, T., Levy, M. J., Knight, Y. E., & Goadsby, P. J. (2005). Inhibition of nociceptive dural input in the trigeminal nucleus caudalis by somatostatin receptor blockade in the posterior hypothalamus. *Pain*, *117*, 30-39.
- Beeley, N. R. F., Rossi, J. V., Mello-Filho, P. A. A., Mahmoud, M. I., Fujii, G. Y., de Juan, E., & Varner, S. E. (2005). Fabrication, implantation, elution, and retrieval of a steroid-loaded polycaprolactone subretinal implant. *Journal of Biomedical Materials Research Part A*, *73*, 437-444.
- Bei, J.-Z., Li, J.-M., Wang, Z.-F., Le, J.-C., & Wang, S.-G. (1998). Polycaprolactone-poly(ethylene-glycol) block copolymer. IV: Biodegradation behavior in vitro and in vivo. *Polymers for advanced technologies*, *8*, 693-696.

- Benko, R., Antwi, A., & Bartho, L. (2012). The putative somatostatin antagonist cyclo-somatostatin has opioid agonist effects in gastrointestinal preparations. *Life Sci*, *90*, 728-732.
- Benoit, M. A., Baras, B., & Gillard, J. (1999). Preparation and characterization of protein-loaded poly(ϵ -caprolactone) microparticles for oral vaccine delivery. *International Journal of Pharmaceutics*, *184*, 73-84.
- Benuck, M., & Marks, N. (1976). Differences in the degradation of hypothalamic releasing factors by rat and human serum. *Life Sci*, *19*, 1271-1276.
- Berezovsky, D. E., Patel, S. R., McCarey, B. E., & Edelhauser, H. F. (2011). In Vivo Ocular Fluorophotometry: Delivery of Fluoresceinated Dextrans via Transscleral Diffusion in Rabbits. *Investigative ophthalmology & visual science*, *52*, 7038-7045.
- Berkland, C., Kim, K., & Pack, D. W. (2001). Fabrication of PLG microspheres with precisely controlled and monodisperse size distributions. *J Control Release*, *73*, 59-74.
- Bigiani, A., Petrucci, C., Ghiaroni, V., Dal Monte, M., Cozzi, A., Kreienkamp, H. J., Richter, D., & Bagnoli, P. (2004). Functional correlates of somatostatin receptor 2 overexpression in the retina of mice with genetic deletion of somatostatin receptor 1. *Brain research*, *1025*, 177-185.
- Blaauwgeers, H. G. T., Holtkamp, G. M., Rutten, H., Witmer, A. N., Koolwijk, P., Partanen, T. A., Alitalo, K., Kroon, M. E., Kijlstra, A., & van Hinsbergh, V. W. M. (1999). Polarized vascular endothelial growth factor secretion by human retinal pigment epithelium and localization of vascular endothelial growth factor receptors on the inner choriocapillaris: evidence for a trophic paracrine relation. *The American journal of pathology*, *155*, 421-428.
- Boddu, S., & Nesamony, J. (2013). Utility of transporter/receptor (s) in drug delivery to the eye. *World J Pharmacol*, *2*, 1.
- Bodvik, R., Dedinaite, A., Karlson, L., Bergström, M., Bäverbäck, P., Pedersen, J. S., Edwards, K., Karlsson, G., Varga, I., & Claesson, P. M. (2010). Aggregation and network formation of aqueous methylcellulose and hydroxypropylmethylcellulose solutions. *Colloids and Surfaces A: Physicochemical and Engineering Aspects*, *354*, 162-171.
- Boehm, B. O., Lang, G. K., Jehle, P. M., Feldman, B., & Lang, G. E. (2001). Octreotide reduces vitreous hemorrhage and loss of visual acuity risk in patients with high-risk proliferative diabetic retinopathy. *Hormone and metabolic research = Hormon- und Stoffwechselforschung = Hormones et métabolisme* *33*, 300-306.
- Bok, D. (1993). Retinal transplantation and gene therapy. Present realities and future possibilities. *Investigative ophthalmology & visual science*, *34*, 473-476.
- Bourlais, C. L., Acar, L., Zia, H., Sado, P. A., Needham, T., & Leverage, R. (1998). Ophthalmic drug delivery systems--recent advances. *Prog Retin Eye Res*, *17*, 33-58.
- Branco, M. C., Pochan, D. J., Wagner, N. J., & Schneider, J. P. (2009). Macromolecular diffusion and release from self-assembled β -hairpin peptide hydrogels. *Biomaterials*, *30*, 1339-1347.
- Brazeau, P., Vale, W., Burgus, R., Ling, N., Butcher, M., Rivier, J., & Guillemin, R. (1973). Hypothalamic polypeptide that inhibits the secretion of immunoreactive pituitary growth hormone. *Science*, *179*, 77-79.
- Buchan, A. M. J., Lin, C.-Y., Choi, J., & Barber, D. L. (2002). Somatostatin, Acting at Receptor Subtype 1, Inhibits Rho Activity, the Assembly of Actin Stress Fibers, and Cell Migration. *Journal of Biological Chemistry*, *277*, 28431-28438.
- Buscail, L., Delesque, N., Estève, J. P., Saint-Laurent, N., Prats, H., Clerc, P., Robberecht, P., Bell, G. I., Liebow, C., & Schally, A. V. (1994). Stimulation of tyrosine phosphatase and inhibition of cell proliferation by somatostatin analogues: mediation by human somatostatin receptor subtypes SSTR1 and SSTR2. *Proceedings of the National Academy of Sciences*, *91*, 2315-2319.
- Byeon, S. H., Lee, S. C., Choi, S. H., Lee, H. K., Lee, J. H., Chu, Y. K., & Kwon, O. W. (2010). Vascular endothelial growth factor as an autocrine survival factor for retinal pigment epithelial cells under oxidative stress via the VEGF-R2/PI3K/Akt. *Invest Ophthalmol Vis Sci*, *51*, 1190-1197.

- Cade, W. T. (2008). Diabetes-Related Microvascular and Macrovascular Diseases in the Physical Therapy Setting. *Physical Therapy*, 88, 1322-1335.
- Caplan, M. R., Schwartzfarb, E. M., Zhang, S., Kamm, R. D., & Luffenburger, D. A. (2002). Control of self-assembling oligopeptide matrix formation through systematic variation of amino acid sequence. *Biomaterials*, 23, 219-227.
- Carmo, A., Cunha-Vaz, J. G., Carvalho, A. P., & Lopes, M. C. (1999). L-arginine transport in retinas from streptozotocin diabetic rats: correlation with the level of IL-1 β and NO synthase activity. *Vision research*, 39, 3817-3823.
- Carrasco, E., Hernandez, C., Miralles, A., Huguet, P., Farres, J., & Simo, R. (2007). Lower somatostatin expression is an early event in diabetic retinopathy and is associated with retinal neurodegeneration. *Diabetes Care*, 30, 2902-2908.
- Castinetti, F., Saveanu, A., Morange, I., & Brue, T. (2009). Lanreotide for the treatment of acromegaly. *Advances in therapy*, 26, 600-612.
- Cattaneo, M. G., Gentilini, D., & Vicentini, L. M. (2006). Deregulated human glioma cell motility: inhibitory effect of somatostatin. *Mol Cell Endocrinol*, 256, 34-39.
- Cejvan, K., Coy, D. H., & Efendic, S. (2003). Intra-islet somatostatin regulates glucagon release via type 2 somatostatin receptors in rats. *Diabetes*, 52, 1176-1181.
- Censi, R., Di Martino, P., Vermonden, T., & Hennink, W. E. (2012). Hydrogels for protein delivery in tissue engineering. *J Control Release*, 161, 680-692.
- Cervia, D., Casini, G., & Bagnoli, P. (2008a). Physiology and pathology of somatostatin in the mammalian retina: a current view. *Mol Cell Endocrinol*, 286, 112-122.
- Cervia, D., Casini, G., & Bagnoli, P. (2008b). Physiology and pathology of somatostatin in the mammalian retina: a current view. *Mol Cell Endocrinol*, 286, 112-122.
- Cervia, D., Catalani, E., Dal Monte, M., & Casini, G. (2012). Vascular endothelial growth factor in the ischemic retina and its regulation by somatostatin. *Journal of Neurochemistry*, 120, 818-829.
- Cervia, D., Catalani, E., Dal Monte, M., & Casini, G. (2012). Vascular endothelial growth factor in the ischemic retina and its regulation by somatostatin. *Journal of Neurochemistry*, 120, 818-829.
- Cervia, D., Martini, D., Ristori, C., Catalani, E., Timperio, A. M., Bagnoli, P., & Casini, G. (2008). Modulation of the neuronal response to ischaemia by somatostatin analogues in wild-type and knock-out mouse retinas. *Journal of Neurochemistry*, 106, 2224-2235.
- Cervia, D., Petrucci, C., Bluet-Pajot, M. T., Epelbaum, J., & Bagnoli, P. (2002). Inhibitory control of growth hormone secretion by somatostatin in rat pituitary GC cells: sst(2) but not sst(1) receptors are coupled to inhibition of single-cell intracellular free calcium concentrations. *Neuroendocrinology*, 76, 99-110.
- Ceulemans, J., & Ludwig, A. (2002). Optimisation of carbomer viscous eye drops: an in vitro experimental design approach using rheological techniques. *Eur J Pharm Biopharm*, 54, 41-50.
- Chan, J. Y. C., Cole, E., & Hanna, A. K. (1985). Diabetic nephropathy and proliferative retinopathy with normal glucose tolerance. *Diabetes care*, 8, 385-390.
- Che, X. I. N., Fan, X.-Q., & Wang, Z.-L. (2014). Mechanism of blood-retinal barrier breakdown induced by HIV-1 (Review). *Experimental and Therapeutic Medicine*, 7, 768-772.
- Checa-Casalengua, P., Jiang, C., Bravo-Osuna, I., Tucker, B. A., Molina-Martínez, I. T., Young, M. J., & Herrero-Vanrell, R. (2011). Retinal ganglion cells survival in a glaucoma model by GDNF/Vit E PLGA microspheres prepared according to a novel microencapsulation procedure. *Journal of Controlled Release*, 156, 92-100.
- Checa-Casalengua, P., Jiang, C., Bravo-Osuna, I., Tucker, B. A., Molina-Martínez, I. T., Young, M. J., & Herrero-Vanrell, R. (2012). Preservation of biological activity of glial cell line-derived neurotrophic factor (GDNF) after microencapsulation and sterilization by gamma irradiation. *International Journal of Pharmaceutics*, 436, 545-554.
- Chen, D. R., Bei, J. Z., & Wang, S. G. (2000). Polycaprolactone microparticles and their biodegradation. *Polymer Degradation and Stability*, 67, 455-459.

- Cheruvu, N. P. S., Amrite, A. C., & Kompella, U. B. (2008). Effect of Eye Pigmentation on Transscleral Drug Delivery. *Investigative ophthalmology & visual science*, *49*, 333-341.
- Cheung, N., Wong, I. Y., & Wong, T. Y. (2014). Ocular anti-VEGF therapy for diabetic retinopathy: overview of clinical efficacy and evolving applications. *Diabetes Care*, *37*, 900-905.
- Cheung, N. W., & Boyages, S. C. (1995). Somatostatin-14 and its analog octreotide exert a cytostatic effect on GH3 rat pituitary tumor cell proliferation via a transient G0/G1 cell cycle block. *Endocrinology*, *136*, 4174-4181.
- Chisholm, C., & Greenberg, G. R. (2002). Somatostatin-28 regulates GLP-1 secretion via somatostatin receptor subtype 5 in rat intestinal cultures. *American journal of physiology. Endocrinology and metabolism*, *283*, E311-317.
- Ciulla, T. A., Harris, A., McIntyre, N., & Jonescu-Cuypers, C. (2014). Treatment of diabetic macular edema with sustained-release glucocorticoids: intravitreal triamcinolone acetonide, dexamethasone implant, and fluocinolone acetonide implant. *Expert Opinion on Pharmacotherapy*, *15*, 953-959.
- Clemens, A., Klevesath, M. S., Hofmann, M., Raulf, F., Henkels, M., Amiral, J., Seibel, M. J., Zimmermann, J., Ziegler, R., Wahl, P., & Nawroth, P. P. (1999). Octreotide (somatostatin analog) treatment reduces endothelial cell dysfunction in patients with diabetes mellitus. *Metabolism: clinical and experimental*, *48*, 1236-1240.
- Coccoli, V., Luciani, A., Orsi, S., Guarino, V., Causa, F., & Netti, P. A. (2008). Engineering of poly(ϵ -caprolactone) microcarriers to modulate protein encapsulation capability and release kinetic. *Journal of Materials Science: Materials in Medicine*, *19*, 1703-1711.
- Cohen, S., Yoshioka, T., Lucarelli, M., Hwang, L. H., & Langer, R. (1991). Controlled delivery systems for proteins based on poly(lactic/glycolic acid) microspheres. *Pharm Res*, *8*, 713-720.
- Collier, J. H., Hu, B. H., Ruberti, J. W., Zhang, J., Shum, P., Thompson, D. H., & Messersmith, P. B. (2001). Thermally and photochemically triggered self-assembly of peptide hydrogels. *J Am Chem Soc*, *123*, 9463-9464.
- Cunha-Vaz, J. (1979). The blood-ocular barriers. *Surv Ophthalmol*, *23*, 279-296.
- Cunha-Vaz, J. G. (1976). The blood-retinal barriers. *Documenta ophthalmologica*, *41*, 287-327.
- Dal Monte, M., Cammalleri, M., Martini, D., Casini, G., & Bagnoli, P. (2007). Antiangiogenic role of somatostatin receptor 2 in a model of hypoxia-induced neovascularization in the retina: results from transgenic mice. *Investigative ophthalmology & visual science*, *48*, 3480-3489.
- Dall, T. M., Narayan, K. M. V., Gillespie, K. B., Gallo, P. D., Blanchard, T. D., Solcan, M., O'Grady, M., & Quick, W. W. (2014). Detecting type 2 diabetes and prediabetes among asymptomatic adults in the United States: modeling American Diabetes Association versus US Preventive Services Task Force diabetes screening guidelines. *Population health metrics*, *12*, 12.
- Daneluzzi, V. Rheological aspects of polysaccharides.
- Dash, T. K., & Konkimalla, V. B. (2012). Poly- ϵ -caprolactone based formulations for drug delivery and tissue engineering: A review. *Journal of Controlled Release*, *158*, 15-33.
- Davis, M. I., Wilson, S. H., & Grant, M. B. (2001). The therapeutic problem of proliferative diabetic retinopathy: targeting somatostatin receptors. *Hormone and metabolic research = Hormon- und Stoffwechselforschung = Hormones et métabolisme*, *33*, 295-299.
- Debiopharm. (2015). Sanvar Product Information. In. www.debiopharm.com.
- Delesque, N., Buscail, L., Estève, J. P., Raully, I., Zeggari, M., Saint-Laurent, N., Bell, G. I., Schally, A. V., Vaysse, N., & Susini, C. (1995). A tyrosine phosphatase is associated with the somatostatin receptor. *Ciba Foundation symposium*, *190*, 187-196; discussion 196.
- Demetriades, A. M., Deering, T., Liu, H., Lu, L., Gehlbach, P., Packer, J. D., Gabhann, F. M., Popel, A. S., Wei, L. L., & Campochiaro, P. A. (2008). Trans-scleral Delivery of Antiangiogenic Proteins. *Journal of Ocular Pharmacology and Therapeutics*, *24*, 70-79.
- Dent, P., Reardon, D. B., Wood, S. L., Lindorfer, M. A., Graber, S. G., Garrison, J. C., Brautigan, D. L., & Sturgill, T. W. (1996). Inactivation of Raf-1 by a Protein-tyrosine Phosphatase Stimulated by GTP and Reconstituted by G Subunits. *Journal of Biological Chemistry*, *271*, 3119-3123.

- Di Leo, M. A., Caputo, S., Falsini, B., Porciatti, V., Greco, A. V., & Ghirlanda, G. (1994). Presence and further development of retinal dysfunction after 3-year follow up in IDDM patients without angiographically documented vasculopathy. *Diabetologia*, *37*, 911-916.
- Di Leo, M. A., Falsini, B., Caputo, S., Ghirlanda, G., Porciatti, V., & Greco, A. V. (1990). Spatial frequency-selective losses with pattern electroretinogram in type 1 (insulin-dependent) diabetic patients without retinopathy. *Diabetologia*, *33*, 726-730.
- dos Santos, A. L. G., Bochot, A., Doyle, A., Tsapis, N., Siepmann, J., Siepmann, F., Schmalzer, J., Besnard, M., Behar-Cohen, F., & Fattal, E. (2006). Sustained release of nanosized complexes of polyethylenimine and anti-TGF- β 2 oligonucleotide improves the outcome of glaucoma surgery. *Journal of Controlled Release*, *112*, 369-381.
- Dunn, K. C., Aotaki-Keen, A. E., Putkey, F. R., & Hjelmeland, L. M. (1996). ARPE-19, a human retinal pigment epithelial cell line with differentiated properties. *Experimental eye research*, *62*, 155-170.
- Duvvuri, S., Majumdar, S., & Mitra, A. K. (2003). Drug delivery to the retina: challenges and opportunities. *Expert Opin Biol Ther*, *3*, 45-56.
- Edelhauser, H. F., Rowe-Rendleman, C. L., Robinson, M. R., Dawson, D. G., Chader, G. J., Grossniklaus, H. E., Rittenhouse, K. D., Wilson, C. G., Weber, D. A., Kuppermann, B. D., Csaky, K. G., Olsen, T. W., Kompella, U. B., Holers, V. M., Hageman, G. S., Gilger, B. C., Campochiaro, P. A., Whitcup, S. M., & Wong, W. T. (2010). Ophthalmic Drug Delivery Systems for the Treatment of Retinal Diseases: Basic Research to Clinical Applications. *Investigative ophthalmology & visual science*, *51*, 5403-5420.
- Einmahl, S., Savoldelli, M., D'Hermies, F., Tabatabay, C., Gurny, R., & Behar-Cohen, F. (2002). Evaluation of a novel biomaterial in the suprachoroidal space of the rabbit eye. *Invest Ophthalmol Vis Sci*, *43*, 1533-1539.
- Ensinck, J. W., Laschansky, E. C., Vogel, R. E., Simonowitz, D. A., Roos, B. A., & Francis, B. H. (1989). Circulating prosomatostatin-derived peptides. Differential responses to food ingestion. *The Journal of clinical investigation*, *83*, 1580-1589.
- Erdemli, Ö., Usanmaz, A., Keskin, D., & Tezcaner, A. (2014). Characteristics and release profiles of MPEG-PCL-MPEG microspheres containing immunoglobulin G. *Colloids and Surfaces B: Biointerfaces*, *117*, 487-496.
- Ewing, F. M., Deary, I. J., Strachan, M. W., & Frier, B. M. (1998). Seeing beyond retinopathy in diabetes: electrophysiological and psychophysical abnormalities and alterations in vision. *Endocr Rev*, *19*, 462-476.
- Ferone, D., Gatto, F., Arvigo, M., Resmini, E., Boschetti, M., Teti, C., Esposito, D., & Minuto, F. (2009). The clinical-molecular interface of somatostatin, dopamine and their receptors in pituitary pathophysiology. *Journal of molecular endocrinology*, *42*, 361-370.
- Ferrante, E., Pellegrini, C., Bondioni, S., Peverelli, E., Locatelli, M., Gelmini, P., Luciani, P., Peri, A., Mantovani, G., Bosari, S., Beck-Peccoz, P., Spada, A., & Lania, A. (2006). Octreotide promotes apoptosis in human somatotroph tumor cells by activating somatostatin receptor type 2. *Endocrine-related cancer*, *13*, 955-962.
- Ferrara, N. (2004). Vascular Endothelial Growth Factor: Basic Science and Clinical Progress. *Endocrine Reviews*, *25*, 581-611.
- Florio, T., Arena, S., Thellung, S., Iuliano, R., Corsaro, A., Massa, A., Pattarozzi, A., Bajetto, A., Trapasso, F., Fusco, A., & Schettini, G. (2001). The activation of the phosphotyrosine phosphatase eta (r-PTP eta) is responsible for the somatostatin inhibition of PC Cl3 thyroid cell proliferation. *Mol Endocrinol*, *15*, 1838-1852.
- Florio, T., & Schettini, G. (1996). Multiple intracellular effectors modulate physiological functions of the cloned somatostatin receptors. *Journal of Molecular Endocrinology*, *17*, 89-100.
- Foo, K. Y., & Hameed, B. H. (2010). Insights into the modeling of adsorption isotherm systems. *Chemical Engineering Journal*, *156*, 2-10.

- Ford, J. L. (1999). Thermal analysis of hydroxypropylmethylcellulose and methylcellulose: powders, gels and matrix tablets. *International Journal of Pharmaceutics*, *179*, 209-228.
- Ford, K. M., Saint-Geniez, M., Walshe, T., Zahr, A., & D'Amore, P. A. (2011). Expression and role of VEGF in the adult retinal pigment epithelium. *Invest Ophthalmol Vis Sci*, *52*, 9478-9487.
- Frangione-Beebe, M., Rose, R. T., Kaumaya, P. T., & Schwendeman, S. P. (2001). Microencapsulation of a synthetic peptide epitope for HTLV-1 in biodegradable poly(D,L-lactide-co-glycolide) microspheres using a novel encapsulation technique. *J Microencapsul*, *18*, 663-677.
- Freitas, S., Merkle, H. P., & Gander, B. (2005). Microencapsulation by solvent extraction/evaporation: reviewing the state of the art of microsphere preparation process technology. *Journal of Controlled Release*, *102*, 313-332.
- Fujii, Y., Gono, T., Yamada, Y., Chihara, K., Inagaki, N., & Seino, S. Somatostatin receptor subtype SSTR2 mediates the inhibition of high-voltage-activated calcium channels by somatostatin and its analogue SMS 201-995. *FEBS Lett*, *355*, 117-120.
- Funatsu, H., Yamashita, H., Ikeda, T., Nakanishi, Y., Kitano, S., & Hori, S. (2002). Angiotensin II and vascular endothelial growth factor in the vitreous fluid of patients with diabetic macular edema and other retinal disorders. *American journal of ophthalmology*, *133*, 537-543.
- Funatsu, H., Yamashita, H., Nakanishi, Y., & Hori, S. (2002). Angiotensin II and vascular endothelial growth factor in the vitreous fluid of patients with proliferative diabetic retinopathy. *British Journal of Ophthalmology*, *86*, 311-315.
- Gander, B., Johansen, P., Nam-Trân, H., & Merkle, H. P. (1996). Thermodynamic approach to protein microencapsulation into poly (D, L-lactide) by spray drying. *International Journal of Pharmaceutics*, *129*, 51-61.
- Gaudana, R., Ananthula, H. K., Parenky, A., & Mitra, A. K. (2010). Ocular Drug Delivery. *The AAPS Journal*, *12*, 348-360.
- Geiger, R. C., Waters, C. M., Kamp, D. W., & Glucksberg, M. R. (2005). KGF prevents oxygen-mediated damage in ARPE-19 cells. *Investigative ophthalmology & visual science*, *46*, 3435-3442.
- Gerber, H. P., McMurtrey, A., Kowalski, J., Yan, M., Keyt, B. A., Dixit, V., & Ferrara, N. (1998). Vascular endothelial growth factor regulates endothelial cell survival through the phosphatidylinositol 3'-kinase/Akt signal transduction pathway. Requirement for Flk-1/KDR activation. *J Biol Chem*, *273*, 30336-30343.
- Ghassemi, A. H., van Steenberg, M. J., Barendregt, A., Talsma, H., Kok, R. J., van Nostrum, C. F., Crommelin, D. J. A., & Hennink, W. E. (2012). Controlled release of octreotide and assessment of peptide acylation from poly (D, L-lactide-co-hydroxymethyl glycolide) compared to PLGA microspheres. *Pharmaceutical Research*, *29*, 110-120.
- Gillies, M. C., Lim, L. L., Campain, A., Quin, G. J., Salem, W., Li, J., Goodwin, S., Aroney, C., McAllister, I. L., & Fraser-Bell, S. (2014). A Randomized Clinical Trial of Intravitreal Bevacizumab versus Intravitreal Dexamethasone for Diabetic Macular Edema: The BEVORDEX Study. *Ophthalmology*, *121*, 2473-2481.
- Gohel, M. C., Panchal, M. K., & Jogani, V. V. (2000). Novel mathematical method for quantitative expression of deviation from the Higuchi model. *AAPS PharmSciTech*, *1*, 43-48.
- Grant, M. B., & Caballero, S. (2002). Somatostatin analogues as drug therapies for retinopathies. *Drugs Today (Barc)*, *38*, 783-791.
- Grant, M. B., Mames, R., Cooper, R., Caballero, S., & Fitzgerald, C. (1996). Octreotide (OCT) does not prevent progression of Diabetic Retinopathy (DR). *Investigative Ophthalmology and Visual Science*, *37*.
- Grant, M. B., Mames, R. N., Fitzgerald, C., Hazariwala, K. M., Cooper-DeHoff, R., Caballero, S., & Estes, K. S. (2000). The efficacy of octreotide in the therapy of severe nonproliferative and early proliferative diabetic retinopathy: a randomized controlled study. *Diabetes Care*, *23*, 504-509.

- Gresh, J., Goletz, P. W., Crouch, R. K., & Rohrer, B. (2003). Structure–function analysis of rods and cones in juvenile, adult, and aged C57BL/6 and Balb/c mice. *Visual Neuroscience*, *20*, 211-220.
- Gromada, J., Hoy, M., Buschard, K., Salehi, A., & Rorsman, P. (2001). Somatostatin inhibits exocytosis in rat pancreatic alpha-cells by G(i2)-dependent activation of calcineurin and depriving of secretory granules. *The Journal of physiology*, *535*, 519-532.
- Gromada, J., Høy, M., Buschard, K., Salehi, A., & Rorsman, P. (2001). Somatostatin inhibits exocytosis in rat pancreatic α -cells by Gi2-dependent activation of calcineurin and depriving of secretory granules. *The Journal of physiology*, *535*, 519-532.
- Grossniklaus, H. E., Ling, J. X., Wallace, T. M., Dithmar, S., Lawson, D. H., Cohen, C., Elner, V. M., Elner, S. G., & Sternberg Jr, P. (2002). Macrophage and retinal pigment epithelium expression of angiogenic cytokines in choroidal neovascularization. *Mol Vis*, *8*, 119-126.
- Guillemin, R. (2008). Somatostatin: the beginnings, 1972. *Mol Cell Endocrinol*, *286*, 3-4.
- Guyer, D. R., Schachat, A. P., & Green, W. R. (2006). Chapter 3 - The Choroid: Structural Considerations. In *Retina (Fourth Edition)* (pp. 33-42). Edinburgh: Mosby.
- Gyr, K., Beglinger, C., Kohler, E., Trautzi, U., Keller, U., & Bloom, S. R. (1987). Circulating somatostatin. Physiological regulator of pancreatic function? *The Journal of clinical investigation*, *79*, 1595-1600.
- Hakert, H., Eckert, T., & Müller, T. (1989). Rheological and electron microscopic characterization of aqueous carboxymethyl cellulose gels Part I: Rheological aging of aqueous gels of carboxymethyl cellulose in the free acid form (HCMC). *Colloid and Polymer Science*, *267*, 226-229.
- Hakkarainen, M., & Albertsson, A. C. (2002). Heterogeneous biodegradation of polycaprolactone– low molecular weight products and surface changes. *Macromolecular Chemistry and Physics*, *203*, 1357-1363.
- Hamalainen, K. M., Kananen, K., Auriola, S., Kontturi, K., & Urtti, A. (1997). Characterization of paracellular and aqueous penetration routes in cornea, conjunctiva, and sclera. *Invest Ophthalmol Vis Sci*, *38*, 627-634.
- Hammes, H. P., Lin, J., Bretzel, R. G., Brownlee, M., & Breier, G. (1998). Upregulation of the vascular endothelial growth factor/vascular endothelial growth factor receptor system in experimental background diabetic retinopathy of the rat. *Diabetes*, *47*, 401.
- Hannon, J. P., Nunn, C., Stolz, B., Bruns, C., Weckbecker, G., Lewis, I., Troxler, T., Hurth, K., & Hoyer, D. (2002). Drug design at peptide receptors: somatostatin receptor ligands. *Journal of molecular neuroscience : MN*, *18*, 15-27.
- Harper, J. D., & Lansbury, P. T., Jr. (1997). Models of amyloid seeding in Alzheimer's disease and scrapie: mechanistic truths and physiological consequences of the time-dependent solubility of amyloid proteins. *Annu Rev Biochem*, *66*, 385-407.
- Harrower, A. D., & Clarke, B. F. (1976). Diabetic retinopathy with normal glucose tolerance. *British Journal of Ophthalmology*, *60*, 459-463.
- Hasskarl, J., Kaufmann, M., & Schmid, H. A. (2011). Somatostatin receptors in non-neuroendocrine malignancies: the potential role of somatostatin analogs in solid tumors. *Future oncology*, *7*, 895-913.
- Heimsath Jr, E. G., Unda, R., Vidro, E., Muniz, A., Villazana-Espinoza, E. T., & Tsin, A. (2006). ARPE-19 cell growth and cell functions in euglycemic culture media. *Current eye research*, *31*, 1073-1080.
- Hernaez-Ortega, M. C., Soto-Pedre, E., & Pinies, J. A. (2008). Lanreotide Autogel for persistent diabetic macular edema. *Diabetes research and clinical practice*, *80*, e8-10.
- Hernandez, C., Carrasco, E., Casamitjana, R., Deulofeu, R., Garcia-Arumi, J., & Simo, R. (2005). Somatostatin molecular variants in the vitreous fluid: a comparative study between diabetic patients with proliferative diabetic retinopathy and nondiabetic control subjects. *Diabetes Care*, *28*, 1941-1947.

- Hernandez, C., Garcia-Ramirez, M., Corraliza, L., Fernandez-Carneado, J., Farrera-Sinfreu, J., Ponsati, B., Gonzalez-Rodriguez, A., Valverde, A. M., & Simo, R. (2013). Topical administration of somatostatin prevents retinal neurodegeneration in experimental diabetes. *Diabetes*, *62*, 2569-2578.
- Hernandez, C., Simo-Servat, O., & Simo, R. (2014). Somatostatin and diabetic retinopathy: current concepts and new therapeutic perspectives. *Endocrine*, *46*, 209-214.
- Hernandez, C., Simo, R., & European Consortium for the Early Treatment of Diabetic, R. (2013). Somatostatin replacement: a new strategy for treating diabetic retinopathy. *Current medicinal chemistry*, *20*, 3251-3257.
- Herrero-Vanrell, R. (2011). Microparticles as drug delivery systems for the back of the eye. In *Drug product development for the back of the eye* (pp. 231-259): Springer.
- Herrero-Vanrell, R., Bravo-Osuna, I., Andres-Guerrero, V., Vicario-de-la-Torre, M., & Molina-Martinez, I. T. (2014). The potential of using biodegradable microspheres in retinal diseases and other intraocular pathologies. *Prog Retin Eye Res*, *42*, 27-43.
- Herrero-Vanrell, R., de la Torre, M. V., Andres-Guerrero, V., Barbosa-Alfaro, D., Molina-Martinez, I. T., & Bravo-Osuna, I. (2013). Nano and microtechnologies for ophthalmic administration, an overview. *Journal of Drug Delivery Science and Technology*, *23*, 75-102.
- Herrero-Vanrell, R., & Ramirez, L. (2000). Biodegradable PLGA microspheres loaded with ganciclovir for intraocular administration. Encapsulation technique, in vitro release profiles, and sterilization process. *Pharmaceutical Research*, *17*, 1323-1328.
- Herrero-Vanrell, R., & Refojo, M. F. (2001). Biodegradable microspheres for vitreoretinal drug delivery. *Advanced drug delivery reviews*, *52*, 5-16.
- Herrmann, J., & Bodmeier, R. (1998). Biodegradable, somatostatin acetate containing microspheres prepared by various aqueous and non-aqueous solvent evaporation methods. *Eur J Pharm Biopharm*, *45*, 75-82.
- Herrmann, J., & Bodmeier, R. (2003). Degradation kinetics of somatostatin in aqueous solution. *Drug Dev Ind Pharm*, *29*, 1027-1033.
- Higgins, R. D., Yan, Y., & Schrier, B. K. (2002). Somatostatin analogs inhibit neonatal retinal neovascularization. *Experimental eye research*, *74*, 553-559.
- Higuchi, T. (1961). Rate of release of medicaments from ointment bases containing drugs in suspension. *J Pharm Sci*, *50*, 874-875.
- Hiljanen-Vainio, M., Karjalainen, T., & Seppälä, J. (1996). Biodegradable lactone copolymers. I. Characterization and mechanical behavior of ϵ -caprolactone and lactide copolymers. *Journal of Applied Polymer Science*, *59*, 1281-1288.
- Hiramatsu, H., & Kitagawa, T. (2005). FT-IR approaches on amyloid fibril structure. *Biochim Biophys Acta*, *1753*, 100-107.
- Hixson, A., & Crowell, J. (1931). Dependence of reaction velocity upon surface and agitation. *Industrial & Engineering Chemistry*, *23*, 1160-1168.
- Hofland, L. J., & Lamberts, S. W. (2003). The pathophysiological consequences of somatostatin receptor internalization and resistance. *Endocr Rev*, *24*, 28-47.
- Holladay, L. A., & Puett, D. (1976). Somatostatin conformation: evidence for a stable intramolecular structure from circular dichroism, diffusion, and sedimentation equilibrium. *Proc Natl Acad Sci U S A*, *73*, 1199-1202.
- Holladay, L. A., Rivier, J., & Puett, D. (1977). Conformational studies on somatostatin and analogues. *Biochemistry*, *16*, 4895-4900.
- Holland, T. A., Tabata, Y., & Mikos, A. G. (2005). Dual growth factor delivery from degradable oligo(poly(ethylene glycol) fumarate) hydrogel scaffolds for cartilage tissue engineering. *Journal of Controlled Release*, *101*, 111-125.
- Holz, F. G., Schmitz-Valckenberg, S., & Fleckenstein, M. (2014). Recent developments in the treatment of age-related macular degeneration. *The Journal of Clinical Investigation*, *124*, 1430-1438.

- Hornof, M., Toropainen, E., & Urtti, A. (2005). Cell culture models of the ocular barriers. *Eur J Pharm Biopharm*, *60*, 207-225.
- Hosoya, K.-i., Tomi, M., & Tachikawa, M. (2011). Strategies for therapy of retinal diseases using systemic drug delivery: relevance of transporters at the blood–retinal barrier. *Expert opinion on drug delivery*, *8*, 1571-1587.
- Hou, C., Gilbert, R. L., & Barber, D. L. (1994). Subtype-specific signaling mechanisms of somatostatin receptors SSTR1 and SSTR2. *Journal of Biological Chemistry*, *269*, 10357-10362.
- Hu, M., & Tomlinson, B. (2010). Pharmacokinetic evaluation of lanreotide. *Expert Opinion on Drug Metabolism & Toxicology*, *6*, 1301-1312.
- Huang, M. H., Li, S., Hutmacher, D. W., Schantz, J. T., Vacanti, C. A., Braud, C., & Vert, M. (2004). Degradation and cell culture studies on block copolymers prepared by ring opening polymerization of ϵ -caprolactone in the presence of poly (ethylene glycol). *Journal of Biomedical Materials Research Part A: An Official Journal of The Society for Biomaterials, The Japanese Society for Biomaterials, and The Australian Society for Biomaterials and the Korean Society for Biomaterials*, *69*, 417-427.
- Hughes, P., Delahaye, L., Boix, M., Chang, J., & Lyons, R. (2005). Therapeutic ophthalmic compositions containing retinal friendly excipients and related methods. In: Google Patents.
- Hughes, P. M., Olejnik, O., Chang-Lin, J.-E., & Wilson, C. G. (2005). Topical and systemic drug delivery to the posterior segments. *Advanced Drug Delivery Reviews*, *57*, 2010-2032.
- Hyer, S. L., Sharp, P. S., Brooks, R. A., Burrin, J. M., & Kohner, E. M. (1989). Continuous subcutaneous octreotide infusion markedly suppresses IGF-I levels whilst only partially suppressing GH secretion in diabetics with retinopathy. *Acta endocrinologica*, *120*, 187-194.
- Ionov, I. D., & Severtsev, N. N. (2012). Somatostatin antagonist potentiates haloperidol-induced catalepsy in the aged rat. *Pharmacology Biochemistry and Behavior*, *103*, 295-298.
- Ipsen. (2015). Somatuline Product Information. In (Vol. 2015). www.ipsen.com.
- Jain, R. A. (2000). The manufacturing techniques of various drug loaded biodegradable poly(lactide-co-glycolide) (PLGA) devices. *Biomaterials*, *21*, 2475-2490.
- Janoria, K. G., Gunda, S., Boddu, S. H., & Mitra, A. K. (2007). Novel approaches to retinal drug delivery. *Expert Opin Drug Deliv*, *4*, 371-388.
- Jenkins, M. J., & Harrison, K. L. (2006). The effect of molecular weight on the crystallization kinetics of polycaprolactone. *Polymers for advanced technologies*, *17*, 474-478.
- Joshi, S. C. (2011). Sol-gel behavior of hydroxypropyl methylcellulose (HPMC) in ionic media including drug release. *Materials*, *4*, 1861-1905.
- Kadam, R. S., Williams, J., Tyagi, P., Edelhauser, H. F., & Kompella, U. B. (2013). Suprachoroidal delivery in a rabbit ex vivo eye model: influence of drug properties, regional differences in delivery, and comparison with intravitreal and intracameral routes. *Mol Vis*, *19*, 1198-1210.
- Kalsi, G., Silver, H., & Rootman, J. (1991). Ocular pharmacokinetics of dacarbazine following subconjunctival versus intravenous administration in the rabbit. *Canadian journal of ophthalmology. Journal canadien d'ophtalmologie*, *26*, 247-251.
- Kamei, M., Misono, K., & Lewis, H. A study of the ability of tissue plasminogen activator to diffuse into the subretinal space after intravitreal injection in rabbits. *American Journal of Ophthalmology*, *128*, 739-746.
- Kamei, M., Misono, K., & Lewis, H. (1999). A study of the ability of tissue plasminogen activator to diffuse into the subretinal space after intravitreal injection in rabbits. *American journal of ophthalmology*, *128*, 739-746.
- Kannan, R., Zhang, N., Sreekumar, P. G., Spee, C. K., Rodriguez, A., Barron, E., & Hinton, D. R. (2006). Stimulation of apical and basolateral VEGF-A and VEGF-C secretion by oxidative stress in polarized retinal pigment epithelial cells. *Molecular Vision*, *12*, 1649-1659.
- Katz, S. E., Klisovic, D. D., O'Dorisio, M. S., Lynch, R., & Lubow, M. (2002). Expression of somatostatin receptors 1 and 2 in human choroid plexus and arachnoid granulations: implications for idiopathic intracranial hypertension. *Archives of Ophthalmology*, *120*, 1540-1543.

- Kaur, I. P., & Kakkar, S. (2014). Nanotherapy for posterior eye diseases. *J Control Release*, *193*, 100-112.
- Kaur, I. P., & Kanwar, M. (2002). Ocular preparations: the formulation approach. *Drug Dev Ind Pharm*, *28*, 473-493.
- Kavanagh, G. M., & Ross-Murphy, S. B. (1998). Rheological characterisation of polymer gels. *Progress in Polymer Science*, *23*, 533-562.
- Kennedy, B. G., & Mangini, N. J. (2002). P-glycoprotein expression in human retinal pigment epithelium. *Mol Vis*, *8*, 30.
- Kennedy, B. G., & Mangini, N. J. (2002). P-glycoprotein expression in human retinal pigment epithelium. *Molecular vision*, *8*, 422-430.
- Khorshid, F. (2005). The Effect of the Medium Viscosity on the Cells Morphology in Reaction of Cells to Topography—I. *Abstract presented at the Proc 2nd Saudi Sci Conl, Fac Sci, KAU*, 67-98.
- Kiernan, D., & Lim, J. (2010). Topical Drug Delivery for Posterior Segment Disease Novel formulations offer possibilities for efficacious therapies through topical routes. *Retina Today*, *48*, 48-54.
- Kilic, U., Kilic, E., Jarve, A., Guo, Z., Spudich, A., Bieber, K., Barzena, U., Bassetti, C. L., Marti, H. H., & Hermann, D. M. (2006). Human vascular endothelial growth factor protects axotomized retinal ganglion cells in vivo by activating ERK-1/2 and Akt pathways. *J Neurosci*, *26*, 12439-12446.
- Kim, H., Robinson, M. R., Lizak, M. J., Tansey, G., Lutz, R. J., Yuan, P., Wang, N. S., & Csaky, K. G. (2004). Controlled Drug Release from an Ocular Implant: An Evaluation Using Dynamic Three-Dimensional Magnetic Resonance Imaging. *Investigative ophthalmology & visual science*, *45*, 2722-2731.
- Kim, J.-H., & Bae, Y. H. (2004). Albumin loaded microsphere of amphiphilic poly (ethylene glycol)/poly (α -ester) multiblock copolymer. *European Journal of Pharmaceutical Sciences*, *23*, 245-251.
- Kim, S. H., Lutz, R. J., Wang, N. S., & Robinson, M. R. (2007). Transport Barriers in Transscleral Drug Delivery for Retinal Diseases. *Ophthalmic Research*, *39*, 244-254.
- Kim, Y. C., Park, J. H., & Prausnitz, M. R. (2012). Microneedles for drug and vaccine delivery. *Adv Drug Deliv Rev*, *64*, 1547-1568.
- Kirchhof, S., Gregoritzka, M., Messmann, V., Hammer, N., Goepferich, A. M., & Brandl, F. P. (2015). Diels–Alder hydrogels with enhanced stability: First step toward controlled release of bevacizumab. *European Journal of Pharmaceutics and Biopharmaceutics*, *96*, 217-225.
- Kirkegaard, C., Norgaard, K., Snorgaard, O., Bek, T., Larsen, M., & Lund-Andersen, H. (1990). Effect of one year continuous subcutaneous infusion of a somatostatin analogue, octreotide, on early retinopathy, metabolic control and thyroid function in Type I (insulin-dependent) diabetes mellitus. *Acta endocrinologica*, *122*, 766-772.
- Klein, R., Klein, B. E., Moss, S. E., & Cruickshanks, K. J. (1998). The Wisconsin Epidemiologic Study of Diabetic Retinopathy: XVII. The 14-year incidence and progression of diabetic retinopathy and associated risk factors in type 1 diabetes. *Ophthalmology*, *105*, 1801-1815.
- Klettner, A., Westhues, D., Lassen, J., Bartsch, S., & Roeder, J. (2013). Regulation of constitutive vascular endothelial growth factor secretion in retinal pigment epithelium/choroid organ cultures: p38, nuclear factor kappaB, and the vascular endothelial growth factor receptor-2/phosphatidylinositol 3 kinase pathway. *Mol Vis*, *19*, 281-291.
- Kleuss, C., Hescheler, J., Ewel, C., Rosenthal, W., Schultz, G., & Wittig, B. (1991). Assignment of G-protein subtypes to specific receptors inducing inhibition of calcium currents. *Nature*, *353*, 43-48.
- Klisovic, D. D., O'Dorisio, M. S., Katz, S. E., Sall, J. W., Balster, D., O'Dorisio, T. M., Craig, E., & Lubow, M. (2001). Somatostatin receptor gene expression in human ocular tissues: RT-PCR and immunohistochemical study. *Investigative ophthalmology & visual science*, *42*, 2193-2201.
- Koch, B. D., Blalock, J. B., & Schonbrunn, A. (1988). Characterization of the cyclic AMP-independent actions of somatostatin in GH cells. I. An increase in potassium conductance is responsible

- for both the hyperpolarization and the decrease in intracellular free calcium produced by somatostatin. *Journal of Biological Chemistry*, 263, 216-225.
- Kociok, N., Heppekausen, H., Schraermeyer, U., Esser, P., Thumann, G., Grisanti, S., & Heimann, K. (1998). The mRNA expression of cytokines and their receptors in cultured iris pigment epithelial cells: a comparison with retinal pigment epithelial cells. *Experimental eye research*, 67, 237-250.
- Koenig, M. F., & Huang, S. J. (1995). Biodegradable blends and composites of polycaprolactone and starch derivatives. *Polymer*, 36, 1877-1882.
- Koevary, S. B. (2003). Pharmacokinetics of topical ocular drug delivery: potential uses for the treatment of diseases of the posterior segment and beyond. *Curr Drug Metab*, 4, 213-222.
- Kokona, D., Mastrodinou, N., Pediaditakis, I., Charalampopoulos, I., Schmid, H. A., & Thermos, K. (2012). Pasireotide (SOM230) protects the retina in animal models of ischemia induced retinopathies. *Experimental eye research*, 103, 90-98.
- Korsmeyer, R. W., Gurny, R., Doelker, E., Buri, P., & Peppas, N. A. (1983). Mechanisms of solute release from porous hydrophilic polymers. *International Journal of Pharmaceutics*, 15, 25-35.
- Kouvidi, E., Papadopoulou-Daifoti, Z., & Thermos, K. (2006). Somatostatin modulates dopamine release in rat retina. *Neuroscience letters*, 391, 82-86.
- Kowluru, R. A., Engerman, R. L., Case, G. L., & Kern, T. S. (2001). Retinal glutamate in diabetes and effect of antioxidants. *Neurochemistry international*, 38, 385-390.
- Kowluru, R. A., & Odenbach, S. (2004). Role of interleukin-1 β in the pathogenesis of diabetic retinopathy. *British Journal of Ophthalmology*, 88, 1343-1347.
- Krimm, S., & Bandekar, J. (1986). Vibrational spectroscopy and conformation of peptides, polypeptides, and proteins. *Adv Protein Chem*, 38, 181-364.
- Kuijpers, R. W., Baarsma, S., & van Hagen, P. M. (1998). Treatment of cystoid macular edema with octreotide. *The New England journal of medicine*, 338, 624-626.
- Kumar, U., & Grant, M. (2010). Somatostatin and somatostatin receptors. *Results and problems in cell differentiation*, 50, 137-184.
- Lam, X. M., Duenas, E. T., Daugherty, A. L., Levin, N., & Cleland, J. L. (2000). Sustained release of recombinant human insulin-like growth factor-I for treatment of diabetes. *J Control Release*, 67, 281-292.
- Lamberts, S. W., van der Lely, A. J., & Hofland, L. J. (2002). New somatostatin analogs: will they fulfil old promises? *European journal of endocrinology / European Federation of Endocrine Societies*, 146, 701-705.
- Lambooi, A. C., Kuijpers, R. W., van Lichtenauer-Kaligis, E. G., Kliffen, M., Baarsma, G. S., van Hagen, P. M., & Mooy, C. M. (2000). Somatostatin receptor 2A expression in choroidal neovascularization secondary to age-related macular degeneration. *Investigative ophthalmology & visual science*, 41, 2329-2335.
- Langer, R., & Peppas, N. (1983a). Chemical and physical structure of polymers as carriers for controlled release of bioactive agents: a review. *Journal of Macromolecular Science-Reviews in Macromolecular Chemistry and Physics*, 23, 61-126.
- Langer, R., & Peppas, N. (1983b). Chemical and Physical Structure of Polymers as Carriers for Controlled Release of Bioactive Agents: A Review. *Journal of Macromolecular Science, Part C*, 23, 61-126.
- Ławnicka, H., Stępień, H., Wyczółkowska, J., Kolago, B., Kunert-Radek, J., & Komorowski, J. (2000). Effect of somatostatin and octreotide on proliferation and vascular endothelial growth factor secretion from murine endothelial cell line (HECa10) culture. *Biochemical and biophysical research communications*, 268, 567-571.
- Lawrence, M. S., & Miller, J. W. (2004). Ocular tissue permeabilities. *Int Ophthalmol Clin*, 44, 53-61.
- Le Goff, M., & Bishop, P. (2008). Adult vitreous structure and postnatal changes. *Eye (Lond)*, 22, 1214-1222.

- Leach, W. T., Simpson, D. T., Val, T. N., Anuta, E. C., Yu, Z., Williams, R. O., 3rd, & Johnston, K. P. (2005). Uniform encapsulation of stable protein nanoparticles produced by spray freezing for the reduction of burst release. *J Pharm Sci*, *94*, 56-69.
- Lee, H. K., Suh, K. I., Koh, C. S., Min, H. K., Lee, J. H., & Chung, H. (1988). Effect of SMS 201-995 in rapidly progressive diabetic retinopathy. *Diabetes Care*, *11*, 441-443.
- Lee, R., Wong, T. Y., & Sabanayagam, C. (2015). Epidemiology of diabetic retinopathy, diabetic macular edema and related vision loss. *Eye and Vision*, *2*, 17.
- Li, X., Wang, Y., Yang, C., Shi, S., Jin, L., Luo, Z., Yu, J., Zhang, Z., Yang, Z., & Chen, H. (2014). Supramolecular nanofibers of triamcinolone acetonide for uveitis therapy. *Nanoscale*, *6*, 14488-14494.
- Li, X., Zhang, Z., & Chen, H. (2013). Development and evaluation of fast forming nano-composite hydrogel for ocular delivery of diclofenac. *International Journal of Pharmaceutics*, *448*, 96-100.
- Liang, L., Xu, X. D., Chen, C. S., Fang, J. H., Jiang, F. G., Zhang, X. Z., & Zhuo, R. X. (2010). Evaluation of the biocompatibility of novel peptide hydrogel in rabbit eye. *Journal of Biomedical Materials Research Part B: Applied Biomaterials*, *93B*, 324-332.
- Lieth, E., LaNoue, K. F., Antonetti, D. A., & Ratz, M. (2000). Diabetes reduces glutamate oxidation and glutamine synthesis in the retina. The Penn State Retina Research Group. *Exp Eye Res*, *70*, 723-730.
- Lin, C.-Y., Varma, M. G., Joubel, A., Madabushi, S., Lichtarge, O., & Barber, D. L. (2003). Conserved Motifs in Somatostatin, D2-dopamine, and α 2B-Adrenergic Receptors for Inhibiting the Na-H Exchanger, NHE1. *Journal of Biological Chemistry*, *278*, 15128-15135.
- Lin, S. Y., Chen, K. S., Teng, H. H., & Li, M. J. (2000). In vitro degradation and dissolution behaviours of microspheres prepared by three low molecular weight polyesters. *J Microencapsul*, *17*, 577-586.
- Lin, X., Voyno-Yasenetskaya, T. A., Hooley, R., Lin, C. Y., Orłowski, J., & Barber, D. L. (1996). Galpha12 differentially regulates Na⁺-H⁺ exchanger isoforms. *J Biol Chem*, *271*, 22604-22610.
- Lopez, F., Estève, J.-P., Buscail, L., Delesque, N., Saint-Laurent, N., Théveniau, M., Nahmias, C., Vaysse, N., & Susini, C. (1997). The Tyrosine Phosphatase SHP-1 Associates with the sst2 Somatostatin Receptor and Is an Essential Component of sst2-mediated Inhibitory Growth Signaling. *Journal of Biological Chemistry*, *272*, 24448-24454.
- Lopez, F., Estève, J. P., Buscail, L., Delesque, N., Saint-Laurent, N., Vaysse, N., & Susini, C. Molecular mechanisms of antiproliferative effect of somatostatin: Involvement of a tyrosine phosphatase. *Metabolism - Clinical and Experimental*, *45*, 14-16.
- Lopez, F., Ferjoux, G., Cordelier, P., Saint-Laurent, N., Estève, J. P., Vaysse, N., Buscail, L., & Susini, C. (2001). Neuronal nitric oxide synthase: a substrate for SHP-1 involved in sst2 somatostatin receptor growth inhibitory signaling. *The FASEB journal : official publication of the Federation of American Societies for Experimental Biology*, *15*, 2300-2302.
- Loveday, S., Wang, X., Rao, M., Anema, S., & Singh, H. (2012). β -Lactoglobulin nanofibrils: Effect of temperature on fibril formation kinetics, fibril morphology and the rheological properties of fibril dispersions. *Food Hydrocolloids*, *27*, 242-249.
- Lovett, M. L., Wang, X., Yucel, T., York, L., Keirstead, M., Haggerty, L., & Kaplan, D. L. (2015). Silk hydrogels for sustained ocular delivery of anti-vascular endothelial growth factor (anti-VEGF) therapeutics. *European Journal of Pharmaceutics and Biopharmaceutics*, *95*, 271-278.
- Luna, J. D., Chan, C. C., Derevjani, N. L., Mahlow, J., Chiu, C., Peng, B., Tobe, T., Campochiaro, P. A., & Viores, S. A. (1997). Blood-retinal barrier (BRB) breakdown in experimental autoimmune uveoretinitis: Comparison with vascular endothelial growth factor, tumor necrosis factor α , and interleukin-1 β -mediated breakdown. *Journal of neuroscience research*, *49*, 268-280.
- Lynn, S. A., Ward, G., Keeling, E., Scott, J. A., Cree, A. J., Johnston, D. A., Page, A., Cuan-Urquizo, E., Bhaskar, A., Gossel, M. C., Tumbarello, D. A., Newman, T. A., Lotery, A. J., & Ratnayaka, J. A. (2017). Ex-vivo models of the Retinal Pigment Epithelium (RPE) in long-term culture faithfully

- recapitulate key structural and physiological features of native RPE. *Tissue and Cell*, *49*, 447-460.
- Mains, J., & Wilson, C. G. (2012). The Vitreous Humor As a Barrier to Nanoparticle Distribution. *Journal of Ocular Pharmacology and Therapeutics*, *29*, 143-150.
- Maji, S. K., Perrin, M. H., Sawaya, M. R., Jessberger, S., Vadodaria, K., Rissman, R. A., Singru, P. S., Nilsson, K. P. R., Simon, R., Schubert, D., Eisenberg, D., Rivier, J., Sawchenko, P., Vale, W., & Riek, R. (2009). Functional Amyloids As Natural Storage of Peptide Hormones in Pituitary Secretory Granules. *Science*, *325*, 328-332.
- Maji, S. K., Schubert, D., Rivier, C., Lee, S., Rivier, J. E., & Riek, R. (2008). Amyloid as a Depot for the Formulation of Long-Acting Drugs. *PLoS Biology*, *6*, e17.
- Makadia, H. K., & Siegel, S. J. (2011). Poly lactic-co-glycolic acid (PLGA) as biodegradable controlled drug delivery carrier. *Polymers*, *3*, 1377-1397.
- Mallet, B., Vialettes, B., Haroche, S., Escoffier, P., Gastaut, P., Taubert, J. P., & Vague, P. (1992). Stabilization of severe proliferative diabetic retinopathy by long-term treatment with SMS 201-995. *Diabete & metabolisme*, *18*, 438-444.
- Mandal, A., Pal, D., Agrahari, V., Trinh, H. M., Joseph, M., & Mitra, A. K. (2018). Ocular delivery of proteins and peptides: Challenges and novel formulation approaches. *Advanced drug delivery reviews*, *126*, 67-95.
- Martin-Gago, P., Ramon, R., Aragon, E., Fernandez-Carneado, J., Martin-Malpartida, P., Verdaguier, X., Lopez-Ruiz, P., Colas, B., Cortes, M. A., Ponsati, B., Macias, M. J., & Riera, A. (2014). A tetradecapeptide somatostatin dicarba-analog: Synthesis, structural impact and biological activity. *Bioorganic & medicinal chemistry letters*, *24*, 103-107.
- Martínez-Sancho, C., Herrero-Vanrell, R. o., & Negro, S. a. (2004). Study of gamma-irradiation effects on aciclovir poly(d,l-lactic-co-glycolic) acid microspheres for intravitreal administration. *Journal of Controlled Release*, *99*, 41-52.
- Massa, A., Barbieri, F., Aiello, C., Arena, S., Pattarozzi, A., Pirani, P., Corsaro, A., Iuliano, R., Fusco, A., Zona, G., Spaziante, R., Florio, T., & Schettini, G. (2004). The Expression of the Phosphotyrosine Phosphatase DEP-1/PTP η Dictates the Responsivity of Glioma Cells to Somatostatin Inhibition of Cell Proliferation. *Journal of Biological Chemistry*, *279*, 29004-29012.
- Mastrodimou, N., Kiagiadaki, F., Hodjarova, M., Karagianni, E., & Thermos, K. (2006). Somatostatin receptors (sst 2) regulate cGMP production in rat retina. *Regulatory peptides*, *133*, 41-46.
- Mastrodimou, N., Lambrou, G. N., & Thermos, K. (2005). Effect of somatostatin analogues on chemically induced ischaemia in the rat retina. *Naunyn-Schmiedeberg's Archives of Pharmacology*, *371*, 44-53.
- Maurice, D. M. (2002). Drug delivery to the posterior segment from drops. *Surv Ophthalmol*, *47 Suppl 1*, S41-52.
- McCombe, M., Lightman, S., Eckland, D. J., Hamilton, A. M., & Lightman, S. L. (1991). Effect of a long-acting somatostatin analogue (BIM23014) on proliferative diabetic retinopathy: a pilot study. *Eye (Lond)*, *5 (Pt 5)*, 569-575.
- Mei, S., Cammalleri, M., Azara, D., Casini, G., Bagnoli, P., & Dal Monte, M. (2011). Mechanisms underlying somatostatin receptor 2 down-regulation of vascular endothelial growth factor expression in response to hypoxia in mouse retinal explants. *The Journal of Pathology*, *226*, 519-533.
- Meriney, S. D., Gray, D. B., & Pilar, G. R. (1994). Somatostatin-induced inhibition of neuronal Ca²⁺ current modulated by cGMP-dependent protein kinase. *Nature*, *369*, 336-339.
- Merkli, A., Tabatabay, C., Gurny, R., & Heller, J. (1998). Biodegradable polymers for the controlled release of ocular drugs. *Progress in polymer science*, *23*, 563-580.
- Mezger, T. G. (2006). *The rheology handbook: for users of rotational and oscillatory rheometers*: Vincentz Network GmbH & Co KG.

- Miranda, S., González-Rodríguez, Á., García-Ramírez, M., Revuelta-Cervantes, J., Hernández, C., Simó, R., & Valverde Ángela, M. (2011). Beneficial effects of fenofibrate in retinal pigment epithelium by the modulation of stress and survival signaling under diabetic conditions. *Journal of cellular physiology*, *227*, 2352-2362.
- Mishima, S., Gasset, A., Klyce, S. D., Jr., & Baum, J. L. (1966). Determination of tear volume and tear flow. *Invest Ophthalmol*, *5*, 264-276.
- Mishra, G. P., Bagui, M., Tamboli, V., & Mitra, A. K. (2011). Recent applications of liposomes in ophthalmic drug delivery. *Journal of drug delivery*, *2011*.
- Misra, G. P., Singh, R. S. J., Aleman, T. S., Jacobson, S. G., Gardner, T. W., & Lowe, T. L. (2009). Subconjunctivally implantable hydrogels with degradable and thermoresponsive properties for sustained release of insulin to the retina. *Biomaterials*, *30*, 6541-6547.
- Modlin, I. M., Pavel, M., Kidd, M., & Gustafsson, B. I. (2010). Review article: somatostatin analogues in the treatment of gastroenteropancreatic neuroendocrine (carcinoid) tumours. *Alimentary pharmacology & therapeutics*, *31*, 169-188.
- Mohamed, Q., Gillies, M. C., & Wong, T. Y. (2007). Management of diabetic retinopathy: a systematic review. *Jama*, *298*, 902-916.
- Mohanan, D., Gander, B., Kündig, T. M., & Johansen, P. (2012). Encapsulation of antigen in poly(D,L-lactide-co-glycolide) microspheres protects from harmful effects of γ -irradiation as assessed in mice. *European Journal of Pharmaceutics and Biopharmaceutics*, *80*, 274-281.
- Moller, L. N., Stidsen, C. E., Hartmann, B., & Holst, J. J. (2003). Somatostatin receptors. *Biochimica et biophysica acta*, *1616*, 1-84.
- Moon, H. T., Lee, Y.-K., Han, J. K., & Byun, Y. (2002). Improved blood compatibility by sustained release of heparin–deoxycholic acid conjugates in a PCL–PEG multiblock copolymer matrix. *Journal of Biomaterials Science, Polymer Edition*, *13*, 817-828.
- Moore, D. J., & Clover, G. M. (2001). The effect of age on the macromolecular permeability of human Bruch's membrane. *Investigative Ophthalmology and Visual Science*, *42*, 2970-2975.
- Morita, T., Sakamura, Y., Horikiri, Y., Suzuki, T., & Yoshino, H. (2000). Protein encapsulation into biodegradable microspheres by a novel S/O/W emulsion method using poly(ethylene glycol) as a protein micronization adjuvant. *Journal of Controlled Release*, *69*, 435-444.
- Morlock, M., Kissel, T., Li, Y. X., Koll, H., & Winter, G. (1998). Erythropoietin loaded microspheres prepared from biodegradable LPLG-PEO-LPLG triblock copolymers: protein stabilization and in-vitro release properties. *J Control Release*, *56*, 105-115.
- Mugisho, O. O., Green, C. R., Kho, D. T., Zhang, J., Graham, E. S., Acosta, M. L., & Rupenthal, I. D. (2018). The inflammasome pathway is amplified and perpetuated in an autocrine manner through connexin43 hemichannel mediated ATP release. *Biochimica et Biophysica Acta (BBA) - General Subjects*, *1862*, 385-393.
- Nakatani, M., Shinohara, Y., Takii, M., Mori, H., Asai, N., Nishimura, S., Furukawa-Hibi, Y., Miyamoto, Y., & Nitta, A. (2011). Periocular injection of in situ hydrogels containing Leu-Ile, an inducer for neurotrophic factors, promotes retinal ganglion cell survival after optic nerve injury. *Exp Eye Res*, *93*, 873-879.
- Narasimhan, B., & Peppas, N. (1997). The role of modeling studies in the development of future controlled-release devices. *Controlled Drug Delivery: Challenges and Strategies*, American Chemical Society, Washington, DC, 529-557.
- Ng, Y. K., Zeng, X. X., & Ling, E. A. (2004). Expression of glutamate receptors and calcium-binding proteins in the retina of streptozotocin-induced diabetic rats. *Brain Research*, *1018*, 66-72.
- Nishijima, K., Ng, Y. S., Zhong, L., Bradley, J., Schubert, W., Jo, N., Akita, J., Samuelsson, S. J., Robinson, G. S., Adamis, A. P., & Shima, D. T. (2007). Vascular endothelial growth factor-A is a survival factor for retinal neurons and a critical neuroprotectant during the adaptive response to ischemic injury. *Am J Pathol*, *171*, 53-67.
- Nomoto, H., Shiraga, F., Kuno, N., Kimura, E., Fujii, S., Shinomiya, K., Nugent, A. K., Hirooka, K., & Baba, T. (2009). Pharmacokinetics of Bevacizumab after Topical, Subconjunctival, and

- Intravitreal Administration in Rabbits. *Investigative ophthalmology & visual science*, 50, 4807-4813.
- NovartisEuropharm. (2012). SIGNIFOR 0.3mg solution for injection. In *Novartis Europharm*. www.novartis.com.
- Ohno-Matsui, K., Morita, I., Tombran-Tink, J., Mrazek, D., Onodera, M., Uetama, T., Hayano, M., Murota, S. i., & Mochizuki, M. (2001). Novel mechanism for age-related macular degeneration: An equilibrium shift between the angiogenesis factors VEGF and PEDF. *Journal of cellular physiology*, 189, 323-333.
- Olsen, T. W. (2003). Drug Delivery to the suprachoroidal space shows promise. *Retina Today*, 36-39.
- Olsen, T. W., Aaberg, S. Y., Geroski, D. H., & Edelhauser, H. F. (1998). Human sclera: thickness and surface area. *American journal of ophthalmology*, 125, 237-241.
- Osswald, C. R., & Kang-Mieler, J. J. (2016). Controlled and extended in vitro release of bioactive anti-vascular endothelial growth factors from a microsphere-hydrogel drug delivery system. *Current eye research*, 41, 1216-1222.
- Pace, C. S., & Tarvin, J. T. (1981). Somatostatin: Mechanism of Action in Pancreatic Islet β -Cells. *Diabetes*, 30, 836-842.
- Paganelli, F., Cardillo, J. A., Dare, A. R. J., Melo Jr, L. A. S., Lucena, D. R., Silva Jr, A. A., Oliveira, A. G., Pizzolitto, A. C., Lavinsky, D., & Skaf, M. (2010). Controlled transscleral drug delivery formulations to the eye: establishing new concepts and paradigms in ocular anti-inflammatory therapeutics and antibacterial prophylaxis. *Expert opinion on drug delivery*, 7, 955-965.
- Pagès, P., Benali, N., Saint-Laurent, N., Estève, J.-P., Schally, A. V., Tkaczuk, J., Vaysse, N., Susini, C., & Buscail, L. (1999). sst2 Somatostatin Receptor Mediates Cell Cycle Arrest and Induction of p27 Kip1 : EVIDENCE FOR THE ROLE OF SHP-1. *Journal of Biological Chemistry*, 274, 15186-15193.
- Pal, K., Paulson, A. T., & Rousseau, D. (2013). *14–Biopolymers in controlled-release delivery systems*: sn.
- Pan, M. G., Florio, T., & Stork, P. J. S. (1992). G Protein Activation of a Hormone-Stimulated Phosphatase in Human Tumor Cells. *Science*, 256, 1215-1217.
- Papadaki, T., Tsilimbaris, M., Pallikaris, I., & Thermos, K. (2010). Somatostatin receptor activation (sst1–sst5) differentially influences human retinal pigment epithelium cell viability. *Acta ophthalmologica*, 88, e228-e233.
- Park, H., & Park, K. (1996). Biocompatibility issues of implantable drug delivery systems. *Pharmaceutical Research*, 13, 1770-1776.
- Patch, D., & Burroughs, A. (2002). Vapreotide in variceal bleeding. *J Hepatol*, 37, 167-168.
- Patel, S. R., Berezovsky, D. E., McCarey, B. E., Zarnitsyn, V., Edelhauser, H. F., & Prausnitz, M. R. (2012). Targeted administration into the suprachoroidal space using a microneedle for drug delivery to the posterior segment of the EyeMicroneedle use for targeted drug delivery. *Investigative ophthalmology & visual science*, 53, 4433-4441.
- Patel, Y. C. (1999a). Somatostatin and its receptor family. *Front Neuroendocrinol*, 20, 157-198.
- Patel, Y. C. (1999b). Somatostatin and its receptor family. *Frontiers in Neuroendocrinology*, 20, 157-198.
- Patel, Y. C., Greenwood, M. T., Warszynska, A., Panetta, R., & Srikant, C. B. (1994). All five cloned human somatostatin receptors (hSSTR1-5) are functionally coupled to adenylyl cyclase. *Biochem Biophys Res Commun*, 198, 605-612.
- Pean, J. M., Boury, F., Venier-Julienne, M. C., Menei, P., Proust, J. E., & Benoit, J. P. (1999). Why does PEG 400 co-encapsulation improve NGF stability and release from PLGA biodegradable microspheres? *Pharm Res*, 16, 1294-1299.
- Peeters, T. L., Depraetere, Y., & Vantrappen, G. R. (1981). Simple extraction method and radioimmunoassay for somatostatin in human plasma. *Clinical chemistry*, 27, 888-891.

- Penman, E., Wass, J. A., Medbak, S., Morgan, L., Lewis, J. M., Besser, G. M., & Rees, L. H. (1981). Response of circulating immunoreactive somatostatin to nutritional stimuli in normal subjects. *Gastroenterology*, *81*, 692-699.
- Petersen, H., Bizec, J.-C., Schuetz, H., & Delporte, M.-L. (2011). Pharmacokinetic and technical comparison of Sandostatin(®)LAR(®) and other formulations of long-acting octreotide. *BMC Research Notes*, *4*, 344-344.
- Pitkänen, L., Ranta, V.-P., Moilanen, H., & Urtti, A. (2005). Permeability of Retinal Pigment Epithelium: Effects of Permeant Molecular Weight and Lipophilicity. *Investigative ophthalmology & visual science*, *46*, 641-646.
- Pitkänen, L., Ruponen, M., Nieminen, J., & Urtti, A. (2003). Vitreous Is a Barrier in Nonviral Gene Transfer by Cationic Lipids and Polymers. *Pharm Res*, *20*, 576-583.
- Poitout, L., Roubert, P., Contour-Galcera, M. O., Moinet, C., Lannoy, J., Pommier, J., Plas, P., Bigg, D., & Thurieau, C. (2001). Identification of potent non-peptide somatostatin antagonists with sst(3) selectivity. *J Med Chem*, *44*, 2990-3000.
- Pola, S., Cattaneo, M. G., & Vicentini, L. M. (2003). Anti-migratory and anti-invasive effect of somatostatin in human neuroblastoma cells: involvement of Rac and MAP kinase activity. *The Journal of biological chemistry*, *278*, 40601-40606.
- Prausnitz, M. R., & Noonan, J. S. (1998). Permeability of cornea, sclera, and conjunctiva: A literature analysis for drug delivery to the eye. *Journal of Pharmaceutical Sciences*, *87*, 1479-1488.
- Pulido, J. E., Pulido, J. S., Erie, J. C., Arroyo, J., Bertram, K., Lu, M. J., & Shippy, S. A. (2007). A role for excitatory amino acids in diabetic eye disease. *Experimental diabetes research*, *2007*, 36150.
- Rai, U., Thrimawithana, T. R., Dharmadana, D., Valery, C., & Young, S. A. (2017). Release kinetics of somatostatin from self-assembled nanostructured hydrogels. *Biopolymers*.
- Ramos, D., Carretero, A., Navarro, M., Mendes-Jorge, L., Nacher, V., Rodriguez-Baeza, A., & Ruberte, J. (2013). Mimicking microvascular alterations of human diabetic retinopathy: a challenge for the mouse models. *Current medicinal chemistry*, *20*, 3200-3217.
- Ranta, V.-P., & Urtti, A. (2006). Transscleral drug delivery to the posterior eye: prospects of pharmacokinetic modeling. *Advanced drug delivery reviews*, *58*, 1164-1181.
- Rathi, R. C., Zentner, G. M., & Jeong, B. (2000). Biodegradable low molecular weight triblock poly (lactide-co-glycolide) polyethylene glycol copolymers having reverse thermal gelation properties. In: Google Patents.
- Raviola, G. (1977). The structural basis of the blood-ocular barriers. *Exp Eye Res*, *25 Suppl*, 27-63.
- Reardon, D. B., Dent, P., Wood, S. L., Kong, T., & Sturgill, T. W. (1997). Activation In Vitro of Somatostatin Receptor Subtypes 2, 3, or 4 Stimulates Protein Tyrosine Phosphatase Activity in Membranes from Transfected Ras-Transformed NIH 3T3 Cells: Coexpression with Catalytically Inactive SHP-2 Blocks Responsiveness. *Molecular Endocrinology*, *11*, 1062-1069.
- Reardon, D. B., Wood, S. L., Brautigam, D. L., Bell, G. I., Dent, P., & Sturgill, T. W. (1996). Activation of a protein tyrosine phosphatase and inactivation of Raf-1 by somatostatin. *Biochemical Journal*, *314*, 401-404.
- Renström, E., Ding, W.-G., Bokvist, K., & Rorsman, P. Neurotransmitter-Induced Inhibition of Exocytosis in Insulin-Secreting β Cells by Activation of Calcineurin. *Neuron*, *17*, 513-522.
- Ritger, P. L., & Peppas, N. A. (1987). A simple equation for description of solute release II. Fickian and anomalous release from swellable devices. *Journal of Controlled Release*, *5*, 37-42.
- Roelfsema, F., Biermasz, N. R., Pereira, A. M., & Romijn, J. A. (2008). Therapeutic options in the management of acromegaly: focus on lanreotide Autogel®. *Biologics: targets & therapy*, *2*, 463.
- Ross-Murphy, S. B. (1994). Rheological characterization of polymer gels and networks. *Polymer Gels and Networks*, *2*, 229-237.
- Roy, D. S., & Rohera, B. D. (2002). Comparative evaluation of rate of hydration and matrix erosion of HEC and HPC and study of drug release from their matrices. *European Journal of Pharmaceutical Sciences*, *16*, 193-199.

- Saenz-de-Viteri, M., Fernández-Robredo, P., Hernandez, M., Bezunartea, J., Reiter, N., Recalde, S., & Garcia-Layana, A. (2016). Single-and repeated-dose toxicity study of bevacizumab, ranibizumab, and aflibercept in ARPE-19 cells under normal and oxidative stress conditions. *Biochemical pharmacology*, *103*, 129-139.
- Saint-Geniez, M., Kurihara, T., Sekiyama, E., Maldonado, A. E., & D'Amore, P. A. (2009). An essential role for RPE-derived soluble VEGF in the maintenance of the choriocapillaris. *Proc Natl Acad Sci U S A*, *106*, 18751-18756.
- Saint-Geniez, M., Maharaj, A. S., Walshe, T. E., Tucker, B. A., Sekiyama, E., Kurihara, T., Darland, D. C., Young, M. J., & D'Amore, P. A. (2008). Endogenous VEGF is required for visual function: evidence for a survival role on muller cells and photoreceptors. *PLoS One*, *3*, e3554.
- Sall, J. W., Klisovic, D. D., O'Dorisio, M. S., & Katz, S. E. (2004). Somatostatin inhibits IGF-1 mediated induction of VEGF in human retinal pigment epithelial cells. *Exp Eye Res*, *79*, 465-476.
- Sandostatin, L. (2000). Depot (octreotide acetate for injectable suspension) prescribing information. *East Hanover, NJ: Novartis Pharmaceuticals Corp.*
- Santiago, A. R., Gaspar, J. M., Baptista, F. I., Cristovao, A. J., Santos, P. F., Kamphuis, W., & Ambrosio, A. F. (2009). Diabetes changes the levels of ionotropic glutamate receptors in the rat retina. *Molecular vision*, *15*, 1620-1630.
- Sarao, V., Veritti, D., Boscia, F., & Lanzetta, P. (2014). Intravitreal Steroids for the Treatment of Retinal Diseases. *The Scientific World Journal*, *2014*, 14.
- Sarkar, N. (1979). Thermal gelation properties of methyl and hydroxypropyl methylcellulose. *Journal of Applied Polymer Science*, *24*, 1073-1087.
- Sathaye, S., Mbi, A., Sonmez, C., Chen, Y., Blair, D. L., Schneider, J. P., & Pochan, D. J. (2015). Rheology of peptide- and protein-based physical hydrogels: are everyday measurements just scratching the surface? *Wiley Interdiscip Rev Nanomed Nanobiotechnol*, *7*, 34-68.
- Schlegel, W., Wuarin, F., Zbaren, C., Wollheim, C. B., & Zahnd, G. R. (1985). Pertussis toxin selectively abolishes hormone induced lowering of cytosolic calcium in GH3 cells. *FEBS Lett*, *189*, 27-32.
- Schlingemann, R. O., Hofman, P., Vrensen, G. F. J. M., & Blaauwgeers, H. G. T. (1999). Increased expression of endothelial antigen PAL-E in human diabetic retinopathy correlates with microvascular leakage. *Diabetologia*, *42*, 596-602.
- Schwesinger, C., Yee, C., Rohan, R. M., Jousen, A. M., Fernandez, A., Meyer, T. N., Poulaki, V., Ma, J. J. K., Redmond, T. M., & Liu, S. (2001). Intrachoroidal neovascularization in transgenic mice overexpressing vascular endothelial growth factor in the retinal pigment epithelium. *The American journal of pathology*, *158*, 1161-1172.
- Seger, R., & Krebs, E. G. (1995). The MAPK signaling cascade. *FASEB Journal*, *9*, 726-735.
- Seiler, G. S., Salmon, J. H., Mantuo, R., Feingold, S., Dayton, P. A., & Gilger, B. C. (2011). Effect and Distribution of Contrast Medium after Injection into the Anterior Suprachoroidal Space in Ex Vivo Eyes. *Investigative ophthalmology & visual science*, *52*, 5730-5736.
- Senthilkumari, S., Sharmila, R., Chidambaranathan, G., & Vanniarajan, A. (2016). Epalrestat, an Aldose Reductase Inhibitor Prevents Glucose-Induced Toxicity in Human Retinal Pigment Epithelial Cells In Vitro. *Journal of Ocular Pharmacology and Therapeutics*, *33*, 34-41.
- Senthilkumari, S., Sharmila, R., Chidambaranathan, G., & Vanniarajan, A. (2017). Epalrestat, an Aldose Reductase Inhibitor Prevents Glucose-Induced Toxicity in Human Retinal Pigment Epithelial Cells In Vitro. *Journal of Ocular Pharmacology and Therapeutics*, *33*, 34-41.
- Sharma, K., Patel, Y. C., & Srikant, C. B. (1996). Subtype-selective induction of wild-type p53 and apoptosis, but not cell cycle arrest, by human somatostatin receptor 3. *Molecular Endocrinology*, *10*, 1688-1696.
- Sharma, R. K., Orr, W. E., Schmitt, A. D., & Johnson, D. A. (2005). A functional profile of gene expression in ARPE-19 cells. *BMC ophthalmology*, *5*, 25.
- Sheedlo, H. J., Li, L., & Turner, J. E. (1992). Effects of RPE-cell factors secreted from permselective fibers on retinal cells in vitro. *Brain research*, *587*, 327-337.

- Shen, E., Kipper, M. J., Dziadul, B., Lim, M.-K., & Narasimhan, B. (2002). Mechanistic relationships between polymer microstructure and drug release kinetics in bioerodible polyanhydrides. *Journal of Controlled Release, 82*, 115-125.
- Shirao, Y., & Kawasaki, K. (1998). Electrical responses from diabetic retina. *Prog Retin Eye Res, 17*, 59-76.
- Shoelson, S. E., Polonsky, K. S., Nakabayashi, T., Jaspan, J. B., & Tager, H. S. (1986). Circulating forms of somatostatinlike immunoreactivity in human plasma. *The American journal of physiology, 250*, E428-434.
- Sigurdsson, H. H., Konráðsdóttir, F., Loftsson, T., & Stefánsson, E. (2007). Topical and systemic absorption in delivery of dexamethasone to the anterior and posterior segments of the eye. *Acta Ophthalmologica Scandinavica, 85*, 598-602.
- Silva-Cunha, A., Fialho, S. L., Naud, M.-C., & Behar-Cohen, F. (2009). Poly-ε-caprolactone intravitreal devices: an in vivo study. *Investigative ophthalmology & visual science, 50*, 2312-2318.
- Simó-Servat, O., Hernández, C., & Simó, R. (2018). Somatostatin and diabetic retinopathy: an evolving story. *Endocrine, 60*, 1-3.
- Simó, R., & Hernández, C. (2008). Intravitreal anti-VEGF for diabetic retinopathy: hopes and fears for a new therapeutic strategy. *Diabetologia, 51*, 1574.
- Simó, R., & Hernández, C. (2015). Novel approaches for treating diabetic retinopathy based on recent pathogenic evidence. *Progress in retinal and eye research, 48*, 160-180.
- Simo, R., Hernandez, C., & European Consortium for the Early Treatment of Diabetic, R. (2012). Neurodegeneration is an early event in diabetic retinopathy: therapeutic implications. *Br J Ophthalmol, 96*, 1285-1290.
- Simo, R., Lecube, A., Sararols, L., Garcia-Arumi, J., Segura, R. M., Casamitjana, R., & Hernandez, C. (2002). Deficit of somatostatin-like immunoreactivity in the vitreous fluid of diabetic patients: possible role in the development of proliferative diabetic retinopathy. *Diabetes Care, 25*, 2282-2286.
- Simó, R., Sundstrom, J. M., & Antonetti, D. A. (2014). Ocular anti-VEGF therapy for diabetic retinopathy: the role of VEGF in the pathogenesis of diabetic retinopathy. *Diabetes Care, 37*, 893-899.
- Simó, R., Villarroya, M., Corraliza, L., Hernández, C., & Garcia-Ramírez, M. (2010). The Retinal Pigment Epithelium: Something More than a Constituent of the Blood-Retinal Barrier—Implications for the Pathogenesis of Diabetic Retinopathy. *Journal of Biomedicine and Biotechnology, 2010*, 190724.
- Sims, S. M., Lussier, B. T., & Kraicer, J. (1991). Somatostatin activates an inwardly rectifying K⁺ conductance in freshly dispersed rat somatotrophs. *The Journal of physiology, 441*, 615-637.
- Singh, A., Suri, S., & Roy, K. (2009). In-situ crosslinking hydrogels for combinatorial delivery of chemokines and siRNA-DNA carrying microparticles to dendritic cells. *Biomaterials, 30*, 5187-5200.
- Sinha, V. R., Bansal, K., Kaushik, R., Kumria, R., & Trehan, A. (2004). Poly-ε-caprolactone microspheres and nanospheres: an overview. *International Journal of Pharmaceutics, 278*, 1-23.
- Skamene, A., & Patel, Y. C. (1984). Infusion of graded concentrations of somatostatin in man: pharmacokinetics and differential inhibitory effects on pituitary and islet hormones. *Clinical endocrinology, 20*, 555-564.
- Smith, G., McLeod, D., Foreman, D., & Boulton, M. (1999). Immunolocalisation of the VEGF receptors FLT-1, KDR, and FLT-4 in diabetic retinopathy. *British Journal of Ophthalmology, 83*, 486-494.
- Smith, L. E., Kopchick, J. J., Chen, W., Knapp, J., Kinose, F., Daley, D., Foley, E., Smith, R. G., & Schaeffer, J. M. (1997). Essential role of growth hormone in ischemia-induced retinal neovascularization. *Science, 276*, 1706-1709.

- Smith, P. A. (2009). N-Type Ca²⁺-Channels in Murine Pancreatic β -Cells Are Inhibited by an Exclusive Coupling with Somatostatin Receptor Subtype 1. *Endocrinology*, *150*, 741-748.
- Sone, H., Deo, B. K., & Kumagai, A. K. (2000). Enhancement of glucose transport by vascular endothelial growth factor in retinal endothelial cells. *Investigative ophthalmology & visual science*, *41*, 1876-1884.
- Sone, H., Kawakami, Y., Kumagai, A. K., Okuda, Y., Sekine, Y., Honmura, S., Segawa, T., Suzuki, H., Yamashita, K., & Yamada, N. (1999). Effects of intraocular or systemic administration of neutralizing antibody against vascular endothelial growth factor on the murine experimental model of retinopathy. *Life sciences*, *65*, 2573-2580.
- Sone, H., Kawakami, Y., Okuda, Y., Kondo, S., Hanatani, M., Suzuki, H., & Yamashita, K. (1996). Vascular Endothelial Growth Factor Is Induced by Long-Term High Glucose Concentration and Up-Regulated by Acute Glucose Deprivation in Cultured Bovine Retinal Pigmented Epithelial Cells. *Biochemical and biophysical research communications*, *221*, 193-198.
- Spenlehauer, G., Vert, M., Benoit, J. P., & Boddaert, A. (1989). In vitro and in vivo degradation of poly (D, L lactide/glycolide) type microspheres made by solvent evaporation method. *Biomaterials*, *10*, 557-563.
- Sprecher, U., Mohr, P., Martin, R. E., Maerki, H. P., Sanchez, R. A., Binggeli, A., Künnecke, B., & Christ, A. D. (2010). Novel, non-peptidic somatostatin receptor subtype 5 antagonists improve glucose tolerance in rodents. *Regulatory Peptides*, *159*, 19-27.
- Srikant, C. B. (1995). Cell cycle dependent induction of apoptosis by somatostatin analog SMS 201-995 in AtT-20 mouse pituitary cells. *Biochem Biophys Res Commun*, *209*, 400-406.
- Srikant, C. B., & Shen, S. H. (1996). Octapeptide somatostatin analog SMS 201-995 induces translocation of intracellular PTP1C to membranes in MCF-7 human breast adenocarcinoma cells. *Endocrinology*, *137*, 3461-3468.
- Stitt, A. W., Li, Y. M., Gardiner, T. A., Bucala, R., Archer, D. B., & Vlassara, H. (1997). Advanced glycation end products (AGEs) co-localize with AGE receptors in the retinal vasculature of diabetic and of AGE-infused rats. *The American journal of pathology*, *150*, 523.
- Strowski, M. Z., Dashkevicz, M. P., Parmar, R. M., Wilkinson, H., Kohler, M., Schaeffer, J. M., & Blake, A. D. (2002). Somatostatin receptor subtypes 2 and 5 inhibit corticotropin-releasing hormone-stimulated adrenocorticotropin secretion from AtT-20 cells. *Neuroendocrinology*, *75*, 339-346.
- Strowski, M. Z., Kohler, M., Chen, H. Y., Trumbauer, M. E., Li, Z., Szalkowski, D., Gopal-Truter, S., Fisher, J. K., Schaeffer, J. M., Blake, A. D., Zhang, B. B., & Wilkinson, H. A. (2003). Somatostatin receptor subtype 5 regulates insulin secretion and glucose homeostasis. *Molecular Endocrinology*, *17*, 93-106.
- Sun, H., Mei, L., Song, C., Cui, X., & Wang, P. (2006). The in vivo degradation, absorption and excretion of PCL-based implant. *Biomaterials*, *27*, 1735-1740.
- Sun, Y. D., Ma, Y., Jiang, Y. J., Zhao, Q. D., Guan, H., & Han, Y. (2014). Effect of somatostatin on early electroretinogram in diabetic rats. *Journal of Jilin University Medicine Edition*, *40*, 1192-1196.
- Szabadfi, K., Pinter, E., Reglodi, D., & Gabriel, R. (2014). Neuropeptides, trophic factors, and other substances providing morphofunctional and metabolic protection in experimental models of diabetic retinopathy. In *International review of cell and molecular biology* (Vol. 311, pp. 1-121): Elsevier.
- Takada, S., Yamagata, Y., Misaki, M., Taira, K., & Kurokawa, T. (2003). Sustained release of human growth hormone from microcapsules prepared by a solvent evaporation technique. *J Control Release*, *88*, 229-242.
- Tallent, M., Liapakis, G., O'Carroll, A. M., Lolait, S. J., Dichter, M., & Reisine, T. (1996). Somatostatin receptor subtypes SSTR2 and SSTR5 couple negatively to an L-type Ca²⁺ current in the pituitary cell line AtT-20. *Neuroscience*, *71*, 1073-1081.
- Tate, P. (2009). *Seeley's principles of anatomy & physiology*: McGraw-Hill.

- Teijeiro, R., Rios, R., Costoya, J. A., Castro, R., Bello, J. L., Devesa, J., & Arce, V. M. (2002). Activation of human somatostatin receptor 2 promotes apoptosis through a mechanism that is independent from induction of p53. *Cellular physiology and biochemistry : international journal of experimental cellular physiology, biochemistry, and pharmacology*, *12*, 31-38.
- Thakur, A., Kadam, R. S., & Kompella, U. B. (2011). Influence of Drug Solubility and Lipophilicity on Transscleral Retinal Delivery of Six Corticosteroids. *Drug Metabolism and Disposition*, *39*, 771-781.
- Thangaraju, M., Sharma, K., Leber, B., Andrews, D. W., Shen, S. H., & Srikant, C. B. (1999). Regulation of acidification and apoptosis by SHP-1 and Bcl-2. *J Biol Chem*, *274*, 29549-29557.
- Thatcher, J. E., Welch, T., Eberhart, R. C., Schelly, Z. A., & DiMaio, J. M. (2012). Thymosin beta4 sustained release from poly(lactide-co-glycolide) microspheres: synthesis and implications for treatment of myocardial ischemia. *Ann N Y Acad Sci*, *1270*, 112-119.
- Thrimawithana, T. (2011). Polymeric Systems for Transscleral Delivery of Antisense Oligonucleotides: A Novel Treatment Strategy for Age-Related Macular Degeneration.
- Trevino, S. G., Schuschereba, S. T., Bowman, P. D., & Tsin, A. (2005). Lecithin: retinol acyltransferase in ARPE-19. *Experimental eye research*, *80*, 897-900.
- Troxler, T., Hurth, K., Schuh, K.-H., Schoeffter, P., Langenegger, D., Enz, A., & Hoyer, D. (2010). Decahydroisoquinoline derivatives as novel non-peptidic, potent and subtype-selective somatostatin sst3 receptor antagonists. *Bioorganic & medicinal chemistry letters*, *20*, 1728-1734.
- Tsuda, K., Sakurai, H., Seino, Y., Seino, S., Tanigawa, K., Kuzuya, H., & Imura, H. (1981). Somatostatin-like immunoreactivity in human peripheral plasma measured by radioimmunoassay following affinity chromatography. *Diabetes*, *30*, 471-474.
- Tuvia, S., Almagor, A., Bitler, A., Levin, S., Korenstein, R., & Yedgar, S. (1997). Cell membrane fluctuations are regulated by medium macroviscosity: evidence for a metabolic driving force. *Proceedings of the National Academy of Sciences*, *94*, 5045-5049.
- Urtti, A. (2006). Challenges and obstacles of ocular pharmacokinetics and drug delivery. *Advanced drug delivery reviews*, *58*, 1131-1135.
- Urtti, A., Pipkin, J. D., Rork, G., & Repta, A. J. (1990). Controlled drug delivery devices for experimental ocular studies with timolol 1. In vitro release studies. *International Journal of Pharmaceutics*, *61*, 235-240.
- Vaishya, R. D., Mandal, A., Patel, S., & Mitra, A. K. (2015). Extended release microparticle-in-gel formulation of octreotide: effect of polymer type on acylation of peptide during in vitro release. *International Journal of Pharmaceutics*, *496*, 676-688.
- Valery, C., Artzner, F., Robert, B., Gulick, T., Keller, G., Grabielle-Madelmont, C., Torres, M. L., Cherif-Cheikh, R., & Paternostre, M. (2004). Self-association process of a peptide in solution: from beta-sheet filaments to large embedded nanotubes. *Biophys J*, *86*, 2484-2501.
- Valéry, C., Paternostre, M., Robert, B., Gulik-Krzywicki, T., Narayanan, T., Dedieu, J. C., Keller, G., Torres, M. L., Cherif-Cheikh, R., Calvo, P., & Artzner, F. (2003). Biomimetic organization: Octapeptide self-assembly into nanotubes of viral capsid-like dimension. *Proceedings of the National Academy of Sciences of the United States of America*, *100*, 10258-10262.
- van der Hoek, J., Hofland, L. J., & Lamberts, S. W. (2005). Novel subtype specific and universal somatostatin analogues: clinical potential and pitfalls. *Current pharmaceutical design*, *11*, 1573-1592.
- Van Grondelle, W., Iglesias, C. L., Coll, E., Artzner, F., Paternostre, M., Lacombe, F., Cardus, M., Martinez, G., Montes, M., & Cherif-Cheikh, R. (2007). Spontaneous fibrillation of the native neuropeptide hormone Somatostatin-14. *Journal of structural biology*, *160*, 211-223.
- van Grondelle, W., Iglesias, C. L., Coll, E., Artzner, F., Paternostre, M., Lacombe, F., Cardus, M., Martinez, G., Montes, M., Cherif-Cheikh, R., & Valery, C. (2007). Spontaneous fibrillation of the native neuropeptide hormone Somatostatin-14. *J Struct Biol*, *160*, 211-223.

- van Grondelle, W., Lecomte, S., Lopez-Iglesias, C., Manero, J.-M., Cherif-Cheikh, R., Paternostre, M., & Valery, C. (2013). Lamination and spherulite-like compaction of a hormone's native amyloid-like nanofibrils: spectroscopic insights into key interactions. *Faraday Discussions*, *166*, 163-180.
- van Hagen, P. M., Baarsma, G. S., Mooy, C. M., Ercoskan, E. M., ter Averst, E., Hofland, L. J., Lamberts, S. W., & Kuijpers, R. W. (2000). Somatostatin and somatostatin receptors in retinal diseases. *Eur J Endocrinol*, *143 Suppl 1*, S43-51.
- Vapreotide. (2003). *Drugs in R & D*, *4*, 326-330.
- Varde, N. K., & Pack, D. W. (2004). Microspheres for controlled release drug delivery. *Expert Opinion on Biological Therapy*, *4*, 35-51.
- Vasquez, B., Harris, V., & Unger, R. H. (1982). Extraction of somatostatin from human plasma on octadecylsilyl silica. *The Journal of clinical endocrinology and metabolism*, *55*, 807-809.
- Veloso, A. A., Zhu, Q., Herrero-Vanrell, R., & Refojo, M. F. (1997). Ganciclovir-loaded polymer microspheres in rabbit eyes inoculated with human cytomegalovirus. *Investigative ophthalmology & visual science*, *38*, 665-675.
- Villarroel, M., García-Ramírez, M., Corraliza, L., Hernández, C., & Simó, R. (2011). Fenofibric acid prevents retinal pigment epithelium disruption induced by interleukin-1 β by suppressing AMP-activated protein kinase (AMPK) activation. *Diabetologia*, *54*, 1543-1553.
- Villarroel, M., García-Ramírez, M., Corraliza, L., Hernández, C., & Simó, R. (2009). Effects of high glucose concentration on the barrier function and the expression of tight junction proteins in human retinal pigment epithelial cells. *Experimental eye research*, *89*, 913-920.
- Virgili, G., Parravano, M., Menchini, F., & Brunetti, M. (2012). Antiangiogenic therapy with anti-vascular endothelial growth factor modalities for diabetic macular oedema. *Cochrane Database Syst Rev*, *12*, CD007419.
- Vogt, R. R., Unda, R., Yeh, L. C. C., Vidro, E. K., Lee, J. C., & Tsin, A. T. (2006). Bone morphogenetic protein-4 enhances vascular endothelial growth factor secretion by human retinal pigment epithelial cells. *Journal of cellular biochemistry*, *98*, 1196-1202.
- Wang, W., Matsukura, M., Fujii, I., Ito, K., Zhao, J. E., Shinohara, M., Wang, Y. Q., & Zhang, X. M. (2012). Inhibition of high glucose-induced VEGF and ICAM-1 expression in human retinal pigment epithelium cells by targeting ILK with small interference RNA. *Molecular Biology Reports*, *39*, 613-620.
- Weckbecker, G., Lewis, I., Albert, R., Schmid, H. A., Hoyer, D., & Bruns, C. (2003). Opportunities in somatostatin research: biological, chemical and therapeutic aspects. *Nature reviews. Drug discovery*, *2*, 999-1017.
- Wei, X., Gong, C., Gou, M., Fu, S., Guo, Q., Shi, S., Luo, F., Guo, G., Qiu, L., & Qian, Z. (2009). Biodegradable poly(ϵ -caprolactone)-poly(ethylene glycol) copolymers as drug delivery system. *International Journal of Pharmaceutics*, *381*, 1-18.
- Wen, H., Hao, J., & Li, S. K. (2013). Characterization of Human Sclera Barrier Properties for Transscleral Delivery of Bevacizumab and Ranibizumab. *Journal of Pharmaceutical Sciences*, *102*, 892-903.
- Wild, S., Roglic, G., Green, A., Sicree, R., & King, H. (2004). Global prevalence of diabetes: estimates for the year 2000 and projections for 2030. *Diabetes care*, *27*, 1047-1053.
- Wilkinson, C. P., Ferris, F. L., 3rd, Klein, R. E., Lee, P. P., Agardh, C. D., Davis, M., Dills, D., Kampik, A., Pararajasegaram, R., Verdager, J. T., & Global Diabetic Retinopathy Project, G. (2003). Proposed international clinical diabetic retinopathy and diabetic macular edema disease severity scales. *Ophthalmology*, *110*, 1677-1682.
- Williamson, J. R., Chang, K., Frangos, M., Hasan, K. S., Ido, Y., Kawamura, T., Nyengaard, J. R., van Den Enden, M., Kilo, C., & Tilton, R. G. (1993). Hyperglycemic pseudohypoxia and diabetic complications. *Diabetes*, *42*, 801-813.
- Wilson, S. H., Davis, M. I., Caballero, S., & Grant, M. B. (2001). Modulation of retinal endothelial cell behaviour by insulin-like growth factor I and somatostatin analogues: implications for

- diabetic retinopathy. *Growth hormone & IGF research : official journal of the Growth Hormone Research Society and the International IGF Research Society*, 11 Suppl A, S53-59.
- Witmer, A. N., Blaauwgeers, H. G., Weich, H. A., Alitalo, K., Vrensen, G. F. J. M., & Schlingemann, R. O. (2002). Altered expression patterns of VEGF receptors in human diabetic retina and in experimental VEGF-induced retinopathy in monkey. *Investigative Ophthalmology and Visual Science*, 43, 849-857.
- Wolin, E. M., Manon, A., Chassaing, C., Lewis, A., Bertocchi, L., Richard, J., & Phan, A. T. (2016). Lanreotide Depot: An Antineoplastic Treatment of Carcinoid or Neuroendocrine Tumors. *Journal of Gastrointestinal Cancer*, 1-9.
- Wu, C., Jim, T. F., Gan, Z., Zhao, Y., & Wang, S. (2000). A heterogeneous catalytic kinetics for enzymatic biodegradation of poly (ϵ -caprolactone) nanoparticles in aqueous solution. *Polymer*, 41, 3593-3597.
- Wu, M. P., Tamada, J. A., Brem, H., & Langer, R. (1994). In vivo versus in vitro degradation of controlled release polymers for intracranial surgical therapy. *Journal of biomedical materials research*, 28, 387-395.
- Wu, P. C., Liu, C. C., Chen, C. H., Kou, H. K., Shen, S. C., Lu, C. Y., Chou, W. Y., Sung, M. T., & Yang, L. C. (2003). Inhibition of experimental angiogenesis of cornea by somatostatin. *Graefe's archive for clinical and experimental ophthalmology = Albrecht von Graefes Archiv fur klinische und experimentelle Ophthalmologie*, 241, 63-69.
- Wu, X. S. (1995). Synthesis and properties of biodegradable lactic/glycolic acid polymers. *Encyclopedic handbook of biomaterials and bioengineering*, 2, 1015-1054.
- Xie, X., Yang, Y., Chi, Q., Li, Z., Zhang, H., Li, Y., & Yang, Y. (2014). Controlled Release of Dutasteride from Biodegradable Microspheres: In Vitro and In Vivo Studies. *PLoS One*, 9, e114835.
- Xu, Y., Li, L., Zheng, P., Lam, Y. C., & Hu, X. (2004). Controllable Gelation of Methylcellulose by a Salt Mixture. *Langmuir*, 20, 6134-6138.
- Yamashita, N., Shibuya, N., & Ogata, E. (1986). Hyperpolarization of the membrane potential caused by somatostatin in dissociated human pituitary adenoma cells that secrete growth hormone. *Proceedings of the National Academy of Sciences*, 83, 6198-6202.
- Yan, C., Altunbas, A., Yucel, T., Nagarkar, R. P., Schneider, J. P., & Pochan, D. J. (2010). Injectable solid hydrogel: mechanism of shear-thinning and immediate recovery of injectable beta-hairpin peptide hydrogels. *Soft Matter*, 6, 5143-5156.
- Yang, S.-K., Parkington, H. C., Blake, A. D., Keating, D. J., & Chen, C. (2005). Somatostatin Increases Voltage-Gated K⁺ Currents in GH3 Cells through Activation of Multiple Somatostatin Receptors. *Endocrinology*, 146, 4975-4984.
- Yasin, M. N., Svirskis, D., Seyfoddin, A., & Rupenthal, I. D. (2014). Implants for drug delivery to the posterior segment of the eye: a focus on stimuli-responsive and tunable release systems. *J Control Release*, 196, 208-221.
- Yasukawa, T., Ogura, Y., Tabata, Y., Kimura, H., Wiedemann, P., & Honda, Y. (2004). Drug delivery systems for vitreoretinal diseases. *Progress in retinal and eye research*, 23, 253-281.
- Yatani, A., Codina, J., Sekura, R. D., Birnbaumer, L., & Brown, A. M. (1987). Reconstitution of Somatostatin and Muscarinic Receptor Mediated Stimulation of K⁺ Channels by Isolated GK Protein in Clonal Rat Anterior Pituitary Cell Membranes. *Molecular Endocrinology*, 1, 283-289.
- Yau, J. W. Y., Rogers, S. L., Kawasaki, R., Lamoureux, E. L., Kowalski, J. W., Bek, T., Chen, S.-J., Dekker, J. M., Fletcher, A., Grauslund, J., Haffner, S., Hamman, R. F., Ikram, M. K., Kayama, T., Klein, B. E. K., Klein, R., Krishnaiah, S., Mayurasakorn, K., O'Hare, J. P., Orchard, T. J., Porta, M., Rema, M., Roy, M. S., Sharma, T., Shaw, J., Taylor, H., Tielsch, J. M., Varma, R., Wang, J. J., Wang, N., West, S., Xu, L., Yasuda, M., Zhang, X., Mitchell, P., & Wong, T. Y. (2012). Global Prevalence and Major Risk Factors of Diabetic Retinopathy. *Diabetes Care*, 35, 556-564.
- Yedgar, S., & Reisfeld, N. (1990). Regulation of cell membrane function and secretion by extracellular fluid viscosity. *Biorheology*, 27, 581-588.

- Yeung, M., & Treit, D. (2012). The anxiolytic effects of somatostatin following intra-septal and intra-amygdalar microinfusions are reversed by the selective sst2 antagonist PRL2903. *Pharmacology Biochemistry and Behavior*, *101*, 88-92.
- Yu, Y., Lau, L. C. M., Lo, A. C.-y., & Chau, Y. (2015). Injectable chemically crosslinked hydrogel for the controlled release of bevacizumab in vitreous: a 6-month in vivo study. *Translational vision science & technology*, *4*, 5-5.
- Zarnbaux, M. F., Bonneaux, F., Gref, R., Maincent, P., Dellacherie, E., Alonso, M. J., Labrude, P., & Vigneron, C. (1998). Influence of experimental parameters on the characteristics of poly (lactic acid) nanoparticles prepared by a double emulsion method. *Journal of Controlled Release*, *50*, 31-40.
- Zatelli, M. C., Tagliati, F., Piccin, D., Taylor, J. E., Culler, M. D., Bondanelli, M., & degli Uberti, E. C. (2002). Somatostatin receptor subtype 1-selective activation reduces cell growth and calcitonin secretion in a human medullary thyroid carcinoma cell line. *Biochemical and biophysical research communications*, *297*, 828-834.
- Zhang, S. X., Wang, J. J., Gao, G., Parke, K., & Ma, J.-x. (2006). Pigment epithelium-derived factor downregulates vascular endothelial growth factor (VEGF) expression and inhibits VEGF–VEGF receptor 2 binding in diabetic retinopathy. *Journal of molecular endocrinology*, *37*, 1-12.
- Zhang, X., Wang, N., Barile, G. R., Bao, S., & Gillies, M. (2013). Diabetic retinopathy: neuron protection as a therapeutic target. *The international journal of biochemistry & cell biology*, *45*, 1525-1529.
- Zhou, S., Deng, X., & Yang, H. (2003a). Biodegradable poly (ε-caprolactone)-poly (ethylene glycol) block copolymers: characterization and their use as drug carriers for a controlled delivery system. *Biomaterials*, *24*, 3563-3570.
- Zhou, S., Deng, X., & Yang, H. (2003b). Biodegradable poly(ε-caprolactone)-poly(ethylene glycol) block copolymers: characterization and their use as drug carriers for a controlled delivery system. *Biomaterials*, *24*, 3563-3570.